UNIVERSITY OF LEICESTER

Sensor applications based on molecularly imprinted polymers prepared by solid phase approach

Thesis submitted for the degree of Doctor of Philosophy at the University of Leicester

By

Omar Abdulhay Sheej Ahmad

Department of Chemistry

University of Leicester

2019

Abstract

Molecularly imprinted polymers (MIPs) have received considerable attention due to their low cost preparation, robustness and high stability. MIP nanoparticles (MIP NPs) offer significant advantages over bulk materials as they have a high surface-to-volume ratio resulting in enhanced chemical reactivity and binding kinetics. This thesis demonstrates the use of MIP NPs as sensing elements for the direct detection of analyte in biomimetic sensors.

Chapter two describes a potentiometric sensor for cocaine based on MIP NPs. MIP NPs were prepared in water and organic solvents. Imprinted polymers produced in organic solvent using acrylamide as a functional monomer demonstrated high yield and affinity. Nanoparticles were incorporated within a PVC matrix which was then used to prepare an ion-selective membrane integrated with a potentiometric transducer. The developed sensor has successfully detected cocaine in blood serum in the range of concentrations 1 $x10^{-9}$-$1x10^{-3}$ M.

Chapter three describes a QCR sensor based on MIP NPs to detect gram-negative bacterial quorum signalling molecules *N*-Acyl homoserine lactone (AHL). The affinity of MIP NPs was analysed using BIAcore 3000. After that, a novel acoustic technique based on Fixed Frequency Drive (FFD) combined with MIPs was used for the detection of AHL exploiting *N*-hexanoyl-L-homoserine lactone (C6 HSL) as a model molecule. The FFD technique enabled sensitive, label-free, rapid and real-time detection of C6 HSL in spiked PBS solution with a minimum quantification limit $1x10^{-3}$ M.

Chapter four describes an electrochemical sensor based on an electroactive molecularly imprinted polymer (EMIP) containing an electroactive mediator. Different polymerisation strategies were used to fabricate the EMIP for three different targets: HSL, trypsin and glucose. Differential pulse voltammetry (DPV) was used to evaluate the selectivity and sensitivity of EMIP towards these targets. The detection limits for these targets were $0.3x10^{-9}$, $0.22x10^{-9}$ and $0.13x10^{-6}$ M respectively.

Acknowledgements

Firstly, I would like to say Alhamdulillah and all praises to Allah for the strengths and his blessing in completing my PhD thesis. Secondly, I would like to express my great appreciation to my supervisors, Professor Sergey Piletsky and Dr Elena Piletska. I really appreciate their patience, encouragement and motivation, not just supervisors but like a parents who made me think deeply. Professor Sergey Piletsky was my research guide, a great source of support and motivation during my research.

I would like to acknowledge the contribution of Dr Kal Karim for running the molecular modelling. As well as, I would like to thank the contribution of Dr Antonio Guerreiro for running the BIAcore experiments.

I am also grateful to the staff in the Biotechnology group (Mike, Francesco, Joanna, Katarzyna and Alvaro) for their unfailing support and assistance.

I would like to show my gratitude to Dr Thomas Bedwell for his time and efforts in reviewing my thesis.

I would like to thank my fellow lab mates (Asma, Fabiana, Kaseb and Todd) for the stimulating discussions and for all the fun we had during my PhD journey.

I greatly appreciate all the hard work and the tremendous support of the collaborators Dr Sourav K. Ghosh and Arnab Guha for the great collaboration.

I am grateful to my friends Dr Mohamed Al-hmeda, Dr Mohammed Alenzii, Dr Hamza Al-Husseini, Dr Mohammed Thanon and Dr Mohammad Bashar for their moral and emotional support during my PhD journey.

A very special gratitude goes out to the Ministry of Higher Education and Scientific Research of Iraq and the Iraqi Cultural Attaché in the UK for the financial contribution to my PhD. As well as, a special thanks to the Department of Chemistry, College of Education for Pure Science / University of Mosul, Iraq for supporting my PhD.

Most importantly, I must express my warmest thanks and most profound appreciation to my parent, sisters and brothers for all their prayers, support and unconditional love throughout this journey. Mum, dad I do not know how to thank you enough for providing me with the opportunity to be where I am today. I love you so much and may Allah bless you.

I would like to express my deeper thanks to my wife's family for their support and prayers. I do not know how to extend my gratitude towards you.

Last but not least, I do not know how to begin with saying thanks to my soul mate, my dearest wife and my best friend, Omamah. I love you for everything, for being so understanding and for putting up with me through the toughest moments of my life. In addition, I dedicate this PhD thesis to my lovely kids (Sama, Dima, Noor and Abdullah). You are the pride and joy of my life. I love you more than anything else.

I am using this opportunity to express my gratitude to everyone who supported me throughout the PhD journey.

Table of Contents

List of Tables

List of Figures

Abbreviations list

3-oxo-C6-HSL	N-(3-Oxohexanoyl)-L-homoserine lactone
AAc	Acrylic acid
ABL	Butyrolactone hydrobromide
ACN	Acetonitrile
AHL	Acyl-homoserine lactone
AIs	Autoinducers
APTMS	3-aminopropyltrimethyloxysilane
C 4 HSL	N-Butyryl-L-homoserine lactone
C6-HSL	Hexanoyl-L-homoserine lactone
CE	Counter electrode
CV	Cyclic voltammetry
DEAEM	2-(Diethylamino)ethyl methacrylate
DLS	Dynamic light scattering
DMF	N,N'-dimethylformamide
DPV	Differential pulse voltammetry
EDC	N-(3-Dimethylaminopropyl)-N′-ethylcarbodiimide hydrochloride
EGDMA	Ethylene glycol dimethacrylate
EIS	Electrochemical impedance spectroscopy
ELISA	Enzyme-Linked Immunosorbent Assay
FC	Ferrocene
FCA	Ferrocene carboxylic acid
FMAA	Ferrocenylmethyl methacrylate
GA	Glutaraldehyde
GSPE	Gold screen-printed electrode
HPLC-MS	High performance liquid chromatography-mass spectrometry
HSL	Homoserine Lactone
IA	Itaconic acid
LC-MS/MS	Liquid Chromatography Mass Spectrophotometry
MAA	Methacrylic Acid
MES buffer	2-[Morpholino]ethanesulfonic acid

MIP NPs	Molecularly Imprinted Polymer Nanoparticles
MIP	Molecularly imprinted polymer MNPs
MIPT	Molecularly imprinted technology
NPs	Nanoparticles
PBS	Phosphate buffered saline
Pt	Platinum
QS	Quorum Sensing
SEM	Scanning electron microscopy
SPE	Screen-Printed Electrode
SPR	Surface plasmon resonance
TRIM	Trimethylolpropane trimethacrylate
WE	Working electrode

Chapter One: General Introduction

1.1 A Short History of Molecular Imprinting

An early example of research on molecular imprinting was published by Polyakov (1931), who was the first researcher to describe molecular imprinting[1,2]. It was experimentally observed that when silica gels were prepared in the presence of a solvent additive, the resulting silica showed superior binding capacity for that solvent. It was the first time that experiments of this kind were accompanied by explanations of this nature. The mechanism proposed by Polykov was mainly overlooked by the scientific community[1,2]. To confirm this concept, in 1949, a study was performed by Frank Dickey, which involved performing molecular imprinting in silica matrices in the presence of dyes[3]. He noticed that after removal of the 'patterning' dye, the silica would preferentially bind the same dye, even in the presence of others. Dickey's silica can be considered the first imprinted material.

Dickey's approach to introduce the template in the sodium silicate pre-polymerisation mixture produced a more definite influence on the structure of the silica, while Polykov introduced the template after the silica framework had been formed. Dickey's work is similar to present methodologies, thus this method has became the most widely used in subsequent studies[4].

Two decades of studies have provided considerable information related to the molecular imprinting of silica, followed by the introduction of the first works on a molecularly imprinted organic polymer. In 1972, Wulff and Klotz's research groups independently described the preparation of organic polymers with predetermined ligands. Template molecules present during the polymerisation process were recognised by the resultant molecularly imprinted polymers (MIPs)[5]. At the same time, Takagishi and Klotz reported that the introduction of a cross-linker during the imprinting process could control polymer chain mobility and improve (specific) adsorption capacity[6,7]. Thereafter, Wulff described the "covalent approach" to prepare an organic molecularly imprinted polymer with the capability to differentiate between glyceric acid enantiomers[8]. In his work, monomers formed covalent bonds with a template, which had to be hydrolysed prior to re-binding. Subsequently, a considerable amount of the literature was derived from Wulff's *et. al*.

Later on, Mosbach and Arshady designed imprinted polymers using non-covalent interactions[2,9]. The prepared MIPs possess several advantages over the conventional immunosorbents (IS)[10]. MIPs showed similar levels of selectivity and affinity but had much greater stability and were easier to prepare[11]. Furthermore, these MIPs could be used repeatedly without decrease in their level of activity. They possessed a high level of mechanical strength and durability, even in harsh chemical media and at elevated temperatures and pressures compared to biological receptors[12].

As a development of the previous work, in 1993, Mosbach and co-researchers published a study in Nature, where for the first time the non-covalent molecular imprinting approach was employed in a competitive binding assay for theophylline and diazepam detection in clinical samples (human serum)[13]. They suggested that non-covalent interactions were preserving the template-functional monomer complex during the polymerisation process.

Research based on this technology has grown rapidly due to its potential application in numerous fields, such as chemical, pharmaceutical, engineering, material and biotechnological industries. As an example, Zhao and Hao have developed molecularly imprinted core-shell polymers[14]. Tert-butylhydroquinone (TBHQ) imprinted core-shell were prepared using silica nanoparticles as a core material. These materials were used as a receptor for electrochemical sensor utilising the molecular imprinting technique in order to determine levels of TBHQ in foodstuffs. Moreover, due to the high surface-to-volume ratio inherent to the nanoscale structure, silica nanoparticles, as core material, showed superior accessibility to the target species and low mass-transfer resistance.

Piletsky and co-workers subsequently developed a novel methodology for direct synthesis and purification of MIPs based on a reusable solid phase for both small and big molecules, which could be used for either aqueous or organic polymerisation[15]. Piletsky and his team further developed this technique into the first automated synthesis of MIP NPs, utilising the template-immobilised glass beads for large industrial-scale manufacturing[16]. As an example, MIP NPs for pepsin A, α-amylase and trypsin were prepared using an automated reactor which contains template-derivatised glass beads. The protocol used an automatic reactor to perform synthesis and purification of MIP NPs under computer control to create nanoMIPs with sub-nanomolar affinity in only 4 hours.

Currently, molecularly imprinted polymers have been widely recognised as extremely promising materials for applications across different fields of scientific research[16].

1.2 Molecularly Imprinting Polymer Technology (MIPT)

Analytical techniques require both selective and sensitive recognition of their target species. Natural antibodies and enzymes meet these requirements; however, their use is limited due to their short shelf-lives, high production costs and poor stability in harsh condition such as organic solvents and extremes of temperature and pH. Furthermore, immobilisation of natural receptors is challenging and can potentially result in changes to their binding properties. In addition, natural antibodies are expensive and require long time to synthesise and purify. To answer these limitations, artificially synthesised receptors have been developed[17-19]. The MIPT is a newly developed synthetic method to produce robust materials capable of mimicking natural recognition entities such as antibodies and biological receptors[8,20,21]. MIPs are generated by the polymerisation of monomers in the presence of a template molecule to forms synthetic analogue to antibody. MIPs utilise a "lock and key" mechanism to selectively bind to the template molecule used in the polymerisation.

MIPs can recognise both chemical and biological molecules including nucleotide derivatives[22], amino acids, proteins[23,24], drugs and food components[25,26]. MIPs have been applied in various areas of research, including separation sciences[27,28], chemical sensors[29], catalysis[30], drug delivery[31], biological antibodies and receptor systems[22,23].

MIPs possess the most important properties of biological receptors - the ability to recognise and bind specific target molecules. However, in contrast to biological receptors, MIPs are large, rigid and insoluble, whereas, biological receptors are smaller, flexible, and in most cases soluble in aqueous solvents. Furthermore, MIPs are larger in size and have the potential to possess thousands of binding sites, whereas in contrast biological receptors usually only have a few or even just one such site[18]. Furthermore, the population of binding sites in MIPs, especially those imprinted using non-covalent monomer-template interactions, is heterogeneous because of the impact of the equilibria

that manage the monomer-template complex formation and the dynamics of the growing polymer chains before copolymerisation.

In molecular imprinting, a three-dimensional polymer network is formed when a large excess of a cross-linking monomer is used. The template is removed from the polymer after polymerisation, leaving specific recognition sites which have a similar shape, size and complementary chemical functionality to the analyte molecule (

Figure 1.1). The functional monomers initially form a complex with the imprinting molecule. Because of the polymerisation process, the monomer functional groups will be held in position by the highly cross-linked polymeric structure of the polymer allowing for specific rebinding of the template[17].

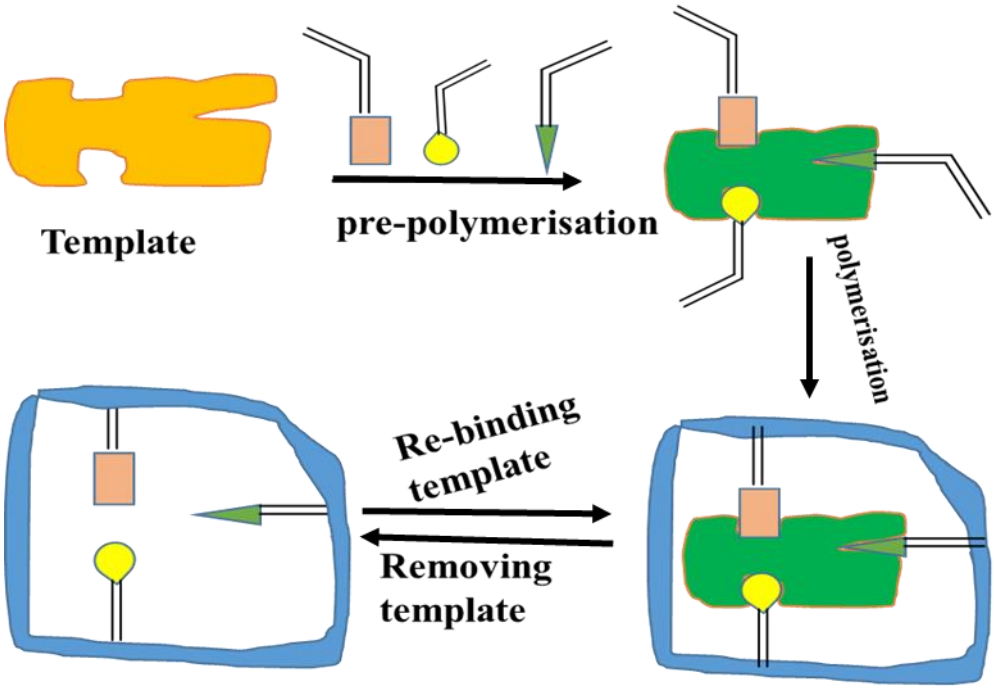

Figure 1.1: Molecular imprinting

The interaction between template and MIP is caused by self-assembly of the functional monomers in solution around the template. For example, positive charges in the monomers will orient themselves around negative charges in the analyte molecule. This principle works with any non-covalent interaction, such as ionic, π–π, hydrophobic and hydrogen bond interactions. The non-covalent interactions between the template and functional groups in an imprinted cavity are ideal, as the template molecule can be removed easily. The resulting cavities reproduce the size and shape of the template, which is washed away[9]. The affinity between the template and the functional monomer should be strong enough to allow strong binding of the imprinted molecule to the polymer and fixation within the polymer matrix while still allowing reversible binding.

Furthermore, they should not react irreversibly with the template. In particular, when the template is a large molecule such as a protein or peptide, the polymer needs, at least to some extent, to be porous to allow template removal as well as rebinding[32]. However, improving MIP technology with enhanced recognition properties necessitates further research into understanding the main mechanisms responsible for selectivity in molecularly imprinted materials.

1.3 Approaches for Preparation of MIPs

To understand the main mechanisms of producing molecular imprinted materials, the general approaches to MIP synthesis can be categorised as being covalent, non-covalent and semi-covalent in nature (Figure 1.2).

1.3.1 Covalent Approach

The covalent approach has been described by Wulff *et al*. as the formation of reversible chemical bonds between monomers and template during polymerisation, with the same bonds being reformed during the rebinding step[4]. The benefits of this method are that only the functional groups on the monomers interact with the template via homogeneous binding sites. The functionalities remaining in the binding sites allow binding to the target molecule by reformation of the covalent bonds. However, only a restricted range of

functional groups including alcohols, aldehydes, ketones, primary amines and carboxylic acids can be imprinted by this approach. The majority of covalent imprinting strategies involve a condensation reaction that requires addition or loss of a water molecule during the cleavage or rebinding processes, respectively[4].

As an example for the covalent approach, carboxylic groups have been imprinted by Shea *et al*. utilising a carboxylic ester linkage[33-35]. Following removal of the template, rebinding can occur by the interaction of a carbonyl chloride with an alcohol, or via the displacement of bromide by a carboxylate anion. However, due to slow rebinding kinetics and an requirement for activated intermediate to facilitate the reaction, carboxylic acids have limited use in the covalent approach[4,36]. In contrast, the main advantages of this method is that the monomer/template complexes are stoichiometric and very stable, allowing for a wide range of polymerisation conditions to be employed[37,38].

1.3.2 Non-covalent Approach

The non-covalent approach was described by Mosbach and co-workers utilising electrostatic and hydrophobic interactions. Since the interactions that take place are weak, additional functional monomers are usually required to increase stability of the monomer-template complex. The chosen monomers utilise hydrogen bonding, ionic interactions, π-π interactions, hydrophobic interactions and van der Waals interactions to form complexes between monomer and template. Moreover, the rebinding process between the template molecules and MIPs are achieved via non-covalent intermolecular interactions. Generally, association/dissociation kinetics of non-covalent binding MIPs are faster than those prepared via covalent approach. It is therefore straightforward to form template/monomer complex and to remove the template from polymer network. As a result of rapid rebinding process, many potential applications utilising a wide range of target molecules has been considered[37,39]. As an example, theophylline and diazepam have been used to fabricate MIPs for separation appicaitons[13]. In addition, a wide range of functional monomers which can be used in non-covalent approach are commercially available; for example, the most common acidic functional monomer, methacrylic acid (MAA), which was first reported in imprinting by Mosbach *et al.*[13].

Other popular monomers, widely employed for MIP synthesis, include 4-vinyl pyridine (4-vpy) and 2-hydroxethyl methacrylate (HEMA)[40,41]. The combination of HEMA in methacrylate-based MIP makes the polymer less hydrophobic, aiding in the diffusion of hydrophilic template[42].

1.3.3 Semi-covalent Approach

The final approach utilised for the preparation of MIPs is a semi-covalent polymerisation. This is a hybrid approach combining the initial formation of the template/monomer complex via covalent bonding, with subsequent rebinding to the polymer occurring via non-covalent interactions[39,43]. Whitcombe *et al.* developed a new synthetic method of polymerisation by linking the monomer functional group with the template through a linker group which is then "sacrificed" during template removal[43], in order to overcome crowding in the binding cavity and to allow unhindered non-covalent rebinding to occur[4]. Semi-covalent imprinting of the cholesterol as a template was the first example of the use of the sacrificial spacer approach. As cholesterol has limited functionality, it was a difficult molecule to imprint through conventional routes. Cholesterol was attached via a carbonyl spacer to 4-vinylphenol forming cholesteryl 4-vinylphenyl carbonate as the template monomer. During polymerisation, cholesterol was cleaved from the polymer by hydrolysis. A phenolic hydroxyl group then left in the binding site which is capable of binding with cholesterol through hydrogen bond formation. Adequate space between the functional groups remained in order to establish hydrogen bonding and to createof an imprinted site, displaying a recognition site matching that of the cholesterol molecule. MIPs prepared for cholesterol via this approach exhibited higher chromatographic efficiency compared to non-covalent imprinted polymers, when used as stationary phases in the HPLC method[44].

Semi-covalent imprinting combines the disadvantages and advantages of the previous two approaches, primarily stable and stoichiometric complexes formed via the use of the covalent imprinting process and fast template-MIP binding of non-covalent imprinting[4].

Finally, many variables should be considered in order to achieve high affinity molecularly imprinted polymers such as the nature and amount of the template, functional monomer(s), cross-linker(s), solvent(s) and the initiator, the method of initiation and the duration of the polymerisation.

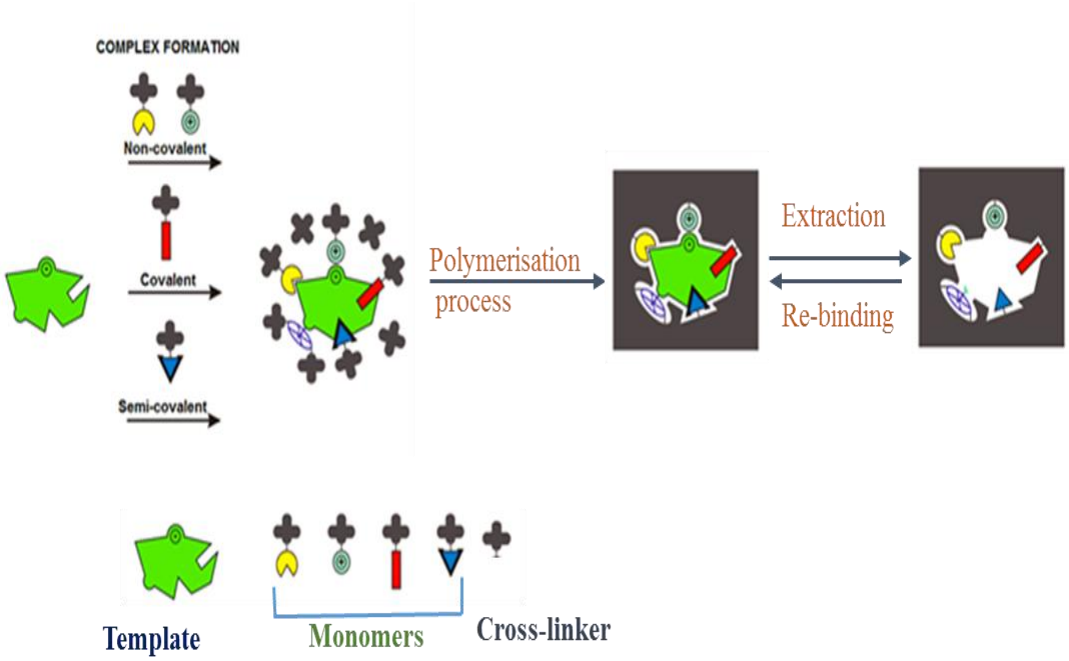

Figure 1.2: MIPs preparation approaches. Adapted from reference

[145] with permission

1.4 Components of MIPs

The effective synthesis of MIP particles depends on the MIP's components such as template, functional monomers, cross-linking species, polymerisation solvent and initiator species. Consequently, the physical and chemical properties of the resultant MIPs, such as the particle size, binding affinity, solubility in various solvents, template selectivity, stability and rigidity, can be affected by these components.

1.4.1 Functional Monomers

Functional monomers are responsible for forming the binding points located within the binding sites of an imprinted polymer generated by self-assembly around a template molecule[45]. Generally, functional monomers used in non-covalent imprinting are chosen from previous experimentation or from the literature. The choice of functional monomers determines the structure of the recognition site, whilst the concentration used will influence the number of binding sites in the MIPs[46,47]. The selection of functional monomers is essential for preserving stable monomer-template complexes during the imprinting process. The functional group is chosen as to complement the chemical functionality of the template molecule. Generally, for templates with acidic groups, monomers with basic functionality are preferred, and vice versa, for example, methacrylic acid (MAA) is frequently used for basic templates[48]. For templates carrying carboxylic acid moieties, vinylpyridine has been chosen to be the most suitable monomers. To ensure stronger interactions between the template and the monomers, the functional groups of the monomers used should be complementary to the template functionality. For example, for a template containing carboxylic or sulfonic acid groups, an amine group of a functional monomer is likely to be chosen as it allows formation of a strong ionic interactions with the template[49].

Monomer selection is very important in order to ensure that highly specific cavities designed for the template molecule are produced. Typical functional monomers used for molecular imprinting are carboxylic acids, such as acrylic acid, methacrylic acid and vinyl benzoic acid, and heteroaromatic bases, such as (vinyl pyridine and vinyl imidazole) (Figure 1.3).

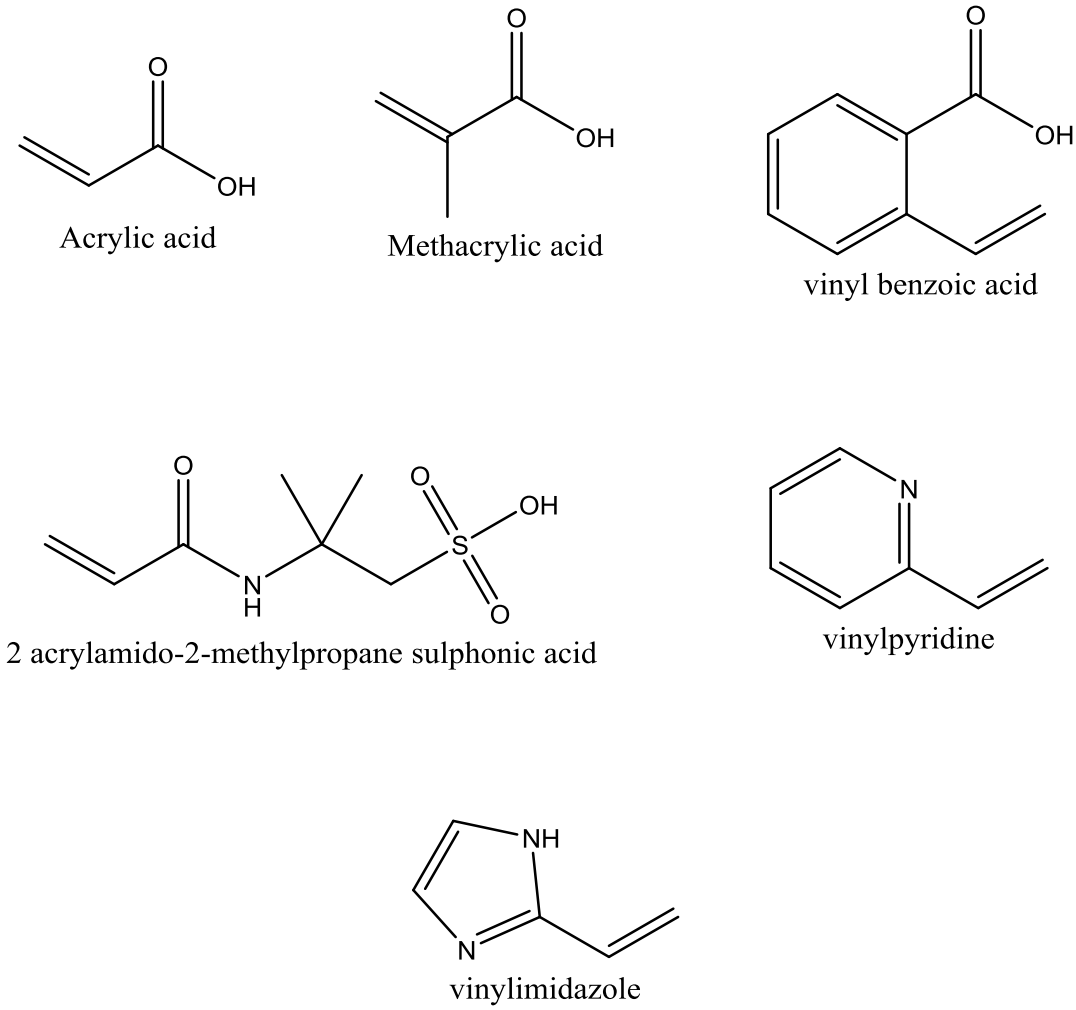

Figure 1.3: Structures of the most common monomers used in molecular imprinting. Adapted from reference [151]

The extensive use of MAA is due to its capability to act as both a hydrogen donor and acceptor. It can ionically interact with an amine group and interact with a variety of polar functional groups such as carboxylic acids, carboxylic esters and carbamates[50] via hydrogen bonding. In addition, it has the ability to be involved in interactions such as ion-ion, ion-dipole and dipole-dipole interactions due to its amphoteric nature, because it can simultaneously act as a Lewis acid and base, and hydrogen donor and acceptor[4]. Stronger acid, 2-(trifluoromethyl)acrylic acid (TFMAA) has been used as a functional monomer for basic templates to achieve superior selectivity and affinity compared to MAA[51,52]. Some functional monomers can form metal coordination complexes with templates such as amino acids and peptides[53]. Urraca *et al*. utilised a functional monomer with multipoint interactions derived from polymerisable amidines and ureas to imprint β-lactam antibiotics[54]. In some cases, a greater degree of recognition was observed with combinations of two or more functional monomers compared to polymers which contained only one functional monomer species[40,51]. There has been a significant increase in the development and application of theoretical and computational strategies to aid in choosing the optimal functional monomer for the synthesis of high affinity biomimetic materials[55-57].

1.4.2 Template

The template carries out a fundamental role in the molecular imprinting processes. The structure of a template determines the type and species of functional monomer to be used in the polymerisation due to the chemical bonds that can be formed between the functional monomer and template, determining the extent of molecular recognition and success of molecular imprinting. Binding strength of the polymer and selective recognition rely on the type of interaction sites, number of interactions, the shape of the template and the rigidity of monomer-template complex[58]. Templates which present multiple binding points for the functional monomers form polymers with high specificity and affinity.

In some cases, the shape and size of the template molecule are sufficient to generate a complementary binding site that is specific to the steric isomer of a molecule, allowing enantiomers to be separated, or separating molecules with protected groups from non-protected molecule[59]. Templates that possess conformational rigidity can adpt into the polymer cavity with greater affinity and selectivity[60]. However, due to the fact that proteins can change their conformation, as well as locations of any charged atoms, protein imprinting can be challenging[61].

Many factors need to be considered when choosing a template molecule. These include solubility of the molecule in the chosen solvent and the electrostatic functionalities of the molecule. Also, consideration needs to be given to whether the molecule is chemically inert and stable under UV light and at elevated temperatures during polymerisation process to be suitable for use in free radical polymerisation[4,62]. Furthermore, the effect of very high monomer to template ratios has been studied and significant imprinting effects has been observed with very low template concentrations[63].

Effect of intermolecular hydrogen bonding in the template on its imprint was assessed by Zhang *et al.*[64]. By comparing the structures of the three templates (4-hydroxybenzoic acid, gentisic acid and salicylic acid), it was noticed that molecular recognition ability is reduced, when the template itself can form intramolecular hydrogen bonds during the molecular imprinting process.

The removal of the template provides a free cavity, which is physically and chemically complementry to the template. Any similarities in the structure of the target species to a structurally similar molecule can influence the selectivity of the polymers. In some cases, it may not be possible to imprint desired template due to high purchase costs or the template being insoluble in the chosen polymerisation solvent, at which point a dummy template can be used to simulate the desired template[65]. In other cases, a dummy template can be used instead of the desired template when the desired target has no functional groups in its structure[66].

1.4.3 Cross-linking Monomers

Cross-linking monomers form a cross-linked network of polymer chains via the use of two or more double bonds forming functional groups. Cormack and Elorza proposed three main roles for the cross-linker:

- ❖ The cross-linker is essential for controlling polymer matrix morphology (gel-type, macroporous or a microgel).
- ❖ The cross-linker helps to stabilise the imprinted binding site.
- ❖ The cross-linker imparts mechanical stability to the polymer matrix.

Ethylene glycol dimethacrylate (EGDMA), trimethylolpropane trimethacrylate (TRIM) and divinylbenzene (DVB) are widely used in research as cross-linking monomers[67].

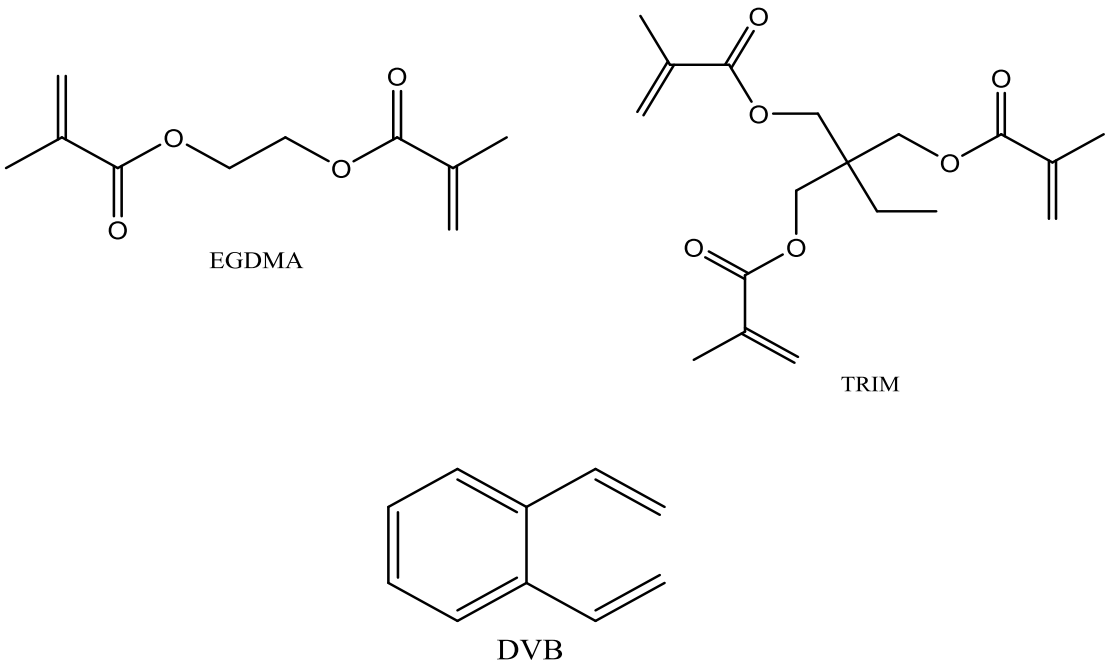

Figure 1.4: Structure of common cross-linkers

Commonly, large amounts of cross-linking monomers are preferred during polymerisation in order to create permanently porous materials whilst maintaining adequate mechanical stability[62]. The main purpose of a cross-linking monomer is to stabilise the binding sites of the polymer. Cross-linking monomers fix the functional monomer-template complex in place via formation of a highly cross-linked rigid polymer network. Variation of cross-linking monomer concentration can have a significant impact on the interaction between the template and nanoparticles, by interfering with molecular interactions, or by enhancing stability of monomer-template complex. In addition, high amounts of cross-linking monomers are commonly required to ensure the accessibility and mechanical strength of the polymer. A large amount of cross-linking monomers (80% of the overall molecules in the polymerisation mixture) needs to be used to protect MIP binding sites[68].

An appropriate degree of cross-linking is important for preserving binding specificity of an imprinted polymer. When the percentage of cross-linking is too low (typically below 20%), binding specificity of imprinted polymer decreases. However, when these levels are too high (above 80%), the loading capacity of the polymers is reduced, and the diffusion of substrates into the imprinted cavities during rebinding may also be obstructed.

During the initial research, the cross-linking monomers used in organic solvent-based molecular imprinting were restricted to monomers with two methacrylate groups. These polymers were commonly prepared using EGDMA as the cross-linking monomer. TRIM, which possesses three methacrylate groups, has been shown to be superior to EGDMA in certain applications, as reported by Kemp and Mosbach[69]. TRIM, as the cross-linker, was used in combination with MAA to imprint a dipeptide. This composition showed a high loading capacity and an improved template resolution. The use of TRIM in the polymerisation mixture yielded materials which possessed improved recognition properties compared to EGDMA[70]. Generally, poly (MAA-co-TRIM) has a higher load capacity than the poly (MAA-co-EGDMA), since TRIM has one more vinyl group than EGDMA and therefore less monomer is required to ensure the same backbone rigidity that contributes to binding specificity[69]. Additionally, TRIM and EGDMA produce polymers with high levels of rigidity, structural order and specificity of binding sites. EGDMA is considered the best cross-linking agent for use in the formation of MIPs. This

is due to the combination of EGDMA being a short and flexible cross-linking monomer and the rigidity and pro-chiral nature of methacrylate group[4].

In a later study, Mosbach *et al*. demonstrated that cross-linking monomer has strong influence over the size and yield of MIP particles produced in precipitation polymerisation[71]. It was confirmed that the use of DVB as the cross-linking monomer, produced low yield polydisperse MIP particles, whereas trimethylolpropane trimethacrylate (TRIM) led to a high yield highly uniform nanoparticles[71]. In recent years researchers have used a combination of TRIM and EGDMA as cross-linking monomers to produce a rigid polymer with a high concentration of binding sites[70].

1.4.4 Solvent

The solvent is an essential part of the polymerisation mixture as it helps to stabilise the formation of the monomer-template complexes. Thus, it is known that electrostatic interactions are stronger in hydrophobic solvents[72]. Polar solvents tend to result in dissociation of the prepolymer complex when used in non-covalent based imprinting, and this is particularly true in the case of protic solvents. Toluene, chloroform, dichloromethane and acetonitrile are the most commonly used solvents for MIPs synthesis. The additional roles of the solvent is to bring all the MIP components into one phase in the polymerisation mixture, and to control the shape and size of pores formed in macroporous polymers[62]. Moreover, the imprinting process and the physical state (morphology, pore structure and swellability) is affected by the choice and amount of the porogenic solvent used in the polymerisation, as described by Sellergren and Shea[73]. In non-covalent imprinting, the porogen needs to be carefully considered to ensure that the solvent supports the formation of the template-monomer complex without impeding the interactions between the functional monomers and template molecule. A study conducted by Sellergren and Shea have shown that there was no obvious connection between selectivity and polymer morphology, but that there was a link between the hydrogen bonding capacity of the porogen and polymer selectivity[73].

Recently highly efficient MIPs were prepared in polar solvent mixtures, such as acetonitrile/water or methanol/water during the investigation of template-monomer interactions in different solvent mixtures. In one such example, a water-compatible molecularly imprinted polymer with a high affinity for 1-methyladenosine (1-MA) has been produced in acetonitrile/water (4:1). The template was dissolved in a solvent mixture with MAA, EGDMA and AIBN as the functional monomer, cross-linker and initiator, respectively. The synthesised MIPs were then successfully utilised as solid phase extraction sorbent for extraction of the target drug from spiked urine samples[74].

In addition, it was noticed experimentally that the template rebinding behaviour was more efficient when performed in the same solvent that was used for imprinting, which suggests that the rebinding requires the use of similar conditions to those used for polymerisation[72]. Thus Yoshizako has prepared MIP imprinted with *o- and p*-xylene. It was confirmed that the optimum rebinding of the template is achieved the same solvent employed in the initial polymerisation process[75]. Generally, selection of an appropriate solvent is essential, and is expected to improve the development of more efficient MIPs.

1.4.5 Initiator

Free radical polymerisation is the most widely used method to produce MIPs. Generally, synthesis is performed under mild reaction conditions with a temperature lower than 80°C, at the atmospheric pressure, either in bulk or solution. This is used for a wide range of functional groups and template molecules. Various chemical initiators with different properties can be used as the initial radical source. Commonly, initiators are used at a low concentration in comparison to the monomers in solution, at around 1% by weight or mol concerning the total moles or weight of monomers in the polymerisation mixture. Heating or light exposure can be used to initiate and control the rate and mode of initiator decomposition. For example, the azo-based initiator azobisisobutyronitrile (AIBN) can undergo decomposition through exposure to UV light or thrombolysis to generate stabilised carbon-centred radicals which are capable of initiating the growth of vinyl polymers[72].

Photo-initiated polymerisation at lower temperatures decreases the kinetic energy of the pre-polymerisation mixture, thus, increasing stability and allowing a greater binding capacity and specificity in comparison to thermally initiated polymerisation, which generally requires temperatures higher than 40°C[25,76,77]. Another example is the use of an iniferter such as *N*,*N'*-diethyldithiocarbamic acid benzyl ester. When exposed to UV light, the iniferter acts as initiator, chain transfer agent and terminator. It has been used to prevent auto-acceleration and allow better control over particle size. In iniferter-controlled polymerisation reaction there is a fast termination process which occurs immediately when the UV light is switched off[78]. Overall, iniferter-controlled photo-initiated polymerisation produces greater recognition properties in the final MIPs in comparison to thermally initiated polymerisation[79,80]. Furthermore, the use of an iniferter in the polymer enables the grafting of additional layers around the polymer core[81].

However, when a high concentration of initiator is used, it can affect the polymerisation process and can interfere with the template-functional monomer interactions[82]. Furthermore, oxygen can interfere with free radical polymerisations, and therefore, free oxygen needs to be removed from the polymerisation mixture, as oxygen is present in the air and dissolve in the solvent. This can be achieved by purging the monomer solution with nitrogen gas[72].

1.5 Molecular Modelling

A selection of suitable functional monomers is essential for the preparation of a molecularly imprinted polymer. Nowadays, computational modelling has become a routine technique in the design and planning of the production of MIPs. This allows the appropriate functional monomers, cross-linker(s) and solvent to be identified, with the optimal ratio of functional monomer and template to generate the greatest selectivity[83].

Consequently, a large amount of efforts have been directed towards the development of monomer screening protocols in which the strongest binding functional monomer can be identified and used in the imprinting of a specific target. In 2001, Piletsky and co-workers developed the first successful approach for screening functional monomers for a chosen template based on molecular mechanics (MM) and molecular dynamics (MD)

simulation[84]. The process involved creating and utilising a virtual monomer library containing 20 potential functional monomers which were screened against one of the enantiomers of ephedrine[84]. Depending on the binding scores, functional monomers were selected and the corresponding MIPs were fabricated and evaluated by the HPLC technique proving efficiency of computaitonal approach.

In 2017, Karim *et al*. published a paper in which they described a protocol for the computational design of high affinity molecularly imprinted polymer[55]. The protocol involved the design and synthesis of high affinity MIPs in any format such as micro- and nanoparticles, films or monoliths). This protocol is particularly suitable for use with low molar mass templates and where the development of high affinity MIPs is required.

Chianella at al. employed computational modelling to rank potential functional monomer molecules[85]. The monomers showing the highest binding energy were chosen and tested using a simulated annealing process to investigate their interaction with the template - Microcystin-LR. The results of modelling were validated by analysing the binding of MIP. The selected monomers were copolymerised with ethylene glycol dimethacrylate (EGDMA) as the cross-linking monomer in the presence of the template molecule[85]. The affinity of the computationally designed MIP was three times greater than the MIPs made from the standard methacrylic acid-co-EGDMA polymer.

Based on the work by the Piletsky research group, similar strategies that utilised a virtual library of functional monomers were developed by Wei *et al*.[86]. To prepare a templated MIP for 17β-estradiol (BE_2), a virtual library of monomers was screened against the chosen template to identify the ideal functional monomers: methacrylic acid, methacrylamide and 2-(diethylamino)ethyl methacrylate. The results obtained from actual rebinding experiments confirmed the predicted computational results.

Silva and co-workers used a computational approach to identify the best monomer for dinotefuran (DNF)[87]. A theoretical study was performed using density functional theory (DFT) to calculate the binding energy between template and monomer to determine a suitable monomer-template ratio. Using a similar method, a novel MIP for vanillin was prepared via photo-initiated polymerisation using dichloromethane as a solvent. From the results of a density functional theory computational method, acrylamide was chosen as the functional monomer, with both semi-covalent and non-covalent imprinting strategies

carried out to prepare the MIPs. It was shown by the DFT calculations that the specific binding of vanillin in the cavities was due to non-covalent interactions between the vanillin and the hydroxyphenyl- and amide-moieties. The produced MIP showed high selectivity for vanillin and was successfully used to extract vanillin from vanilla pods and red wine spiked with vanillin[88].

Recently, Bates *et al*. expanded the virtual library of functional monomers to include a range of acidic, basic and neutral functional monomers as well as charged structures of the monomer[89]. The virtual library included cross-linking monomers such as *m- and p*-DVB, mono-, di-, tri and tetra-EGDMA and TRIM. A combination of frequently used solvents such as dimethylformamide, acetonitrile, chloroform, ethanol, methanol, acetone, DMSO and water with known melamine solubility were modelled. Divinylbenzene and itaconic acid were chosen as the cross-linking and functional monomers respectively. The design of the molecularly imprinted polymer for melamine was achieved using a combination of computational techniques and laboratory testing. The prepared polymer was used in high-performance liquid chromatography (HPLC) for the rapid detection of melamine in spiked milk samples[89]. This approach demonstrated the potential of virtual tools in accelerating the design of MIPs for practical applications. The selectivity of the MIPs toward melamine has been characterised for several structural analogues in the range of 1–100 μM concentrations.

In the recent literature, there are numerous examples where researchers have investigated the strength of monomer-template interactions through the use of molecular mechanics (MM)[90-93], molecular dynamics (MD)[94-96] and quantum mechanical (QM)[97,98] based molecular modelling techniques. The use of a virtual library of functional monomers is an essential step in reducing the overall time and cost of MIP synthesis. Indeed, it could be argued that the most significant development in molecularly imprinted polymer science and nanotechnology during recent years has been increasingly driven by the use of computational techniques, as reflected in the significant increase in the number of studies employing computational approaches. Consequently, computational techniques will enhance the quality of binding sites and have a significant impact on the evolution of new applications of MIPs[99]. Additonally selection of the optimum composition of the MIP components could improve the function and the morphology of the subsequent MIP.

1.6 Molecularly Imprinted Polymer Nanoparticles and Microbeads - Polymerisation Methods

Conventional MIPs were initially prepared as bulk monoliths. This process leads to the synthesis of particles with irregular shapes and sizes, furthermore, the procedure is time-consuming as the MIPs need to be ground down to produce nanoparticles of the desired particulate size, which leads to low yields[100]. This also reduces the capacity site accessibility for the template as a result of the grinding process. Incomplete elution of polymers formed using bulk polymerisation is a common result due to highly crossed-linked nature of the polymer[101]. This incomplete removal of the template can lead to significant issues with the template rebinding process.

To overcome these shortcomings, efforts have been made to synthesise MIPs as nanoparticles which possess regular shapes and sizes. MIP NPs possess improved homogeneity of binding sites and can facilitate quantitative template removal.

Nanocomposite materials can be tailored to include additional functionality such as magnetic properties, electroactive mediation and semi-conductive cores[102, 103]. The most commonly used methods to prepare MIP NPs include precipitation polymerisation, emulsion polymerisation and solid phase polymerisation.

1.6.1 Precipitation Polymerisation

Precipitation polymerisation is a straightforward and low-cost method of synthesising polymer particles with high yield and purity. This synthetic approach was first used in 1999 to obtain MIP NPs with high selectivity and load capacity[104]. Precipitation polymerisation is achieved by cross-linking multiple polymer chains in diluted monomer solutions containing template species. The polymer is not soluble in this continuous phase when it grows beyond a critical molecular mass. Polymerisation under these conditions produces spherical-shaped MIPs which are a few micrometres in diameter[104,105]. Wulff *et al*. reported a post-dilution polymerisation which was intended to enhance selectivity and increase the reusability of the template. It required the dilution of the pre-polymerised polymer after the initial polymerisation to prevent the aggregation and continued

polymerisation of the diluted mixture to obtain the required nanogels[106,107]. The size of the particles produced can be affected by the following parameters:

- The ratio between cross-linkers and functional monomer: this can be used to tune the morphology of the imprinted NPs[71].
- The type and amount of template molecule: for example, adding smaller amounts of template can result in a homogeneous particle size distribution[108].
- Solvent: different solvents and their combinations affect the surface area of the NP due to their changing porosity[32]. Thus, adding small amounts of aqueous ammonia instead of water in the case of inorganic MIP NPs leads to an approximate four-fold decrease in particle size[109].

Precipitation polymerisation is a direct approach which can be applied for most template molecules. Compared to particles synthesised by grinding bulk monoliths, precipitated particles have a uniform size distribution and can be obtained in higher yield, making them ideal for standard industrial manufacturing[110,111]. Also, surfactants are not necessary for producing MIPs when using precipitation polymerisation[102]. However, the highly diluted monomer solution is one of the main issues with precipitated MIP NPs compared to imprinted monoliths. It can have negative affect on the interaction between the functional monomer and the template, causing a decrease in polymer affinity and selectivity[112]. This issue, however, is compensated by the significantly higher surface-to-volume ratio of nanoparticles compared to the bulk polymers. In sensor applications, MIP nanoparticles were determined to be more sensitive than the respective thin films[109,113]. A further advantage of precipitation polymerisation compared to other MIP syntheses approaches, such as emulsion polymerisation, is the lower consumption of reagents during the polymerisation process. However, a considerable amount of solvents is required, and the parameters of the polymerisation need to be optimised for each template molecule and copolymer monomer individually[114].

1.6.2 Emulsion Polymerisation

Emulsion polymerisation emulsifies cross-linking monomers, functional monomers and template molecules in an aqueous surfactant phase via sonication. The addition of a co-stabiliser such as sodium dodecyl sulphate (SDS) aids the dispersion of the separate phases into the semi-continuous phase. This process, called mini-emulsion polymerisation results in stable emulsions possessing homogeneous droplet sizes[115]. Emulsion polymerisation also requires the use of liquid polymers or polymer solutions as a disperse phase. Mini-emulsion polymerisation further applies stabilisers to generate particles in the dispersed phase with sizes between 50-1000 nm, where the process takes place in a dispersion made of water, oil and surfactant[105]. As an example, Lysozyme MIP NPs with 50 nm diameter were prepared by using mini-emulsion polymerisation. This was achived by producing two aqueous phases containing SDS as a surfactant and stabiliser, cross-linking monomer and additional additives, mixed stepwise with the organic phase containing the cross-linking monomer and functional monomer, with the template being added to the initial emulsion. The resulted MIP nanoparticles only have binding sites on the surface of the nanoparticles surrounding a stable core created by the copolymerisation of the cross-linking monomer and surfactant. MIP NPs show a high adsorption capacity for the purification of lysozyme in the presence of different analogues (BSA and cytochrome)[116]. However, using SDS in the polymerisation reduces the application of MIP NPs in biological fields due to its toxicity towards cells and the considerable difficulty encountered in removing it from the nanoparticles[102].

To overcome this issue, surfactant-free emulsion polymerisation has been recently tested using a continuous phase stabilised with a poly(vinyl alcohol). Initially, the template was pre-complexed with the functional monomer in the organic phase. The two phases were combined and sonicated before the initiating the polymerisation process via addition of potassium persulphate to the solution. The size of the resultant MIP particles was 200 nm in diameter[117].

In summary, emulsion polymerisation is an excellent technique for the synthesis of MIP NPs sizes down to nanometre range. Furthermore, the resulting MIP NPs exhibit imprinted surfaces with greater homogeneity and accessibility of binding sites compared to ground and sieved monoliths. However, in terms of commercial applications, the procedure requires too many synthetic steps to be commercially viable[118,119].

Furthermore, the main drawback with emulsion polymerisation in comparison to precipitation polymerisation is that it requires a greater amount of chemicals to be used, including surfactants, buffer components and stabilisers, which need to be removed after the MIP nanoparticle synthesis, requiring sophisticated washing procedures. This can reduce the yield and affinity of micro and nanoparticles.

1.6.3 Membrane Template Synthesis Approach

In order to carry out *in-situ* polymerisation, porous support membranes are required to form surface-imprinted MIP NPs in their pores. By changing the viscosity of the polymerisation solvent, particles with nanometres diameter can be synthesised. Such MIP NPs can be embedded in the support material and used for membrane separation[120]. Nano and microstructured materials, such as polycarbonate or alumina membranes, can be used as a sacrificial mould to synthesise different shaped MIPs, such as microrods and nanowires[121,122]. The use of supporting materials enables the formation of well-defined MIPs which exhibit high surface areas. However, only a few nanosized MIPs based on template synthesis in membranes have been successfully validated to date[122,123].

In 2000, Yılmaz *et al*. presented "the use of immobilised template" as a new approach. Immobilisation of the template was achieved through the formation of amide bonds by EDC/NHS chemistry[124]. This approach includes use of a silica based solid support to which the template is immobilised. It provides numerous advantages to these systems. For the insoluble templates in the polymerisation mixture, this approach might be used as a good alternative. The aggregation of template in pre-polymerisation mixtures which might be seen in some cases can be prevented by this method. Comparing to classical MIPs, where a solvent capable of creating pores is important to yield a macroporous structure, no porogen was used for the imprinting of the immobilised template molecule in this approach. The pore structure of the prepared polymers was generated by dissolving the silica gel backbone. Because of this, all imprinted sites were found at or close to the

surface of the pores which is the main advantage in facilitating the diffusion of the analyte to the binding sites[125].

1.6.4 Iniferter Polymerisation

The most useful synthetic approach to obtain organic imprinted polymers is via free radical polymerisation. Free radical polymerisation can be achieved under mild reaction conditions such as room temperature and atmospheric pressure, and the process can be carried out in bulk or in solution with a wide range of low cost commercially available functional monomers. Since this technique is simple and inexpensive, it represents an ideal choice for the synthesis of molecularly imprinted polymers[126]. However, it is difficult to control the dimensional characteristics of MIP particles in terms of chain length and distribution of the cross-linking monomer during the free radical polymerisation, which is caused by side processes from the chain transfer and termination reactions.

To overcome this limitation, a new type of polymerisation utilises a new kind of initiator known as an iniferters, which are so-named as they act as the initiator, transfer agent and terminator. In this kind of polymerisation, iniferters can reversibly decompose to a pair of free radicals, one of which is the active propagating species, while the second less reactive species act as a transfer agent and terminates formation of the polymer chains in solution, generating a new initiating species in the process. This leads to better control over the polymerisation process, as well as the possibility of reinitiating the polymerisation process simply by applying an energy source, which is usually a UV light source[127]. Recently, diethyldithiocarbamic acid benzyl ester, diethylthiocarbamoylsulfanyl acetic acid and sodium diethyldithiocarbamate trihydrate have seen widespread use in MIP and core-shell MIP processes[67,128-131].

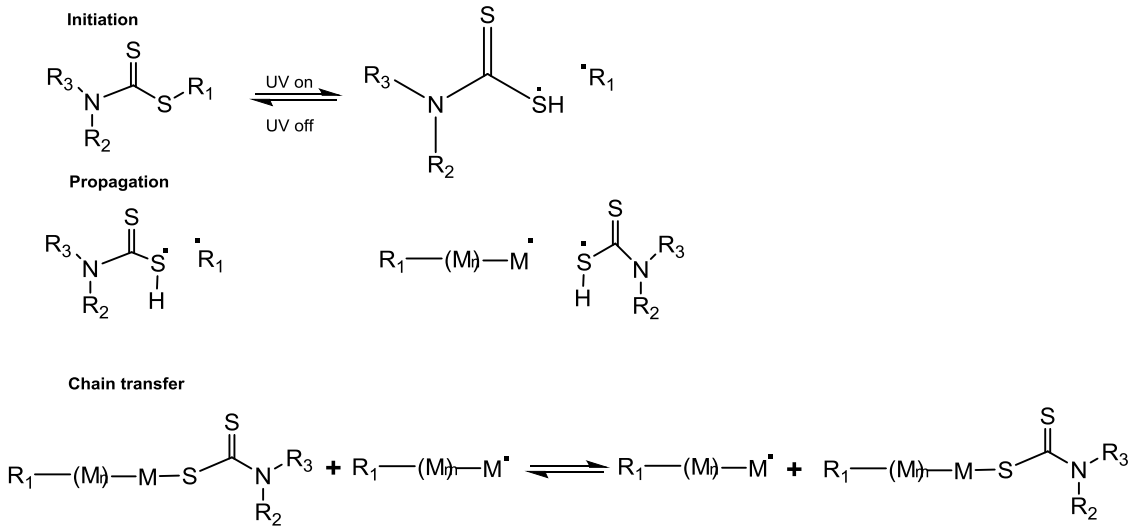

Figure 1.4: Scheme of a general iniferter polymerisation mechanism

As an example of iniferter polymerisation, a simple approach for the controlled coating of gold microelectrodes with thin film of MIPs was presented by García-Mutio and co-workers[131]. The iniferter contains a terminal thiol group capable of forming self-assembled monolayers on gold substrates via activation under UV light after the immersion of a microelectrode in a polymerisation mixture containing 4-ethylphenol (4EP), 4-vinylpyridine (4-VPD) and EGDMA as the template, functional monomer and cross-linker respectively. The voltammetric behaviour of the MIP-coated microsensor was evaluated. The linearity range of the sensor was 1 x 10^{-6}-1 x 10^{-3} M. The sensor has remarkable selectivity toward the template with no interference detected from the template analogues.

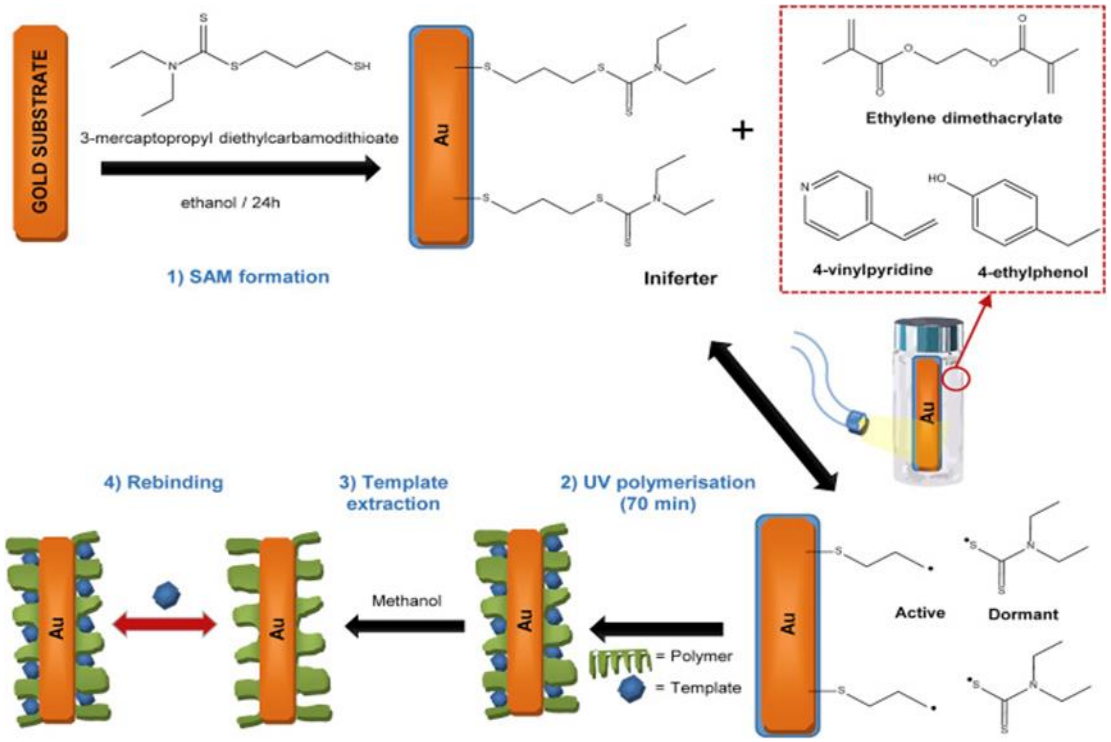

Figure 1.5: Schematic illustration of the free radical polymerisation procedure used to develop the MIP sensor. Adapted from reference [126] with permission

1.6.5 Solid Phase Molecularly Imprinted Polymer Nanoparticles (MIP NPs)

MIPs prepared via traditional synthetic methods with the free template in solution have limited binding site access and suffer from complications when removing the bound template, which is due to the presence of residual template molecules and the fact that the production methods are challenging to standardise[128]. Furthermore, interaction sites are not only present on the surface of the respective sensor material but they are also distributed within the whole bulk of the matrix. Bulk imprinting fails to produce suitable recognition sites and the resulting materials could be too thick for most sensor applications[132].

To overcome these limitations and combine the advantages of the iniferter polymerisation, Poma *et al*. established a new method for the synthesis of MIP NPs using an innovative solid-phase approach. In this method, the template is covalently immobilised onto the surface of a solid support phase such as glass beads[19]. The MIP NPs obtained form on the solid phase are free of the template and exhibit high affinities for their template molecules. Low affinity MIPs and incomplete polymers are removed through the use of an affinity separation technique performed on the solid phase after completion of the polymerisation step. The MIPs produced by this method have more uniform binding characteristics and while the particle size have been controlled by the iniferter[128].

In solid-phase molecular imprinting, the template is covalently immobilised on the surface of glass beads with an average diameter of 65-90 μm[133]. The solid phase bearing the immobilised template is placed in the monomer mixture and the polymerisation initiated under conditions that promote formation of polymer nanoparticles. This polymerisation methods requires only short polymerisation time and a high dilution of monomers in solution as opposed to macrogels or monoliths. After the polymerisation process is completed, the solid support acts as an affinity medium to separate the high-affinity MIP NPs from the unreacted monomers, oligomers and low-affinity polymers. These are eluted by washing the beads under conditions where the high affinity nanoparticles remain attached (Figure 1.6)[128].

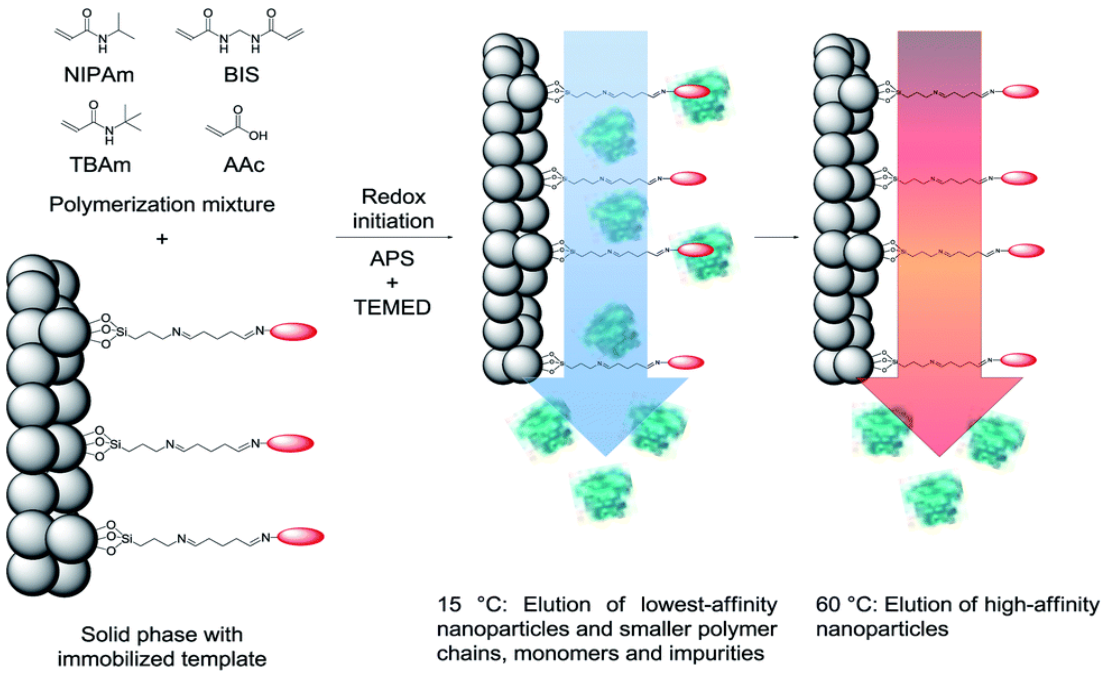

Figure 1.6: Schematic representation of the solid-phase synthesis process, washing step and purification and collection of high-affinity MIP NPs exploiting the different interaction strengths at different temperatures. Adapted from reference [16] with permission

As described earlier, Poma *et al*. created an automated system to produce robust MIP NPs in only 2–3 hours including the synthesis and affinity purification[16] (Figure 1.7). As a result of the affinity purification step, the MIP NPs have a high affinity and specificity toward their target molecules allowing them to exhibit a homogeneous distribution of binding sites in similar manner to monoclonal antibodies[133]. The MIP NPs obtained are free from templates, while traditional MIP production approaches require up to three days of dialysis to remove the template. The method is generic and can be applied for water-based (persulfate-initiated polymerisation) and organic solvents-based (a UV-triggered process) polymerisations[134].

Water polymerisation (chemical initiated polymerisation) has been used to produce MIP NPs imprinted with peptides and proteins, while the organic polymerisation (light initiated polymerisation) has proven to be more suitable for the imprinting of small molecules with a molecular weight less than 500 Da[19,130,135-137]. In particular, as an example, Chianella *et al*. demonstrated that these materials could be used as a direct replacement for natural antibodies in bioanalytical and diagnostic assays[130]. Canfarotta *et al*. have utilised both synthetic protocols to produce MIP NPs that are useful in a broad range of applications[128]. The solid-phase imprinting process can be scaled up or down by changing the amount of solid phase used during polymerisation while keeping the ratio of polymerisation mixture to glass beads constant[128]. However, when scaling up the UV-initiated synthesis of MIP NPs, the thickness of the solid-phase layer inside the polymerisation vessel and density of monomer mixture should be relatively low otherwise the UV penetration into the interior of the solid phase will be inefficient and will adversely affect the yield of MIP NPs[128].

MIP NPs have a higher surface-to-volume ratio and larger surface area per unit weight of polymer compared to bulk polymerisation and this allows the template to have better accessibility to the binding sites of the nanoparticles, reducing the amount of template required. Furthermore, it possible to obtain template-free polymer avoiding the time-consuming methods otherwise required for template extraction from the polymer[138, 139]. As an example, a solid phase approach[19], has recently been used for potentiometric sensing using PVC membranes[134,137], voltammetric sensing[140], electrochemical sensors and SPR sensors[141]. Moreover, this approach allows the production of fluorescent and electroactive nanoparticles, as shown by Ambrosini *et al*. who used it to prepare specific protein-imprinted polymer[133]. In this method is that the binding sites have the same orientation and are located at the surface of the particle assuring binding site homogeneity and accessibility, especially for bulky protein[133]. Additionally, depending on the stability under the reaction conditions, the protein may be able to be re-used[133]. In lihgt of these advantages, the solid-phase approach has been used in this work.

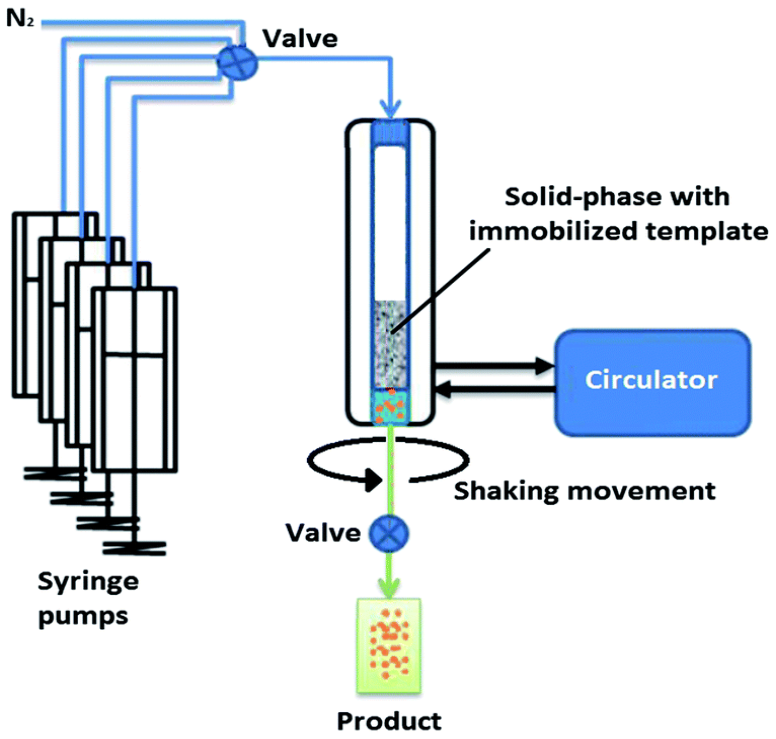

Figure 1.7: Schematic of the automatic reactor used for the synthesis of MIP NPs based on solid- phase approach. Adapted from reference [16] with permission

1.7 Applications and Limitations of Solid -phase MIPs

Molecularly imprinted polymers produced by the solid-phase imprinting approach can be applied in sensors and assays due to their excellent recognition properties[135,141-143]. For example, MIP NPs templated for vancomycin have been successfully used as a direct replacement for antibodies in enzyme-linked immunosorbent assay (ELISA)[130]. The MIP NPs were used in a competitive binding assay in combination with a conjugate of horseradish peroxidase and vancomycin. The MIP assay was capable of detecting the target molecule in a clinical sample (plasma) in a concentration range of 0.001–70 nM. MIP NPs have also been used as the recognition elements in potentiometric sensors[134]. MIP NPs prepared by the solid-phase approach have been combined with PVC membranes for the detection of cocaine, where it was demonstrated that the sensor was able to detect nanomolar concentrations of cocaine in blood serum samples[134].

However, the solid-phase method described suffers from a low polymer yield in comparison with traditional methods. This is primarily due to low-affinity MIP NPs and polymer chunks being removed during washing steps at low temperatures. Even though the total amount of polymer produced is lower, most of the nanoparticles produced have high-affinity binding sites, unlike bulk polymer, which produce a high yield of nanoparticles with non-specific binding. Yield can be increased by running multiple subsequent syntheses on the same solid phase, although the reusability dependes on the template used[19, 128]. However, in the case of protein templates, the solid phase cannot be reused due to the protein being denatured during the hot wash. In addition, lower temperatures (~40 °C) or other elution conditions such as pH or ionic strength variations can be used. Nevertheless, the alternative solutions could decrease the yield of the high affinity nanoparticles.

The second limitation of the solid-phase approach is related to the template molecule. The solid-phase approach requires the template to have a functional group which can be used for immobilisation on the glass beads such as COOH, NH_2 and SH. However, if the template has no functional groups available, analogue or dummy template can be used as alternative for the immobilisation process[134]. Moreover, a template analogue can also be used if the target molecule is toxic or expensive[128].

Furthermore, polymerisation time, duration of UV irradiation and the power of the radiation should be carefully considered to maintain the particle size within the nanometre range[128]. However, the automatic solid phase synthesiser was designed to overcome the problems with poor reproducibility of different batches and as well as to maintain the power of the radiation.

1.8 Molecularly Imprinted Polymer for Sensor Application

Sensors are analytical devices containing a sensing element that recognises a specific analyte molecule in a complex environment, producing an output signal. The use of MIPs in sensor applications is beneficial as MIP NPs exhibit high mechanical and thermal stabilities.

There are three main types of sensors, namely catalytic (not reviewed here), affinity and receptor sensors[144]. The detection process in affinity sensor strategies is based on the concentration of template bound to the MIP, which is immobilised on the sensor surface. Receptor sensors strategies are based on the ability of the MIP to change conformation upon binding with the template, leading to a change in a determinate property, such as conductivity, permeability or surface potential (Figure 1.9)[145]. Furthermore, sensors can be formed which relies on the ability of the functional monomer to change its property upon interaction with the template species such as an environment-sensitive florescence sensor[146].

The advantages of MIPs in sensor applications include their high binding capacities, specificities and high affinities for their target molecules, which makes them promising alternatives to antibodies and natural receptors. However, there are limitations to the development of MIP sensors including (i) the absence of a general protocol for MIP preparation (ii) integrating the polymer with the transducer is crucial and (iii) the difficulty in converting the binding event into an electrical signal in solution[144]. Moreover, the fabrication of selective sensors requires a recognition element that is in close contact with a transducer surface. The recognition element should bind selectively with the template or a class of molecules found within a complex matrix. The transducer then translates the analyte binding signal, as caused by a change in: mass, electrical energy, thermal energy or capacitance into a quantifiable output signal proportional to the template concentration.

To address this, MIPs can be fabricated directly in situ on the surface of transducer to act as a molecular recognition layer for template detection. The main problem associated with *in situ*-fabrication is that, there is a degree of inaccessibility of a large fraction of the template binding sites due to the layers' density. With *ex situ*-prepared MIP-based

sensors, this issue can be avoided because these MIPs can be synthesised as nanoparticles with a large surface-to-volume ratio[147].

Additionally, in the case of MIP NPs having one or more functional groups, the self-assembled monolayer (SAM) mechanism offers simple route to functionalise electrode surfaces using organic molecules containing free anchor groups such as thiols, disulphides, amines and acid (Figure 1.8)[148]. The main advantages of SAM-based biosensors is that their stability coupled with the behaviour of electroactive SAMs in terms of selective electron tunnelling, makes them beneficial as suitable substrates for monitoring biomolecular interactions[148].

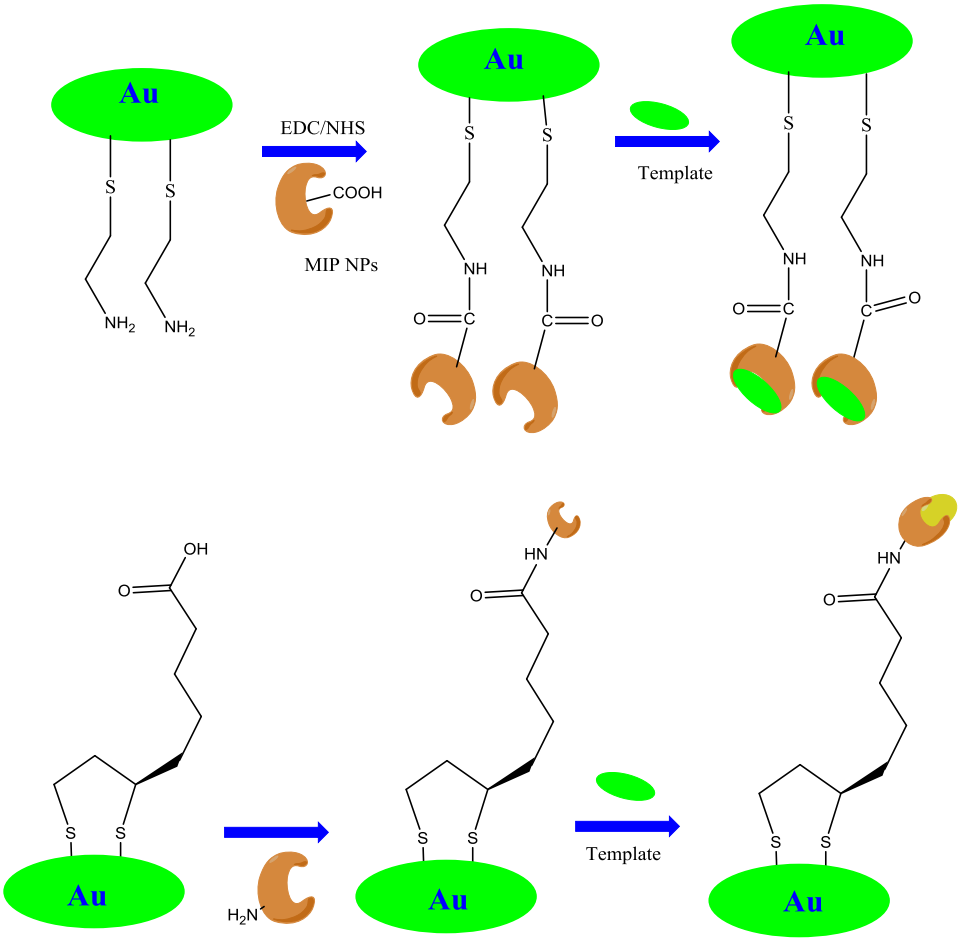

Figure 1.8: Schematic representation of a self-assembled monolayer (SAM)

In addition, a composite conductive MIP system can be prepared by depositing the MIP onto the electrode, by electropolymerisation of monomers, or loading the conductive material into the pre-produced MIPs. MIP functionalisation can be obtained before or during the preparation of the composite system. The mainstream approach consists of immobilisation of the MIP NPs close to the electrode surface with a high degree of control over the molecular architecture of the recognition interface[149]. Moreover, the sensitivity of the technique relies on the affinity properties of the receptor and the sensitivity of the physical transducer.

The solid-phase imprinting approach revolutionised the production of MIP NPs. This approach allows for automation and large-scale fabrication of MIP NPs, significantly contributing to the improved reproducibility and efficiency of MIP NP synthesis[16, 150]. Similarly, the combination of nanomaterials and printing technologies could transform the mass production of MIP-based sensors and allow for real-time and online medical monitoring.

Furthermore, the detection limit of MIPs can be further enhanced by particle engineering. The incorporation of metals[151], graphene[152] and carbon nanotubes[153] redox mediators[154] into a MIP can improve the performances of the final systems in terms of their sensitivities. Developments in polymer science and nanotechnology have contributed to the enhancement and performance of MIP based sensors. Encouragingly we have seen an increase in the literature describing the use of MIP-based sensors for the detection and quantification of biomolecules, drugs of abuse, toxins, explosive compounds and food samples[134,155-159].

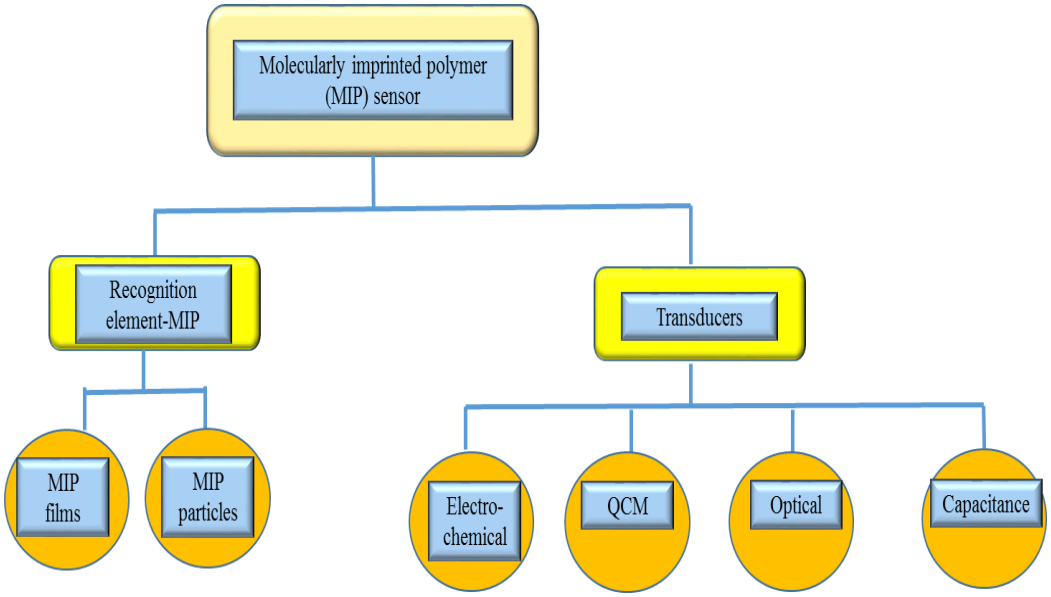

Figure 1.9: Schematic representation of MIP-based sensor

1.8.1 Gravimetric and Electrochemical Sensors Based on MIPs

The selection of a transduction device principally depends on the nature and physicochemical properties of the sensitive layer material that changes when exposed to the analyte. Since the addition of a labelling agent sometimes result in a certain complexity of the receptor's binding mechanism and thus might also affect its sensitivity, the development of a label-free sensor, such as gravimetric sensor and electrochemical sensors, is required[160].

The initial attempts to use bulk imprinted polymers in sensor applications were made in 1992 by Piletsky and co-workers[161]. It was shown that templates such as amino acids, nucleic acids and cholesterol increase the current passing through a membrane made of imprinted polymers[145]. The prime function of MIPs exploited in sensors is that of selective binding to a target analyte. A sensor registers the binding of the target analyte to the MIP as a change in mass (QCM and SAW), or impedance (in electrochemical sensors). There are also numerous examples of sensors which rely on MIPs capable of generating an electrochemical signal in response to template binding to the functional groups in an imprinting site, such as in potentiometry and voltammetry.

Generally, electrochemical sensors have continued to be the most popular type in use, mainly due to their simplicity and ease of production and the low cost of the associated devices and instrumentation[154]. In addition, they are suitable for a wide range of analytes. Moreover, there is evidence of significant improvement in sensitivity of the analysis with the detection of target analyte reaching nano and picomolar levels of concentrations. To enhance sensitivity, MIP NPs materials can be tailored to include additional functionality such as magnetic, electroactive mediator and semi-conductive cores. Moreover, the combination of MIPs recognition phases and flow injection systems offers the possibility of reusing the same polymeric material for multiple measurements without loss of sensitivity and the possibility of real-time monitoring[50]. Nowadays, the trend is shifting towards the development of real-life applications where the analyte is measured in clinical samples, rather than modelled samples.

1.8.1.1 Gravimetric Sensor

The quartz crystal microbalance (QCM) also known as the quartz crystal resonator (QCR) is a technique based on the detection of small mass changes on the sensor surface. An increase in mass on the crystal surface is associated with a binding reaction and causes an associated decrease in the fundamental frequency of the crystal. QCM sensors are useful monitoring tools because of their sensitivity, high accuracy, stability, straightforward operation and reproducibility. QCM techniques can be used to convert the recognition process achieved using MIP-based interactions into a sensor signal. Therefore, the integration of the QCM technique and MIPs as synthetic receptors enhances sensitivity through the immobilisation of MIPs on the crystal surface[162]. QCM offers one of the most promising sensor technologies based on its low cost, rapid response, portability, operational safety, and as label-free, real-time procedure and which is ideal for the sensitive online detection of analytes.

The technique is valuable for analysis of both gas and liquid samples, although liquid measurements need to account for other simultaneous changes caused by solvent viscosity and temperature. The sensors operate through a surface coated with MIPs and offer real-time measurements. The QCM consists of a thin piezoelectric quartz crystal

sandwiched between couples of metal electrodes. Under an applied electric field, a stress force is created that causes the crystal to vibrate at its natural resonant frequency. When the target molecule adsorbs onto the MIP surface, it causes increase in the mass of the crystal, which leads to a change in its resonant frequency as shown by the following equation:

$$\Delta f = - C\Delta m$$

Where C is the mass sensitivity constant (ng cm^{-2} Hz^{-1}), Δm is the increase in mass, and Δf is the change in the resonant frequency. The microbalance uses an oscillation circuit with either a frequency counter or a network analyser to detect the frequency change, and an intermediate layer is often used to increase the adhesion of the MIP and to change the baseline frequency by increasing mass (Figure 1.10). With this method sensitivity of 1 ng cm^{-2} can be achieved[163].

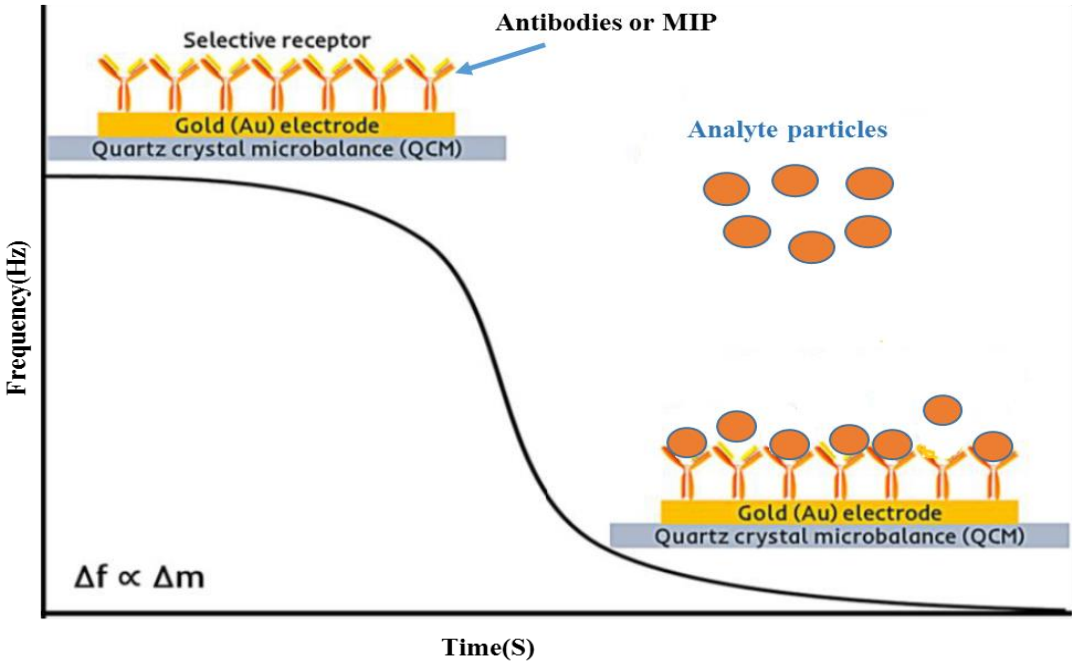

Figure 1.10: The principle of a QCM sensor. The receptor-analyte binding can be detected as a change in frequency

Gravimetric MIP sensors are the simplest and most straightforward types of sensors which allow template detection by measuring the weight of molecules re-adsorbed by the immobilised MIPs. Gravimetric sensors such as piezoelectric devices have advantages such as: a) relative simplicity of the sensor design; b) easy interpretation of the sensor response; and c) compatibility with a variety of solvents and a variety of templates.

Seifner *et al*. reported a QCM-based sensor utilising MIPs imprinted with erythrocytes and formed via UV polymerisation of 1-vinyl-2-pyrrolidone as the functional monomer and N,N-methylenebis(acrylamide) as the cross-linker. The prepared MIP-based QCM sensor showed high affinity and selectivity toward erythrocytes[164]. It can be used to distinguish the subgroups A1 and A2 from another with selectivity factors of two to three. These results can be explicated by the different antigenic patterns on the two erythrocyte surface types having been transferred to the polymer.

Ayankojo *et al*. prepared a molecularly imprinted poly(meta-phenylenediamine) film to recognise amoxicillin[165]. Amoxicillin (AMO) MIPS-COATED thin films were generated electrochemically from meta-phenylenediamine (M-PD) directly onto the QCM transducer. Computational modelling and spectroscopic studies were used to confirm the formation of a complex between the template (AM) and the monomer molecules (M-PD) prior to the polymerisation process. The electrodeposition process was studied to allow for the selection of the ideal parameters for stable AM-MIP film deposition to occur and to achieve the desired nanomolar detection limit.

A surface acoustic wave (SAW) sensor functionalised with a polypyrrole molecularly imprinted polymer was created for the selective detection of dopamine (DA)[166]. To achive high sensitivity and selectivity in the sensor, the pyrrole/DA ratio, polymerisation and immersion times were optimised. Before and after extraction of DA, the morphology and related roughness parameters of molecularly imprinted polymer surfaces were characterised via atomic force microscopy (AFM). The chemosensor selectively recognised DA without the cross-activity of 4-hydroxyphenethylamine and ascorbic acid being detected, having a LOD of 1×10^{-10} M.

Ayankojo and co-researchers have developed a label-free SAW sensor for the detection of sulfamethizole (SMZ)[167]. Selective recognition was ensured by a homogeneous thin film on the sensing surfaces of the SAW chip created by oxidative electropolymerisation of m-phenylenediamine in the presence of the template. The functional monomer was chosen using a computational approach. Furthermore, the sensor was used to detect SMZ in the presence of structurally similar molecules such as sulfanilamide and sulfadimethoxine. The SAW sensor based MIP had a LOD of 11 x 10^{-10} M.

1.8.1.2 Electrochemical Sensor

An electrochemical sensor is a device that translates the interaction of an analyte with a receptor on the surface of an electrode into a useful analytical signal[168]. Electrochemical sensors employ different electroanalytical techniques: voltammetry, when current is measured as the potential difference is varied, amperometry; when current is measured at a fixed voltage, and potentiometry; when voltage is measured at zero current, conductivity, and capacitance or impedance changes. These sensing techniques were designed for analysis of liquid-based samples. Typically, an electrochemical cell contains three electrodes: the working electrode which contains the MIPs, and the counter and the reference electrodes. Voltammetric methods include cyclic voltammetry (CV), linear sweep voltammetry (LSV), square wave voltammetry (SWV) and differential pulse voltammetry (DPV) which is used in this work to create electrochemical sensor based MIP.

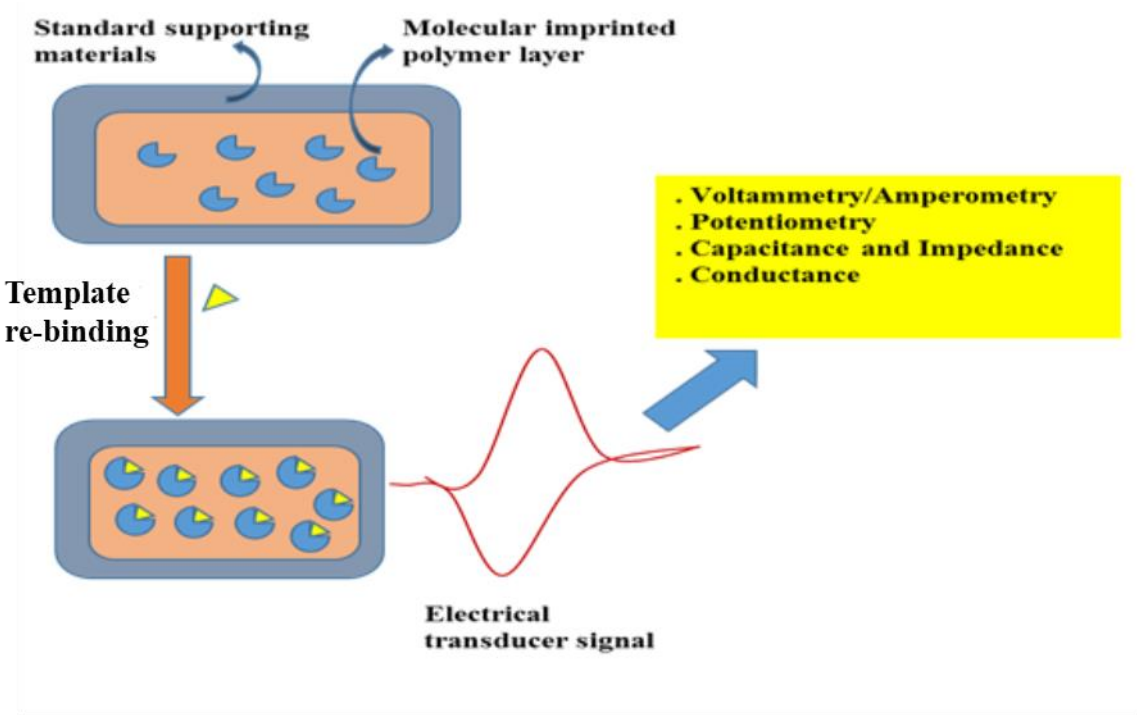

Figure 1.11: Basic mechanisms of electrochemical MIP-based biomimetic sensors

As an example for electrochemical sensor-based on MIPs, one of the modern trends in the development of electrochemical sensor-based MIPs is the use of micro- or nanoparticles and nanostructured coatings. Bates and Del Valle presented a sol-gel-based method for immobilisation of unmodified MIP particles for use in an electrochemical sensor. Differential pulse voltammetry (DPV) technique was used to detect micromolar concentration of theophylline[169]. The enhancement in sensor signal was achieved by integrating sol-gel MIPs with multi-walled carbon nanotubes (MWCNTs). As an example of the latter, a new sensor was fabricated using the micro-contact imprinting technique for the detection of L-cysteine (Figure 1.12)[170]. The combined effect of the molecularly imprinted polymer@graphite/MWCNTs/gold nanoparticles/sol–gel composite led to the growth of a nanometre thik film coating on the surface of a sandpaper electrode. Analyte detection (L-cysteine) was directly performed electrochemically in blood serum sample, the limit of detection for which were found as 0.26×10^{-9} M when free from any cross-reactivity. The enhancement in the sensitivity of electrochemical detection was caused by the use of a large surface area, strong adsorptive ability, and the electron-transfer properties of the MWCNTs.

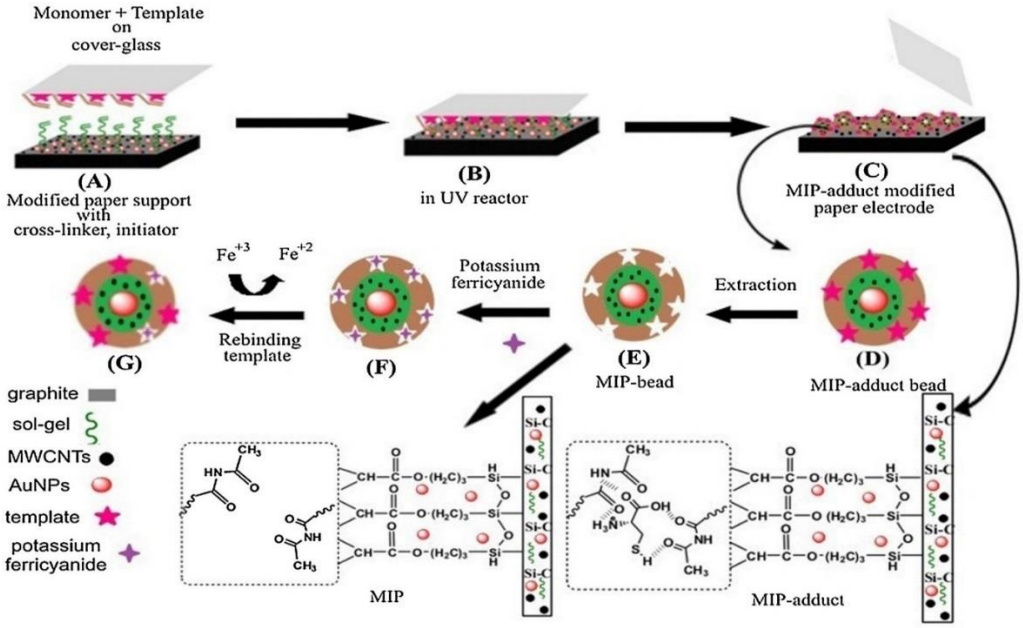

Figure 1.12: Preparation of L-cysteine micro-contact imprinting: adapted with permission from reference [150]

By way of illustration, Mazzotta *et al*. developed a voltammetric sensor based-MIPs for the detection of ephedrine[171]. A novel method based on the immobilisation of an imprinted polymer for ephedrine (MIP) in an electrosynthesised polypyrrole (PPY) film. The developed sensor revealed promising results for ephedrine detection at micromolar concentrations, but shows some non-specific binding of ephedrine and interfering compounds through a PPY matrix. In order to deactivate the chemical groups responsible for the non-specific binding, employing of electropolymerisable monomers or chemical derivatisation of polypyrrole is required.

As another example, Bai *et al*. created a sensitive electrochemical sensor based on MIP for artemisinin (ARM). The receptor (MIP) was prepared by *in situ* polymerisations of a monomer mixture on the surface of a graphene-modified glassy carbon electrode[172]. Under optimum conditions, the sensor showed high selectivity, sensitivity and cross-reactivity for ARM analogues such as dihydroartemisinin, artemether and artesunate. The detection limit was 2×10^{-9} M, MIP showed a long shelf-life, where the DPV sensor based on MIPs was reusable and stable for two months at room temperature.

In order to improve the sensitivity of MIP-based sensors, MIPS can be modified with AuNPs, quantum dots (QDs), CNTs, nanowires, magnetic nanoparticles, graphene and redox markers. For example, Bai *et al*. developed electrochemical sensor for the detection of diethyl-stilbestrol[173]. They combined AuNPs and an MWCNT-chitosan composite by drop-casting the sample onto a GC electrode to increase the surface area and enhance the electron transfer rate, and to thus amplify the sensor signal. Also, a sol-gel produced MIP was electrodeposited on a GC electrode surface. The sensor was characterised using cyclic voltammetry and impedance with DPV being used for electrochemical measurements. Under optimal conditions, the detection limit reached nanomolar concentrations[173].

Intrapment of MIP particles within gels or membranes has been suggested for electrochemical transducers[174]. On the other hand, a suspension of MIP particles and conductive materials (graphite or carbon black) in a solution of an inert soluble polymer (PVC) has been spin-coated on the electrode surface[175]. However, these approaches suffer from certain limitations such as slow diffusion kinetics, long response times, non-specific binding, suppressed binding capacity, difficult control of layer thickness and electrochemical area[175].

To overcome this limitation, redox markers such as dyes and ferrocene derivatives have been used to facilitate electron movement between the enzyme catalytic sites and the electrode surface. The main advantages of redox markers are their low oxidation and reduction potentials which help to eliminate interference signals. The use of redox markers helps in the creation of electrochemical MIP sensors[176]. Generally, soluble redox markers were used in combination with MIPs for indirect detection of effects related to polymer-template interactions. Therefore, it is known that analyte binding to MIPs-coated electrodes reduces the permeability of redox markers such as ferricyanide, and this can be used to measure the concentration of the analyte[130,177,178].

As an example, Alizadeh *et al*. created electroactive MIP NPs[179] which incorporated both ferrocene and the MIPs into a carbon paste electrode. Electroactive MIP NPs were used to detect a weak electroactive compound, thiamine which was detected indirectly via a redox probe formed of ferrocene and using SWV. For the non-electroactive template, electroactive monomers such as vinyl ferrocene (VF) and ferrocenylmethyl methacrylate (FMMA) were added to the polymerisation mixture to create an electroactive MIP NPs[180].

The redox properties of the ferrocene derivatives can be conferred to MIP NPs, which was applied in the electrochemical detection of non-electroactive template such as vancomycin.

Rebocho *et al*. developed a new disposable sensor for Bisphenol A (BPA) based on MIPs[181]. Ferrocenylmethyl methacrylate (FMMA) was co-polymerised with ethylene glycol dimethacrylate in which supercritical carbon dioxide ($scCO_2$) used as a porogenic solvent. A differential pulse voltammetry technique (DPV) was used with carbon ink used as the working electrode and silver ink as a pseudo-reference electrode. The LOD was 2×10^{-9} M.

Recently, electroactive molecularly imprinted polymers (EMIPs) have been introduced onto the surface of screen-printed carbon electrodes (SPCE) as the sensing receptor for the detection of an organic pollutant and as screen-printed carbon electrodes. Ekomo *et al*. created a new sensor utilising MIPs for the detection of bisphenol A (Bis A) using FMAA as copolymer to create the EMIPs. The FMAA was mixed with 4- vinylpyridine as a functional monomer and ethylene glycol dimethacrylate as the cross-linking monomer for the recognition of the endocrine disruptor[182]. The electrochemical properties of EMIP-SPCE revealed a high sensitivity to Bis in the presence of BPA in an aqueous medium compared to NIP-SPCE which had a LOD 6×10^{-10} M. Sensor shows low cross-reactivity toward the template analogues such as carbamazepine and ketoprofen. Screen-printed electrodes (SPE) present a particular advantage over traditional electrodes, as they are cheaper due to the use of established technology that can used for their mass production. In addition, SPE only requires a small sample volume and can be used at high temperatures[183]. Howecer, there is a difference in results between one experiment and another as a result of non-control of the concentration of the MIP so optimising the concentration are required.

Multi-channel screen-printed electrode (MCSPE) can be used to run experiments where the analyte and reference are tested simultaneously. In addition, the electrochemical transducer can detect small molecules unlike mass sensitive technique such as QCM and SPR which struggle to detect low molecular weight molecules. With regards to sensor applications, MIP NPs have led to a significant increase in sensitivity and selectivity of sensors. Furthermore, nanocomposite materials can be tailored to include additional functionality such as magnetic, electroactive mediator and semi-conductive cores.

1.9 The aims and objectives of the project

The aim of the thesis is to study the development and application of MIP NPs, prepared by solid phase, to sensors.

To achieve this aim, the objectives of this research are to:

1. To develop a general procedure for the design of MIP NPs with improved affinity and selectivity to detect different types of template.
2. To perform computational modeling experiments to determine the best functional monomers capable of forming strong interactions with the template.
3. Evaluation of the affinity of MIP NPs using the surface plasmon resonance technique.
4. Testing the cocaine sensor in a real sample (blood).
5. To develop a generic approach applicable to the transformation of the MIP-template binding event into measureable mass/electrical signal.
6. To investigate appropriate transduction mechanisms for the synthesised MIP NPs.
7. To demonstrate the possibility of using open gate theory for the development of EMIP NPs sensors for different types of target using an electrochemical mediator such as FC, FCA and FMAA.
8. Validating the process by detecting target analytes such as proteins, drugs and small molecules such as HSL.
9. Testing different types of ink paste and mixing it with MIP NPs to create a layer on the working electrode surface.

Chapter Two: A New Potentiometric Sensor Based on Molecularly Imprinted Polymer Nanoparticles for Cocaine Detection

Abstract

A potentiometric sensor for cocaine detection based on molecularly imprinted polymer nanoparticles produced by the solid-phase imprinting technique has been described here. Molecular mechanics (MM) and molecular dynamics (MD) were used to predict the interaction energies between a cocaine analogue (benzoylecgonine) and functional monomers from a monomer database. The compositions of polymers with high affinities for cocaine were optimised using molecular modelling. Four compositions were selected, and polymers prepared using two protocols: chemical polymerisation in water and UV-initiated polymerisation in an organic solvent. All synthesised nanoparticles were found to have good affinity for cocaine, with dissociation constants between 0.6 nM and 5.3 nM. The imprinted polymers produced in an organic solvent using acrylamide as a functional monomer demonstrated the highest yield and affinity. For further sensor development, nanoparticles were incorporated within a PVC matrix which was then used to prepare an molecule-selective membrane integrated with a potentiometric transducer. Preliminary results showed that cocaine could be successfully detected with high selectivity and sensitivity. It was demonstrated that the sensor was able to quantify cocaine in blood serum samples over the range of concentrations from $1x10^{-9}$-$1x10^{-3}$ M.

2.1 Introduction

The abuse of cocaine is a worldwide problem[184]. Cocaine is an effective central nervous system stimulant that induces a state of high alertness and euphoria[185]. Doses as low as 0.2 mg can be quickly absorbed, generating physiological effects in 30 seconds after nasal or intravenous administration, or as little as 5 seconds when smoked[186,187]. The typical biological fluids analysed to detect cocaine consumption are blood and urine[188]. Futhermore, cocaine can also be detected using saliva for anywhere between 2–10 days after consumption[189]. Cocaine is an alkaloid extracted from coca leaves, being the most common drug of abuse in European countries after cannabis.

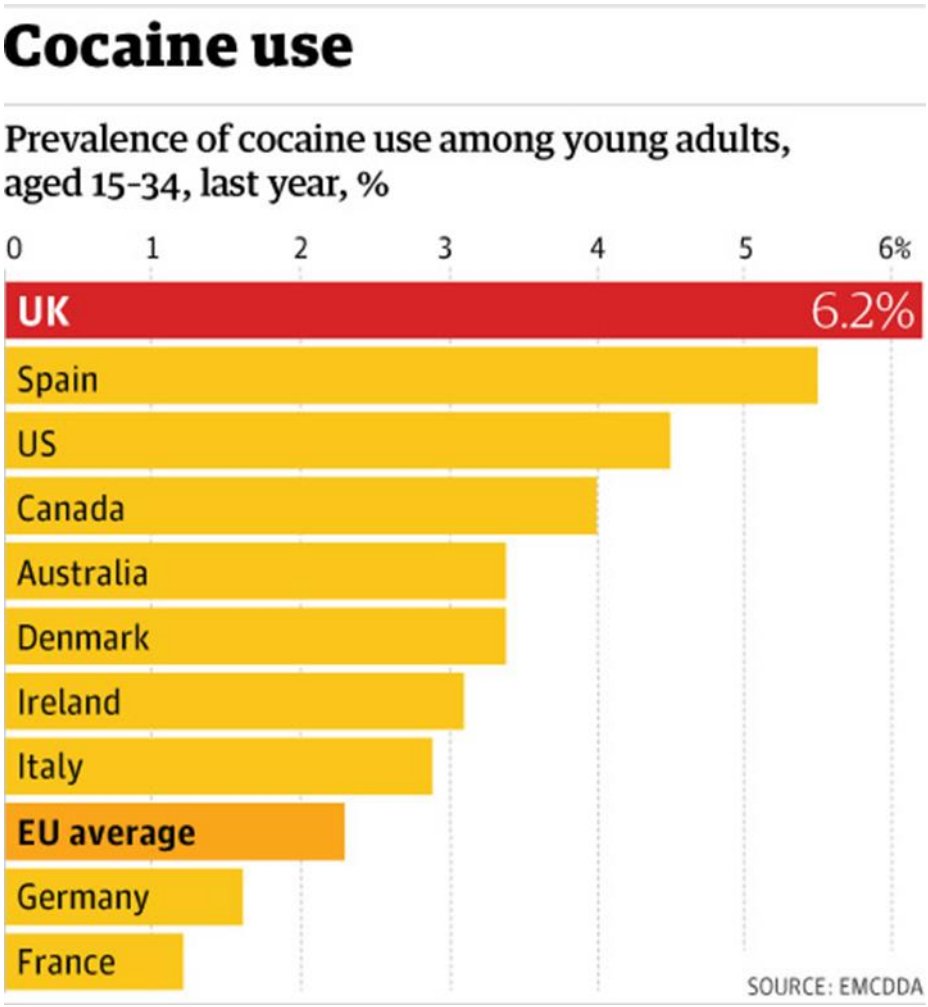

Figure 2.1: Statistics of cocaine use in the UK for 2010. Adapted from reference [167]

Cocaine use has rapidly increased between 2010−2012 in Western and Central Europe, as reported by the United Nations Office on Drugs and Crime[190]. Cocaine is one of the most widely used recreational drugs in the world, with the number of users estimated between 13.8–20.7 million for the population aged 15-64[191]. It is obvious that cocaine addiction can cause many side-effects in users, such as anxiety, organ damage and cardiac arrest. In addition, it has an impact on social and economic life[192, 193]. The major metabolites excreted in urine as a result of cocaine consumption are benzoylecgonine (BZE) and ecgonine methyl ester, followed by minor metabolites such as norcocaine, *p*-hydroxycocaine, *m*-hydroxycocaine, *p*-hydroxybenzoylecgonine and *m*-

hydroxybenzoylecgonine (Figure 2.2). Due to its abundance, benzoylecgonine (BZE) is considered a critical metabolite. It is known that BZE can form under physiological conditions through hydrolysis of the methyl ester of cocaine, and does not have significant biological activity in humans. However, norcocaine contributes to hepatotoxic effects that can be observed in cocaine users[194].

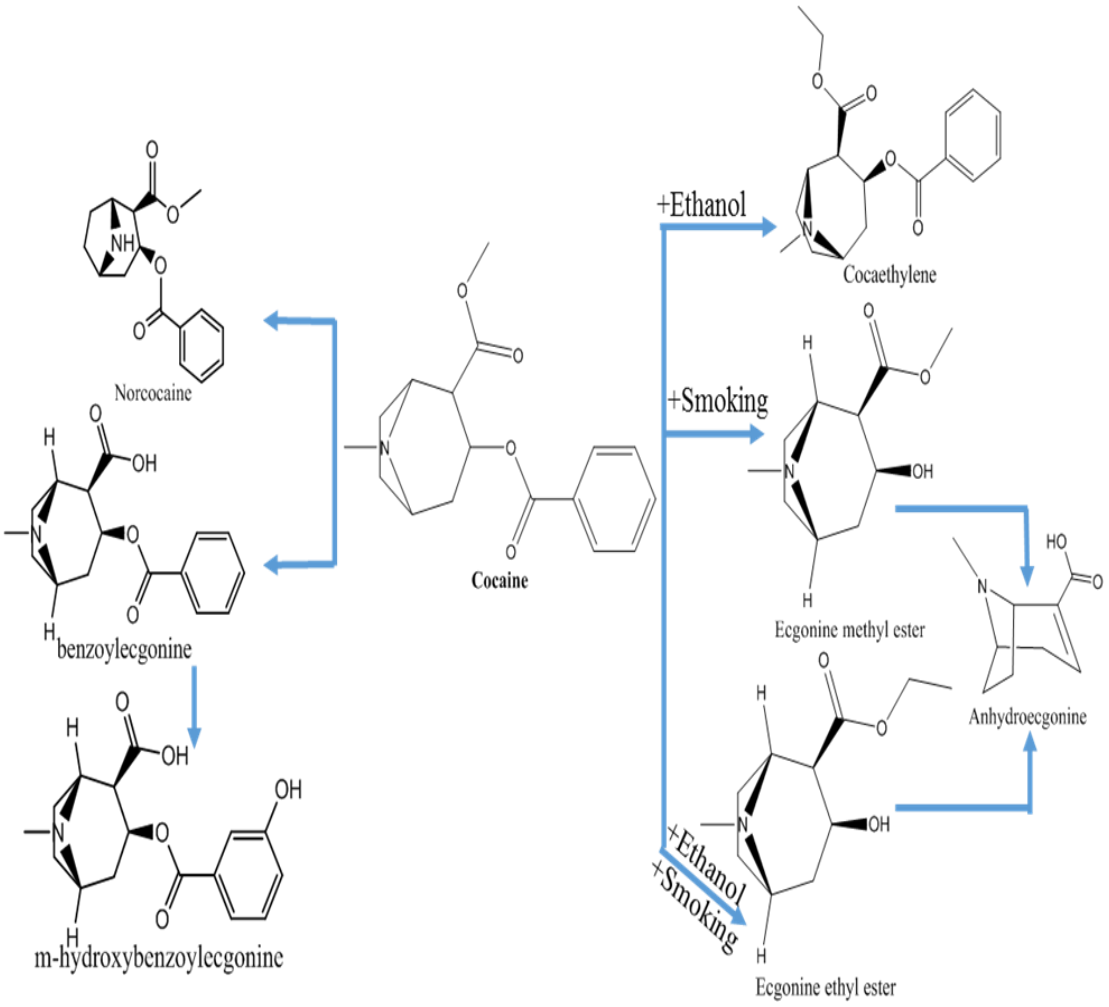

Figure 2.2: Cocaine metabolites

Researchers have created a wide range of cocaine sensors, but the analytical techniques used for cocaine detection are still mostly based on HPLC, LC-MS/MS, electrochemical techniques and ELISA[195-197]. These traditional methods are time-consuming, require the use of complex and expensive tools that demand a laboratory setting, cannot offer real-time measurement and require sample clean-up and derivatisation of cocaine[198,199]. Therefore, such sensors are physically and chemically robust and are particularly appropriate for working in harsh environments such as temperature and pH due to their immunity to electromagnetic interference. In addition, utilising molecularly imprinted polymers (MIP) is a key strength, because preparation of synthetic molecular receptors allows recognition of any given target molecule. Other advantages of such sensors are their durability, low cost and long shelf-life plus MIP-based sensing, provides a more stable alternative to biological receptors. Small number of the sensing solutions for Cocaine detection (e.g. aptamer-based biosensors) are in existence but a compact, hand-held monitor utilising stable synthetic molecular receptors does not exist[200-202]. For these reasons, the development and improvement of sensitive, simple, fast and inexpensive methods for the detection of cocaine are essential for medical diagnostics and law enforcement purposes. The potentiometric sensor is a simple and inexpensive analytical technique which is commonly referred to under the generic term 'sensors'. Potentiometric sensing involves the use of molecule-selective electrodes (ISEs) and reference electrodes used to electrochemically determine the concentration of target ions in a variety of chemical environments. Moreover, only a small sample volume was required for the measurements.

2.2 Materials and Methods

2.2.1 Materials

Benzoylecgonine (BE), norcocaine, ethylcocaine, anhydrogonine methyl ester, cocaine, histamine, acrylamide (ACRYL), *N*,*N*-diethylamino ethyl metacrylate (DEAEM), acrylic acid (AA), *N*-isopropylacrylamide (NIPAm), *N*,*N′*-methylenebisacrylamide [105], *N*-tert-butylacrylamide (TBAm), ammonium persulfate (APS), tetramethylethylene-diamine (TEMED), 3-aminopropyltrimethyloxysilane (APTMS), sodium hydroxide (NaOH), glutaraldehyde (GA), *N*-hydroxy-succinimide (NHS), 1-ethyl-3-(3-dimethylaminopropyl)-carbodiimide hydrochloride (EDC), ethylene glycol dimethacrylate (EGDMA), trimethylolpropane trimethacrylate (TRIM), pentaerythritol tetrakis(3-mercaptopropionate) (PETMP), low molecular weight poly(vinyl chloride) (PVC), nitrophenyl octyl ether (NPOE), potassium tetrakis(4-chlorophenyl)borate (kTpBCl), sterile-filtered human serum (from male clotted whole blood of AB group, USA), potassium chloride (KCl) were supplied by Sigma-Aldrich, UK. Dimethylformamide (DMF), acetonitrile (ACN), tetrahydrofuran (THF) and acetone were supplied by Fisher Scientific, UK. *N*,*N*-diethyldithiocarbamic acid benzyl ester (Iniferter) from TCI Europe. *N-(*3-Aminopropyl*)*methacrylamide hydrochloride>98% (NAPMA) was supplied by from Polyscience Inc, UK. Phosphate-buffered saline (PBS), consisting of phosphate buffer (0.01 M), potassium chloride (0.00268 M), and sodium chloride (0.14 M), pH 7.4 (Gibco Life Technologies Ltd, UK), and carbonate-biscarbonate buffer (CBB), pH 9.5 (Sigma-Aldrich, UK), was prepared from buffer tablets. All solvents were HPLC Grade. Glass beads with diameters in the range of 53-106 µm were purchased from Potters Industries, while glass beads with a diameter of 9-13 µm were supplied by Sigma Aldrich, and silica gel particles with a diameter of 35-70 µm were purchased from Acros, UK. Double-distilled ultrapure water (Millipore, UK) was used for the experiments. All chemicals and solvents were used without further purification.

2.2.2 Molecular Modelling

Molecular modelling was performed as described in previous works[203-205]. The virtual library of monomers was screened for monomer interactions with the template using the LEAPFROG™ algorithm (SYBYL® 7.3 software package, Tripos International, USA). Therefore, LEAPFROG was applied to recognise the monomers with the strongest interactions for the target. Simulated annealing or molecular dynamics are other essential steps in the rational design of polymers. These tools are used to obtain low-energy conformations of either a single molecule or more complex systems (multiple molecules). Before polymerisation, pre-arrangement of the functional monomer and the template in the monomer mixture was determined by simulated annealing. The functional monomer library used for this study contained 24 functional monomers frequently used in molecular imprinting, which possess polymerisable residues and functional groups that can interact with a template through ionic and hydrogen bonds, van der Waals and dipole-dipole interactions[206,207]. Energy minimisation for each monomer was conducted to a minimum of 0.001 kcal mol^{-1} using the following molecular mechanics parameters: method - Powell; force field – Tripos; and charges Gasteiger-Hückel. In order to screen the monomers in the database and select the functional monomers with the highest affinities towards cocaine, the LEAPFROG algorithm was applied over 60,000 iterations. The list of the functional monomers obtained was organised according to binding energy, where the monomers with the lowest binding energy values were subsequently selected for the polymer preparation.

2.2.3 Solid-phase Synthesis of MIP NPs

2.2.3.1 Functionalisation of Glass Beads

Glass beads were functionalised following the method described by Canfarotta and colleagues with slight modifications[128]. A Retsch Vibratory Sieve Shaker AS 200 basic (Retsch, Germany) with 70% amplitude for 3 hours was used to strip out the glass beads' surface coating. The glass beads were then activated by boiling them in 2 M NaOH for 10-15 min and were then washed with DI water followed by acetone, and then dried under vacuum and then in oven at 80°C for 24 h. The beads were then incubated for 24 h in a dry toluene solution of APTMS (3%), followed by washing with methanol, ethanol and acetone and again dried in the oven at 80°C. In the case of histamine immobilisation, the beads were incubated for 2 h at 4°C in a solution of GA in PBS (pH 7.4). The template was immobilised on the surface of glass beads by incubating the beads with a solution of the appropriate template (1 mg ml^{-1}) in PBS (pH 7.4) overnight at 4°C. Unbound histamine was then removed from the solid phase by washing with DI and incubating with $NaBH_4$ (1 mg ml^{-1}) in PBS (0.4 ml of solution per gram of beads) for 30 min at RT to reduce the Schiff base bonds on the glass beads. Finally, the beads were washed with DI water and dried under vacuum and stored at 4°C.

For benzoylecgonine immobilisation, a 10-fold excess of EDC and 15-fold excess of NHS were added to the template solution. After 1 h of incubation, the modified glass beads were washed with DI water, dried, and stored in the fridge at 4°C.

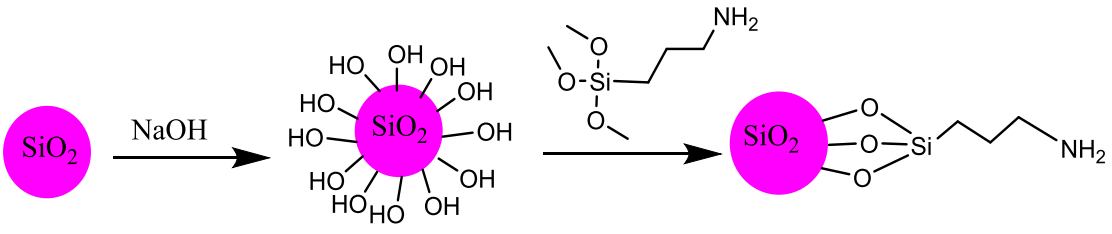

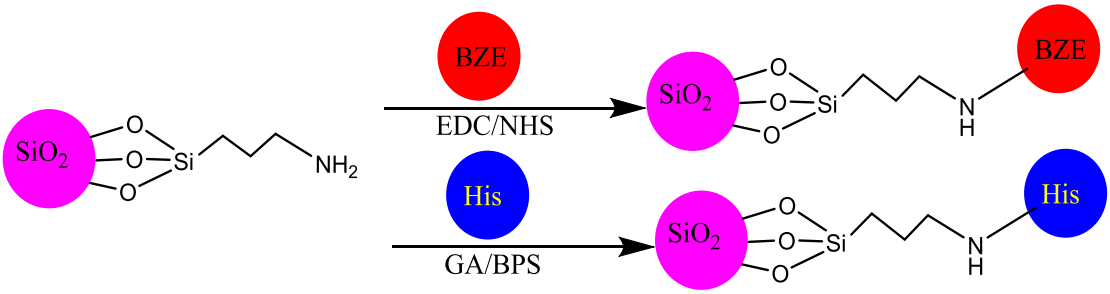

Figure 2.3: Scheme showing the modification of the glass beads with 3-aminopropyltrimethoxysilane and template immobilisation

2.2.3.2 Synthesis of MIP NPs

MIP NPs were polymerised in both water and DMF. In both cases, the components were dissolved in the corresponding solvent, sonicated for 10-15 min, and purged with nitrogen for 30 min to ensure deoxygenation. The polymerisation mixture was added to the glass beads functionalised with the corresponding template (Table 2.1,Table 2.2). Polymerisation in water was initiated by adding 30 mg ml^{-1} solution of APS and 15 µl of TEMED, while polymerisation in DMF was initiated via UV radiation using a UV lamp system (Philips, UK) for 2 min. After polymerisation, all the content was transferred into a cartridge (60 ml syringe tube) fitted with polyethylene frit (20 mm porosity). Unreacted monomers and low-affinity polymeric particles were removed by washing with DI water at room temperature or cold DMF/ACN (0°C), as shown in Figure 2.4. Next, the temperature was raised to 60°C in order to break down the non-covalent interactions between the template attached to the solid-phase and MIP NPs, thus allowing a pure fraction of the high-affinity particles free of residual template and monomers to be collected (Figure 2.4). The surface imprinting approach figure out the mass transfer issue in the target removing process and target rebinding process.

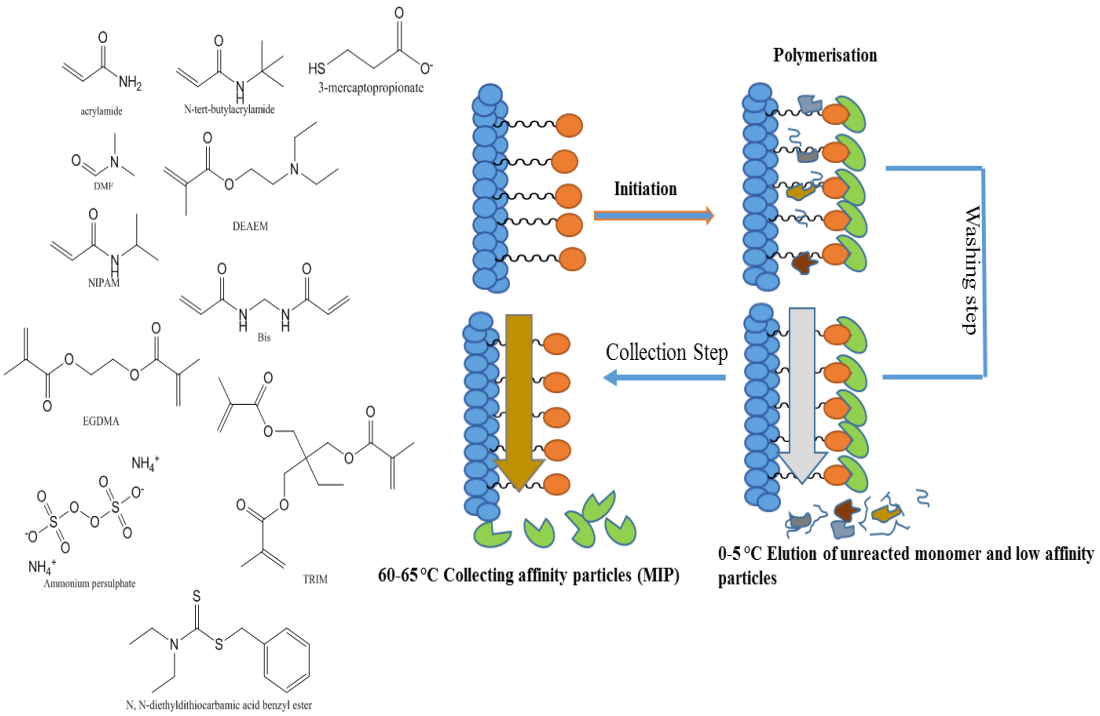

Figure 2.4: Schematic to present the solid-phase synthesis of MIP NPs

Table 2.1: Composition of monomer mixture and polymerisation conditions for polymerisation in water.

Components	**MIP NPs prepared in water**			
	1	2	3	4
Glass beads, g	30	30	30	30
Water, g	50	50	50	50
ACRYL, mg	13.2	10.5	6.6	8.6
DEAEM, mg	-	6.9	8.6	8.6
BIS, mg	1	1	8.2	1
NIPAm, mg	2.2	22	2.2	2.2
TBAm, mg	16.5	16.5	16.5	16.5
APS, mg	30	30	30	30
TEMED, µl	15	15	15	15
Conditions				
Time, min	90 min			
Cold wash, ml	6-8 x 15 ml water (R.T)			
Elution, ml	5x 20 ml hot water (60 °C)			

Table 2.2: Composition of monomer mixture and polymerisation conditions for polymerisation in DMF.

Components	MIP NPs prepared in DMF			
	1	2	3	4
Glass beads, g	30	30	30	30
DMF, g	25	25	25	25
ACRYL, g	2.5	1.9	1.2	1.8
DEAEM, g	-	1.2	1.6	1.6
BIS, g	-	-	1.3	0
NIPAm, g	0.11	0.11	0.11	0.11
EGDMA, g	3.2	3.2	3.2	3.2
TRIM, g	3.2	3.2	3.2	3.2
Iniferter, g	0.18	0.18	0.18	0.18
PETMP, g	0.75	0.75	0.75	0.75
Conditions				
Radiation time, (UV)min	1.5 min			
Cold wash, ml	2x 20 ml of DMF+6x 20 ml ACN			
Elution, ml	5x 20 ml hot ACN (65 °C)			

2.2.4 Preparation of Sensor Membranes Containing MIP NPs

The preparation of the sensor membranes was adapted from Basozabal *et al.* with some modifications[137]. The immobilisation solutions were prepared by dissolving 0.1 g of PVC in 3 ml tetrahydrofuran (THF) followed by adding 5 or 10 mg of nanoparticles, 0.2 g of plasticiser (NPOE), and 0.2 g kTpBCl. The kTpBCl was added in order to increase the membrane's conductivity and reduce anion interference. The mixture was sonicated for 25 minutes and placed in a 10 ml beaker, where it was left to dry for 48 h at room temperature, obtaining a membrane with 0.2 mm thickness. A 7 mm diameter disk was punched from the membrane and placed inside an ion-selective electrode (ISE) body (Sigma-Aldrich, Spain), which was internally filled with aqueous solution of 1 mM cocaine in 0.01 M PBS. The membrane composition in relation to the quantities of MIP NPs and kTpBCl were optimised as described in Table 2.3.

Table 2.3: Membrane composition for potentiostatic measurements.

No.	Nanoparticles, mg	PVC g	NPOE g	KTpBCl g	Slope, mV decade^{-1}	Working conc. range
1	5 (MIPs)	0.1	0.2	0.15	4.2	1 nM-1 mM
2	10 (MIPs)	0.1	0.2	0.2	22.3	1 nM-1 mM
3	10 (NIPs)	0.1	0.2	0.2	-	-

2.3 Characterisation of Physical and Chemical Properties of MIP NPs

2.3.1 DLS Measurements

The sizes and quality of the MIP NPs were verified using Dynamic Light Scattering (DLS). Prior to size analysis, an aliquot (10 ml) of nanoparticle stock solution of the high-affinity fraction of MIP NPs was concentrated using a stream of nitrogen. Acetonitrile was changed to DI water using centrifugal filter units (Amicon Centriplus®, 30 kDa MWCO, Millipore, UK) followed by ultrasonication for 20 minutes. An aliquot of MIP NPs was analysed in disposable polystyrene cuvettes at 25ºC using a Zetasizer Nano (Nano-S) from Malvern Instruments Ltd. (Malvern, UK). All measurements were performed in triplicate.

2.3.2 BIAcore analysis

BIAcore is a technique based on the surface plasmon resonance (SPR), capable of monitoring the binding properties of a given analyte. In BIAcore system, one binding partner is immobilised on the gold surface (MIP NPs) and the analyte and its analogue were injected and passes over the gold surface. The variation in mass on the gold surface due to the binding event is identified and registered in a sensorgram, whose typical shape is shown in (Figure 2.5). This binding event can be sensed down to changes in mass of a few picograms/mm^2 on the chip, which corresponds to pico- nanomolar concentrations. This capability to detect such low concentrations is possible due to the SPR phenomenon, which occurs at the interface between two media with different refractive index (RI). In

BIAcore case, the glass layer of the chip and the sample solution have different RI. For the SPR to occur, a conducting film (gold in BIAcore systems) is necessary between the two media[67]. The light incident on the glass generates an electric field called evanescent wave. Actually, at a specific angle, this incident light generates electron charge oscillations (called plasmons) in the gold layer and such absorption of energy is registered as a drop in intensity of the reflected light. For MIP NPs synthesised for C6 HSL, BIAcore analysis was performed to confirm that affinity and specificity of the MIP NPs.

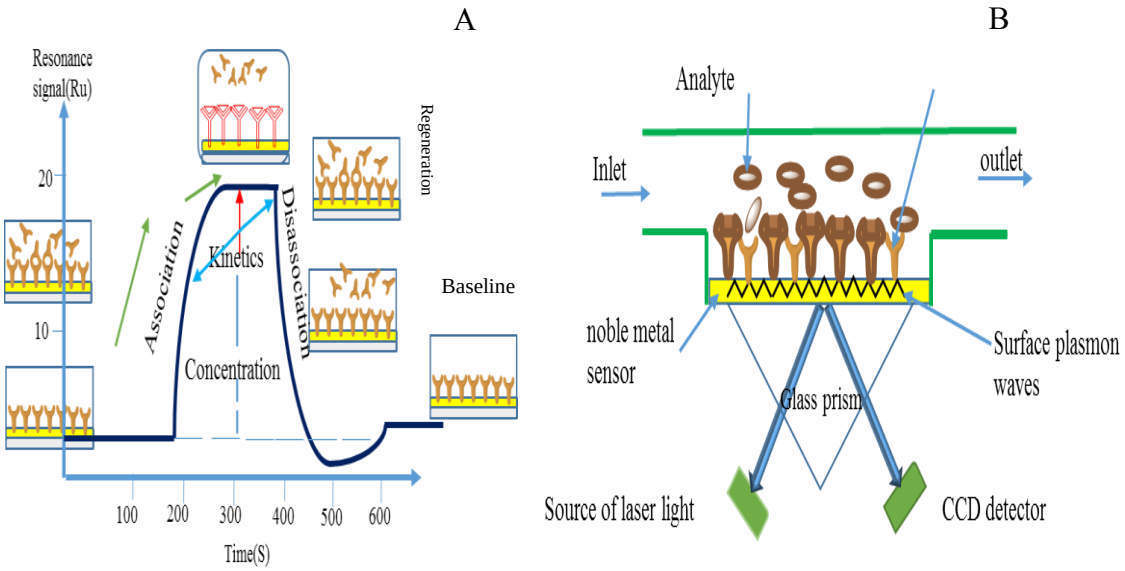

Figure 2.5: A typical BIAcore sensorgram (a). Mechanism of detection based on the SPR effect (b)

2.3.3 BIAcore Gold Chip Treatment and Surface Immobilisation

The interactions of cocaine, cocaine analogues (benzoylecgonine, norcocaine, ethylcocaine, anhydrogonine), and histamine (ref MIP) with MIP NPs were tested using a BIAcore 3000 instrument (GE Healthcare Life Sciences, USA). Au-coated chips (SIA Kit Au, BIAcore) were cleaned to remove residual glue with a mixture of tetrahydrofuran (THF), methanol and were then cleaned via plasma treatment (RF, 13.56 MHz, EMITECH K1050X, UK). The chips were then carefully rinsed with DI water and stored in ethanolic solution until the template immobilisation. For template immobilisation, lipoic acid was immobilised on the chip by incubating in an absolute ethanolic solution of 0.3 mg ml^{-1} lipoic acid and 5% acetic acid (v/v) for 24 h at 4ºC. Before subsequent use, the sensor surfaces were washed with ethanol. After immobilisation, chips were assembled on their holders and stored under argon at 4 °C until use.

2.3.4 Surface Plasmon Resonance Analysis

Affinity analysis was performed using a BIAcore 3000 SPR system (BIAcore, GE Healthcare, UK). In order to ensure successful immobilisation of MIP NPs on the sensor chip, all affinity experiments were performed in PBS, pH 7.4, at 25 °C as a running buffer at a flow rate of 15 µl min^{-1}. Surface activation of the chip was performed on-line by injecting aqueous solution of EDC and NHS at 0.6 and 0.4 mg ml^{-1} respectively at a flow rate of 15 µl min^{-1}. Immediately after activation, the nanoMIPs (suspended in PBS, pH 7.4) were injected on the sensor chip at a flow rate of 15 µl min^{-1}. For the binding experiment, the flow rate was increased to 25 µl min^{-1} and 100 µl aliquots of various analytes were injected in the KINJECT mode, which allowed the dissociation and the sensor response for 2-3 min to be evaluated. To assess their specificity, MIP NPs were evaluated by testing a cocaine MIP against cocaine analogues and histamine as NIPs. Kinetic data were fitted using the BIAevaluation Software v. 4.1 (GE Healthcare Life Sciences, USA).

Dissociation constants (KD) were calculated by BIAevaluation software v 4.1 using a 1:1 (analyte: ligand) binding model with drifting baseline fitting. This model assumes a basic interaction between analyte and ligand. Since a 1:1 binding model has been chosen for data fitting, the affinity constant is equal to the ratio of the rate constants (equilibrium association $K_A = K_a/K_d$ and $K_D = K_d/ K_a$), where K_a is the association rate constant and K_d is the dissociation rate constant. Using known concentrations of analyte, it was possible to determine the apparent equilibrium concentration (K_D).

2.3.5 Potentiometric Measurements Using Model Samples

Sensor performance was assessed potentiometrically using Autolab type II potentiostat/galvanostat (Metrohm, Netherland). Measurements were carried out at ambient temperature using an Ag/AgCl (model 5241) reference electrode (Crison, Barcelona, Spain). The assembly of the potentiometric cell was as follows: Ag/AgCl(s), KCl (3 mM)//test solution/MIP membrane/AgCl(s), 1 mM cocaine and 0.1 M KCl/Ag. A membrane containing NIP nanoparticles (histamine nanoparticles) was used as the control. Sensor responses for cocaine solutions with concentrations ranging between 1 nM and 1 mM were recorded.

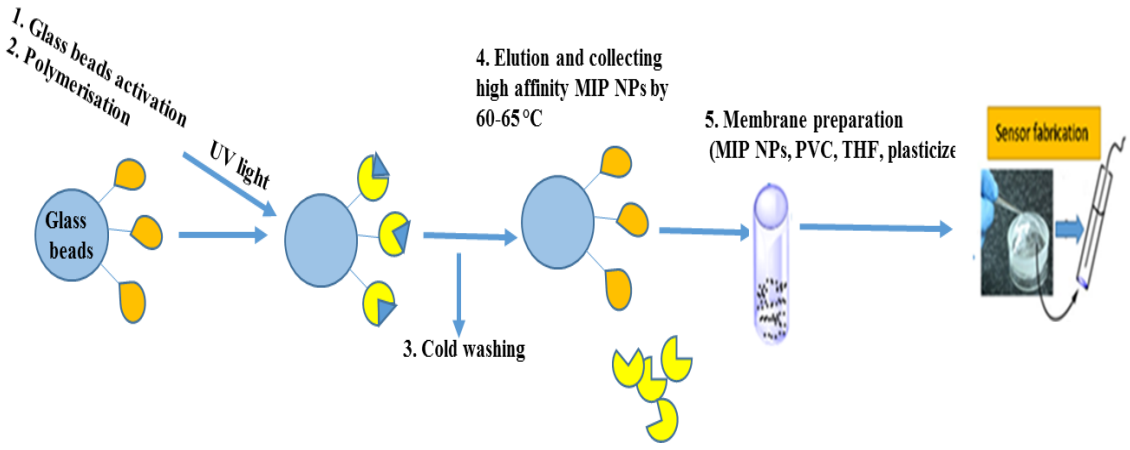

Figure 2.6: Schematic to illustrate the MIP NPs synthesis and sensor fabrication

2.4 Results and Discussion

2.4.1 Computational Design of High-affinity MIP NPs for Cocaine

Computational design was used to optimise the composition of the MIPs and reduce time, cost and chemical waste. Briefly, the chemical structure of a cocaine analogue (benzoylecgonine) was simulated and its energy minimised and screened against a virtual library containing a set of 20 monomers (acidic, basic and neutral), which are commonly used in molecular imprinting. Benzoylecgonine was used as template because it has functional group (COOH) while cocaine does not have a functional group that can interact and bind with the monomer, also it is difficult to immobilise on glass beads surface. Befor the polymerisation, computional modelling has been performed and the monomers giving the strongest binding interactions with benzoylecgonine were identified and used for the synthesis of the molecularly imprinted polymer (Table 2.4). Histamine MIP was used as a reference MIP. Organic and water polymerisation were performed (Table 2.1, Table 2.3). Various compositions of the monomer mixture and polymerisation conditions have been applied to obtain high-affinity MIP NPs and high polymerisation yields (Table 2.5).

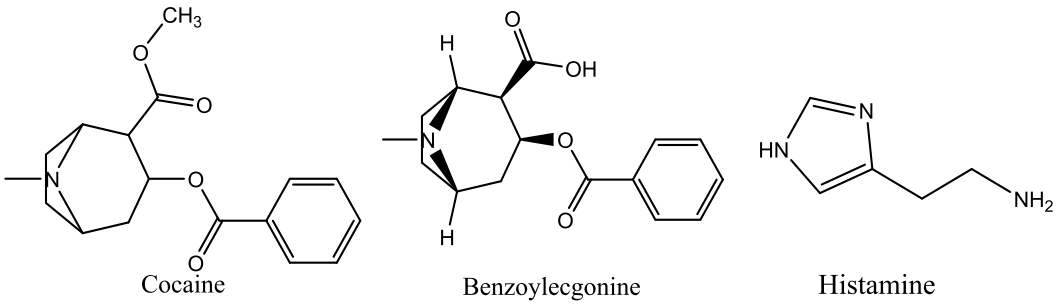

Figure 2.7: Structure of cocaine, benzoylecgonine and histamine

Table 2.4: Functional monomer binding scores for benzoylecgonine.

Functional Monomers	Binding Score kcal/mol
ACRYL	-32.43
BIS	-30.11
DEAEM	-29.77
EGMP	-27.57
NPEDMA	-26.18

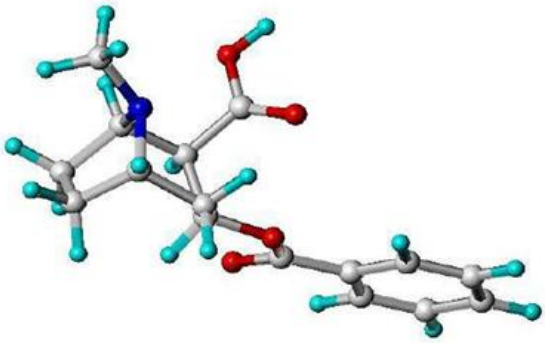

Figure 2.8: Minimised structure of benzoylecgonine [red (O), dark blue (N), cyan (H)]

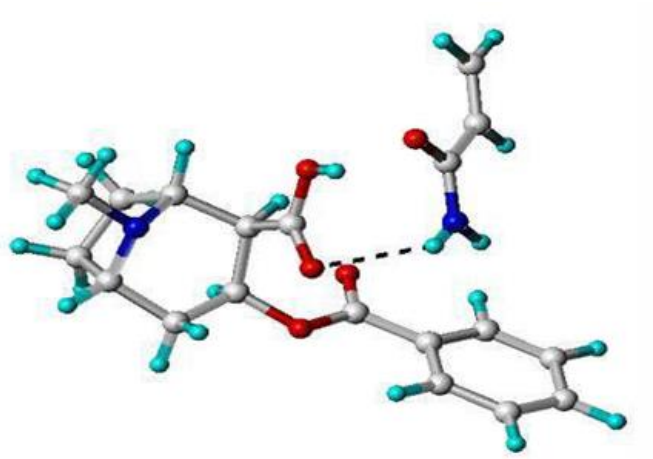

Figure 2.9: Template: monomer complex for benzoylecgonine and acrylamide [Red (O), dark blue (N), cyan (H)]

2.4.2 Synthesis of MIP Nanoparticles

Activation of the glass beads with boiling NaOH (2 M) increases the number of silanol groups (-Si-OH) on the glass beads surface, facilitating the following silanisation reaction with APTMS. When the primary amino groups cover the glass bead surface, GA can be used to link these groups with the amino groups ($–NH_2$) present in the histamine structure, generating a Schiff base bond. Both APTMS and GA allow for the reduction of potential steric hindrance issues during polymerisation, arising from the overcapacity of the template on the bead surface[67], while in the case of benzoylecgonine, the primary amino groups covering the beads surfaces bond to the template's functional group (-COOH) using EDC/NHS chemistry. The NHS compound was used to formulate amine-reactive esters of carboxylate groups for the chemical immobilisation to the glass beads. The carboxylate group (-COOH) (benzoylecgonine) reacted with NHS in the presence of EDC (a carbodiimide), resulting in an unstable NHS ester. This unstable ester can bind to the primary amine ($-NH_2$) to link to the solid phase, i.e., the glass beads.

The immobilised molecule first functions as a template during the imprinting step, after which it operates as a ligand in the temperature-dependent affinity separation, where high-affinity NPs are selectively separated from both low-affinity NPs and unreacted materials. In a regular affinity chromatography method, a column is packed with a material with specific affinity ligands on its surface. When a raw sample is loaded into the system, only the target with affinity for the ligand will be retained, while other compounds can be removed by proper elution conditions. The chosen molecules can subsequently be collected by employing stronger elution conditions, such as increasing the ionic strength of the elution solvent or adding surfactants.

The synthesis of MIP NPs follows the same principle of temperature-based affinity separation. At low temperature (0-5°C), the initial washes remove unreacted and low-affinity materials. A subsequent increase in temperature (60-65°C) disrupts the stronger interactions between high-affinity NPs and the template, making particle collection possible. This method acts to both purify the final product with regards to unreacted materials and allow selection of only high-affinity particles.

N,*N*′-diethyldithiocarbamic acid benzyl ester was used as an initiator. This kind of initiator can act also as a terminator and chain transfer agent, commonly referred to as an iniferter. Iniferters can generate one radical (dithiocarbamyl) after the decomposition step which is capable of controlling the growth of the polymer chains in solution, forming for the second time the initial C-S bond. Consequently, the product formed after termination can further generate a new propagating radical upon application of the stimulus triggering the polymerisation[208]. As a result, sequential polymerisation with other monomers can be reinitiated in order to modify properties or synthesised particles' functionalities[127, 209]. Furthermore, in contrast to conventional radical polymerisation, iniferter-based living polymerisation proceeds at a low rate and without autoacceleration, allowing considerable control over certain parameters like such as polymer chain length and particle size[78]. The UV-irradiation time should be short (1.5-2 min) to avoid excessive heating of the polymerisation mixture, which would decrease the particle affinity for the template[210].

A significant advantage of the solid-phase molecularly imprinted polymer method is that the surface of the MIP particles can be modified without affecting the functionalities within the active sites themselves. The process relies on the production of the MIP NPs in the presence of template-derivatised beads as previously described[69]. In addition, core-shell and labelling MIP NPs can be produced. Interestingly, MIP NPs can be prepared in water using a persulfate-initiated polymerisation or an organic solvent (with UV irradiation). However, organic polymerisation will increase the complex formation while more polar solvents tend to dissociate the non-covalent interactions in the prepolymer complex, especially protic solvents that afford a high degree of disruption of the hydrogen bonds[72].

Futhermore, MIP NPs prepared in organics by photopolymerisation showed high affinities for their targets. This method allows for the synthesis of MIP NPs which can combined with pve to create ISE membrane. Regardless of their composition, NPs can be designed to act as a receptor to qanitify cocaine.

2.4.3 Nanoparticle synthesis

Based on molecular modelling, four different monomer compositions (three different functional monomers with different monomer ratios) were selected. Two approaches to the polymerisation process were attempted (water and DMF) (Table 2.1 and Table 2.2). As a template the cocaine analogue, benzoylecgonine was used while histamine was used in controls and NIP formation.

Table 2.5: Polymerisation yield.

Sample No.	**Monomers composition (mole ratio)**		**Polymerisation yield (mg)**			
			in water		in DMF	
			MIPs	NIPs*	MIPs	NIPs*
1	1BE	3ACRYL	3.84	1.28	22	8.8
2	1BE	4ACRYL:1DEAEM	4.16	1.36	20	11
3	1BE	2ACRYL:1DEAEM:BIS	4.32	0.80	23	11
4	1BE	3ACRYL:1DEAEM	4.32	0.88	25	10

The present results as shown in Table 2.5, confirmed that the acrylmide and n,n-diethylamino ethyl metacrylate with percentage 3:1 gave the hightest polymerasation yield and the next experiments will be built on this results. This allowed us to find monomers capable of interacting with diff erent parts of the template other than the acrylamide binding area. In order to facilitate the immobilisation of the nanoparticles on the surface of a Biacore chip by amine coupling, a small amount of N-(3-aminopropyl) methacrylamide (containing a primary amine) was added to all monomeric compositions.

2.4.4 Concentration and Size

DLS or photon correlation spectroscopy (PCS) was used for particle size measurements. The light will scatter in all directions when it hits a particle, (Rayleigh scattering). If the particles are stationary, the light scattered would be constant. However, since nanoparticles undergo Brownian motion in solution, interference (constructive or destructive) occurs thus causing a change in light intensity because the distance between the scatters (i.e. the particles) in solution and the detector is constantly changing[211].

By monitoring the time of such fluctuations in light intensity, DLS measures the diffusion coefficient of the particles, which can be converted into a size using the Stokes-Einstein equation[211].

$$d(H)=kT/3\pi\eta D$$

Where: d(H)= hydrodynamic diameter; k = Boltzmann's constant; T = absolute temperature; η = viscosity and D = diffusion coefficient.

The nanoparticles were prepared by organic and aqueous polymerisation. Before the measurement, the high-affinity MIP NPs fraction in ACN was concentrated and transferred to DI water using N_2 and centrifugal filter cartridges. For characterisation and testing purposes, four batches of MIP NPs were synthesised and characterised. The polymerisation yield was calculated for all batches. The diameter of dispersed MIP NPs in water and the correlation between the measurements was evaluated via DLS (Zetasizer Nano-S instrument (Malvern Instruments Ltd, UK)). Before the DLS measurements, an

ultrasonic bath was used to reduce possible nanoparticle aggregates, which would otherwise affect the measurements. The concentration of the nanoparticles polymerised in water was about 20 times lower than in the case of organic polymerisation (Table 2.5). This could be explained by the formation of more stable complexes between monomer-template in organics than in water, therefore higher probability of forming particles with high affinity binding sites and, correspondingly, their yield. Another advantage was a shorter time required for the UV-initiated polymerisation than for the chemical polymerisation in water (1.5 min and 90 min, respectively).The results show the average diameter derived from the DLS measurements of all nanoparticles (MIP, NIP) was about 120 ± 15 nm (Table 2.6). There is a similarity regarding nanoparticle sizes in both cases.

Table 2.6: Particles size measured by DLS.

Sample No.	**Nanoparticles size (nm)**			
	Water polymerisation		DMF polymerisation	
	MIPs	NIPs*	MIPs	NIPs*
1	111 ± 10	93 ± 2.4	117 ± 1.7	97 ± 4.7
2	108 ± 4.5	96 ± 1.3	110 ± 4.2	95 ± 7.5
3	104 ± 4.2	99 ± 5.8	125 ± 8.9	96 ± 8.7
4	102 ± 7.5	107 ± 9.4	129 ± 2.0	89 ± 3.4

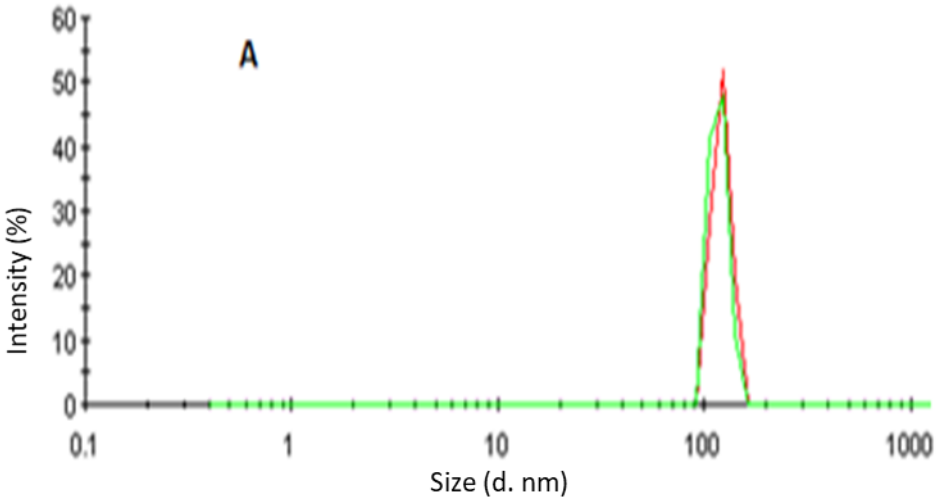

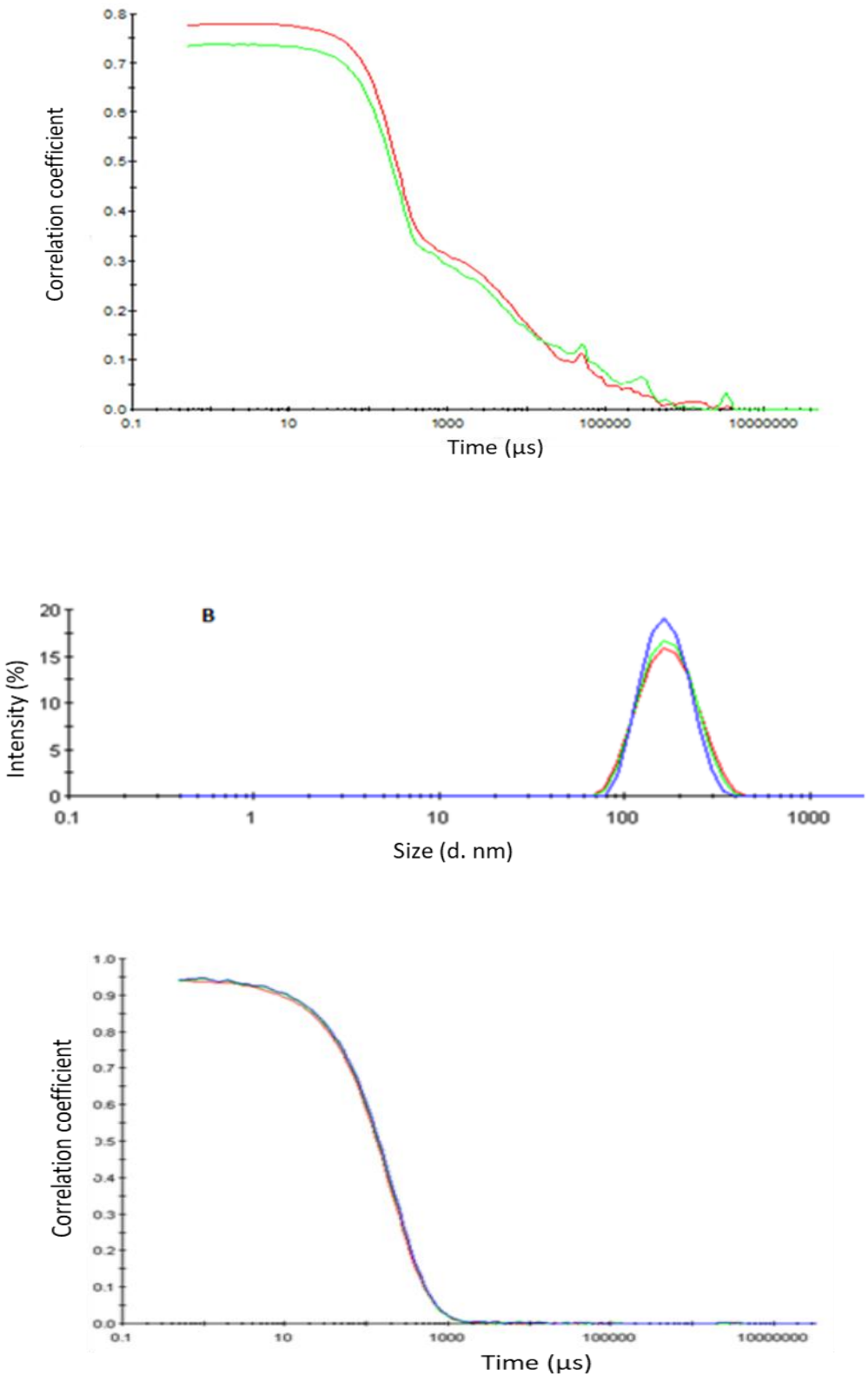

Figure 2.10: Dynamic light scattering (DLS) size distribution and correlation of (A) NIP (B) MIP in water

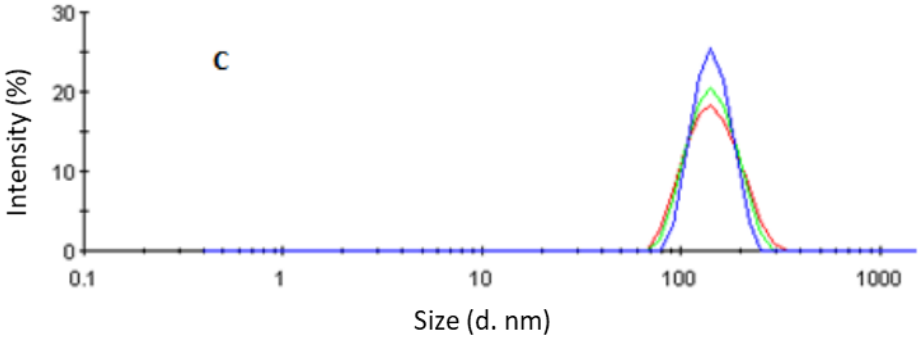
C
Intensity (%)
30
20
10
0
0.1
1
10
100
1000
Size (d. nm)

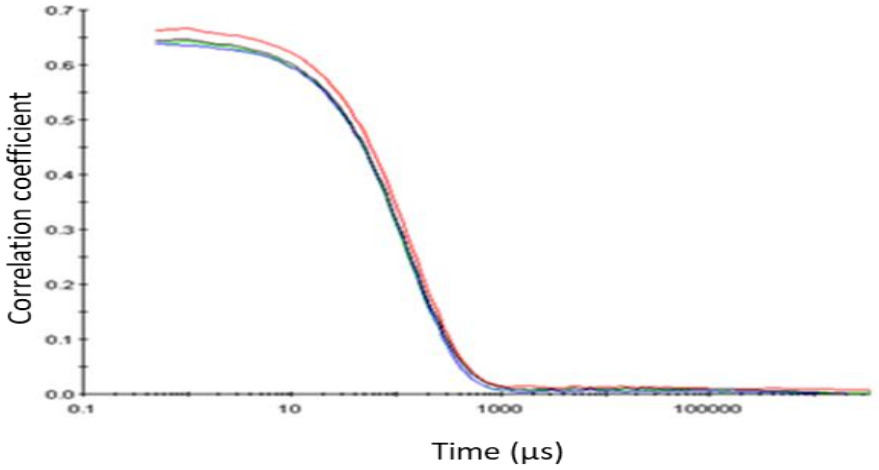
Correlation coefficient
0.7
0.6
0.5
0.4
0.3
0.2
0.1
0.0
0.1
10
1000
100000
Time (µs)

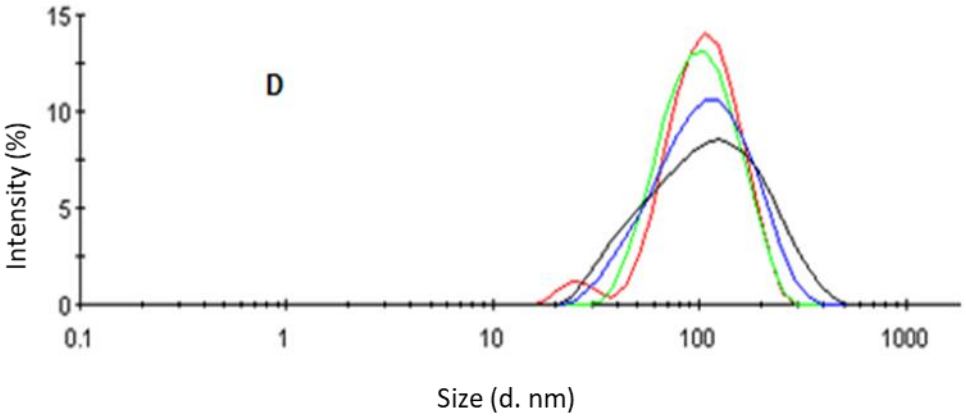
D
Intensity (%)
15
10
5
0
0.1
1
10
100
1000
Size (d. nm)

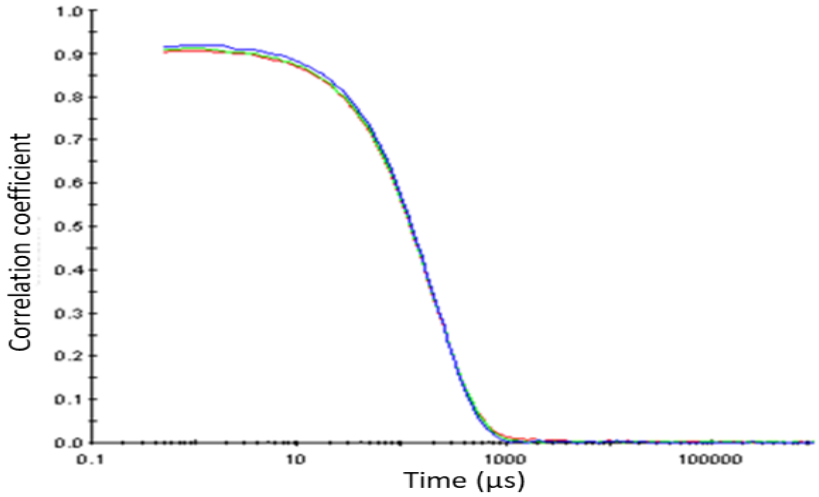

Figure 2.11: Dynamic light scattering (DLS) measurements for size distribution and correlation of (C) NIP (D) MIP in DMF

2.4.5 Nanoparticles Affinity to Benzoylecgonine

The affinity between nanoparticles and benzoylecgonine (cocaine analogue) was tested using surface plasmon resonance (SPR). The nanoparticles (MIP and NIP) were immobilised on a BIAcore gold chip. Different concentrations of BE were then injected in the range 0.01-1 nM, and the binding between the MIP NPs polymerised in water and BE were observed. However, there was no binding between the NIP NPs and BE, and no affinity was noted (Figure 2.12). An analogous situation was observed for nanoparticles polymerised in organics. Dissociation constants for MIP NPs and the template are shown in Table 2.7. For MIP NPs produced in water, the K_D was approximately 3-6 nM, and for MIP NPs made in organics, below 1 nM (0.06-0.22 nM).

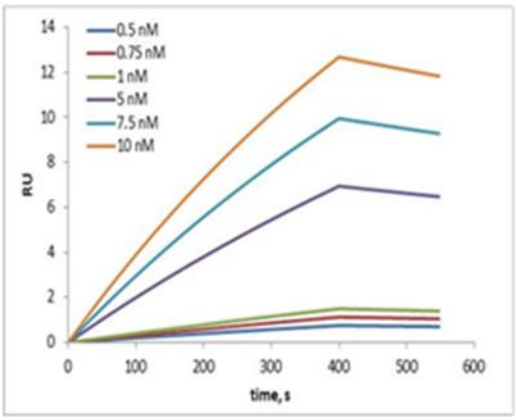

MIP NPs**1**, K_d 4.75nM (Chi^2 0.15)

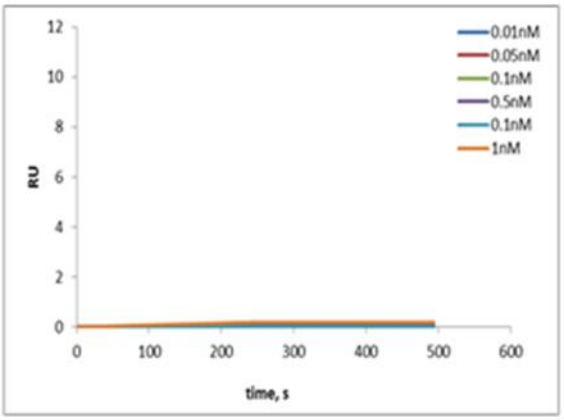

NIP NPs**1**

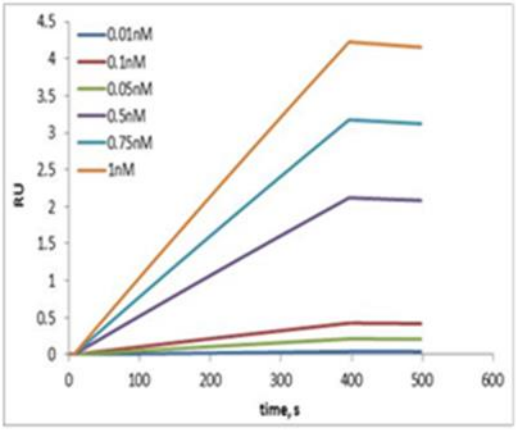

MIP NPs**2**, K_d 5.27nM (Chi^2 0.046)

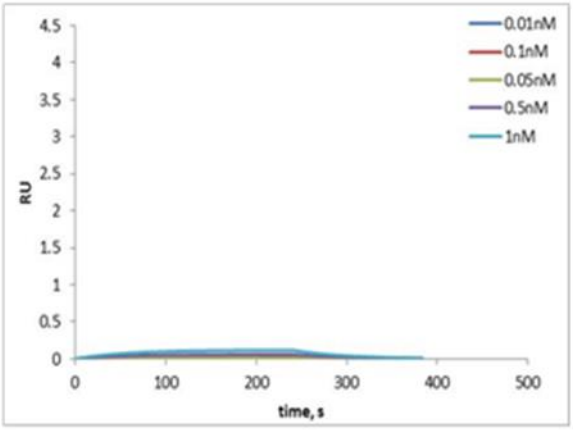

NIP NPs**2**

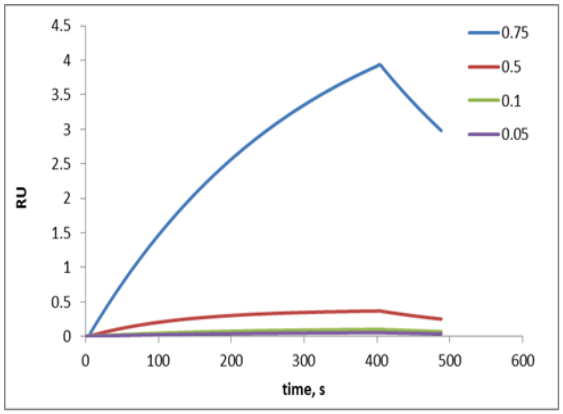

MIP NPs**3**,Kd 0.69nM (Chi^2 0.052)

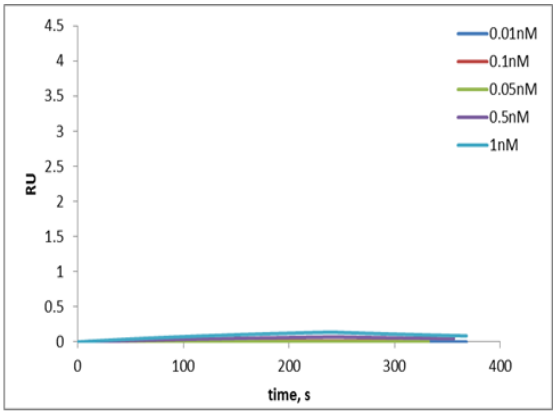

NIP NPs**3**

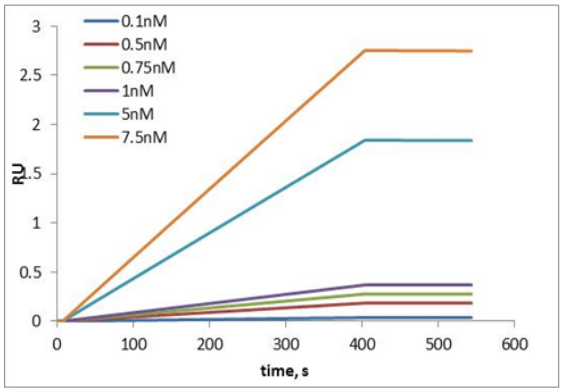

MIP NPs**4**,Kd 3nM (Chi^2 0)

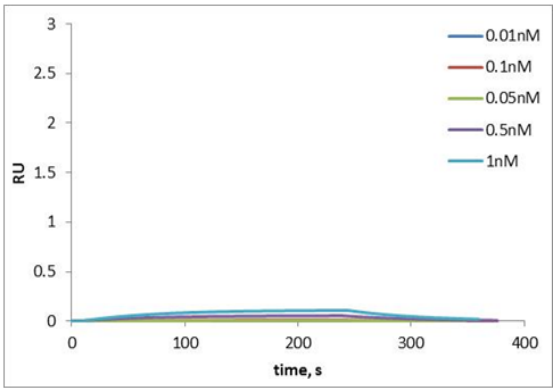

NIP NPs**4**

Figure 2.12: MIP and NIP NIPs binding to benzoylecgonine. Nanoparticles polymerised in water

MIP NPs, **NIP NIPs** 1: composition**1**; **MIP NPs**, **NIP NIPs** 2:composition**2**;
MIP NPs, **NIP NIPs** 3: composition**3**; **MIP NPs**, **NIP NIPs** 4:composition**4**

All MIP NPs polymerised in water showed a good affinity for BE (K_D 0.69-4.75 nM). Additionally, in the same concentration range, the results confirmed that there was no significant affinity for the NIP particles made in water towards the template. Comparing K_D values, response units and binding shape the results indicate that the best nanoparticles produced in water were composition number (1), while as showen in Figure 2.12, the composition number (3) has low response toward the template.

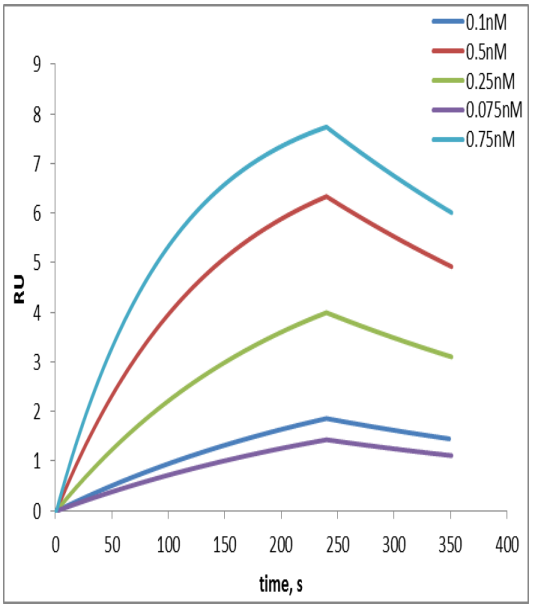

MIP NPs**1**, Kd 0.225 nM (Chi^2 0.13)

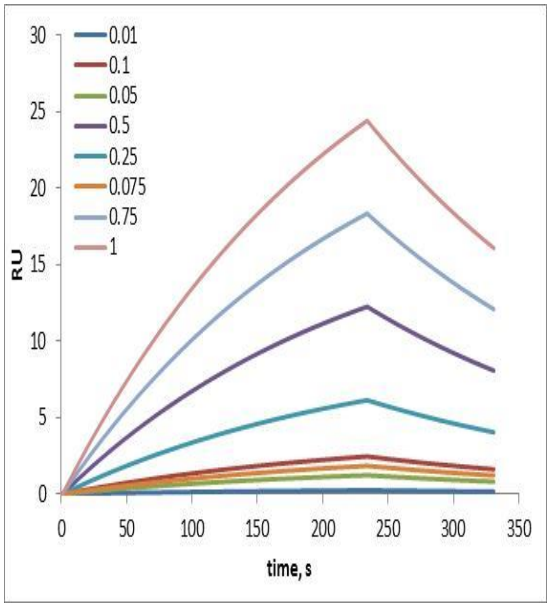

NIP NPs**1,** Kd 45 nM (Chi^2 109)

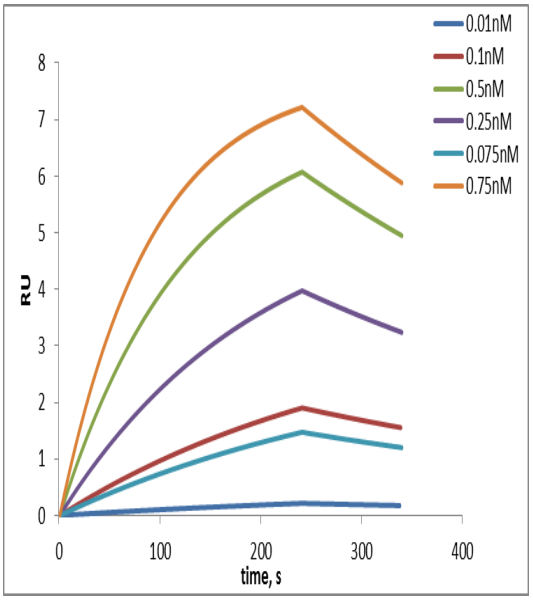

MIP NPs**2**, Kd 0.173 nM (Chi^2 0.169)

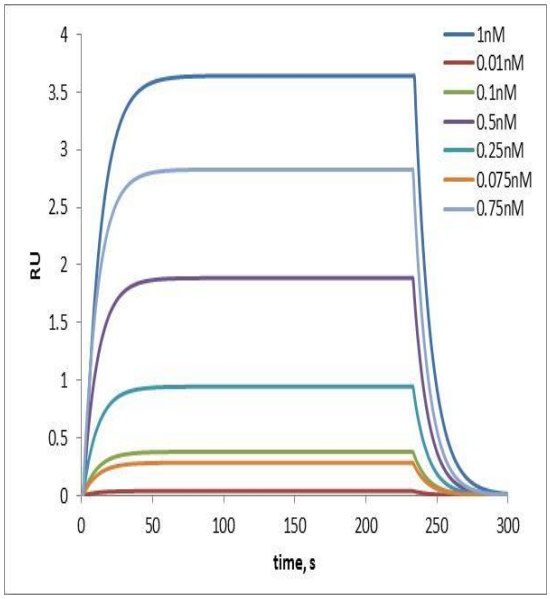

NIP NPs**2**, Kd 448 nM (Chi^2 0.98)

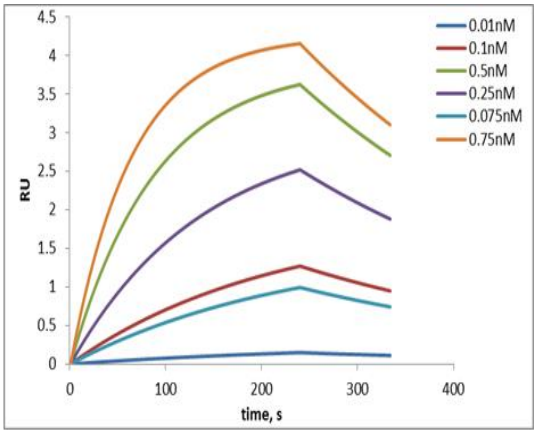

MIP NPs**3**, Kd 0.18nM (Chi^2 0.27)

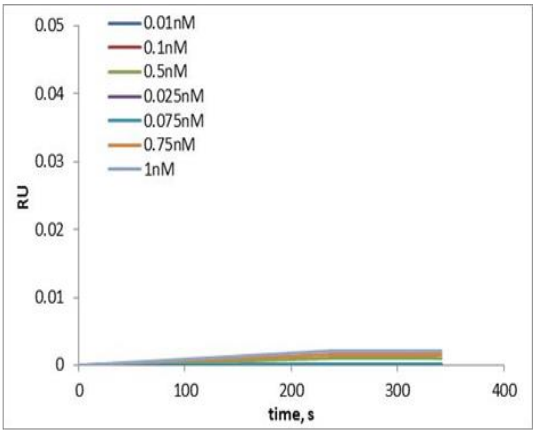

NIP NPs**3,** K_d -

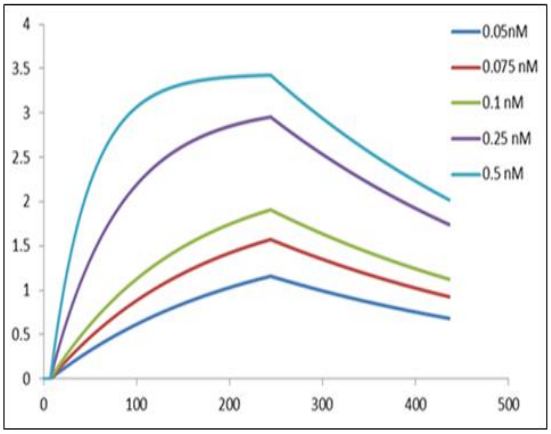

MIP NPs**3**, Kd 0.06nM (Chi^2 0.129)

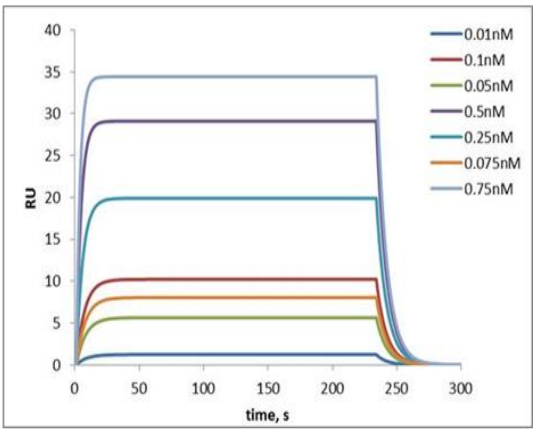

NIP NPs**3,** Kd 0.43nM (Chi^2 0.74)

Figure 2.13: MIP and NIP binding to the Benzoylecgonine. Nanoparticles polymerised in organic solution

MIP NPs, **NIP NIPs**1: composition**1**; **MIP NPs**, **NIP NIPs** 2:composition**2**;

MIP NPs, **NIP NIPs** 3: composition**3**; **MIP NPs**, **NIP NIPs** 4:composition**4**

Table 2.7: Dissociation constants for MIP NPs made in water and organic polymerisation and benzoylecgonine.

MIP NPs	Dissociation constants MIP NPs-BE K_D, nM (Chi^2) polymerisation in water	Dissociation constants MIP NPs -BE K_D , nM (Chi^2) polymerisation in organic
1	4.75nM (0.150)	0.22nM (0.130)
2	5.27nM (0.046)	0.17 nM (0.169)
3	0.69nM (0.052)	0.18 nM (0.270)
4	3.00nM (000)	0.06 nM (0.129)

All MIP NPs made in organic solution show good affinity to the benzoylecgonine than the MIP NPs made in water. However, the NIP NPs made in water showed no affinity for BE. In the case of MIP NPs made in organic solution it seemed that the NIP NPs composition (1) had some affinity to BE (Kd 45 nM), but the fit was not particularly good because the associated Chi^2 is very high (109) (Chi^2 is a sign of the average deviation of the experimental data from the fitted curve). Lower Chi^2 values indicate a better fit assuring the validity of experimental results[212]. In the case of NIP NPs, composition numbers 2 and 4 appeared to show that target was washed out of the nanoparticles immediately after connection. The results demonstrated high K_D value and response units for MIP NPs comparing with NIP NPs toward BE. In addition, MIP NPs number 3 (Kd 0.18 nM) used to be the best polymer composition in modelling.

2.4.6 Nanoparticles Affinity to Cocaine and Analogues

To achieve the aim of this work, all MIP NPs made through both water and organic polymerisations were tested in BIAcore experiments to confirm their affinity toward cocaine (Figure 2.14 and Figure 2.15).

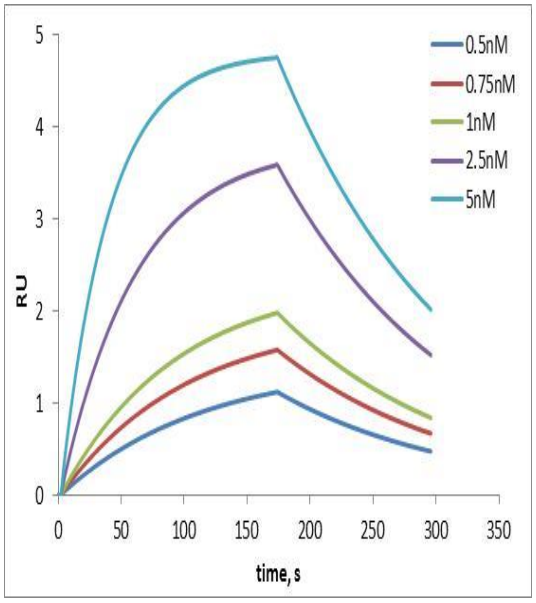

MIP NPs**1**, Kd 1.89nM (Chi^2 0.158)

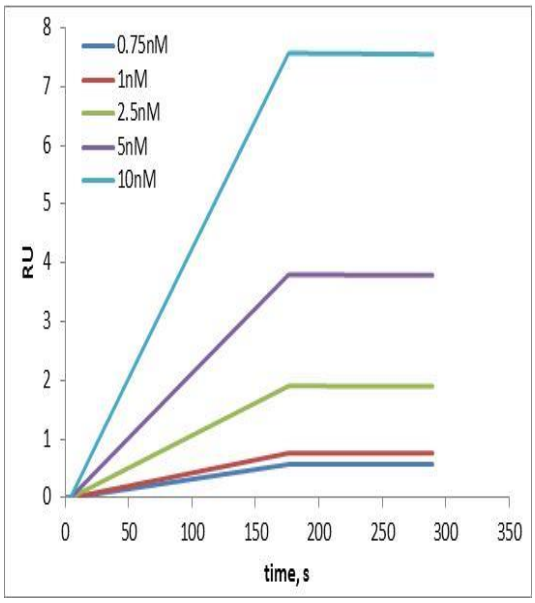

MIP NPs**2**, Kd 2.52nM (Chi^2 0.104)

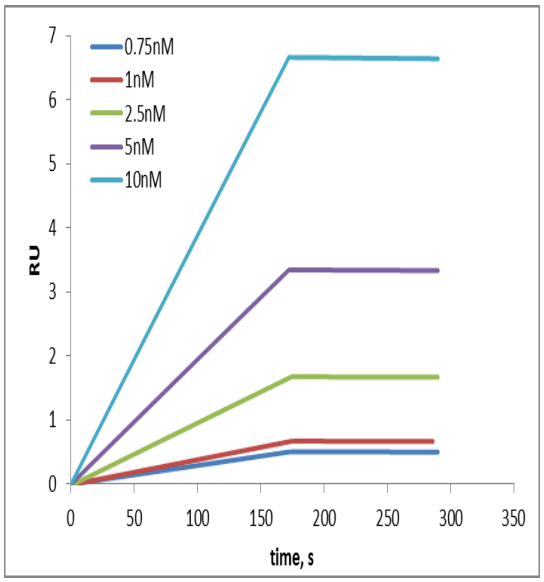

MIP NPs**3**, Kd 2.45nM (Chi^2 0.08)

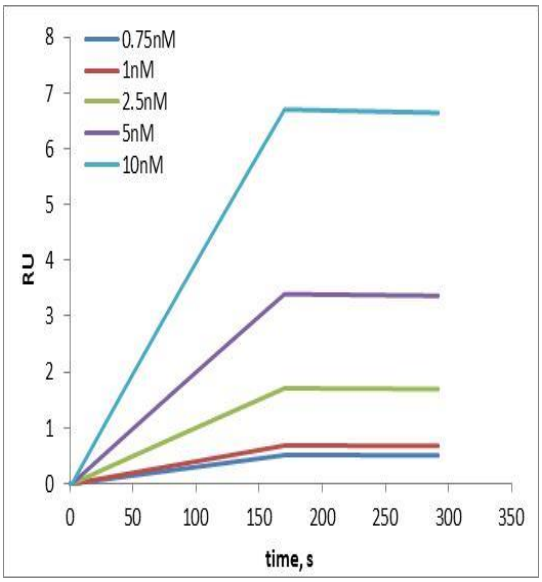

MIP NPs4, Kd 2.64nM (Chi^2 0.105)

Figure 2.14: MIP and NIP NIPs binding to cocaine. Nanoparticles made in water polymerisation

MIP NPs: composition1; MIP NPs: composition2;

MIP NPs: composition3; MIP NPs: composition4.

As shown in Figure 2.14, MIP made in water binding to cocaine. However, MIP 2, 3 and 4 have no koff and it is misleading, the clearly is a k_{off} otherwise you are not be able to calculate the KD with as such a low Chi^2 which indicate a good statistical fit. The reason why they looks like this is because is the component function that have been used they make it looks like this as if no k_{off} but the raw data shows there is k_{off} for all the injected concentration otherwise in impossible to fit the data and getting KD value.

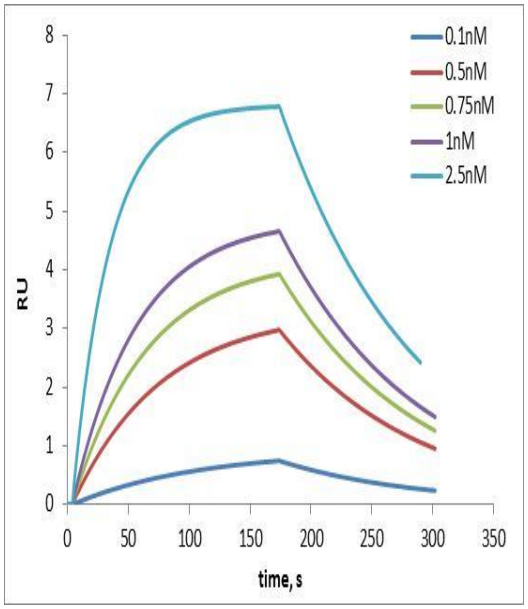

MIP NPs**1**, Kd 0.9nM (Chi^2 0.264)

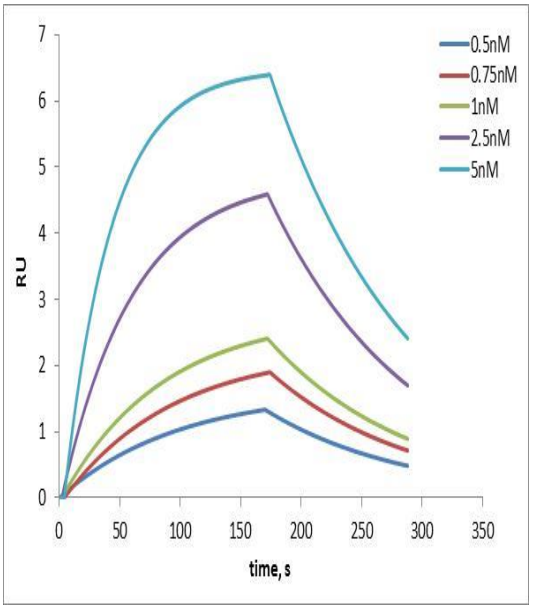

MIP NPs**2**, Kd 2.52nM (Chi^2 0.157)

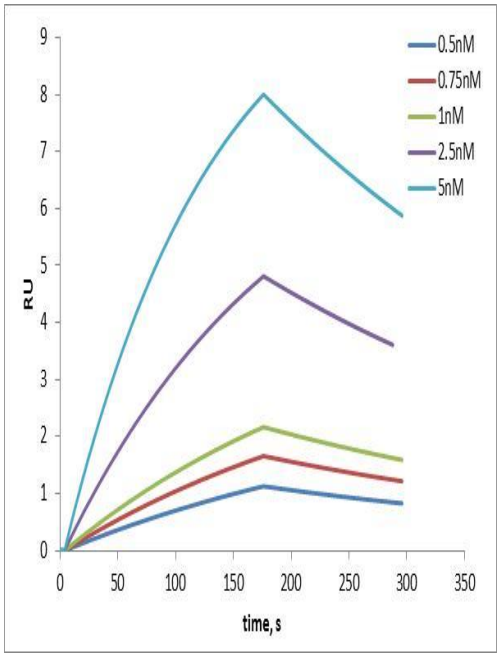

MIP NPs**3**, Kd 2.45nM (Chi^2 0.109)

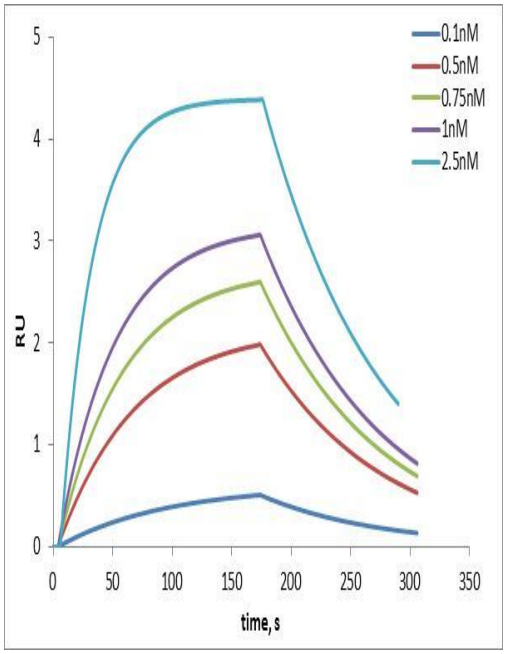

MIP NPs**4**, Kd 0.89nM (Chi^2 0.129)

Figure 2.15: MIP and NIP NIPs binding to cocaine. Nanoparticles made in organic polymerisation

MIP NPs: composition1; MIP NPs: composition2;

MIP NPs: composition3; MIP NPs: composition4.

Table 2.8. Dissociation constants for MIP NPs, made in water and organic polymerisation for cocaine.

MIP	Dissociation constants BE-MIP-Cocaine K_D, nM (Chi^2) polymerisation in water	Dissociation constants BE-MIP-Cocaine K_D, nM (Chi^2) polymerisation in DMF
1	1.89 nM (0.158)	0.90 nM (0.264)
2	2.32 nM (0.104)	2.52 nM (0.157)
3	2.87 nM (0.08)	2.45 nM (0.109)
4	2.28 nM (0.105)	0.89 nM (0.129)

The MIP NPs with BE imprint have an excellent affinity with cocaine. It is well known that the regular half-life of cocaine in the body is 20-90 min[213]. The drug is metabolised into analogues such as norcocaine, benzoylecgonine, cocaethylene and anhydroecgonine (Figure 2.2). The binding of MIP NPs "composition No. 3" to the cocaine metabolites in SPR experiments was determined and the affinities for the cocaine analogue calculated to be as follows: norcocaine, 2.45 mM; cocaethylene, 2.45 nM; and anhydroecgonine, 1.79 nM (Figure 2.16). The low dissociation constants of MIP NPs and metabolites demonstrate the efficiency of MIP binding to cocaine and its metabolites which is vital to the accurate analysis of this drug in body fluids.

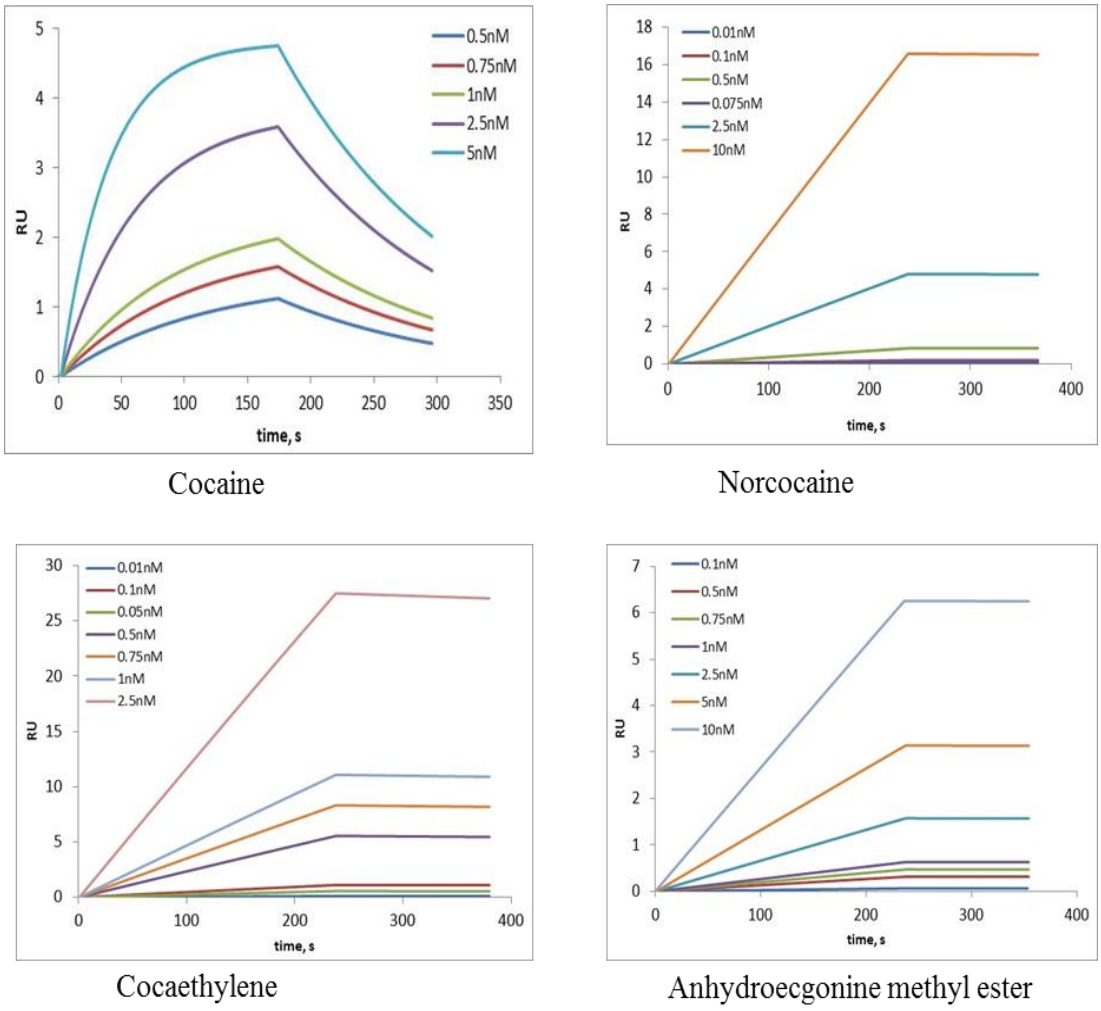

Figure 2.16: The binding sensorgram of cocaine and its analogues, norcocaine (a), cocaethylene (b) and anhydroecgonine methyl ester (c) with MIP NPs

	Norcocaine	Cocaethylene	Anhydroecgonine
K_D, nM	2.45	1.56	1.79
Chi^2	0.857	2.86	0.077

The MIP NP yields produced by organic polymerisation were in all cases larger than the yield from water polymerisation (about 25 mg and 4 mg, respectively). All the prepared MIP NPs that were imprinted for benzoylecgonine showed an affinity for the target. In addition, there was no affinity between BE and the nanoparticles imprinted for histamine in the same range of concentrations as for MIP NPs and BE. All MIP NPs based on the acrylamide monomer showed affinity for cocaine. However, dissociation constants were better for MIP NPs obtained in organic polymerisation. Dissociation constants were found to be in the range of 0.9 to about 3 nM.

2.5 Sensor Development for Cocaine

Potentiometric sensor for cocaine was fabricated based on ion-selective membranes containing MIP NPs as a recognition element. The membrane composition in relation to the amount of either MIP NPs or kTpBCl were optimised as shown in Table 2.9. The sensor response was based on the specific recognition and binding of charged cocaine species to the membrane receptors which then resulted in generation of a potential diff erences cross the membrane. It is also important to highlight that there was no sensor response for compounds such as galantamine (reference). The potentiometric response for cocaine was measured in the concentration range 1 nM and 1 mM. This is in line with data reported for optical cocaine sensors which exhibited a similar working range[199]. Furthermore, the results were better than sensors based on optical fibres for cocaine detection which demonstrated a good sensitivity with a detection range of 1–100 μM[214].

MIP NP-based polymeric membrane potentiometric sensors have been successfully developed for the determination of cocaine. The homogeneous molecular recognition between the analytes and MIPs in the membranes are reasonably efficient due to the particle sizes, high affinity and available binding sites on the MIPs. The potentiometric sensor for cocaine was developed following the standard protocol described earlier[137,215]. The ion exchange membranes containing MIP NPs were used as a recognition element on the sensor.

Table 2.9: The composition of the membrane for potentiometric measurements.

No.	Nanoparticles, mg	PVC g	NPOE g	KTpBCl g	Slope, mV decade^{-1}	Working conc. range
1	5(MIPs)	0.1	0.2	0.15	4.2	1 nM-1 mM
2	10(MIPs)	0.1	0.2	0.2	22.3	1 nM-1 mM
3	10(NIPs)	0.1	0.2	0.2	-	-

The potentiometric response to cocaine was measured over a concentration range of 1 nM – 1 mM (Figure 2.17). In contrast to MIP NPs, the results demonstrated that no response could be detected for a membrane containing NIP NPs. It is also important to highlight that there was no sensor response for compounds such as galantamine (reference MIP) (Figure 2.18).

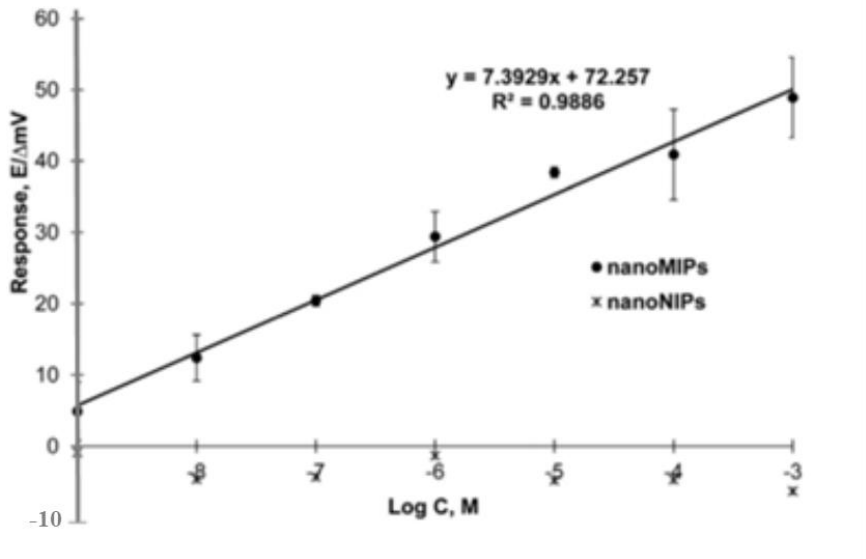

Figure 2.17: Sensor response to cocaine: MIP NPs and NIP NPs. The experiments were repeated in triplicate

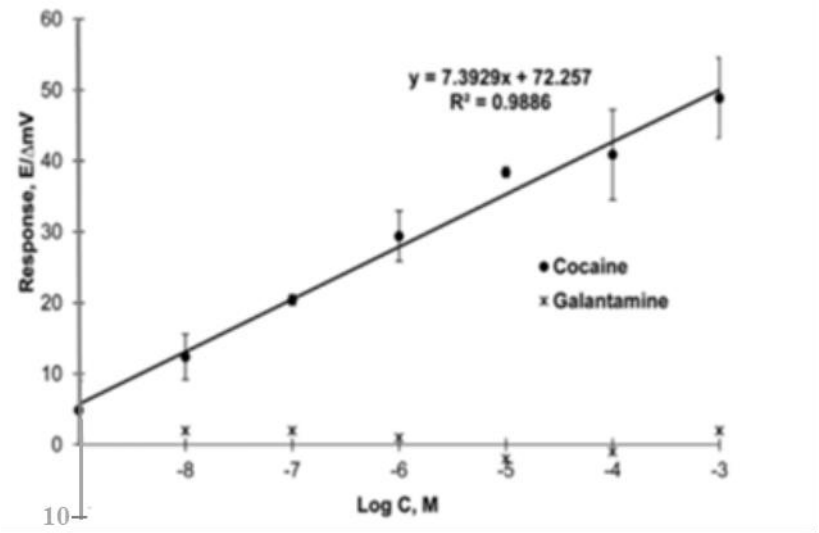

Figure 2.18: Sensor response to cocaine and galantamine. The experiments were repeated in triplicate

2.5.1 Analysis of Cocaine in Biological Samples

To confirm sensor feasibility for real sample applications, the proposed potentiometric sensor was used to detect cocaine in the human blood serum. Human blood serum was spiked with concentrations of cocaine ranging from 1 nM to 1 mM. The detection of cocaine in human blood serum was conducted potentiometrically, accordingly to the protocol described above. Interestingly, the presence of blood serum in the sample had practically no effect on the linearity of the sensor response and its sensitivity (Figure 2.19).

The results indicated that the MIP NPs-based sensor has promising potential for the accurate and rapid determination of cocaine in complex biological fluid samples. The proposed sensor shows excellent characteristics, including the wide dynamic concentration range, high selectivity, quick response and low detection limits which would be required for routine work.

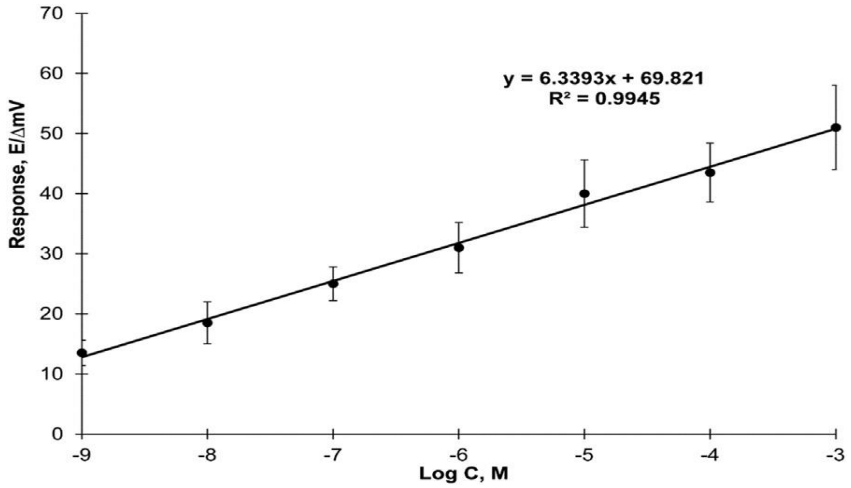

Figure 2.19: Sensor response to cocaine in human blood serum samples. The experiment was performed in triplicate

2.6 Conclusion

MIP NPs with a high affinity to cocaine were prepared using acrylamide as a functional monomer. The nanoparticles had a high affinity to cocaine and cocaine metabolites, with dissociation constants ranging from 0.6 to 5.3 nM. The solid phase approach offers the advantage of using an analogue compound when the target has no functional group. Synthesised MIP NPs were used in a potentiometric sensor for the accurate measurement of drug content in human blood serum across a wide range of concentrations of $1x10^{-9}$-$1x10^{-3}$ M. The opportunity of regenerating the sensor using a short washing steps using PBS suggests that the sensor could be possible to be re-used. In conclusion, we can say that the potentiometric sensor was used successfully for the accurate measurement of cocaine in biological fluid, particularly in blood serum.

In terms of stability, similar MIP NPs has been evaluated in the previous studies[66,137]. It was confirmed that their high stability (especially when compared with natural receptors like antibodies) allows for the development of robust sensor, which do not require cold storage. The new sensor could potentially be used by police and security forces for on-the-spot testing.

Chapter Three: A Quartz Crystal Resonator (QCR) Sensor for Bacterial Sensing Molecules (homoserine lactone)

Abstract

The present study describes the preparation of Molecularly Imprinted Polymer nanoparticles (MIP NPs) for gravimetric sensory applications. MIP NPs were prepared using solid-phase synthesis from high affinity functional monomers identified in previous molecular modelling study. (S)-(−)-α-amino-γ-butyrolactone hydrobromide was used as a starting template model to develop a MIP sensor to detect the gram-negative bacterial quorum signalling molecules, N-acyl homoserine lactone (AHL). To characterise the MIPs properties, particle size of the MIPs was evaluated using Dynamic Light Scattering (DLS) and SEM (Scanning Electron Microscopy). Futhermore, the affinities between the template and different types of MIP NPs were analysed using a BIAcore 3000, the results of which were determined using the BIAevaluation software. A novel acoustic technique based on Fixed Frequency Drive (FFD) coupled with molecularly imprinted polymer nanoparticles as receptors have been used for in vitro detection of AHL using N-hexanoyl-L-homoserine lactone (C6 HSL) as a model molecule. The FFD technique enabled the sensitive, specific, label-free, rapid and real-time detection of C6 HSL in spiked PBS solution with a minimum quantification limit down to 1 μM, which is improvement over the current state-of-the-art acoustic detection of C6 HSL. The novel acoustic sensor can be potentially integrated on a single silicon chip which favours point of care diagnostics of gram-negative bacterial infections.

3.1 Introduction

Deterioration of human health due to bacterial infections is issue of global concern[216, 217]. A reliable and rapid diagnostic platform followed with suitable treatment and prognosis is therefore essential in order to fight bacterial infections. A number of biosensing techniques have been developed in recent years for the rapid and sensitive detection of bacteria[218]. However, while such detection confirms the presence of bacteria, it does not confirm whether it is contamination, colonisation, or infection. The determination of bacterial infection is actually a synthesis of evidence of the presence of bacteria and inflammation or systemic dysfunction and, hence, more than one diagnostic approach is often needed for definitive confirmation[219].

Actually, the number of infections caused by bacteria that are resistant to antibiotics have increased dramatically. Specific bacterial phenotypes are responsible for the growth and production of microorganisms in different environments[220, 221]. Gram-negative and gram-positive microorganisms use cell-to-cell communication systems to control some of their phenotypes[222,223]. The majority of these phenotypes are density-dependent and consequently influenced by the increase of microbial populations[221, 224]. Gram-negative bacteria produce N-acyl homoserine lactone (AHL) to regulate gene expression in a cell density-dependent manner. For example, expression of virulence factors by pathogens such as *Pseudomonas aeruginosa* is induced when AHL threshold concentration is reached, which confirms that the increase in bacterial population is sufficient to cause infection.

Despite the great advances in drugs manufacturing, bacterial infections are a common problem with regards to human health. These issues are magnified by the steadily advancing resistance amongst different bacteria to many common antibiotics. A new method of attacking bacterial infectious diseases, without promoting antimicrobial resistance, is necessary. A successful strategy might well be the detection of low concentrations of the bacterial ‘language’ which bacilli use to communicate. In quorum sensing (QS), bacteria create and release specific small molecule chemicals as signals or autoinducers (AI) into the environment. QS (QS-phenotypes) activity consists of virulence factors, toxin production, antibiotic resistance and biofilm formation.

In addition, the literature notes that many species of wastewater bacteria rely on *N*-acyl homoserine lactone-mediated QS to synchronise activities essential for biofilm formation. The oil industry, for instance, suffers from biological corrosion of its oil pipes by biofilm bacteria,[225] which can lead to massive financial losses.

3.2 The Chemical 'Languages' of Gram-negative Bacteria

In gram-negative bacteria, the most common type of signalling molecules belongs to the *N*-acyl-homoserine lactone family (Figure 3.1)[226]. The chemical structure of AHL consists of a homoserine lactone ring attached, via an amide bond, to an acyl side chain of varying length. To date, naturally occurring AHL that are 4-14 carbons in length have been revealed. They can be saturated or unsaturated, with or without a hydroxyl substituent, oxy substituent, or have no substituent at the 3-position of the *N*-linked acyl chain[226,227].

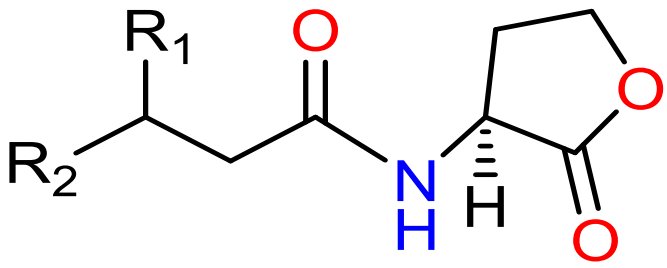

Figure 3.1: Chemical structure of the AHL signal molecule (R1 = H, OH, or O/ R2=C1–C18)

Gram-negative bacteria generally produce AHL at minimal concentrations, which is difficult to detect using common procedures. AHL is capable of controlling bacterial virulence genes and suppressing the immune system in the host body, thereby facilitating bacterial infection. Virulence factor expression is introduced when a cut-off concentration of AHL is attained, which indicates that the bacterial community is sufficiently large to develop an infection in the host body[228]. The exact threshold concentration of AHL required for initiation of different bacterial infections is still unclear in the existing literature and thus calls for further inquiries. However, AHL have been successfully quantified in infectious human biological samples[229-231]. *N*-hexanoyl-L-homoserine lactone (C6 HSL)-mediated QS in opportunistic human pathogen such as *Serratia marcescens* has been found to be involved in nosocomial infections including the respiratory tract, urinary tract, and wound infections, to name a but a few. AHL including *N*-butyryl-L-homoserine lactone (C4 HSL), *N*-hexanoyl-L-homoserine lactone (C6 HSL), *N*-octanoyl-L-homoserine lactone (C8 HSL), *N*-dodecanoyl-L-homoserine lactone (C12 HSL) and *N*-tetradecanoyl-L-homoserine lactone (C14 HSL) have been identified in saliva and stools of patients suffering from bacteria-induced gastrointestinal disorders, such as inflammatory bowel disease, at the nanomolar level[232-234]. *N*-(3-oxododecanoyl-L-homoserine lactone (3-oxo-C12 HSL) has been found in nanomolar concentrations in *Pseudomonas aeruginosa*-affected lungs and sputum tissues of cystic fibrosis patients[235]. Hence, AHL can serve as potential biomarkers for gram-negative bacteria-related infections and disorders.

Generally, detection methods for AHL of genetically engineered bacterial reporter strains are coupled with other methods including TLC (thin layer chromatography)[235-238], PCR (polymerase chain reaction)[231,239,240], colorimetry[231] and fluorescence-based[241]. AHL biosensors employ genetically engineered bacterial whole-cell sensing systems, which suffer from low sensitivity and can produce false negative results with sample concentrations below the detection threshold[242,243].

The detection methods associated with bacterial strains require intensive lab work, specific conditions and expert researchers. Additionally, they suffer from lack of sensitivity and are time-consuming. On the other hand, detection techniques such as HPLC[244], LC-MS[245], HPLC-MS[246], GC-MAS[247], NMR[248] and FTIR [249] have also been used for the detection of AHL from cell-free supernatants of gram-negative bacterial cultures with remarkable sensitivities. Nevertheless, these detection techniques require

sample pre-treatment and/or molecular derivatisation. Additionally, the high costs associated with the extensive instrumentation restricts their use as biosensing tools.

The Quartz Crystal Microbalance (QCM), also known as the Quartz Crystal Resonator (QCR), is a class of label-free acoustic sensors that are widely used for chemical compound detection. QCM provide sensitive tools for determination of the mass adsorbed onto the surface of the sensor during some form of the deposition process. QCM can be incorporated into portable detection platforms, and consequently can serve as a potential biosensing technique for AHL detection. Previously only one article in the literature has provided evidence of real-time detection of C6 HSL using a 27 MHz QCR[232]. Cyclic oligosaccharide cyclodextrins (β-CD) were used as the receptors for C6 HSL in this work. The change in resonance frequency due to the interaction between β-CD immobilised 27 MHz QCR and the aqueous solution of C6 HSL at a given concentration was recorded using electrical admittance or frequency sweep (FS) analysis of QCR[232].

Enzyme-linked immunosorbent assay (ELISA) has been used as a tool for the detection of AHL[250]. Regarding analysis time, ELISA is faster than the techniques mentioned above, but it requires labelling of the target molecule, such as AHL, with an enzyme. Label-free receptor-based biosensing methods with minimal sample processing steps have also been explored in order to overcome some of the limitations of conventional techniques related to AHL detection. Label-free receptor based biosensors transduce the phenomenon of binding into a measurable signal using various transduction techniques including optical, acoustic, thermal, electrochemical and magnetic. Optical biosensors, including surface plasmon resonance[250,251], and electrochemical biosensors including differential pulse voltammetry (DPV)[228] and cyclic voltammetry (CV)[252], have achieved remarkable sensitivities comparable with the standard methods used in the context of AHL detection. However, these methods have certain drawbacks as well. The necessity for an electroactive biomolecular target, high interfacial charge resistance and a well-constructed reversible thermodynamic interface between the receptor layer and the transduction element make operation of miniaturised electrochemical biosensing techniques very challenging[253].

The objective of this work was to develop a gravimetric biosensor for the rapid, label-free, simple, and specific detection of AHL. *N*-hexanoyl-L-homoserine lactone (C6 HSL) was used as a model template in this work. The performance of the biosensor was evaluated by determining a calibration curve and selectivity using dopamine as a reference compound. In addition, the results were supported by a surface plasmon resonance experiment. However, the minimum C6 HSL concentration tried for that work was only 0.1 μM.

Molecularly imprinted polymers (MIPs) have been used as receptors for C6 HSL. Nanoparticles would have the performance features of MIPs such as stability over a wide pH range, pressure and temperatures. They have received increasing attention due to their superior properties such as the large surface area to volume ratio, which results in easily accessible binding sites that are more homogeneous due to the lack of any need for a grinding process[254]. Generally, nanosized particles can help to improve detection range, increase affinity, enhance conductivity, increase surface-to-volume ratio, and would be more beneficial for sensor applications.

The concept behind the formation of the selective binding sites in MIP NPs for HSL is shown schematically in Figure 2.4 . In brief, the template is immobilised on the solid phase support (glass beads). After that, the activate glass beads are polymerised under the UV light in the presence of functional monomers, cross-linking, iniferter, chain transfer agent, and appropriate solvent. Molecular imprinted polymers nanoparticles (MIP NPs) have been used as receptors for C6 HSL.

3.3 Materials and Methods

3.3.1 Materials

α-amino-γ-butyrolactone hydrobromide, *N*-butyryl-L-Homoserine lactone (C4 HSL), *N*-Hexanoyl-L-homoserine lactone (C6 HSL), dopamine, dodecanedioic acid, 2-(*N*-morpholino)ethanesulfonic acid (MES), 3-aminopropyltrimethyloxysilane (APTMS), sodium hydroxide (NaOH), *N*-hydroxy-succinimide (NHS), 1-ethyl-3-(3-dimethylaminopropyl)-carbodiimide hydrochloride (EDC), ethylene glycol dimethacrylate (EGDMA), trimethylolpropane trimethacrylate (TRIM), pentaerythritol tetrakis(3-mercaptopropionate) (PETMP) were from Sigma-Aldrich, UK. Sodium carbonate (Na_2CO_3), sodium chloride (NaCl), dimethylformamide (DMF), acetonitrile (ACN), acetone and Phosphate-Buffered Saline tablets (PBS) were procured from Fisher Scientific, UK. *N*,*N*-diethyldithiocarbamic acid benzyl ester (iniferter) was procured from TCI Europe. All solvents were HPLC Grade. Glass beads with diameters in the range of 63-106 µm were from purchased from Potters Industries. Double-distilled ultrapure water (Millipore, UK) was used for the experiments. All chemicals and solvents were high purity and they used without further purification.

3.3.2 Tools

1. SPR experiments were carried out using a BIAcore 3000 SPR system (GE Healthcare, UK) and the final Data were analysed via BIAevaluation Software v4.1.
2. The main equipment used for these experiments were a SensAND Network Analyser (University of Cambridge, UK) comprising of a signal generator, low-pass filter and high-pass filter, amplifier, flow cell/microfluidic cartridge printed circuit board (PCB) and a desktop computer. A pure sinusoidal wave with a frequency of around 14.3 MHz (1f) was generated by the SensAND instrument and was amplified. The alternating electrical input signal was filtered using the low-pass filter and then passed through the quartz resonator in order to remove any undesirable harmonic distortions. The high-pass filter was included in the output side as a provision to record transduced electrical signals at higher-order harmonics. The in-phase and quadrature components of the transduced electrical

signal measured at the driving frequency (1f) were captured using the SensAND. The transduced electrical signals were amplified before recording. The output signal was recorded by the SensAND control software and then displayed using a desktop computer.

3. Quartz crystal resonator: The quartz crystals have been supplied from LapTech Precision Inc., Bowmanville, Ontario, Canada. The fundamental crystal frequency lay within the range of 14.275 MHz to 14.325 MHz. The quartz substrate was sandwiched between two circular gold electrodes that were 5 mm and 4 mm in diameter, respectively.
4. Software**:** The SensAND control software (University of Cambridge, UK) was run to record the transduced electrical signal. The Wolfram Mathematica 10 software was used to analyse and calculate the resonance frequency shift data.

3.4 Methods

3.4.1 Molecular Modelling

Molecular modelling allows the formation and improvement of molecular geometry through a computational strategy to determine the bond lengths, bond angles and torsions and helping to select low energy conformations of molecules. The computational simulation technique gives information to evaluate the binding energies, electrostatics, interaction geometries and bulk properties such as monomer-template ratio[255].

Based on molecular modelling, previous studies have suggested that MAA and IA can bind strongly with HSL[226,256-258]. Furthermore, itaconic acid and methacrylic acid were selected based on the binding energy as the best monomers due to their strong interactions with 3-oxo-C6 HSL, C4 HSL and C6 HSL[256]. The monomers were selected from a library containing 20 of the most regularly used commercial monomers[84].

MIP NPs containing MAA have the capability to recognise the analyte of interest (AHL). The keto-functional group of the target (AHL) is appropriate for binding with acidic monomers (MAA or IA)[259]. The MAA is one of the most popular commercial monomers and is regularly used as backbone monomer in molecular imprinting. The methyl group present in MAA allows for conformational changes and rotations, and also offers van der Waals interactions, when compared to other monomers such as acrylic acid[80].

Moreover, Cavaleiro used computer modelling to select the most suitable monomers for HSL to synthesise MIP. The IA and MAA monomers as in previous case were selected by computer modelling due to the strong binding with the HSL. Molecularly imprinted polymer nanoparticles (MIP NPs) which contained MAA have a good recognition capability for the analyte[257].

In addition, methacrylic acid (MAA) is one the most commonly used functional monomers in noncovalent approaches for MIP preparation. This monomer can work as a hydrogen bond donor and acceptor, capable of establishing ionic interactions[260].

3.4.2 Molecular Imprinting

Free radical polymerisation included three steps: initiation, propagation and termination. Initiation involved the formation of a free-radical active centre through two steps. The initiator (*N*,*N*-diethyldithiocarbamic acid benzyl ester) formed free radicals, and one of those free radicals was added to the functional monomer (IA or MAA) under UV light. The propagation step, the core of the process, included the growth of the polymer chain by rapid sequential addition of the monomer to the carbon-based free active centre. Basically, a number of monomer units were added to each initiator molecule, and this determined the molecular weight of the final material. In the termination step, the active centre was irreversibly destroyed and propagation ceased[261]. To control the polymerisation process under UV light and particals morphology, a chain transfer agent was also added. Nanoparticles for sensor application were prepared using solid-phase approach to obtain a particle with size range of 100-250 nm.

3.4.3 Solid-Phase Synthesis of MIP NPs

3.4.3.1 Preparation of Derivatives Glass Beads as Solid-Phase Media

Glass beads were prepared following the method described by Cavaleiro with slight modifications[257]. The glass surface coating was stripped out using a Retsch Vibratory Sieve Shaker (AS 200) for 3 hours with 80% amplitude. After that, the beads were boiled in 2 M NaOH for 15 min then cooled down for 30 min. Beads then washed sixteen times (seven times with DI water, one time with 2 M HCl, four times with DI water, two times with PBS and finally two times with DI water) then pH has been adjusted to 6.5. Lastly, beads were washed with acetone and then dried under vacuum and an oven at 150°C for 2 h to remove the acetone residue. Next step to introduce the amino group on the beads surface, beads were then incubated for 24 h in anhydrous toluene solution of APTMS (3%). To remove unreacted APTMS, beads washed six times with ethanol and water and dried for 24 hours in oven at 80°C.

For template immobilisation, in case of dopamine, beads were incubated for 2 h in a 0.01 M PBS solution of glutaraldehyde (GA) at 4°C. After that, beads washed with DI water. The dopamine was immobilised on the beads surface by incubating the beads with a solution of template (1 mg ml^{-1}) in PBS (pH 7.4) overnight at 4°C. Later, unbound dopamine was removed from the beads surface by washing with DI and incubated with $NaBH_4$ (1 mg ml^{-1}) in PBS (0.4 ml per gram of beads) for 30 min at RT to reduce the Schiff base bonds on the glass beads. Finally, the glass beads were washed with DI water and dried under vacuum and stored at 4°C. Dopamine MIP was used as a reference.

For HSL immobilisation, (S)-(−)-α-amino-γ-butyrolactone hydrobromide was used as a starting template. It was connected with dodecanedioic acid by EDC/NHS chemistry to link carboxylic groups with primary amino group according to the Thermo Scientific protocol[262]. The activation reaction with EDC/NHS took place at room temperature, but the pH had to be adjusted to 6.0. Briefly, activation buffer was prepared by mixing 2.17 g of MES (0.1 M) with 2.92 g of NaCl (0.5 M) in DI and then adjusting the pH to 6.0 by adding NaOH (1 M) in a dropwise manner. An activation mixture was then prepared in a 50 ml bottle as follows: 125 mg of dodecanedioic acid (5.43×10^{-4} mol) was dissolved in 20 ml DMF, after which 1 g of EDC (5×10^{-3} mol), and 0.21 g of NHS (18.2×10^{-3}

mol) were dissolved in 10 ml of fresh activation buffer; this was then added to the dodecanedioic acid solution and mixed well. The glass beads functionalised with APTMS were incubated for 20 minutes in this solution and then washed with a DMF: water (1:1), activation buffer and acetone. Template was immobilised on the surface of the beads by incubating the glass beads functionalised with the activated dodecanedioic acid in an aqueous solution (50 ml) containing 79.08 mg of (S)-(−)-α-amino-γ-butyrolactone hydrobromide (4.344 x 10^{-4} mol) and 46.02 mg of sodium carbonate (4.344 x 10^{-4} mol). The immobilisation was carried out for 3 hours. The glass beads were washed with 50% DMF in DI water, followed by DI water alone. Finally, the glass beads were dried under vacuum and stored in the fridge until use.

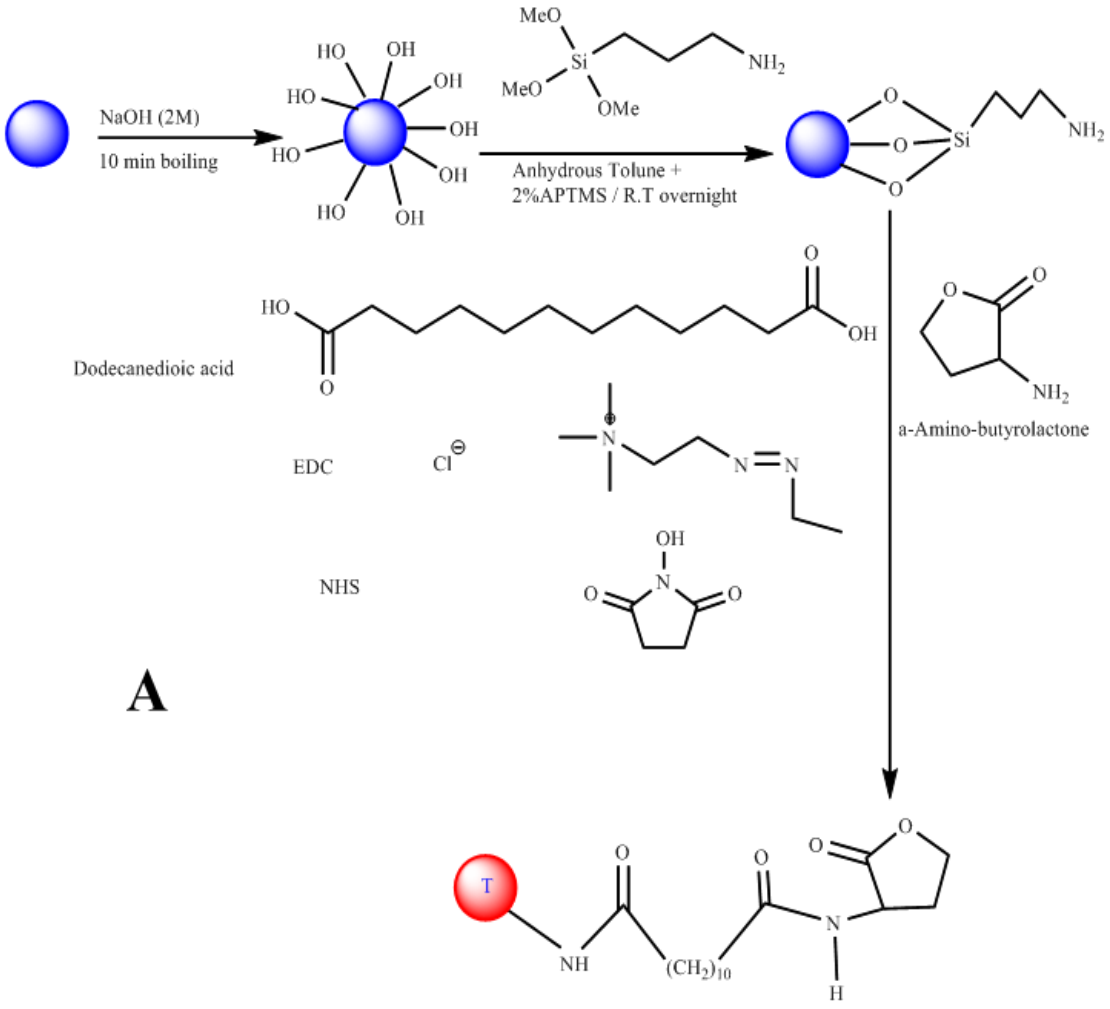

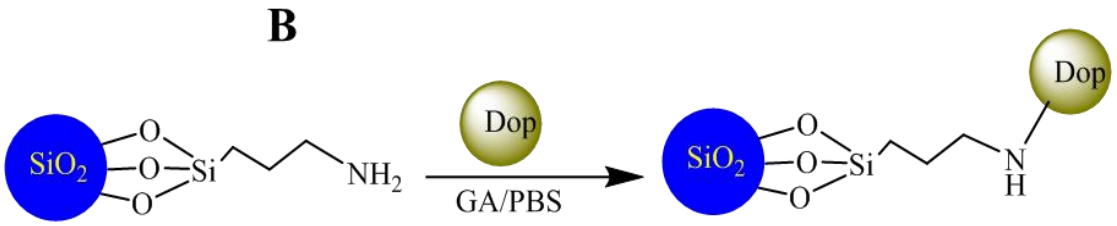

Figure 3.2: Scheme of the glass beads modification with 3-aminopropyltrimethoxysilane (A) HSL immobilisation (B) Dopamine immobilisation

3.4.3.2 Synthesis of MIP NPs

The organic and water polymerisation were performed using different functional monomer. In both cases, the components were dissolved in the corresponding solvent, sonicated for 10-15 min, and purged with nitrogen for 30 min to deoxygenate the solution. The polymerisation mixtures were added to the glass beads functionalised with the corresponding template (

Table 3.1). Organic polymerisation processes were initiated by UV light for 2 min. After polymerisation, the contents were transferred into a cartridge (60 ml syringe tube) fitted with a polyethylene frit (20 mm porosity). Unreacted monomers and low-affinity particles were eluted and washed away by cold DMF/ACN (0-5 °C). For next step, the solvent temperature (ACN) was raised to 60-65°C in order to break down the non-covalent interactions between the template attached to the solid-phase and MIP NPs, thus allowing a pure fraction of the high-affinity particles to be free from residual template and monomer species to be collected (Figure 3.3).

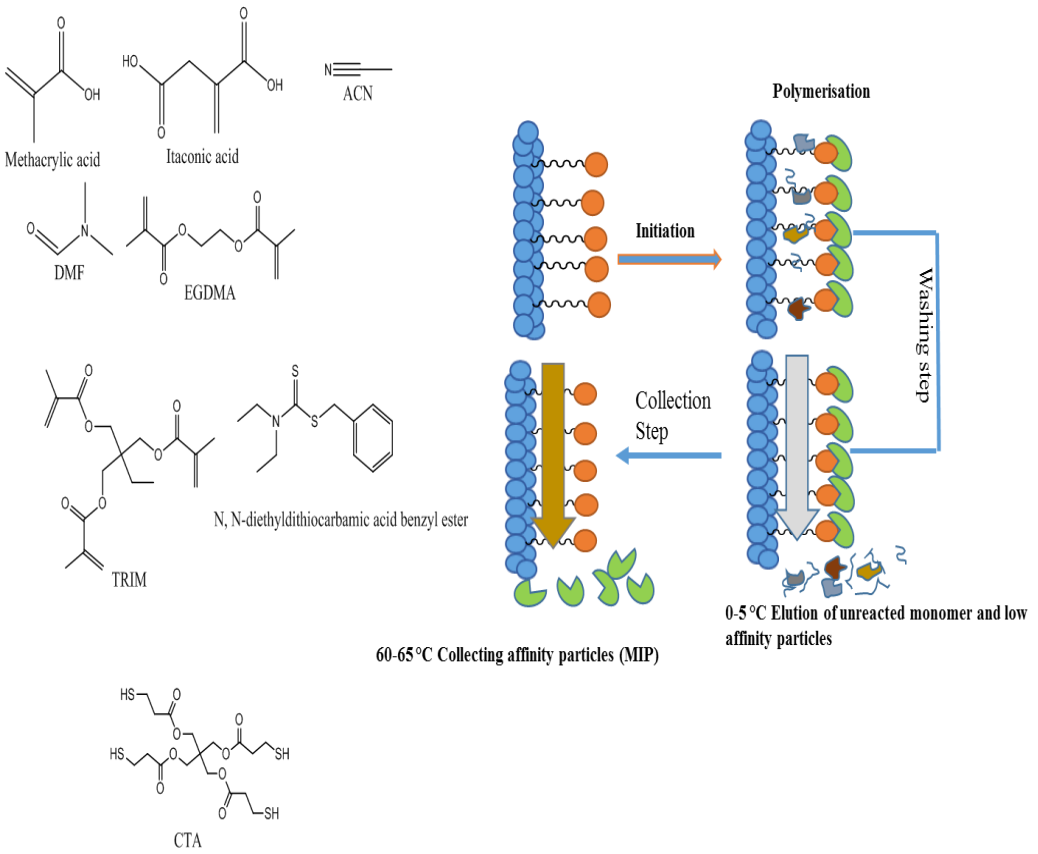

Figure 3.3: Schematic representation of the solid-phase synthesis of MIP NPs

Table 3.1: Polymerisation conditions and mixtures.

Components	Organic MIP NPs		
	HSL MIP (MIP 1)	HSL MIP (MIP 2)	Dopamine (Reference MIP)
Glass beads, g	40	40	40
DMF, g	-	22.4	-
ACN, g	17.55		17.55
MAA, g	4.8	-	4.8
IA, g		7.24	
EGDMA, g	5.4	5.4	5.4
TRIM, g	5.4	5.4	5.4
Iniferter, g	1.255	1.255	1.255
PETMP, g	0.3	0.3	0.3
Radiation time, (UV) min	2.0 min		
Cold wash, ml	2x 20 ml of DMF+ 6x 20 ml of ACN for (MIP based IA) while cold ACN was used only for Reference MIP and MIP based MAA		
Elution, ml	5x 20 ml of hot ACN (60-65°C)		

3.4.4 Dynamic Light Scattering Analysis (DLS) of MIP NPs

DLS has many advantages for measuring MIP particle size and it is commonly used to evaluate the hydrodynamic dimensions of nanoparticles. DLS measurements can be performed in a relatively short time and the sample can be reused for other measurements. In addition, this technique is particularly sensitive to the presence of small aggregates. For this reason, the sample should be sonicated before any measurement to remove or reduce any aggregated particles[263]. The size of the MIP was analysed by taking the eluted fractions and sonicating it for 2 min. After that, the fractions were filtered using a 1.2 μm filter and injected into disposable polystyrene cuvettes and analysed at RT using a Zetasizer Nano (Nano-S) from Malvern Instruments Ltd. (Malvern, UK).

3.4.5 Scanning Electron Microscopy Analysis

Scanning electron microscopy (SEM) was used to characterise the morphological features of the MIP NPs. SEM uses electrons to scan the sample and produce the image. The electrons beam interacts with the sample's surface atoms to give information about the morphological features of the surface. The data is collected by scanning a selected sample area ranging from a few cms to micrometres in size. A Hitachi s3000h scanning electron microscope with an accelerating voltage of 10kv was used to get images of MIPs particles. Samples for the analysis were prepared by depositing a drop of the concentrated MIPs which previously filtered through a 1.2 μm syringe filter on the surface of QCR crystal then mounted onto aluminium stubs using carbon sticky tabs and coated with gold/palladium in a quorum q150 TES coating unit. The measurements were taken at College of Science/the centre for Core Biotechnology services/Electron Microscopy Facility.

3.4.6 Surface Plasmon Resonance

3.4.6.1 Preparation of BIAcore Gold Chips

Au-coated chips (SIA Kit Au, BIAcore) were treated with hydrogen plasma to remove any substances on the surface of the BIAcore chip. After that, the gold chip was placed in a solution containing cystamine (10 mg / 10 ml of EtOH) for 24 h, after that chip washed with ethanol and DI water and dried under N_2. This process presents amino groups onto the surface. EDC/NHS chemistry was used to bind the MIP NPs with the surface (prior measurements MIP NPs have been concentrated, washed and converted to PBS). Reference MIP measurements were performed in the same manner.

3.4.6.2 Preparation of Samples for BIAcore Experiments

The BIAcore chip was modified with cystamine to introduce amino group in the surface. The MIP sample and reference (Dopamine MIP) were sonicated for 3 min prior use. At the same time, serial dilutions of template were made using sample buffer (0.01 M PBS). 500 µl of each concentration were prepared in Eppendorf tubes. The decision to increase or decrease the concentration of the template was determined by the BIAcore experiment itself. Examples of the dilutions used are: 1:1, 1:2, 1:4, 1:8, 1:16, 1:32, 1:64, 1:128 and 1:256.

3.4.6.3 Running the BIAcore Experiment

The BIAcore is an automated system that only requires the sample to be placed into a given compartment. The rest of the experiment is controlled by the BIAcore software. For MIP NPs based MAA as functional monomer and control MIP, EDC/NHS was mixed with MIP and docked onto the BIAcore instrument to activate the carboxylic group of MIP NPs to react with the amino modified chip surface (channel one and two MIP) while (channel three and four for the control MIP). PBS 0.01 M was used as a running buffer and the flow rate was 15 µl/min. For the experiment, 100 µl of C6 HSL injected for the (first and third channel), C4 HSL injected through (second and forth channel). KINJECT mode was used which has fixed times between injections in order to monitor dissociation. Injections started with the most dilute (low concentration) to least dilute (high concentration). The evaluation of the results was carried out using the BIAevaluation software. The same steps were performed for MIP NPs based on IA as functional monomer.

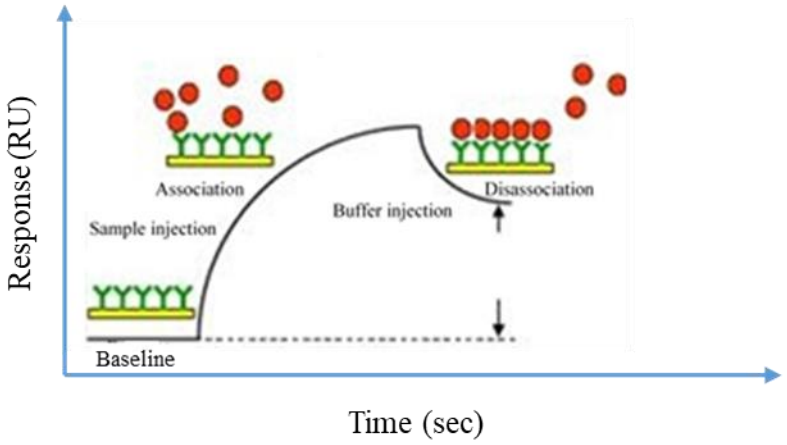

Figure 3.4: SPR sensorgram

3.4.7 QCR Sensor

A novel QCR sensor based on the fixed frequency drive (FFD) technique for rapid, sensitive and label-free detection of AHL using C6 HSL as a model QS molecule has been developed. Molecularly imprinted polymers (MIPs) have been used as receptors for C6 HSL. An experiment involving the detection of the C6 HSL molecule at a particular concentration was carried out using an AT-cut thickness-shear-mode QCRs comprising a fundamental frequency of 14.3 MHz. The QCR was functionalised with MIP NPs. The functionalised QCR was placed between an acrylic microfluidic flow cell to allow a controlled injection of the sample, and a printed circuit board (PCB) to facilitate the electrical connection. The actuation and electrical sensing for the QCR were achieved by employing a custom-built network analyser. The sensor assembly consisted of three main parts: a microfluidic cartridge, quartz crystal resonator (QCR) and a printed circuit board (PCB) (Figure 3.6). A sample chamber of 13 µl volume was formed when the microfluidic cartridge was clamped above the QCR and PCB. A quality factor of 1900 was obtained when the assembled QCR was filled with a liquid solution.

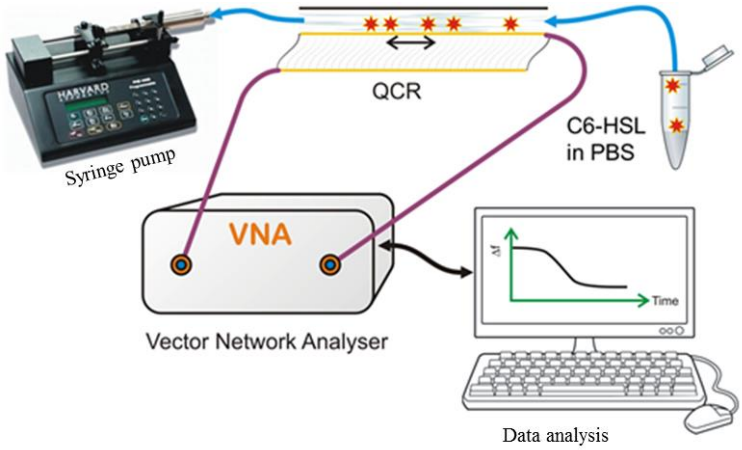

Figure 3.5: QCR experiment process

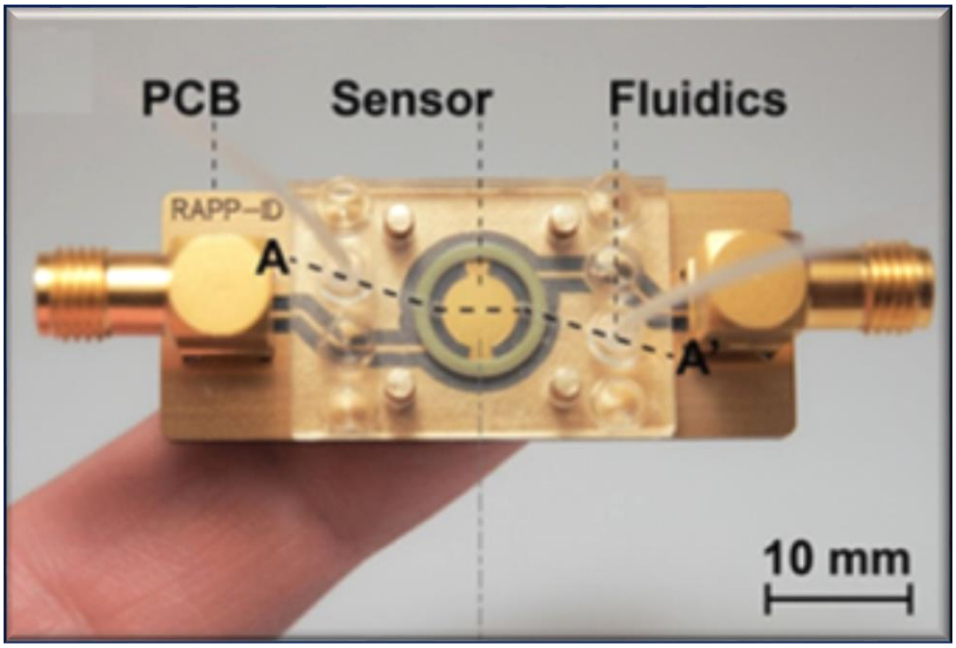

Figure 3.6: Assemble QCM sensor. Adapted from reference [245]

3.4.6.1 Protocol for Cleaning the QCR Crystal

Cleaning of quartz crystals: the quartz crystal was immersed in a petri dish filled with acetone and sonicated for 2-3 minutes followed by further sonication for 4-5 minutes in isopropanol, after which the crystal was dried using nitrogen gas. After that, the crystal was placed in a plasma cleaner for 3 min to remove impurities and contaminants using hydrogen gas.

3.4.7.1 Protocol for Immobilisation of HSL MIP NPs on QCR Crystal

1. The cleaned QCR crystal was incubated overnight in an ethanolic solution of cystamine (0.2 mg/ml). The MIP NPs solution was concentrated under N_2 gas then transferred from the acetonitrile to water by using centrifugal filter cartage. The QCR crystal, after overnight incubation with cystamine, was washed it many times with ethanol and water. The activated MIP NPs solution was prepared by adding EDC to the MIP NP solution (offline activation). The activation with EDC was used more than one time with new MIPs solutions. Cystamine-functionalised QCR was incubated for 20 minutes in an activated MIP NPs solution.

The protocol for preparation of C6 HSL stock solution. 5.9 mg of C6 HSL with a molecular weight of 199.2 Da was added in 3 ml PBS to prepare 0.1 M C6 HSL stock solutions.

2. Immediately pass 200 µl of ethanol through the flow to remove air bubbles. Immediately inject 8 ml of degassed double-distilled water at a high flow rate (syringe handle by hand).
3. Connect PCB to the SensAND/ADT instrument and turn it on.
4. Measurements in PBS: PBS buffer was flowed for 30 minutes as a baseline measurement at a flow rate of 40 µl/min in order to achieve stability.

5. Template was injected directly after the base line at the same flow rate.

3.5 Results and Discussion

3.5.1 Synthesis of MIP Nanoparticles

The first step was to mechanically remove the silane coating from the glass beads, which were then boiled in NaOH to activate their surfaces (i.e., introduce hydroxyl groups). Hydroxyl groups can react with silane compounds (APTMS) to add silyl linkers onto the beads (i.e., introduce amino groups). In order to investigate the modification of glass beads with amino groups, the ninhydrin test was undertaken.

Figure 3.7: Ninhydrin test for amino modified glass beads

In case of Dopamine, when that the primary amino groups cover the glass bead surface, GA was used to connect these groups with the other amino groups present in the dopamine structure, producing a Schiff base bond. Both APTMS and GA allow for the reduction of potential steric hindrance problems during the polymerisation, arising from the overloading of the template on the glass beads surface[67]. After that the same polymerisation process was carried out.

In case of HSL, the amine group on the beads reacted with the dodecanoic acid, which acts as a spacer on the glass surface. The EDC/NHS chemistry starting template (S)-(−)-α-Amino-γ-butyrolactone hydrobromide) can couple to the carbonyl group to form an imine bond (Figure 3.2 A). The iniferter was used for the polymerisation process. Nano MIPs s were prepared using MAA and ITA as monomers, as mentioned previously. The MIP prepared using ITA as a monomer was different to the MIP prepared by MAA because that ITA is not soluble in ACN. Therefore, ITA had to be initially prepared in DMF then ACN was used to remove the low affinity and unreacted polymer after that warm ACN (60 °C) was used to collect the high affinity nanoparticles. The organic polymerisation chosen here was useful, since as confirmed previously, the concentration of the organic polymer particles was about 20 times higher than this in water[256, 257]. The main advantage of the use of solid phase methodology was that since the template is immobilised onto the solid phase, the removal of the template is unnecessary, all that is required is to wash the NPs from the solid phase. Additionally, the template can be modified by different chemical strategies and template analogue can be used, if required. MIPs with binding site on their surface should also have superior binding kinetics. Thus, this approach overcomes the problem of template leeching into the MIP. The use of the solid phase can be automated, which has been achieved by the Leicester Biotechnology Group[16].

3.5.2 Characterisation of MIP NPs

3.5.2.1 Dynamic Light Scattering (DLS)

DLS was used to measure the size of the particles. The main advantages of DLS technique are simplicity, sensitivity and short time of measurement. In addition, it is cheaper than SEM and the sample can be reused. Therefore, this technique is increasingly used for NP characterisation in many fields. Although the DLS technique is widely used for particle characterisation, there are some problems regarding measuring samples with large size distributions. The MIP NPs were filtered through a 0.75 μm filter to remove any larger particulates prior to testing. MIP NPs have been known to aggregate in solution over time. In this circumstance, the MIP NPs should be sonicated for a few minutes to reduce any aggregation. Regarding manufacturing of MIP NPs, better homogeneity of batches can be achieved by using automated synthesizer[16].

Table 3.2: MIP NPs size by DLS.

Type of MIP	Size (nm)±	PDI±
MAA- HSL MIP (MIP1)	223.9 ± 9.51	0.296 ± 0.028
ITA-HSL MIP (MIP2)	269.7 ± 16.3	0.492 ± 0.13
Reference MIP or MIP 3	299.6 ± 17.23	0.459 ± 0.095

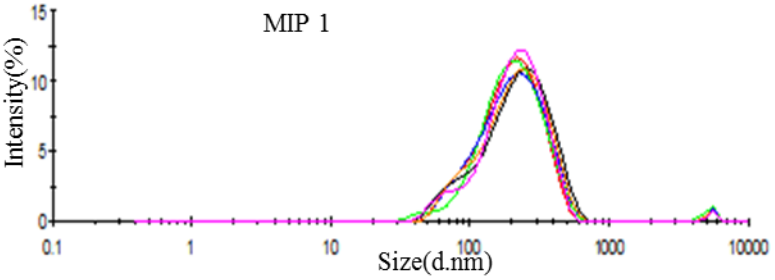
MIP 1
Intensity(%)
Size(d.nm)

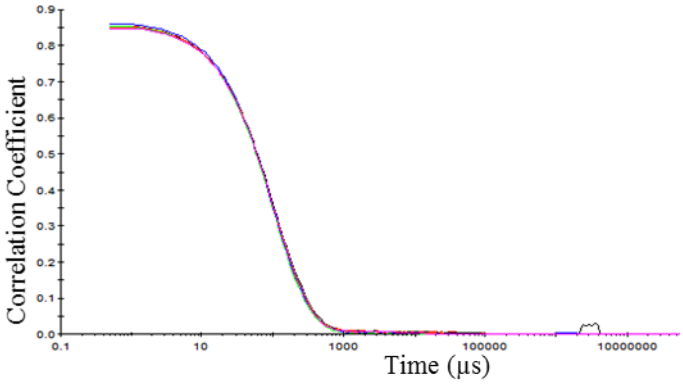
Correlation Coefficient
Time (µs)

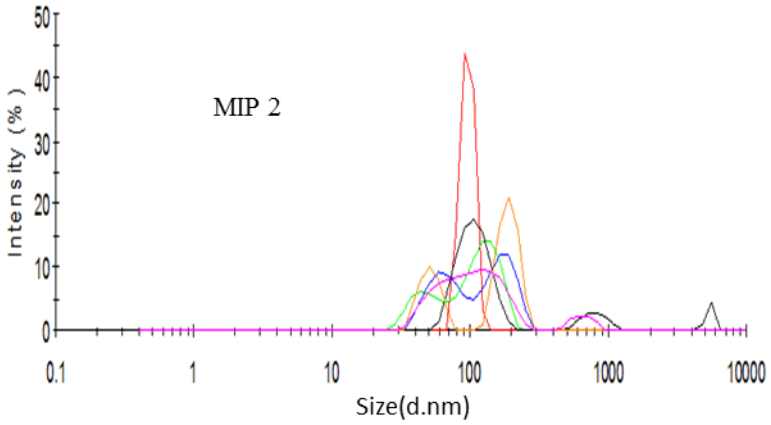
MIP 2
Intensity (%)
Size(d.nm)

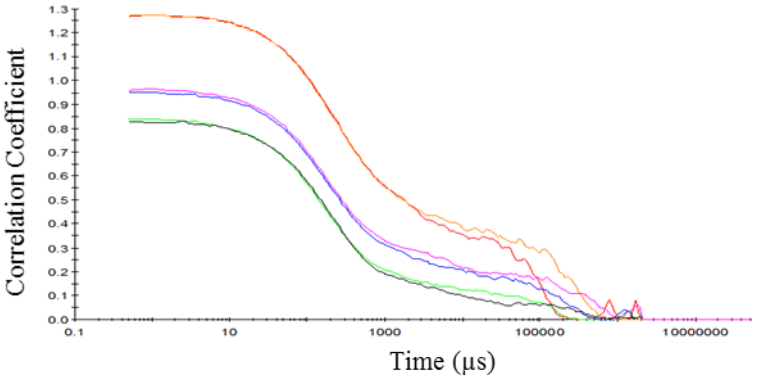
Correlation Coefficient
Time (µs)

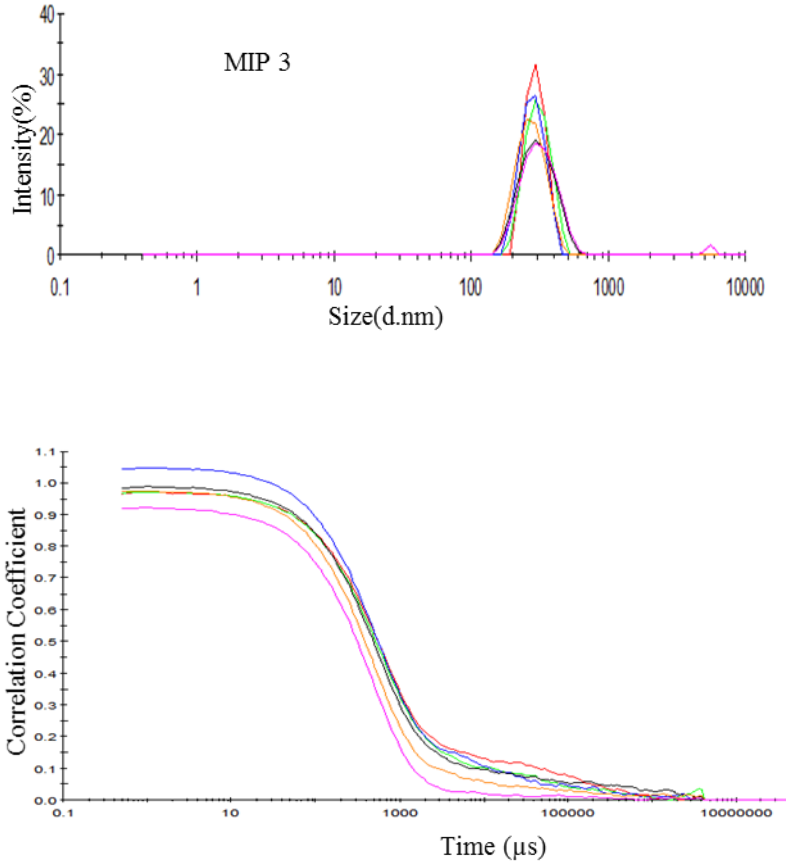

Figure 3.8: Dynamic light scattering (DLS) size distributions and correlation of HSL MIP with reference MIP

From the DLS charts, it can be seen that there is a diffrences between MIP NPs preperd for HSL using different monomer (MAA, ITA). It can be seen that the MIP NPs (MAA) was more homogenious and there is no aggregation effect was found. Futhermore, the particals size was smaller the MIP 2 and MIP 3. The correlogram can give an information about the sampl as the time at which the correlation starts to notebly decay is asign of the mean size of the sample. The steeper the line, the more monodisperse the sample is. Contrariwise, the more extended the decay becomes, the greater the sample polydispersity. Howevor, the MIP 2 looks unpure, aggregate and the sample was polydispersity. As you shown in Figure 3.8, MIP I has uniform particles and one type of particles was present in the sample. Furthermore, there is no aggregation has been noticed. On the other hand, MIP 2 was polydisperse and more than on type of particles

has been shown. However, the sample has been sonicated for 2 min but still has some aggregation effect.

3.5.2.2 Scanning Electron Microscopy

The morphology of the particles is evaluated using scanning electron microscopy. SEM analysis showed more than one population of NPs for the particles synthesised using 2 min of irradiation time (Figure 3.9). SEM images confirmed the successful MIP NPs immobilisation using self-assembling monolayers (SAMs). It should be noted that the size of the particles determined by SEM differs from the results of DLS. It is common for DLS results to be different from the ones obtained by SEM because SEM is performed with dry and concentrated particles. It is clear that the NPs population appeared to include both single particles and small aggre gates.

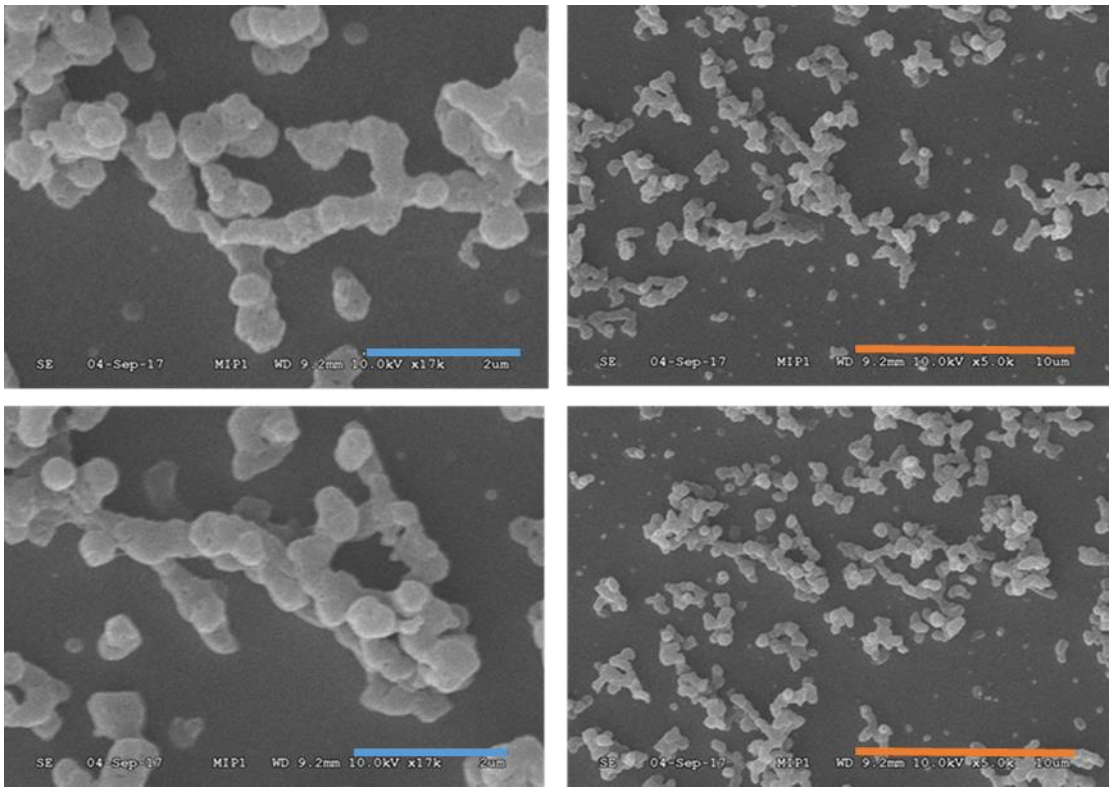

Figure 3.9: SEM images of dry MIP nanoparticles

3.5.2.3 Affinity Analysis

The affinities between MIP NPs and homoserine lactone compounds (C4 and C6 HSL) were evaluated using BIAcore technique. The MIP NPs and NIP (reference MIP) were immobilised on a BIAcore gold chip by self-assembling. For the BIAcore experiments, all MIP NPs were tested with C4 and C6 HSL. MIP based on IA as functional monomer did not show any response for C4 and C6 HSL. However, MIP based on MAA as functional monomer showed response toward C6 HSL only. The sensorgram showed a huge increase in response units compared to control MIP characteristics of a binding to C6 HSL (Figure 3.12). The dissociation constants for C6 HSL was 1 x 10^{-6} M. The level of response is proportional to the mass of the analyte, so when injecting a relatively small molecule (compared to biomolecules which the BIAcore was designed for) such as HSL it gave a small response. The BIAcore 3000 specifies a detection limit greater than 180 g/mol which is nearly identical to C6 HSL. Since there was evidence of some binding using this method, an optimisation of the process would allow this to work. In the following work, MIP based on MAA as functional monomer was used for the QCR sensor.

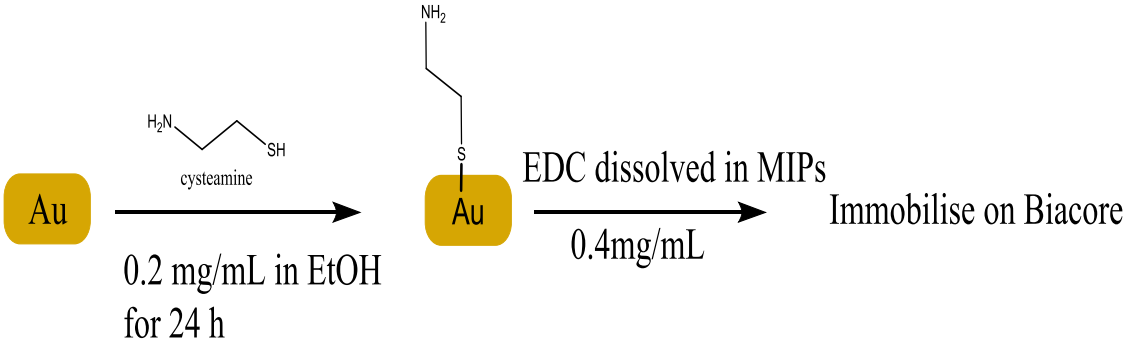

Figure 3.10: Cystamine-derived chip for immobilising MIP NPs on the gold surface

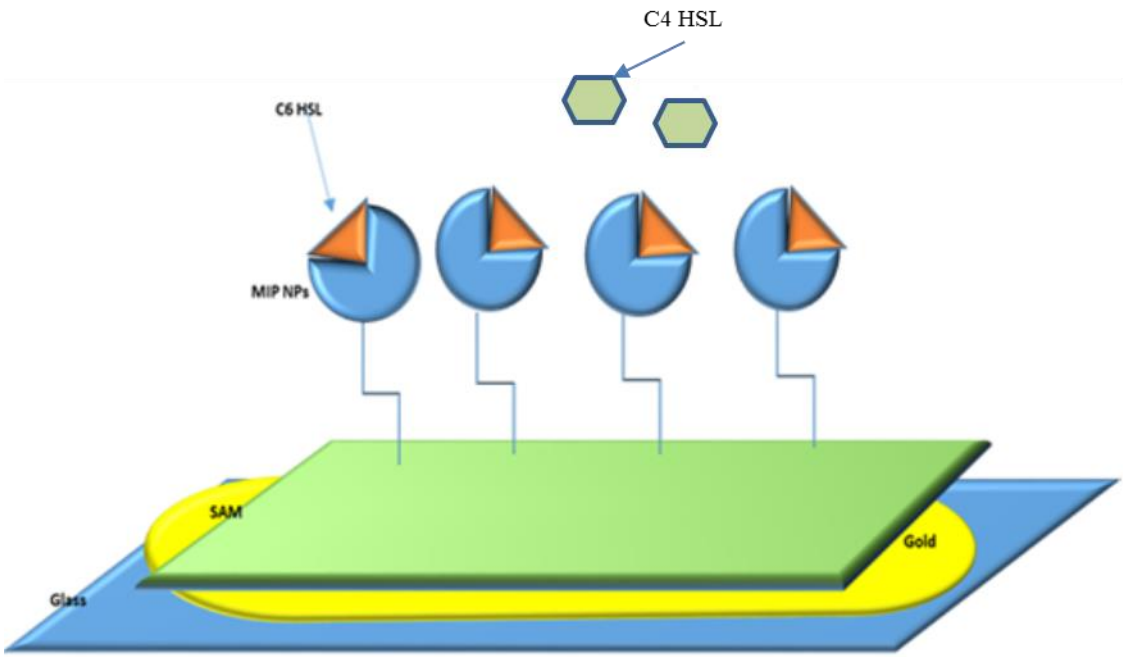

Figure 3.11: Schematic presenting the method used in the BIAcore experiments

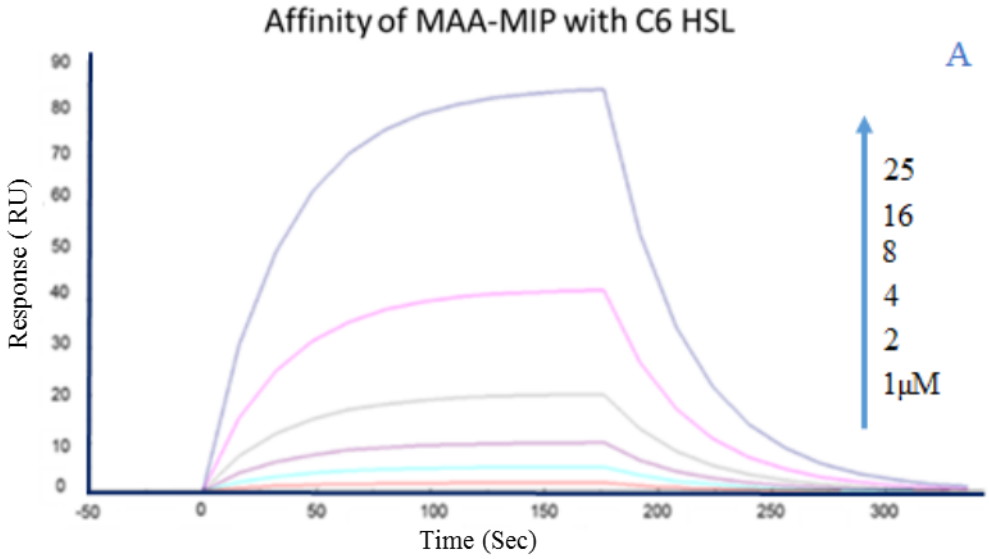

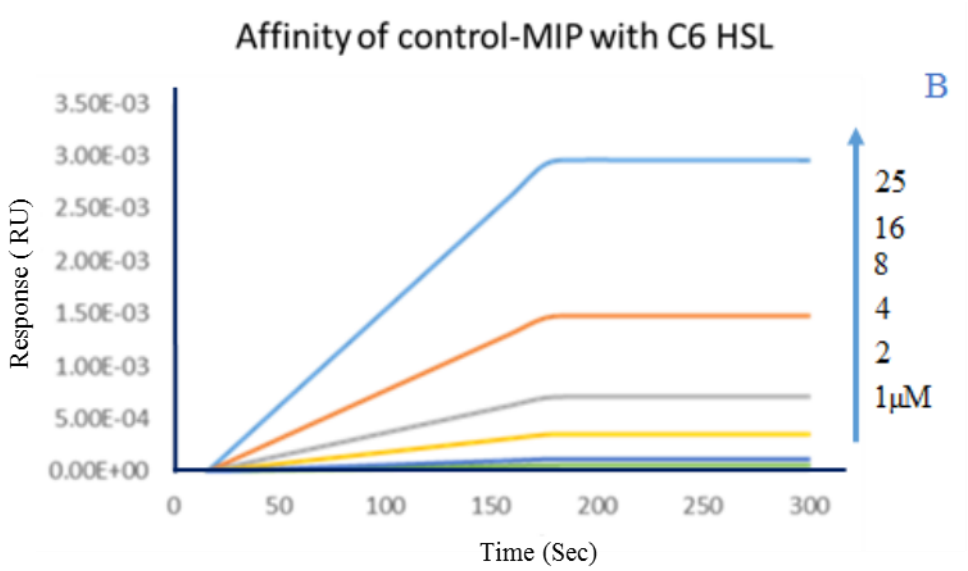

Figure 3.12: (A) MIP based MAA binding to C6 HSL (B) Control MIP binding to C6 HSL

3.6 QCR Sensor for Detection of C6 HSL

The experiment involving detection of the C6 HSL molecule at a particular concentration was performed using an AT-cut thickness-shear-mode QCRs with a fundamental frequency of 14.3 MHz. The functionalised QCR was placed in between an acrylic microfluidic flow cell to allow the controlled injection of the sample and a PCB to enable the electrical connection. The actuation and electrical sensing for the QCR were achieved by employing a custom-built network analyser. The details of the experimental setup and MIP NPs immobilisation procedures have been noted in the **Materials and Methods** section.

A baseline was established for 30 min by recording frequency sweeps (0.1 sec, 0.52 V) and fixed frequency/ FFD scans (0.1 sec, 0.47 V) every 2 min in PBS buffer. During baseline measurements, PBS was flowed (at 40 µl/min) over the functionalised QCR. Subsequently, C6 HSL solution in PBS buffer was injected (at 40 µl/min) after baseline measurements into the microfluidic cartridge for 30 min in order to evaluate binding of C6 HSL with MIP NPs. During the binding phase, similar frequency sweeps and FFD scans as mentioned above were performed. The concentration of C6 HSL solution in PBS

was varied from 1-50 µM. Estimation of the resonance frequency shifts gained from the FFD and FS methods at every measurement point were in good agreement with each other during the baseline and C6 HSL binding phases for a particular concentration (Figure 3.13A). The baseline noise estimated in each case for the FS and FFD methods were 1.48 Hz (SD, $\sigma = 0.63$ Hz) and 1.83 Hz (SD, $\sigma = 0.46$ Hz), respectively. The resonance frequency shifts estimated from each of the two methods after 30 min of C6 HSL injection at a given concentration due to MIP NPs binding also showed reasonable responses (Figure 3.13 B). The agreement varied between -10.33 to 13.46 Hz over the range of C6 HSL concentrations explored (Figure 3.13 C). The C6 HSL biosensor developed was capable of detecting 1 µM C6 HSL solution in PBS in 10 min using a sample volume of 400 µL with linear range of 1-50 µM.

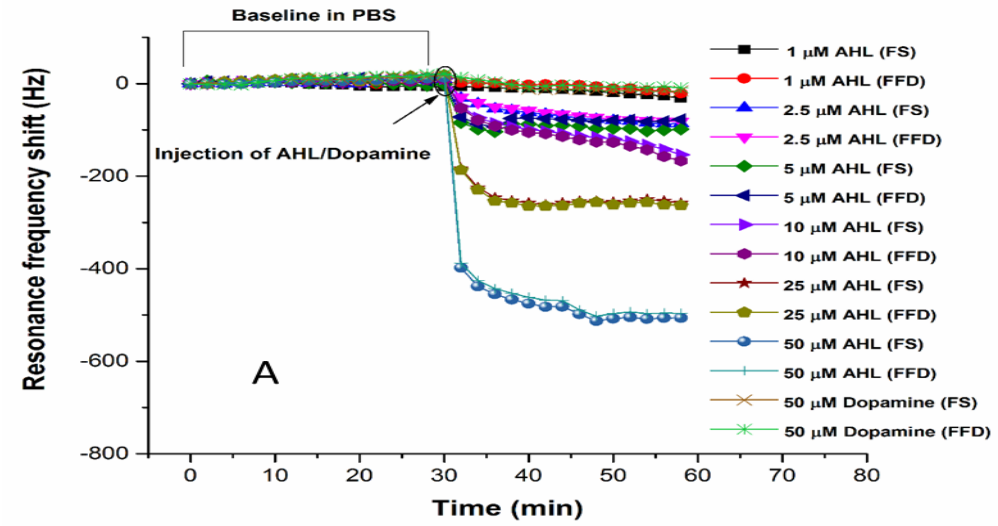

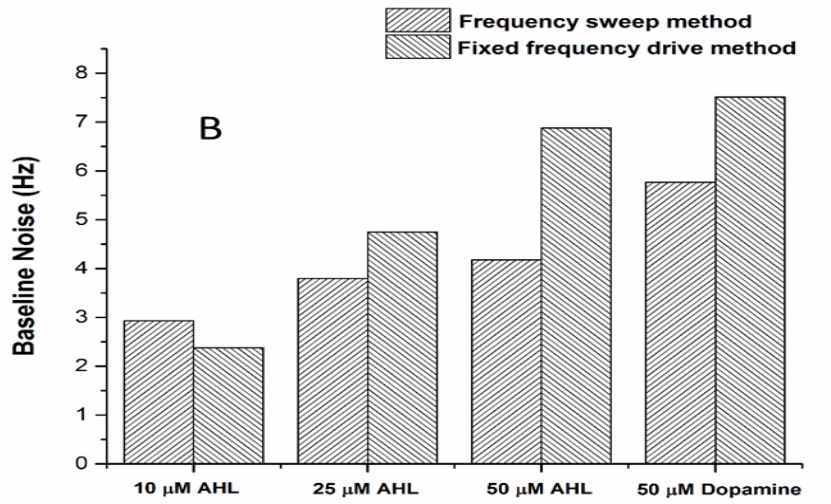

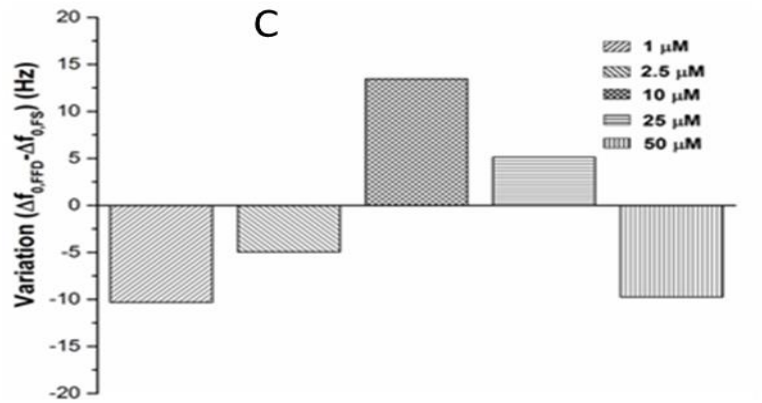

Figure 3.13: (A) Resonance frequency shifts due to C6 HSL binding using the frequency sweep and FFD methods for different concentrations. (B) Resonance frequency shifts 30 min after C6 HSL injection for different concentrations. (C) Variation in the resonance frequency shifts after 30 min for FFD (at different concentrations of the injected C6 HSL) with respect to the frequency sweep (FS) method

3.7 Selectivity of the MIP NPs

Dopamine was selected as a reference for selectivity study because it has similar molecular weight (153.18 Da) to C6 HSL (199.2 Da) and charge appropriate for interaction with MAA. PBS was flowed (at 40 µl/min) over HSL MIP NPs-functionalised QCR for 30 min followed by subsequent injection of 50 µM dopamine at the same flow rate. Similar measurements were taken during PBS and dopamine injections as mentioned in the Detection of C6 HSL section. Another set of experiments with identical measurements were conducted where PBS was flowed (at 40 µl/min) continuously over the functionalised QCR for 60 min. Negligible changes in the conductance spectrum were observed between the two frequency sweeps taken at an interval of 60 min during PBS and 50 µM dopamine injection experiments in comparison to the 50 µM C6 HSL injection experiment (Figure 3.14a). The estimated resonance frequency shifts obtained with respect to the first measurement point after 60 min using the FS technique for PBS, 50 µM C6 HSL and 50 µM dopamine injection experiments, were 3.43, -506.2 and -15.7 Hz, respectively. Dopamine injection experiments for the FS and FFD methods showed satisfactory agreement with each other (Figure 3.14b). The results obtained from 50 µM dopamine injections were compared with those obtained from the 50 µM C6 HSL injection experiment. Resonance frequency shifts for 30 min for the anti-C6 HSL MIP NPs-C6 HSL interaction obtained from the FS and FFD methods were approximately 32.2 and 56.1 times those obtained for the 30 min HSL MIP NPs-dopamine interaction, respectively (Figure 3.14b). The variations in the resonance frequency shift for the FFD method with respect to the FS method were approximately -9.76 and -6.86 Hz for C6 HSL and dopamine injection experiments, respectively (Figure 3.13c).

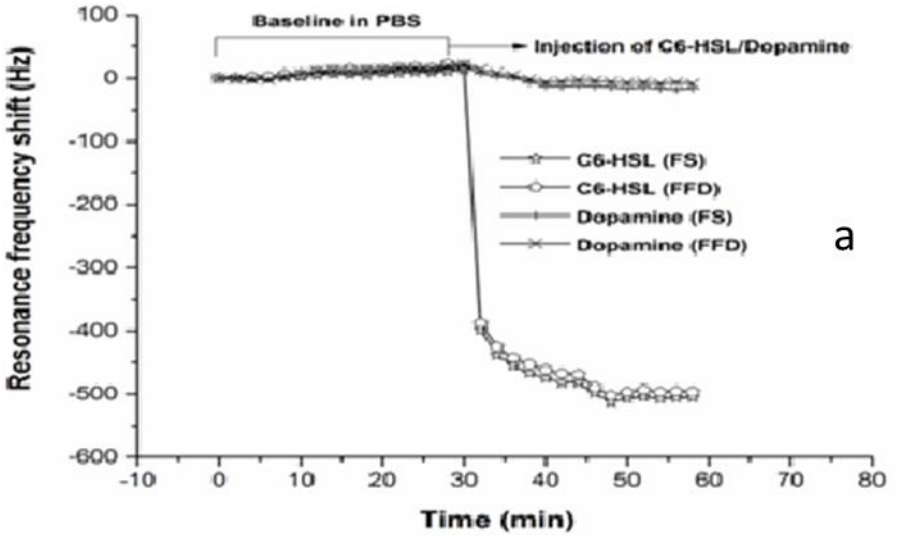

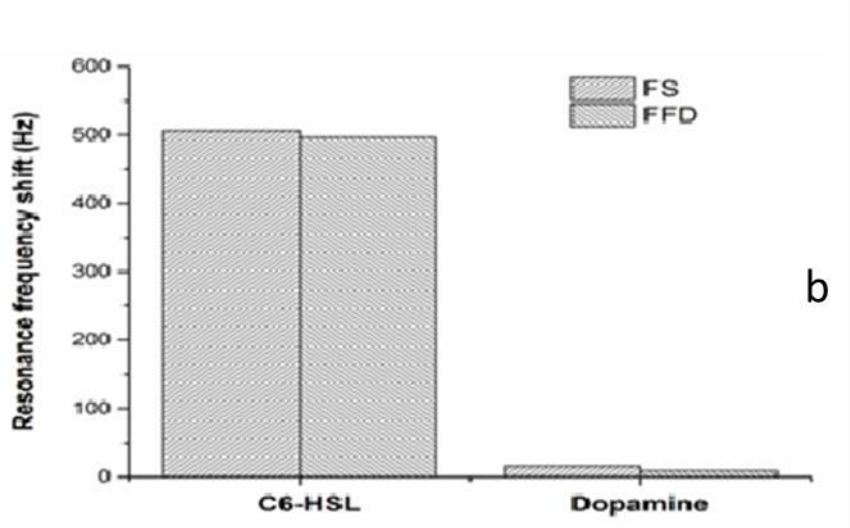

Figure 3.14: (a) Resonance frequency shift due to binding of 50 µM C6 HSL and 50 µM dopamine on functionalised QCR using the Frequency sweep and FFD methods with a 2 min measurement interval. (b) Resonance frequency shifts 30 min after 50 µM C6 HSL and dopamine injections

3.8 Discussion and Conclusions

The QS signal molecule, such as C6 HSL, after reaching a threshold concentration induces the expression of pathogenic factors in gram-negative bacteria and can play a key role in determining virulence. The detection of AHL could well aid clinicians in determining between bacterial and viral infections and confirming more precisely an infection caused by gram-negative bacteria. QCR sensor can be used as bacterial contamination indicator in oil pipe. As a result for bacteria growing, HSL can be produces in high concentration which can led to erodes pipes and in this case the oil company will lose £100,000 per day. Developing sensor, which can be robust and can be integrated in these pipes to give a signal which proportional to HSL concentration can be useful to protect pipes from the corrosion.

MIPs are synthetic materials derived from acrylic or methacrylic monomers which are polymerised in existence of a specific target molecule referred to as the template and have the capability to rebind specific target molecule[260]. In this work MIP NPs were synthesised using a solid-phase molecular imprinting, which was dependent on covalent immobilisation of a modified template molecule on the surface of micro-sized glass beads followed by polymerisation and a subsequent affinity separation step involving the washing of the beads for removal of poor binders and unreacted monomers[257]. Due to the strong binding interactions of MAA with AHL including C4 HSL, C6 HSL and 3-oxo-C6 HSL[256-258], MAA was selected as a monomer, ethylene glycol dimethacrylate (EGDMA) and trimethylolpropane trimethacrylate (TRIM) as a cross-linkers, acetonitrile (ACN) as the solvent, pentaerythritol tetrakis(3-mercaptopropionate) (PETMP) as the chine transfer agent and *N*,*N*-diethyldithiocarbamic acid benzyl ester as the iniferter.

Fixed Frequency Drive (FFD) technique does not require any frequency synthesiser or fast analogue to digital converter for its operation, thereby providing a simple, cost-effective and low-power resonance frequency shift measurement tool for gram-negative bacterial infection diagnosis. The novel acoustic technique also eliminates the fitting requirement for frequency sweep or ring down techniques which allow a greater degree of multiplexability through simultaneous operation of 24 QCRs[264, 265]. The multiplexing capability of the FFD technique can be beneficial for gram-negative bacterial infection diagnosis as more than one AHL molecule is usually found in an infectious sample[234].

The FFD technique also provides a real-time estimation of resonance frequency by utiliing measured reactance values from a fixed frequency drive. The unique attributes of the FFD technique can also favour online monitoring of QS-mediated biofilm formation in oil pipes which leads to biological corrosion and damage of pipes[225, 266-269].

The FFD technique combined with the application of molecular imprinted polymer nanoparticles as receptors were used for the detection of AHL using *N*-hexanoyl-L-homoserine lactone (C6 HSL) as a model molecule in a time of 10 min. The FFD technique allowed analytical estimation of the frequency shift of the QCR crystal when the template was bound to HSL MIP NPs. The driving frequency and characteristic shear wave impedance values were assumed to be constant during the estimation of resonance frequency using the FFD technique. Mass-loading experiments with C6 HSL concentrations varying from 1-50 µM and C6 HSL MIP NPs immobilised on 14.3 MHz QCRs were carried out separately using a customised network analyser. The resonance frequency shifts estimated from the FFD method were compared with those obtained from the frequency sweep (FS) method, a conventional technique for resonance frequency estimation. The specificity of the developed biosensor was also investigated by studying the interactions of 50 µM dopamine (negative control) and 50 µM C6 HSL (analyte) separately with C6 HSL MIP NPs-immobilised QCRs, where a negligible response in terms of resonance frequency shift was obtained from the dopamine experiment (-8.84 Hz) compared to the C6-HSL experiment (-496.44 Hz) using the FFD technique. Herein, we report the acoustic detection of C6 HSL up to 1 µM concentration over 10 min durations, which was lower than that reported for C6 HSL detection using QCM[232]. The novel acoustic sensor not only facilitates bacterial infection diagnosis but can also be used to study drug susceptibility through measurement of virulence expression via AHL concentration after application of antibiotics.

Chapter Four: Electroactive Molecularly Imprinted Polymer Nanoparticles (EMIP NPs) as Recognition Elements for Electrochemical Sensors

Abstract

The present study describes the preparation of electroactive molecularly imprinted polymers (EMIP) for electrochemical sensor applications. The EMIPs have been prepared by the incorporation of an electroactive mediator compound such as ferrocene (FC), ferrocene carboxylic acid (FCA) and ferrocenylmethyl methacrylate (FMAA). Three different targets (HSL, trypsin and glucose) were used to create the EMIPs via three different polymerisation strategies. The DLS and Nanoparticle Tracking Analysis (NTA) were used to evaluate EMIP particle sizes. The EMIP particles were deposited on the gold surface of a screen-printed electrode (GSPE) through a self-assembled monolayer (SAM) and characterised via electrochemical techniques. Differential pulse voltammetry (DPV) was used to characterise the electrochemical signal when the template was bound to the MIP and to further evaluate the selectivity and sensitivity of the sensor. The detection limits for this assay were $0.3x10^{-9}$, $0.22x10^{-9}$ and $0.13x10^{-6}$ M for HSL, trypsin and glucose respectively. The EMIP-based electrochemical sensor is a valuable new tool that allows quantitative measurement with selective analyte molecules. It has potential applications in the fields of clinical diagnosis, food analysis and other industrial applications in terms of real-time detection with high specificity. This chapter describes the improvement and application of EMIP for the direct detection of three different molecules (HSL, trypsin and glucose).

4.1 Introduction

4.1.1 Targets

In all molecular imprinting procedures the template plays an important role, the molecular structure of the template determines the type of functional monomer to be used in the synthesis, since the chemical bonds between both substantiates the molecular recognition. Three different types of template have been chosen (HSL, trypsin and glucose) to create the EMIPs to use them as receptor for electrochemical sensor. Different polymerisation strategies based on solid phase approach (water, organic) and polymerisation in solution have been performed.

4.1.1.1 Acyl Homoserine Lactones (AHLs)

Bacteria can communicate in a cell-to-cell manner using common signalling molecules known as *N*-acyl homoserine lactones (AHL)[270]. Quorum sensing is a process that enables bacteria to communicate using extracellular signalling molecules called autoinducers[271]. The construction and responses to autoinducers to monitor gene expression are cell density dependent[272]. This phenomenon is referred to as "quorum sensing (QS)" as this system enables bacteria to act in unison by coordinating their gene expression[270,273]. The physiological activities of many forms of bacteria are controlled and modified in response to population density via the synchronisation of the signalling molecules that they produce[274].

Biofilm formation is an example of such activity in bacteria. Today's lifestyle has changed the eating habits of consumers with regards to fast-food products. At the same time, there has been a dramatic increase in the incidence and outbreaks of food-borne diseases[275,276]. Many studies have confirmed that the microbiological contamination of food products is mainly due to the naturally occurring phenomenon of biofilm formation[277]. This biofilm formation has been found to be correlated with QS. Small diffusible chemical signalling molecules, or autoinducers, use this mechanism in order to mediate group-coordinated behaviours[278].

Generally, TLC[235-238], PCR[231,239,240] colourimetry[231], fluorescence-based[241] spectrometry, HPLC[244], LC-MS[245], HPLC-MS[246], GC-MAS[247] and NMR[248] are the main techniques as mentioned previously that have been used for the detection of AHLs. However, these detection techniques require sample pre-treatment, additionally, they are expensive, are not generally available in all laboratories (especially in developing countries), and require professional researchers to operate. To overcome these limitations, this work aims to create a cheap, rapid, easy to use, and sensitive sensor for the detection of QS signalling (C4 HSL is used as an example of HSL).

4.1.1.2 Trypsin

Trypsin has been chosen as a second template in this work. Trypsin is one of the serine protease family members. As a result of strict specificity, trypsin is the most commonly used protease in mass spectrometry-based proteomics[279]. Additionally, trypsin is widely used in various biochemical and biomedical applications such as the baby food industry, where it hydrolyses cow milk proteins into peptides and free amino acids for babies who are allergic or intolerant to bovine milk[280].

Additionally, trypsin is probably the most important digestive enzyme, and is formed in the pancreas as the inactive proenzyme trypsinogen[281]. Trypsin plays a key role in controlling the pancreatic exocrine function, and has been used as a cell dissociation reagent to eliminate adherent cells from cell surfaces, and for healing wounds and relieving inflammation by cleaning thick purulent masses in surface infections[281]. Though there is no trypsin in the urine of healthy individuals, the trypsin concentration found for whole-organ pancreas transplant patients is generally extremely high, showing an average concentration of 84.4 µg/ml. These data suggest that trypsinogen is rapidly converted to active trypsin following secretion into the bladder, resulting in the high urinary trypsin levels that has been detected in the majority of patients[282,283]. Moreover, a quantitative study based on an immunoassay found a trypsin concentration of 0.25 ± 0.1 µg/ml in serum of healthy individuals, whereas whole-organ pancreas transplant patients exhibited concentrations of 1.4 ± 0.6 µg/ml[284]. Therefore, the development of an easy to use, selective and sensitive detection method for trypsin would be beneficial to many biotechnological and diagnostic applications. Various techniques have been used

for trypsin detection, for instance surface-enhanced Raman spectroscopy[285] ELISA[286,287] colorimetric assay[288] and fluorescence analysis[289]. Detection by fluorescence enhancement carries certain restrictions, because quenching can result from non-specific interactions, resulting in false-positive responses, and fluorescence shifts are not always sufficiently sensitive[290]. Commercial human trypsin ELISA kits (Sandwich ELISA) are available (Lifespan Bioscience, Inc.) for detection purposes and are widely used.

Nevertheless, the above techniques are either time-consuming or require sophisticated laboratory equipment and trained personnel. Lately, sensitive amperometric and fluorescent probes have been created for trypsin detection[291,292]. Zhang and co-workers described a new, label-free assay for trypsin and inhibitor screening by taking advantage of the AIE (aggregation-induced emission) performance of tetraphenylethene compounds[293]. However, this approach did not allow for the quantitative analysis of trypsin.

MIPs as recognition elements for proteins represents a particularly attractive technique[290,294]. As an example, bulk MIPs for trypsin based on acrylamide as the functional monomer have been prepared by Subrayal and co-workers[295]. Spectrophotometric and QCM techniques have also been used for the detection of trypsin. In a similar approach, surface imprinting has been demonstrated by Hayden *et al*. to show selective recognition for trypsin on a QCM sensor[296], where the detection limits were found to be in the region of 1×10^{-7} M. Another bulk polymer for trypsin has been prepared by Ertürk and co-workers with the aim of creating a capacitive biosensor[297]. Nonetheless, biosensors that use bulk MIPs in their immobilised form have a number of limitations such as challenging integration of bulk MIPs with sensors and a lack of high affinity binding sites as a result of sieving and grinding processes. Furthermore, it is difficult to achieve selectivity at lower concentrations, due to an apparent lack of critical protein agglomeration or complete denaturation of protein molecules during protein binding. To overcome this limitation, MIPs based on a solid phase approach have been prepared to obtain nanosized particles without the need for sieving and grinding processes[70].

4.1.1.3 Glucose

Glucose was selected as third template in this project. As it is known, diabetes is a common health problem which is caused, when the body cannot control or produce sufficient amounts of insulin. The main factor in diabetes is a high level of glucose in the blood, which can either be heredity or occur as a result of an unbalanced diet. Blood glucose concentration is an essential indicator of patient health, mainly in terms of the symptoms associated with diabetes. Glucose is the primary source of energy for cellular activity in the body. However, some patients suffer from metabolic disorders involving processing of glucose. Diabetes mellitus is one of the most pervasive chronic diseases that can result from dysfunctional insulin production[298]. High glucose concentration in the blood plasma can cause hyperglycaemia, which can lead to blindness[299], kidney failure and cardiovascular disorders[300-302]. As a results of the significant increase in the number of diabetics, different methodologies for the measurement of glucose have been suggested to enable continuous, cheap, and accurate glucose level monitoring. Electrochemical analysis has been used in glucose sensors, because it is simple, straightforward and sensitive[303]. This technique has been used for commercial and research-level devices. Electrochemical glucose sensors have wide detection ranges and the electrochemical signals can be directly converted, or equated, to the equivalent concentration of glucose. Improved electrode structure, surface functionality and reducibility are required to achieve direct blood glucose detection.

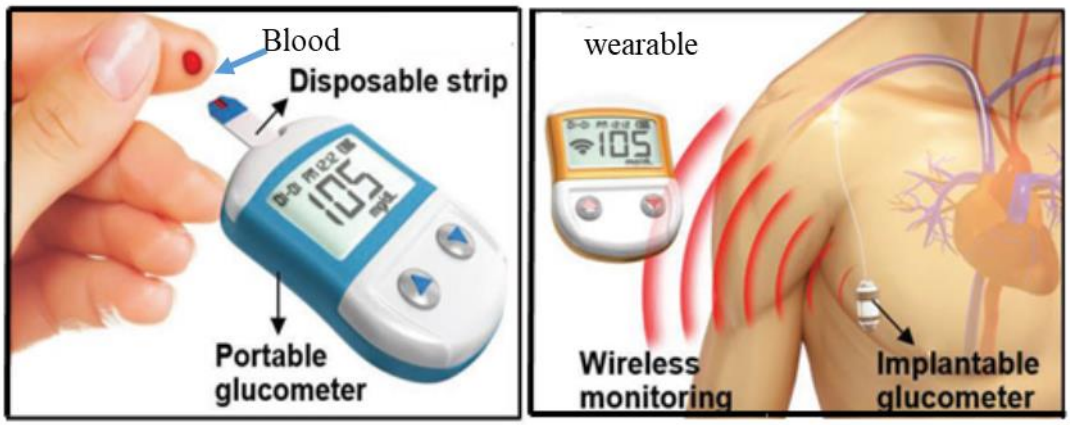

Figure 4.1: Commercial electrochemical glucose sensors

4.1.1.3.1 Generation of Glucose Sensor

Enzymes are commonly used as the main components in building glucose sensors. Glucose oxidase (GOx) react rapidly with glucose as a result of their catalytic turnover, and because the direct oxidation of glucose is energetically favourable. GOx is one of the enzymes associated with glucose metabolism[304]. In principle, GOx oxidises glucose to form gluconic acid and hydrogen peroxide (H_2O_2) via the following reaction.

$$\text{Glucose} + H_2O + O_2 \xrightarrow{\text{GOx}} \text{Gluconic acid} + H_2O_2$$

The first generation of GOx-based sensors monitor H_2O_2 production or O_2 consumption, which react with the electrodes to generate a signal proportional to the amount of glucose consumed. Glucose sensors assessed glucose concentrations in a given sample based on the production of hydrogen peroxide by glucose oxidase utilising dissolved hydrogen. Based on this procedure, in 1975, a company called Yellow Spring Instrument created the first commercial sensor for glucose[305]. However, it is clear that a high positive overpotential above 1 V versus an Ag/AgCl reference electrode needs to be applied to identify the analytes directly and unfortunately this overpotential will reduce the sensor selectivity because it creates side reactions such as oxidation of ascorbic acid, lactic acid and uric acid[306]. Moreover, deactivation of the glucose oxidase will occur due to the production of hydrogen peroxide.

The second generation of glucose sensors are based on a redox mediator to transfer electrons from the glucose oxidase to the surface of the working electrode. Numerous redox mediators have been used, such as ferricyanide, quinines, methylene blue and ferrocene to enhance sensor performance. The use of a redox mediator can reduce or eliminate the need for O_2 for electron transfer to occur at the surface of the electrode, overcoming the limitation of the first generation of sensors related to variations in partial pressure of oxygen. However, the main drawbacks of the second generation of glucose sensors were the high completion between the redox mediator and O_2. In addition, the small size of mediator and highly diffusive nature caused problems associated with it leaching from the electrode surface[307].

The third generation of glucose sensor was based on the direct electron transfer between the active centre of the enzyme and the electrode surface. The essential barrier to electron flow is the globular structure of glucose oxidase with the active site, having a FAD/$FADH_2$ redox factor, buried deep inside a cavity of 13 Å, severely limiting direct electron transfer. Immobilisation of carbon nanotubes on the surface of the electrode provides a suitable orientation for enzyme immobilisation and allow formation of links between the electrode surface and catalytic site[307-309]. However, all of these sensors require some form of enzymatic reaction to generate a response to the analyte.

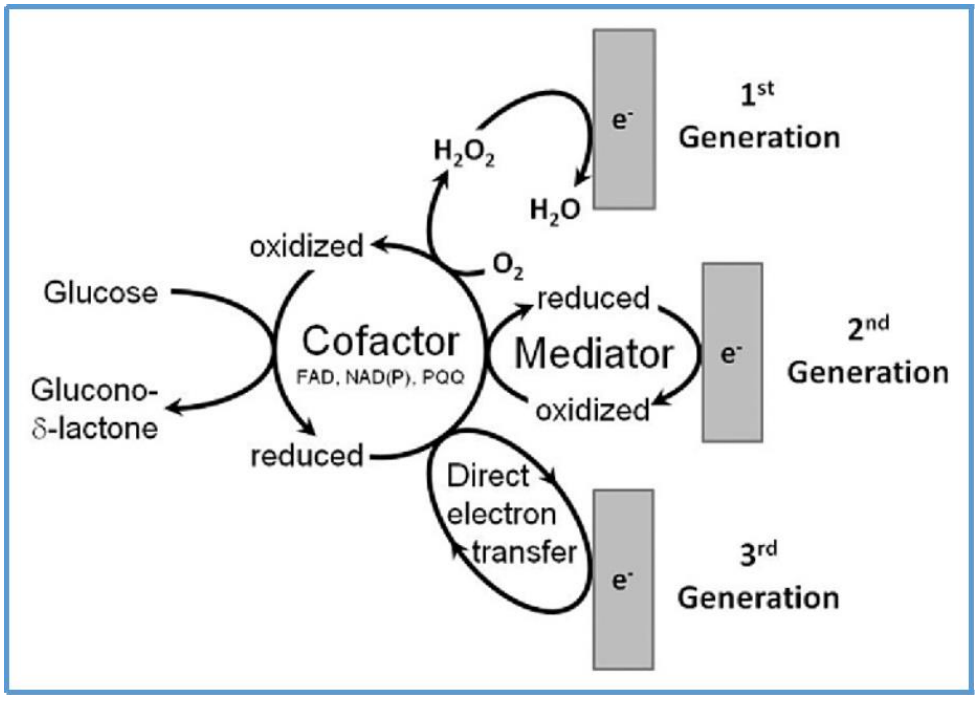

Figure 4.2: Schematic representation of glucose sensor generation. Adapted with permission from reference [293]

Theoretically, Wungu and co-workers demonstrated that MAA-based MIPs could be used as a bio-sensing material[310]. To confirm the interaction between MIP and D-glucose, the density functional theory (DFT) was used. Mulliken population analysis was used to investigate the possible reaction between MAA and D-glucose through the reduced distance between them.

As an example, MIPs based on methacrylic acid (MAA) have been used to create an artificial receptor using glucose as a template. An ion selective potentiometric membrane based on MIPs, prepared via bulk polymerisation, shows a significant difference in potential response to glucose compared to NIP[311]. However, the process involves complex steps for template elution, and, as mentioned, suffers from the effects of sieving and grinding on the binding sites. Also, linearity of the sensor response was limited to between 2×10^{-5}-5×10^{-3} M.

Farid and co-workers developed an enzyme-free glucose sensor by combining the molecular imprinting and MnO_2/CuO loaded onto graphene oxide nanoparticles[312]. First of all, MnO_2/CuO loaded on graphene oxide nanoparticles was mixed and sonicated with sodium dodecyl sulfate, glucose and water. The mixture was then polymerised with polyvinyl acetate, ammonium peroxysulfate and sodium acetate to create the MIP[312]. To gain template free MIP, they were stirred and refluxed for 3h at 80 °C and mixed with carbon paste. The cyclic voltammetry was used to characterise binding between MIP and glucose. The linearity was found was fornd to be in the range of 5×10^{-4} - 44×10^{-2} M with an LOD 3.5×10^{-2} M. However, the process was complex, time-consuming and unsuitable for real sample detection.

MIP NPs offer significant advantages over bulk materials as they have high surface-to-volume ratios, resulting in enhanced chemical reactivity, loading capacity, and enhanced binding kinetics. Additionally, the imprinted cavity is more available and accessible to the template, which improves polymer performance[112]. Furthermore, nanocomposite materials can be tailored to include additional functionality, such as magnetic, electroactive mediator and semi-conductive cores. These functionalities can be used to generate a sensor signal.

4.1.1.4 Signal Generation

In biosensors redox mediators can be used to facilitate electron movement between enzyme catalytic sites and the electrode surface and then convert this electron transport to a detectable electric signal[78,177]. The use of redox markers for creating electrochemical MIP sensors. Generally, soluble redox markers were combined with MIPs to allow indirect detection to be translated from the polymer-template interactions. It is clear that analyte binding to the MIP-coated electrode surface will reduce permeability of the redox marker (such as ferricyanide) and this could be useful in determining the concentration of the analyte[177]. The specific nature of the binding of the polymeric layer with the template molecule can generate morphological changes in the polymer, leading to changes in the redox probe's diffusion rate and the associated faradaic current[313]. Also, there is a possibility of using redox monomers such as pyrrole, aniline and aminophenyl boronic acid to prepare MIPs[314,315]. The conductivities of the MIPs are affected by template rebinding.

This project aims to create EMIP nanoparticles by conjugating ferrocene derivatives as monomer with MIP NPs. It is known that when the template binds, it induces conformational changes in the MIP NPs (Figure 4.3). Consequently, this should affect the density of MIP-ferrocene moieties (and the corresponding electrochemical signal) in contact with the electrode. The detection of a change in the density of the ferrocene electroactive moieties at the MIP-electrode interface triggered by MIP-template interactions is a more appropriate, direct and reliable approach than an indirect determination of the change in diffusion of redox markers through a polymer film in solution. A simple self-assembling monolayer process was used to attach MIP particles to the electrode surface. MIP NPs were functionalised and decorated with redox labels using polymerisable ferrocene derivatives such as ferrocenylmethyl methacrylate[316]. Furthermore, advanced disposable screen-printed electrodes (SPE) based on a gold working surface have been used in this project for electrochemical analysis. They are low-cost, disposable and they designed particularly to work with microliters volum of the sample.

As a result of its simplicity, sensitivity and low instrumentation cost, differential pulse voltammetry (DPV) was used to detect the electrochemical signal. DPV enables analyte detection down to sub-nanomolar level[317]. In DPV, the current is sampled twice in each pulse period, the difference between these two current values is recorded to produce a peaked voltammogram[317]. The heights of these peaks are directly proportional to analyte concentration. DPV has an advantage over other analytical methods, as it can reduce the effect of capacitive current and improves signal-to-noise ratio by attenuating the background current[318]. DPV provides quantitative information and requires only a short time to record a voltammogram.

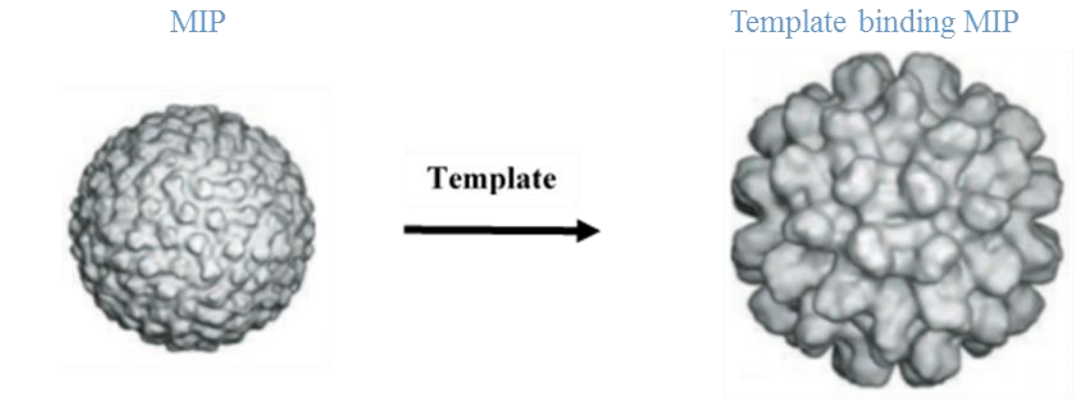

Figure 4.3: Cartoon representation of the change in polymer conformation triggered by the interaction with the template

4.2 Materials and Methods

4.2.1 Materials

N-butyryl-L-homoserine lactone (C4 HSL), α-Amino-γ-butyrolactone hydrobromide, *N*-hexanoyl-L-homoserine lactone (C6 HSL), dopamine, glucose, fructose, lactose, maltose, trypsin, avidin, pepsin, dodecanedioic acid, 2-(*N*-morpholino)ethanesulfonic acid (MES), 3-aminopropyltrimethyloxysilane (APTMS), cysteamine, glutaraldehyde (GA), sodium persulfate (APS), ferrocene (FC), ferrocene carboxylic acid (FCA), ferrocenylmethyl methacrylate (FMAA), sodium hydroxide (NaOH), sodium cyanborate, *N*-hydroxy-succinimide (NHS), 1-ethyl-3-(3-dimethylaminopropyl)-carbodiimide hydrochloride (EDC), 2-(*N*-morpholino)ethanesulfonic acid (MES buffer), *N*-isopropylacrylamide (NIPAm), *N*-tert-butylacrylamide (TBAm), *N*,*N*′-methylenebisacrylamide [105], *N*,*N*,*N*′,*N*′-tetramethylethylenediamine (TEMED), acrylic acid (AAc:99%), *N*-(3-aminopropyl)methacrylamide hydrochloride), EGDMA, TRIM and pentaerythritol tetrakis(3-mercaptopropionate) (CTA) were purchased from Sigma-Aldrich. Sodium carbonate (Na_2CO_3), sodium chloride (NaCl), toluene, dimethylformamide (DMF), acetonitrile (ACN), acetone and PBS tablets were purchased from Fisher Scientific, UK. *N*, *N*-diethyldithiocarbamic acid benzyl ester was purchased from TCI Europe. All solvents were HPLC Grade. Glass beads with diameters in the range of 53-106 μm were purchased from Potters Industries. Double-distilled water (Millipore, UK) was used for the experiments. All chemicals and solvents were used without any further purification.

4.3 Equipment

Polypropylene solid-phase extraction (SPE) tubes (60 ml), polyethylene (PE) that can be used with 60 ml SPE tubes, disposable plastic syringes, syringe filter membrane 0.45 and 0.75 μm, and UV-visible cuvettes were purchased from Sigma-Aldrich. Magnetic stirrer hotplates, sintered disc filter funnels, Buchner filter flasks, Buchner filter cones, flat-bottomed glass vessels, Amicon Ultra-15 centrifugal filter units (UFC9030 (30 kDa) were purchased from Fisher Scientific. Glass vials and disposable plastic cuvettes were obtained from VWR International, UV-visible spectrophotometer (Shimadzu, UV-1800),

UV light source (Philips HB/171/A, 4×15 W lamps). Oven, ultrasonication bath, vacuum pump, Dynamic Light Scattering (DLS). Zetasizer Nano (Nano-S) particle-size analyser from Malvern Instruments Ltd, UK. NanoSight® LM20 device (NanoSight Ltd., Amesbury, UK). Gold screen printed Electrodes (GSPE/ refs. 250AT) with connection cable to potentiostat were purchased from DropSens/Spain. A μAutolab Type II potentiostat (Ecochemie, Netherlands) connected with a GPES 4.9 software package.

4.4 Methods

MIP NPs based on solid-phase approach were used for both small and large molecules (HSL, trypsin). Aqueous and organic polymerisations were carried out using chemical and light-initiated methods. Notably, the template was covalently immobilised on the surfaces of the glass beads. Glass beads were placed in contact with a mixture of the monomers and polymerisation initiated either chemically or by UV light under appropriate conditions to allow the formation of polymer nanoparticles. After synthesis, the solid support functions as an affinity matrix for the separation of the MIP NPs from any remaining, unreacted monomers and low-affinity polymer. Due to affinity purification step, MIP NPs have high affinity/specificity for their target and a homogeneous distribution of binding site affinities, much like monoclonal antibodies[67]. The MIP NPs obtained are practically free from template, an otherwise common problem with traditional approaches that requires lengthy (up to a week) dialysis of the NPs to ensure its removal. This approach tends to be generic and enables polymerisation in water (persulfate-initiated) and organics (UV-triggered process). The water polymerisation was employed successfully to produce hydrophilic MIP NPs imprinted against peptides and proteins. However, the polymerisation in organics tends to be useful for imprinting of small molecules[130,319]. It is assumed that weak polar organic solvents such as toluene, acetone, and chloroform do not interfere with the template–functional monomer interaction during the preassembly step due to their lower polarities and hydrogen bonding abilities compared to aqueous media[320]. Moreover, in this method the solid-phase can be reused several times, so saving template molecules. Furthermore, this method allows for the addition of a mediator and labelling particles for specific applications. Two types of polymerisations were performed to synthesise the MIPs for

three different molecules in this chapter. Polymerisation process were carried out with the aim of labelling MIPs with an electroactive mediator to create EMIP which is appropriate for electrochemical sensor applications.

4.4.1 Glass Bead Activation

A. Placing up to 200g of glass beads in a flask containing 4 M sodium hydroxide (the volume of sodium hydroxide has to be 1-2 cm above the top of the glass beads).
B. Glass beads were boiled in sodium hydroxide for 15-20 min to activat them.
C. Beads were filtered after cooling then washed eight times with DI water. The beads were incubated with sulphuric acid: water (1:1). The beads were then washed with DI water, PBS buffer and DI water again to remove salts and restore pH to between to 6.5– 8.
D. The beads were washed with acetone and left to dry under vacuum at 150 ^{o}C for 60 min.
E. The glass beads were removed from the oven and the silanisation process then performed directly to prevent excessive degradation.

4.4.2 Silanising the Glass Beads

A. A suitable amount of boiling toluene was measured out and then added directly onto the glass beads (0.5 ml/g of beads). Then, a silane compound (3-Aminopropyl)triethoxysilane) (3 ml/100 ml toluene) was added.
B. The dipodal silane (1,2-bis (trimethoxysilyl)ethane) was added to the toluene to obtain a final concentration of 400 µl /100 ml of toluene. After that, the mixture was purged for 30 min under N_2 to remove any remaining O_2.
C. The glass beads were incubated overnight with silane at 70 ^{o}C to react.
D. The beads were cooled and then washed with methanol and acetone (eight times) and dried under vacuum. The beads were then kept it for 30 min at 150 ^{o}C before being collected and cooled. After that, the silane beads were then tested. To evaluate the presence of amino group.

4.4.3 Evaluating the Presence of Amino Groups After Silanisation Step

4.4.3.1 Dansyl Chloride Test

The dansyl chloride reagent reacts with free amino groups producing a fluorescent light under UV light[321]. To do the test, 5 g of silane beads was placed in a 10 ml vial. Then, 5 ml of an acetonitrile solution of dansyl chloride (1mg/ml) was added to the vial. This was maintained at room temperature for 1 h in a dark place. After that, the glass beads were washed with acetonitrile and evaluated under the UV lamp (results: green = silane present, not green = no silane present).

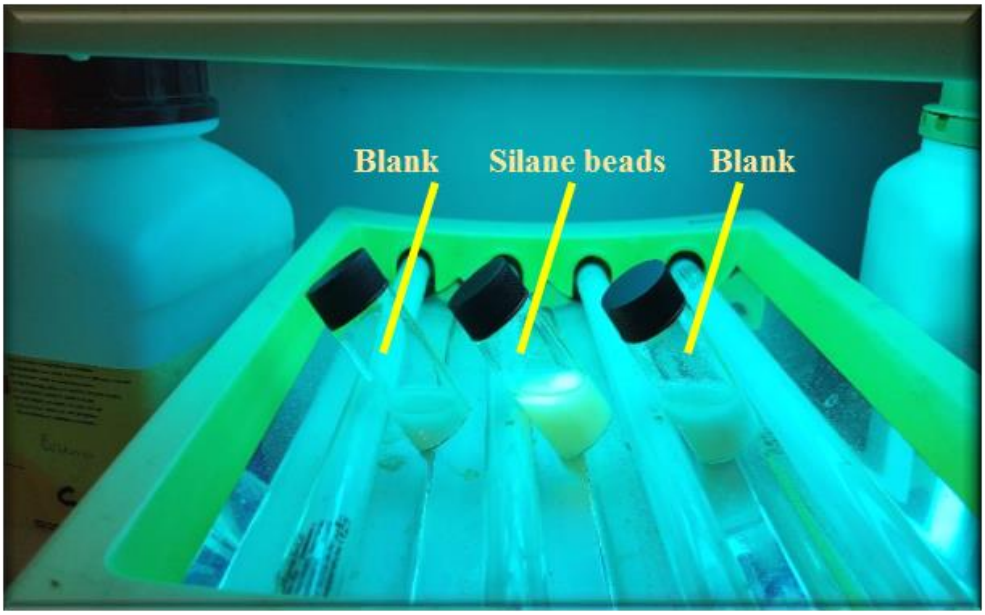

Figure 4.4: Illustration of the dansyl chloride test

4.4.3.2 Kaiser Test

Ninhydrin can react with primary and secondary amino group to produce a blue to purple colour[322]. The intensity of the colour is directly proportional to the concentration of the present primary amino group. To perform the test, 2 mM ethanolic solution of ninhydrin was freshly prepared. After that, 5 g of silane glass beads was weighed into a vial and suspended in 2.5 ml of ethanol, then 2.5 ml of 2 mM ninhydrin solution were added and the result mixture shaken thoroughly (final volume 5 ml, final ninhydrin concentration 1 mM). Vials should be adequately sealed with parafilm and covered to protect the contents from light. Vials were incubated in the shaker for 90 minutes at 60 ^{0}C and 150 rpm. Once the reaction had taken place, the solution was cooled and absorption spectra recorded (λ_{max} = 580 ± 4 nm) using a 1.5 ml quartz cell with a path length of 1 cm. Pure ninhydrin solution was used as a reference. After that, the results were compared to a calibration curve (amino compound instead of glass beads) to evaluate the presence of the amino group in a quantitativ manner.

4.5 Solid-Phase Synthesis of EMIP NPs in Organic Solution (HSL)

4.6 Preparation of Template-derivatives Glass Beads (HSL template)

10 ml of MES buffer solution (pH 6.0) containing 1.9 g of EDC and 0.4 g of NHS was mixed with dodecanedioic acid in DMF (0.125 g/20 ml). After that, 40 g of silane glass beads was incubated for 30 min in this mixture. The beads then were washed with 50% (DMF: water) and acetone. The water solution of the template (0.078 g (S)-(−)-α-amino-γ-butyrolactone hydrobromide and 0.046 g of sodium carbonate) was added to the glass beads and incubated for 120 min. The glass beads with the immobilised template were washed with DI water and dried under vacuum. The template-derivatives beads were kept at 4 °C until use.

4.6.1 The Polymerisation of EMIP NPs

A monomer mixture that included 1.44 g of MAA, 1.62 g EGDMA, 1.62 g TRIM, 0.37 g of *N*,*N*-diethyldithiocarbamic acid benzyl ester (DABE), 0.09 g of pentaerythritol-tetrakis-(3-mercaptopropionate) (PETMP) and X(g) of electroactive mediator (FC, FCA, FMAA) (Table 4.1) were dissolved in ACN (10.52 g). The mixture was sonicated and deoxygenated with nitrogen for 15 min. Glass beads with the immobilised template (25 g) were degassed under vacuum for 20 min and mixed with the monomer mixture. Polymerisation was then initiated by exposing the mixture to UV light for 2 min. After polymerisation, the polymerisation product with the glass beads was transferred into a solid phase extraction (SPE) cartridge fitted with a polyethene frit (20 mm porosity) and washed with cold acetonitrile at 0°C to remove any remaining monomers, residues and low-affinity nanoparticles. The high-affinity EMIP NPs were collected by elution at 60-65 °C. The particle size of high affinity MIP particles was later determined by DLS.

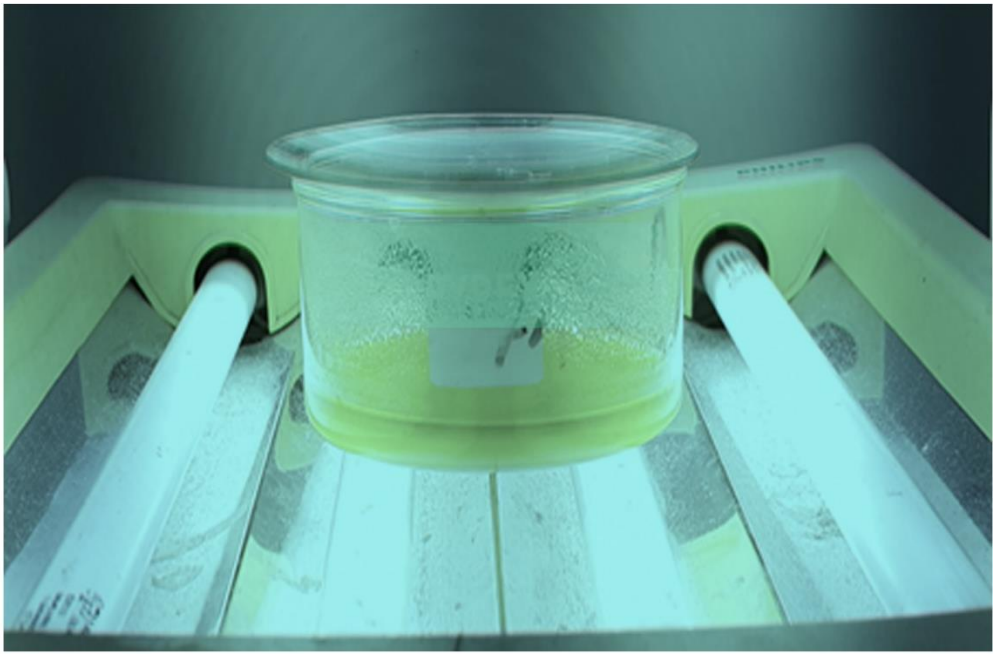

Figure 4.5: Polymerisation under UV light

Table 4.1: Organic polymerisation mixture for EMIP synthesis for HSL.

Polymerisation No.	Glass beads (g)	MAA (g)	EGDMA (g)	TRIM (g)	ACN (g)	CTA (g)	Iniferter (g)	Mediator % from MAA		
								FC	FCA	FMAA
1	25	1.44	1.62	1.62	10.52	0.09	0.37	5	-	-
2	25	1.44	1.62	1.62	10.52	0.09	0.37	10	-	-
3	25	1.44	1.62	1.62	10.52	0.09	0.37	15	-	-
4	25	1.44	1.62	1.62	10.52	0.09	0.37		5	-
5	25	1.44	1.62	1.62	10.52	0.09	0.37		10	-
6	25	1.44	1.62	1.62	10.52	0.09	0.37		15	-
7	25	1.44	1.62	1.62	10.52	0.09	0.37			5
8	25	1.44	1.62	1.62	10.52	0.09	0.37			10
9	25	1.44	1.62	1.62	10.52	0.09	0.37			15

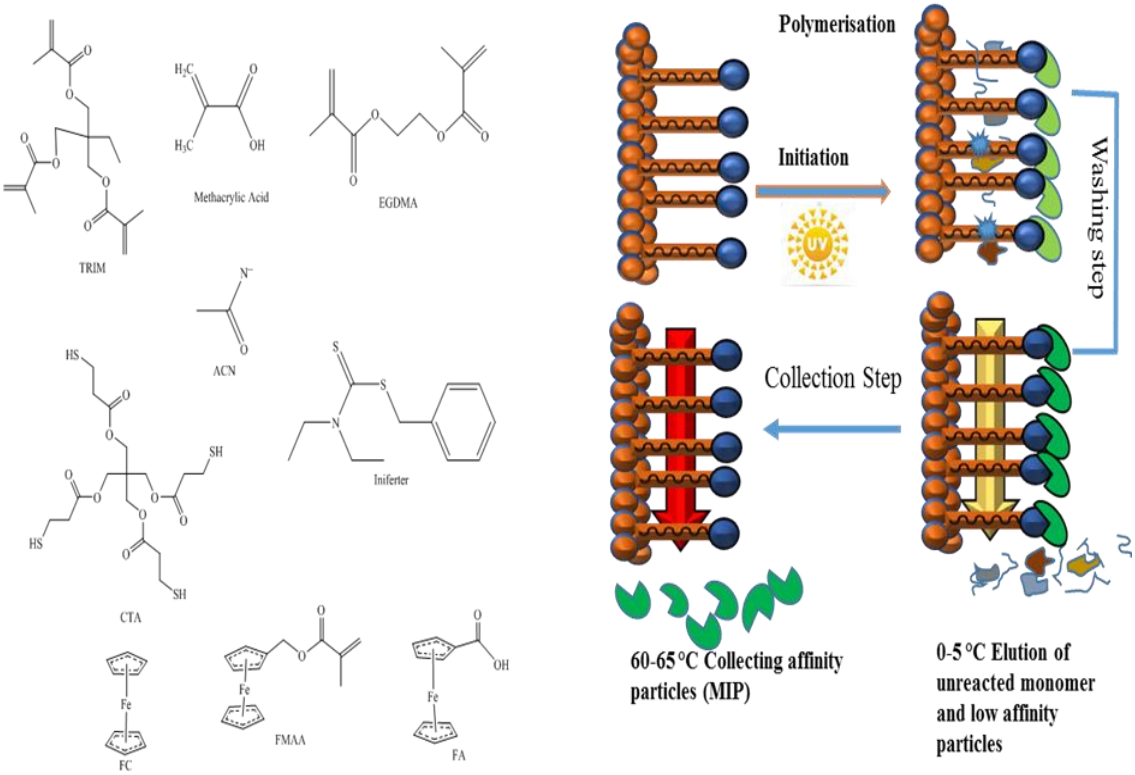

Figure 4.6: Organic polymerisation process to create EMIP for HSL

4.7 Solid-Phase Synthesis of EMIP NPs in Water (Trypsin)

4.7.1 Preparation of Template-derivatives Glass Beads

Silane glass beads were incubated for 2 h in a PBS solution of GA (7% vol/vol). After that, the glass beads were washed with DI water (eight times) in a sintered disc or Buchner funnel under vacuum. The template was immobilised on the surface of the glass beads by incubating the beads in a solution of Trypsin (1 mg/ml) in PBS buffer overnight at 4°C. To reduce the Schiff base bonds, a PBS solution of sodium cyanoborohydride was added to the template-derivatised glass beads (1 mg/ml) and incubated for 30 min. The beads were then washed with DI water, dried under vacuum and stored at 4 °C until use.

4.7.2 The Polymerisation of EMIP NPs

A mixture of NIPAM (39 mg), BIS (2 mg), TBAm (33 mg dissolved in 2 ml of ethanol) was dissolved in 50 ml of water. In a separate vial, 22 µl of AAc was diluted to 1 ml then 0.1 ml of the solution was added to the mixture. Ferrocenylmethyl methacrylate (5 mg) was dissolved in 1 ml ethanol, and then also added to the mixture. The volume was adjusted to 100 ml with water. The mixture was sonicated and purged with nitrogen for 30 min. This solution was then added to 60 g of glass beads. Polymerisation was initiated by adding 0.5 ml of APS (60 mg/ml) containing TEMED (30 µl/ml) at room temperature for 60 min. After that, the beads were transferred into an SPE cartridge (60 ml) that was fitted with a 20 µm porosity PE frit. Unreacted monomers and low-affinity materials were washed away using DI water (10 × 20 ml) at room temperature. Next, to collect the fractions of high-affinity MIP NPs, the temperature was raised to 60-65°C and the beads washed with DI water at 60-65°C (5 × 20 ml). The particle size of the high affinity MIP particles was later determined by DLS.

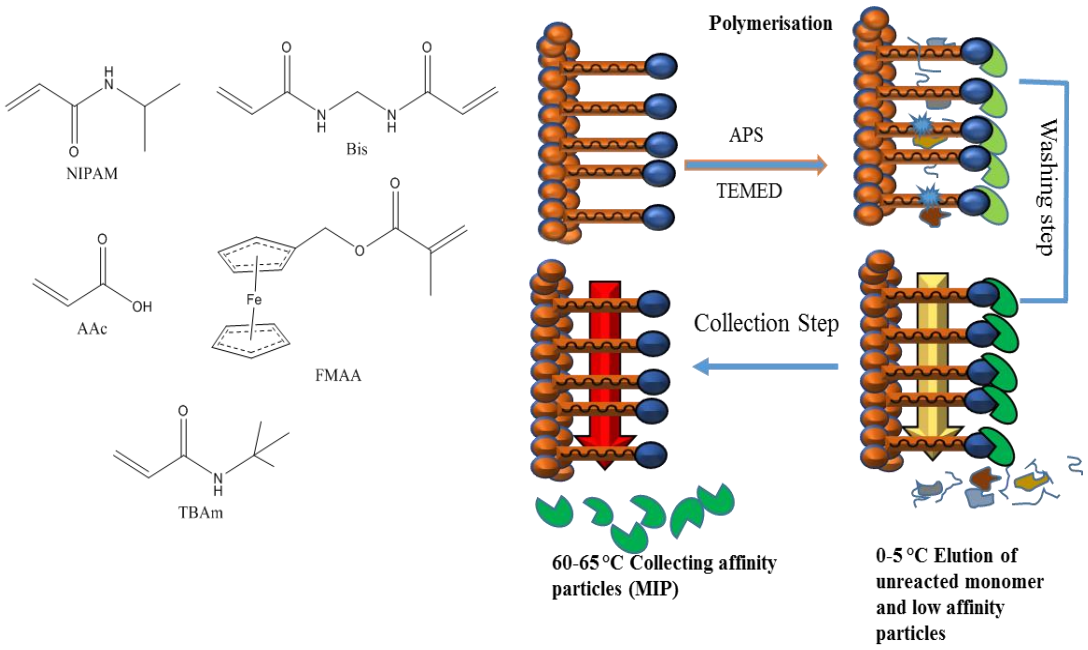

Figure 4.7: Water polymerisation process to create EMIP for Trypsin

4.8 Synthesis of Glucose EMIP in Solution (without glass beads)

A mixture of NIPAM (39 mg), BIS (6 mg), TBAm (33 mg dissolved in 2 ml of ethanol), and AA 2.2 µl in 0.1 ml water was added to the polymerisation mixture. The components were suspended in water (50 ml) and sonicated for 10 minutes. In a separate vial, 6 mg of FMAA was dissolved in 1 ml ethanol. After that, 30 mg of glucose and 5.8 mg of amino monomer (*N*-(3-aminopropyl)methacrylamide hydrochloride) were dissolved in 20 ml of DI and then mixed with the polymerisation mixture. The volume was adjusted to 100 ml with DI water, sonicated and degassed by bubbling with nitrogen for 30 min. After that, the polymerisation was initiated by adding 0.5 ml of water containing APS (60 mg/ml) and 30 µl TEMED at room temperature for 60 min. Next, the resulting MIP particles were collected and concentrated. After that, MIPs were washed with DI water (seven times) using a centrifuge cartridge filter (10 k). The size high fraction EMIP particle was assessed via DLS.

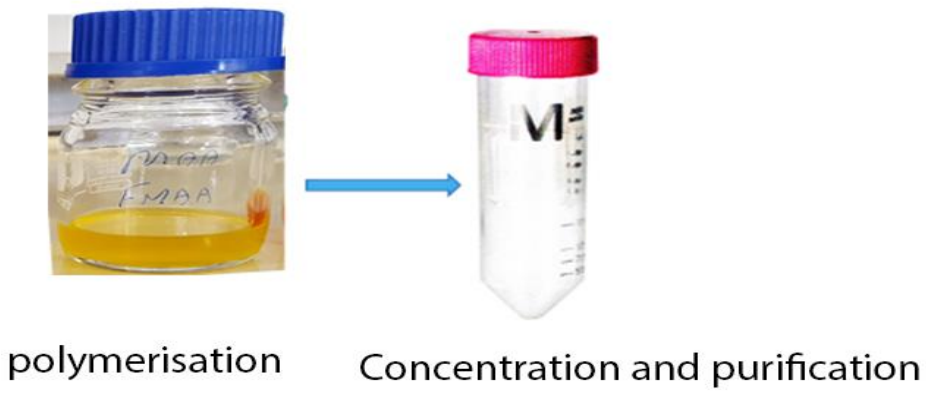

Figure 4.8: Polymerisation in solution for glucose

4.9 The Evaluation of the Size of EMIP Particles

4.9.1 Dynamic Light Scattering Analysis for EMIP NPs

To evaluate the size of the synthesised MIP particles and to be sure of successful synthesis, the dynamic light scattering technique was carried out. All measurements were carried out after the collections of high affinity EMIP particles which were filtered using A 1.2 µm filter membrane. The EMIP solution was placed into 4 ml glass vial and sonicated for 2 min. After that, 1 ml was transferred into a glass cuvette and the DLS measurement carried out at room temperature. The instrument automatically sets up the attenuator position, number of runs and measurement duration, obtaining the particle size as an average of the hydrodynamic diameter and the polydispersity index (PDI), which is an indication of the heterogeneity of the particle sizes in the sample. In a monodisperse sample, PDI values between 0-0.7 are acceptable. Data analysis performed using the solvent parameters for acetonitrile (HSL), water (trypsin) and phosphate buffer solution (glucose). The instrument was allowed to select the attenuator position based upon the observed scattering. The duration of each measurement and the number of runs were also set to automatic. The software included a ‘data quality report’ that indicated the quality of all data obtained.

4.9.2 NanoSight

The nanoparticle tracking analysis (NTA) technique was carried out using a NanoSight NS500 (Malvern, Grovewood Road, UK) to analyse nanoparticle sizes. Samples were diluted appropriately for the contrast and to ensure minimal background levels. The samples were filtered using a syringe filter membrane with a pore size of 0.72 µm, and a particle motion video recorded automatically using the standard measurement mode. After that, the NPs were tracked by the NTA software to evaluate their Brownian motion in solution and calculate the particle size. Particles size analysis was carried out using a NanoSight® LM20 device (NanoSight Ltd., Ames-bury, UK) equipped with the NanoSight® NTA 2.2 software. The sample was first concentrated under nitrogen then solvated in water via an Amicon Centrifugal Filter Unit (MWCO 30 kDa) after which it was diluted ten-fold using milli-Q water. Six independent analyses were performed to record 60 s videos. Then, the NTA software tracked NPs to evaluate their Brownian motion in solution. The latter depend on the particle size, which could be determined by the software.

4.10 Electrochemical Sensor Based on EMIP

4.10.1 Cleaning and Immobilisation of the MIP NPs on the SPE surface

Gold screen-printed electrodes (GSPEs) were immersed in a petri dish filled with isopropanol and sonicated for 2-3 min followed by further washing with ethanol, after which the electrode was dried using nitrogen. A hydrogen plasma was then used for 3 min to remove impurities and contaminants from the electrode surface. Finally, the GSPEs were washed with ethanol and incubated overnight in an ethanolic solution of cysteamine (0.2 mg/ml). At the same time, the EMIP NPs solution was concentrated (10 times). To immobilise EMIP NPs on the GSPEs surface, the carboxylic acid of the EMIP NPs was activated using EDC to bind the modified GSPEs surface with amino group. GSPEs were used due to their small dimensions, the fact that it is easy to connect with transducer and that it only requires microliter volumes of analyte. In order to evaluate the MIP response toward the template, electrochemical characterisation of GSPEs surface (DRP-250AT, 4 mm diameter) was carried out using differential pulse voltammetry

(DPV). The electrochemical experiments were carried out with the Autolab II Instruments (Netherland).

4.10.2 Differential Plus Voltammetry (DPV) Sensor

A self-assembling monolayer was used to immobilise EMIPs on the electrode surface while the DPV technique was employed for the current measurements to evaluate the rebinding (template-MIP) signal. The electrochemical cell includes three elements: the working electrode (gold - 4 mm diameter), an auxiliary electrode (platinum), and a reference electrode (silver). GSPEs with a connection cable for the potentiostat were purchased from DropSens/Spain. The electrochemical experiments were carried out with the Autolab II Instruments (Netherland) connected to the electrochemical system software (GPES) to evaluate the binding between the MIPs and templates on the GSPEs surface.

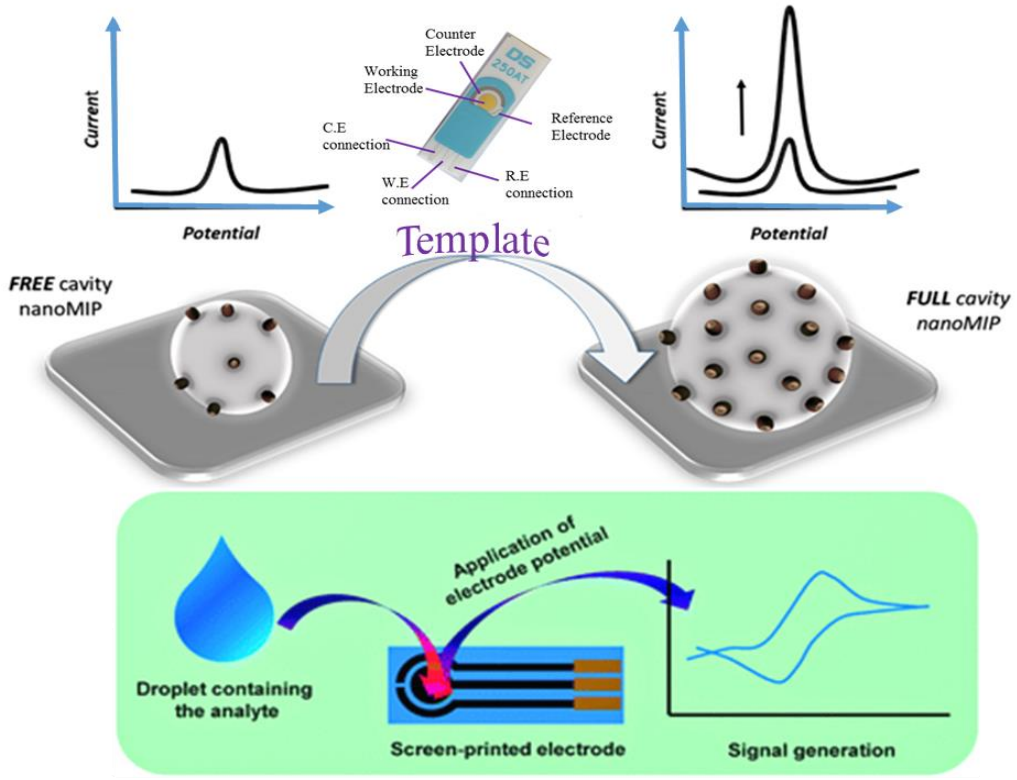

Figure 4.9: Schematic representation of the template-induced change in the number of anchored redox markers exposed onto the electrode surface

4.11 Results and Discussion

4.11.1 Synthesis and Characterisation of EMIPs

The synthesis of EMIP was based on the solid-phase technique for HSL and trypsin. Organic polymerisation was performed for a small molecule to obtain high-affinity EMIP for HSL, which offered high yield and allowed for straightforward control of particle size, while synthesis of EMIPs by persulfate-initiated polymerisation was performed for trypsin using water-soluble acrylate monomers. The presence of APMA and AAc in the polymerisation mixture ensured that both the acidic and basic residues in the peptide sequence could contribute to the formation of the binding sites. To overcome the possiblity of protein denaturation, aqueous polymerisation was the only option for imprinting of proteins. Molecular imprinting of proteins is quite challenging, as the generation of selective imprinted cavities is particularly difficult due to their flexible structure, high molecular-weight and the presence of multiple different functional sites. To overcome this limitation, the solid-phase approach was used to prepare MIPs specific to any protein that could be immobilised in an oriented way on the solid phase[323]. Moreover, in order to offer a range of ionic and hydrophobic interactions in addition to hydrogen bonds between monomers and the large protein template, different monomers were used. Oriented immobilisation was achieved by first immobilising trypsin via glutaraldehyde coupling onto the glass beads and then incubating the beads with trypsin[136].

The subsequent temperature-based affinity separation was first performed at low temperature (0-5°C) to remove low-affinity MIP NPs, followed by elution of the high-affinity MIPs at 65°C, similar to that performed for the imprinted particles produced in acetonitrile (Figure 4.6 and Figure 4.7). Hot washing (60-65 °C) was used to disrupt the interaction of the MIPs with the template and thus collect a fraction of high-affinity MIPs.

Experimentally, MIP NPs can be functionalised with redox labels using polymerisable ferrocene derivatives such as FMAA, FCA and FC. It would be expected that interaction of MIP NPs with template would trigger conformational changes in the polymer that affect the density of electroactive ferrocene moieties on particle surfaces[178]. The detection of change in density of electroactive moieties is more convenient and reliable than

detecting change in diffusion of soluble redox markers through the polymer film triggered by polymer-template interactions.

Furthermore, in case of HSL MIP, standard monomers were used in combination with an electroactive mediator (FC, FA, FMAA) to create electroactive MIPs (EMIPs). Then, FMAA was combined with the standard polymerisation mixture to obtain EMIPs with a high selectivity for trypsin and glucose. In addition, EMIPs were created via a non-covalent approach that could include electrostatic, hydrophobic and van der Waals interactions. This method considers that fact that the EMIPs could interact with the analyte structure in different ways.

The combination of an electroactive mediator into the structure of the NPs offered a promising labelling technique, and it might offer a novel method of electrochemical sensing for different molecules with different size and functionalities. Also, the use of vinyl ferrocene as an electroactive polymer coating on the electrode surface also showed a shift in peak potential which has been reported to be caused by the proximity of the fixed electroactive sites within the polymer cavities[324,325]. It is clear that the redox mediator had affected the template rebinding process, increasing the oxidation peak of the mediator with an increase in template concentration.

4.11.2 Particle Size Measurements

4.11.2.1 Dynamic Light Scattering (DLS)

The standard protocol for DLS measurements of EMIPs involved sample sonication for two minutes before measurement to reduce or eliminate the presence of aggregate particles. The size of the particles differed depending on the template and polymerisation processes. The results shown in (Table 4.2) gives some indication as to the MIP purity and concentration. The polydispersity index (PDI) gave an indication as to the heterogeneity of the particle sizes in the sample, the results of which indicated that the EMIP have an acceptable PDI range. Correlation data showed that there was no aggregation during the measurements, and all runs seemed similar in this regard.

The size distribution by intensity and the correlation data showed the presence of one population of particles for HSL and trypsin at around 180 and 430 nm, respectively, while the size distribution by intensity showed more than one peak for glucose but with the highest intensity appearing at 200 nm.

Table 4.2: Size of MIP particles as determined by DLS.

Template	Size ± (nm)	PDI±	Count rate
HSL	186.5 ± 8.612	0.316 ± 0.005	1449.5 ± 7.1
Trypsin	443.8 ± 14.83	0.196 ± 0.168	254.1 ± 38.4
Glucose	201.8 ± 16.49	0.373 ± 0.033	463.1 ± 33.6

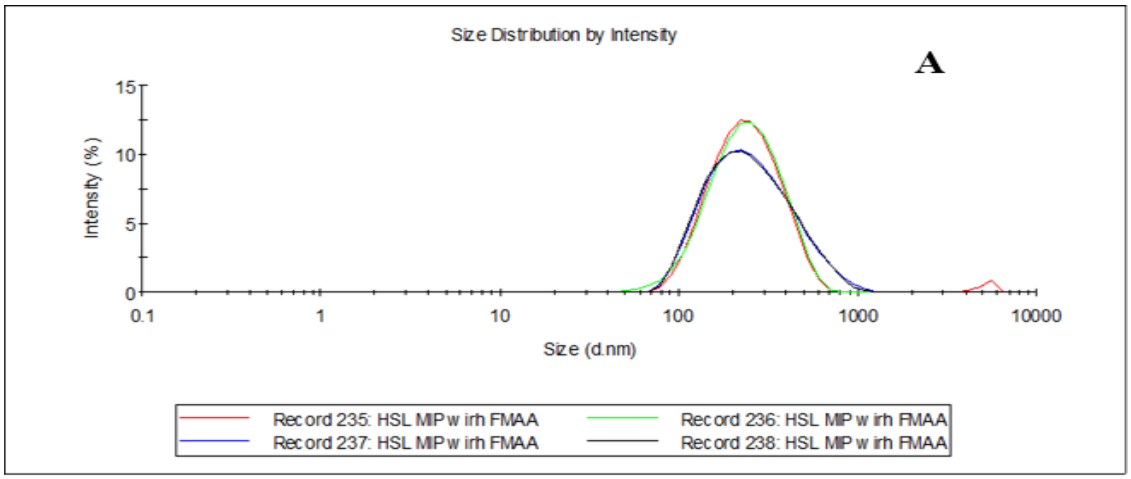

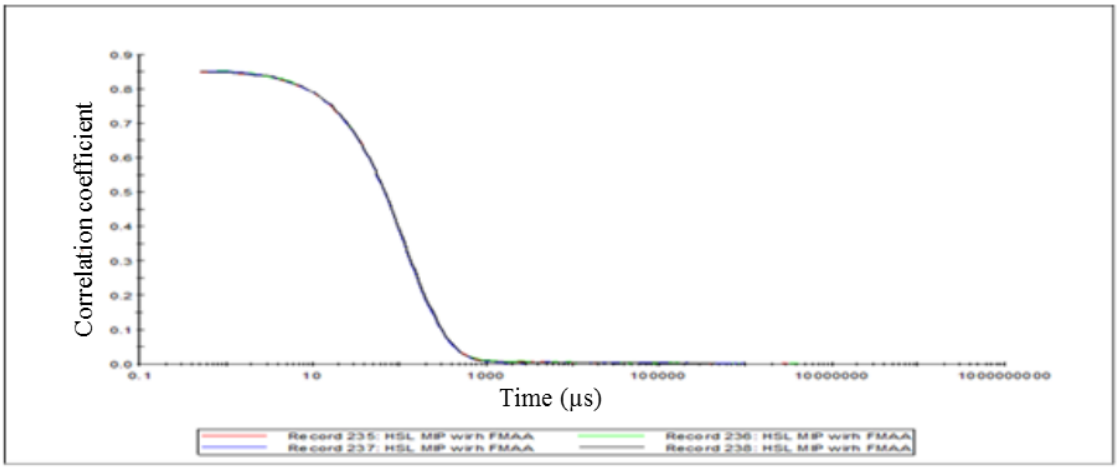
Correlation coefficient
Time (µs)
Record 235: HSL MIP with FMAA
Record 236: HSL MIP with FMAA
Record 237: HSL MIP with FMAA
Record 238: HSL MIP with FMAA

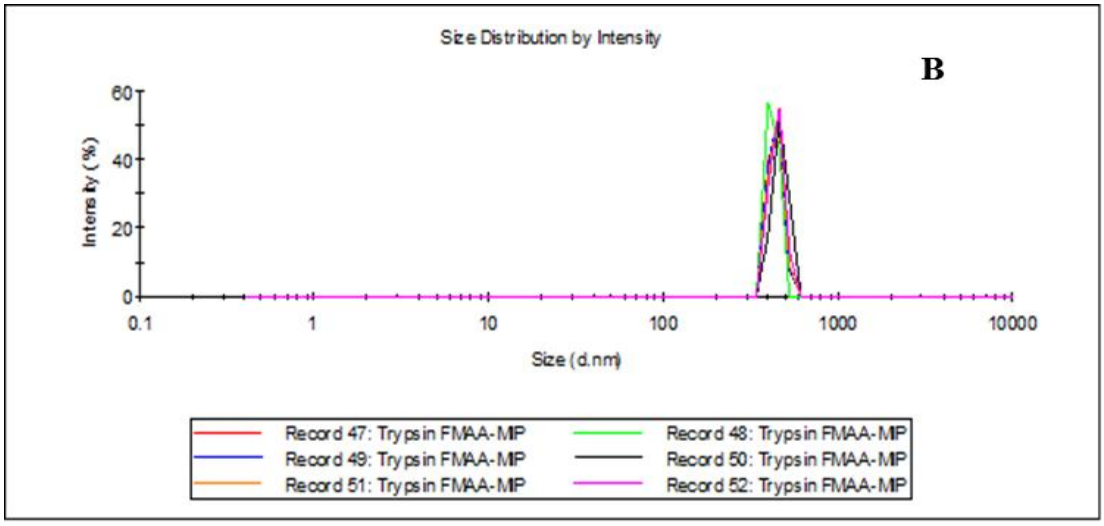
Size Distribution by Intensity
B
Intensity (%)
Size (d.nm)
Record 47: Trypsin FMAA-MIP
Record 48: Trypsin FMAA-MIP
Record 49: Trypsin FMAA-MIP
Record 50: Trypsin FMAA-MIP
Record 51: Trypsin FMAA-MIP
Record 52: Trypsin FMAA-MIP

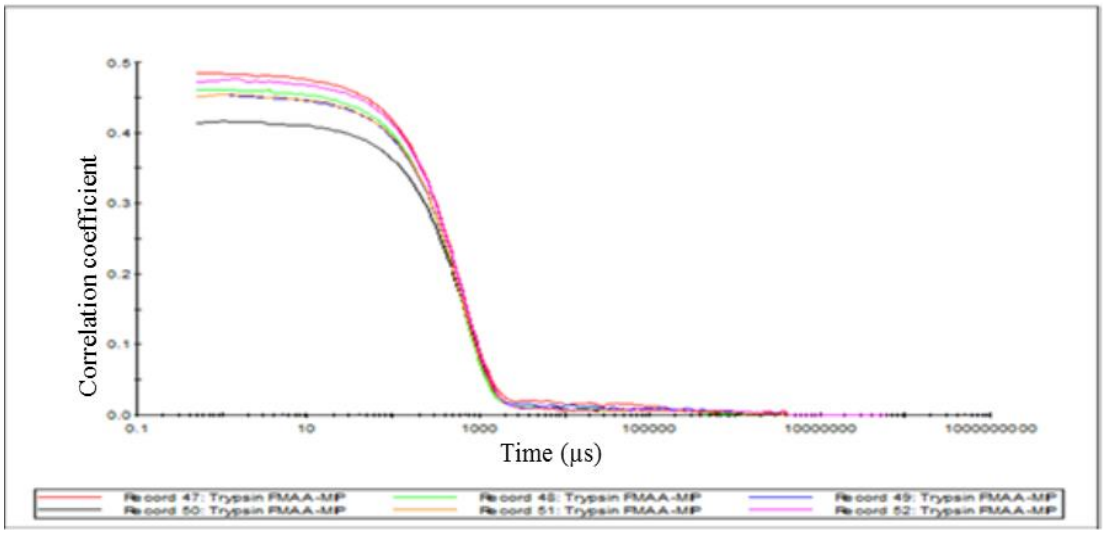
Correlation coefficient
Time (µs)

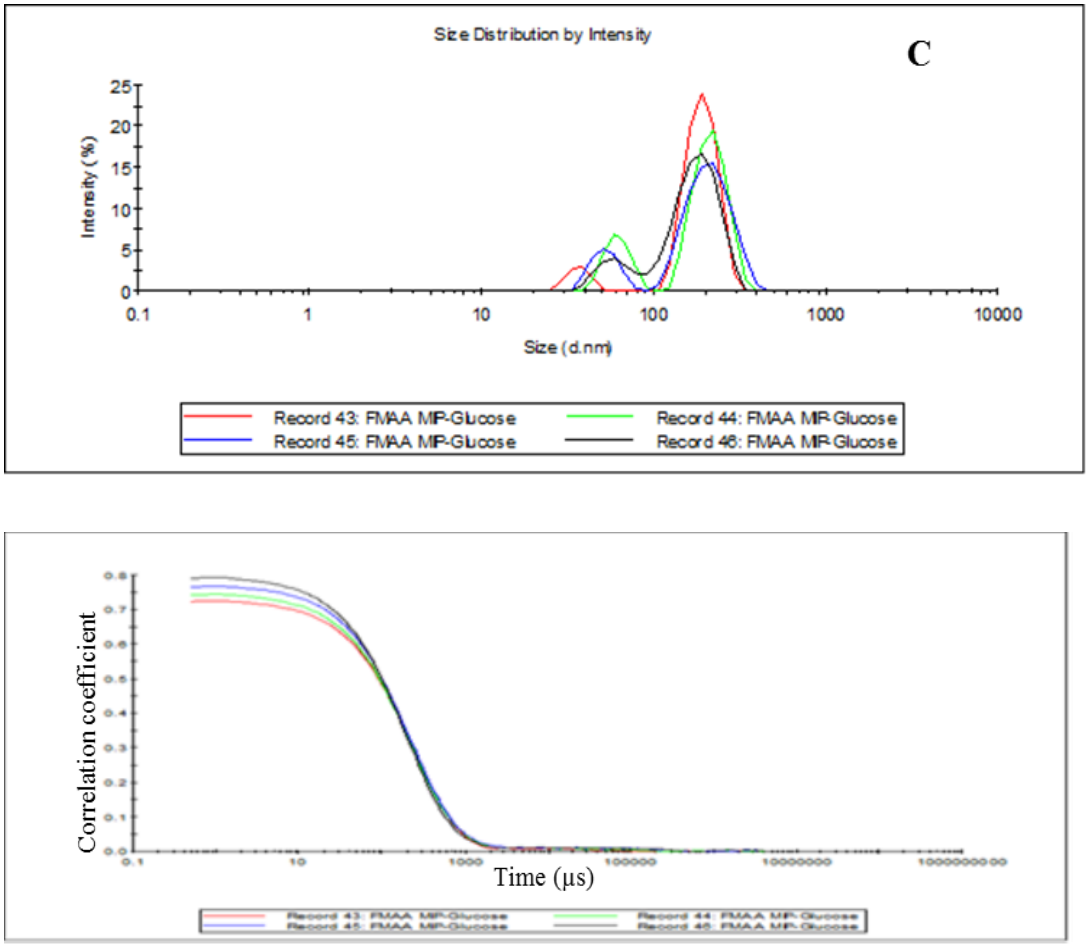

Figure 4.10: Graphs showing size distribution and correlation curves by intensity from the analysis of (A) HSL FMAA-MIP, (B) trypsin FMAA-MIP, and (C) glucose FMAA-MIP with DLS

In analysing the size distribution by intensity graphs (Figure 4.10), it may be noted that the size distributions are quite homogenous, taking into account the absence of other populations of NPs of different sizes. However, in case of glucose, there were two peaks observed, as well as the count rate being high, the reason for which might be insufficient washing. As mentioned, organic polymerisation obtained high yield as the count rate for the HSL-EMIP was around 4 times higher than others[134]. Due to the living nature of the process, this iniferter-based polymerisation enhanced particle size control, since the polymer chains grew at a constant rate compared to non-controlled radical polymerisation. The addition of a small amount of chain transfer agent could also help in controlling the polymerisation process.

4.11.2.2 NanoSight Analysis

NTA is an accurate technique compared to DLS especially when polydisperse samples are analysed the individual nanoparticles were tracked, rather than measuring the overall scattered light. HSL FMAA-MIP NPs only were evaluated using this technique[326]. NTA measures the particles movement through image analysis tracking the movement of the particles on a particle-by-particle basis. For polydisperse samples, in general, the NTA approach is appropriate due to the particle-by-particle measurement. DLS produces an average particle size due to the ensemble measurement (all particles measured at the same time) and is biased towards larger particles within the sample. The NTA technique does not give an average particle size but can give an approximate particle concentration and obtains size information based on the Brownian motion of individual particles[327].

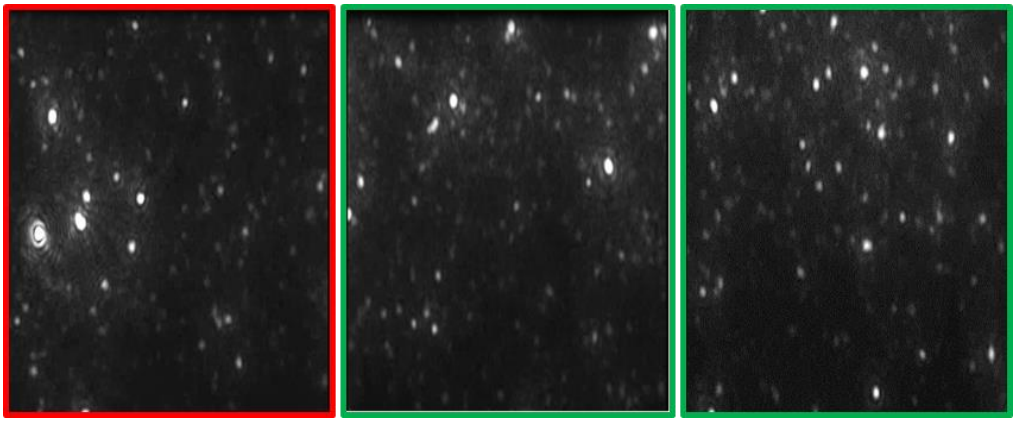

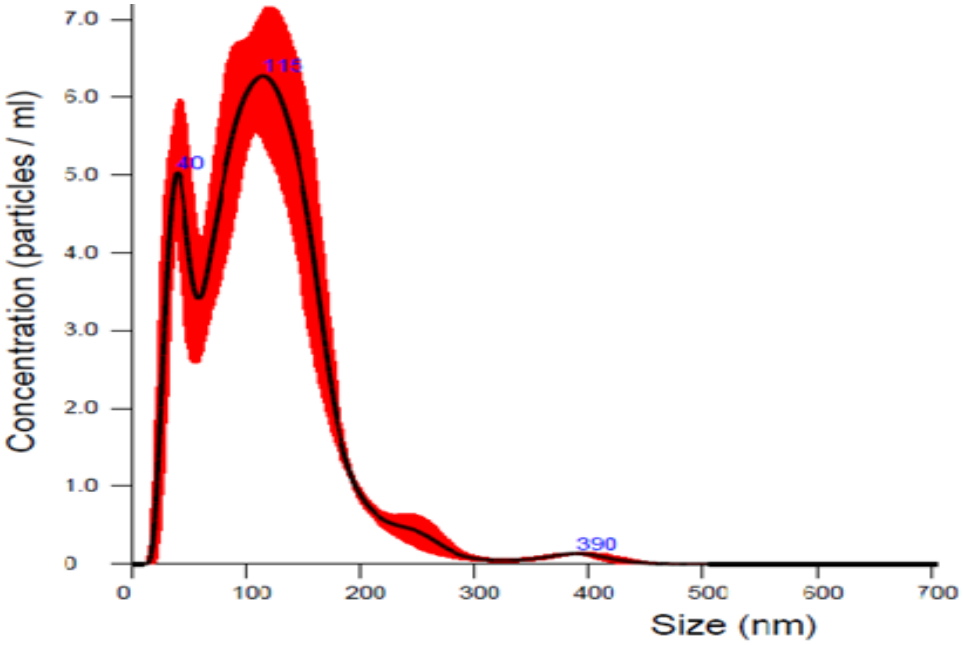

Figure 4.11: Average concentration/size for HSL FMAA-MIP measured by NanoSight

NTA analysis showed two main size populations of MIP NPs for the particles synthesised for HAL using 2 min of irradiation time (Figure 4.11). It should be noted that the size of the particles measured by NTA differs from the results of DLS, since the NTA techniques tracked individual nanoparticles rather than measuring the overall scattered light.

4.11.3 Electrochemical Sensor Measurements

All experiments were carried out via Autolab II using GSPEs. DPV was used and the experimental potential was recorded in the range -0.4 to +0.8 V with the step potential and modulation amplitude set to 50 mV. To obtain precise and reproducible values for the peak potentials, GSPEs included gold (4 mm diameter) as a working electrode and a platinum counter and silver reference electrode.

Gold was used to design the surface material due to its chemical stability, biocompatibility and the property that organic compounds can form well-ordered and packed monolayers on its surface[328]. For the gold surfaces, thiol compounds have been used for surface functionalisation. The high affinity of the thiol group (R-SH) for gold

results in the formation of a well-ordered organic layer with suitable functional groups exposed on the surface for different applications[329]. The robust and fast adsorption of alkylthiolates necessitates a clean Au surface, which can be accomplished by cleaning the latter with piranha solution or by plasma cleaning. Film properties, such as the structure and density of the resulting self-assembled monolayers (SAMs) can be affected by factors such as the solvent, temperature, concentration and purity of the adsorbate, the immersion time, and the concentration of oxygen in the solution.

Thin films of self-assembled monolayers (SAMs) are widely used in electroanalytical chemistry for sensor surface modification. The SAMs process is used due to their exposed surface groups, such as amines ($-NH_2$), which can interact with activated –COOH in the MIP via well-known carbodiimide chemistry[330]. SAMs were used for sensor surface modification with EMIP, after which the rebinding between EMIP and the template might result in an electrochemical signal which can be detected by DPV.

A conformational change in structure which increases the number of exposed electroactive moieties on the electrode-polymer interface, and which can be translated to electrochemical signal when the redox-labelled polymer recognises the analyte, can be detected as well.

In the case of the HLS EMIP based sensor, the current response of the rebinding process for the prepared EMIP with a different mediator (FC, FA and FMAA) was recorded. The response current was higher when FMAA was used in the polymerisation (80 µA). In terms of the percentage of the redox mediator, best results were obtained with 10% of ferrocene. The response current was found to increase with increasing template concentration. Under the chosen experimental conditions, the redox peaks of the probe were recorded in the -0.4 V to +0.8 V range. FMAA displayed a relatively stable oxidation peak, and it was easier to polymerise. The results shown in Figure 4.12 confirm that the MIP sensor based on FMAA has best response.

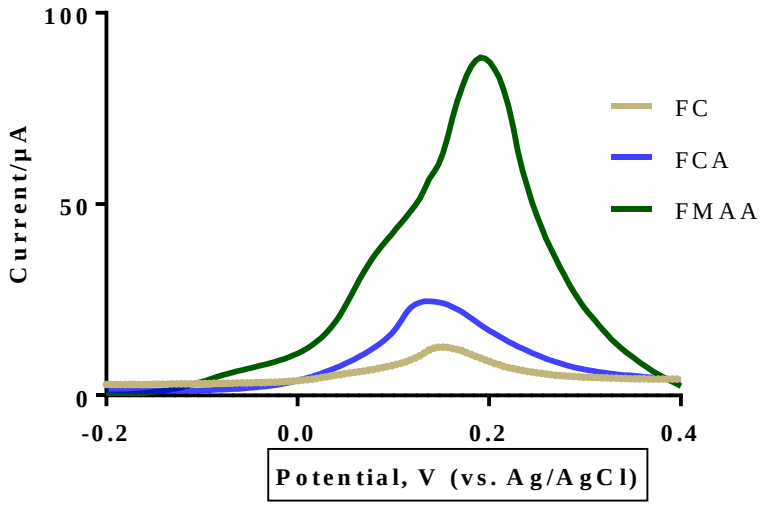

Figure 4.12: Current response for HSL MIP with 10% FC, FCA and FMAA

Subsequently, in order to evaluate the effects of the polymerisation type on the current response, water and organic polymerisation were undertaken using FMAA as a redox mediator. Figure 4.13 reveals that the organic polymerisation showed significant increase in terms of current response as compared to aqueous polymerisation. The reason for this is that amount of redox mediator was higher in the organic polymerisation, as a consequence of the low solubility of FMAA in water.

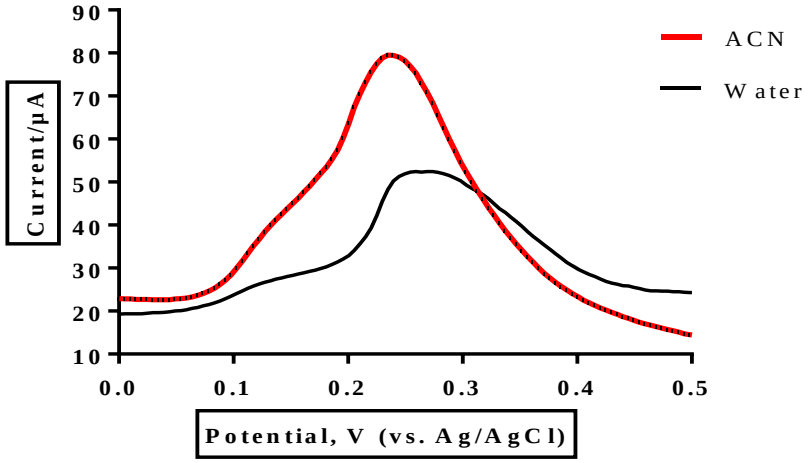

Figure 4.13: Water and organic HSL- FMAA MIP

The next step was to optimise the percentage of FMAA. To this end, three HSL FMAA-MIP were prepared with different percentages of FMAA. Then, DPV was used to evaluate the current response for all EMIPs. As shown in Figure 4.14 , 10% FMAA by weight of MAA gave the optimal current response, which was used in the subsequent experiments.

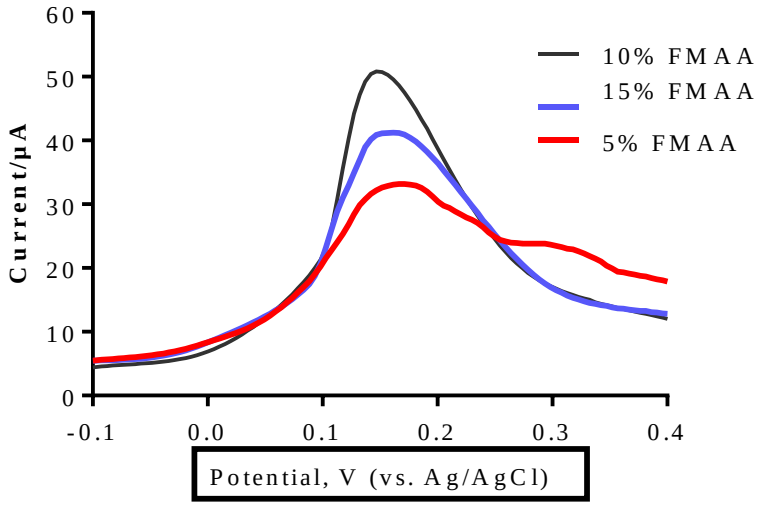

Figure 4.14: Current response for the HSL MIP incorporated with FMAA

4.11.4 Detection of C4 HSL Using the DPV Sensor

After the characterisation steps, DPV was carried out for the real-time detection of C4 HSL in aqueous solution. The sensor surface was modified to immobilise the EMIP, and its signal was recorded as a blank after washing. Subsequently, the solutions, including different concentrations of C4 HSL (1–200 nM), were applied to the DPV sensor system. The DPV signals (current response) were changing with C4 HSL concentration. The amount of C4 HSL could be determined quantitatively due to the correlation between DPV signal and amount of C4 HSL present (Figure 4.15). The calibration curve shows linearity in the range 6.5-100 nM, with a LOD of 0.3×10^{-9} M (Figure 4.17).

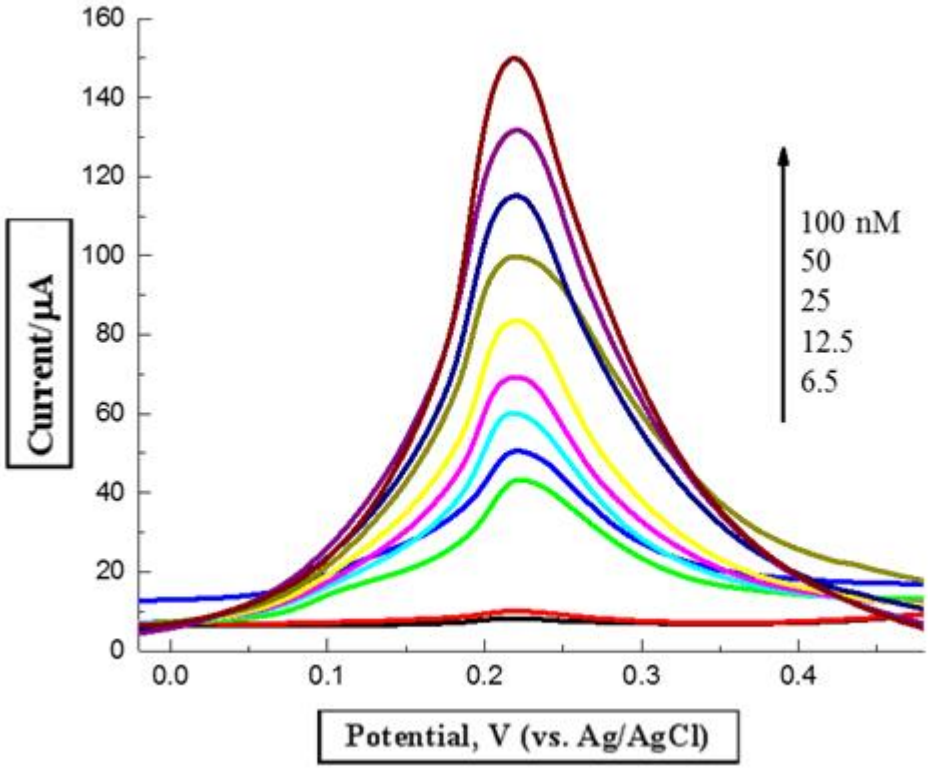

Figure 4.15: DPV voltammogram for the C4 HSL sensor

4.11.5 Selectivity of HSL FMAA-MIP toward C4 HSL

The EMIPs capable of recognising C4 HSL were used in the DPV sensor. During DPV measurements the EMIP nanoparticles were immobilised on the SPE surface using EDC to activate the EMIP carboxylic acid to react with an amino group (cysteamine). Thus, the current intensity response could be correlated to the C4 HSL concentration. To demonstrate the specificity of EMIP as a recognition element, the response of the DPV sensor was recorded for C6 HSL, oxo-C6 HSL and γ-butyrolactone, as shown in Figure 4.16. These molecules were selected as structural analogues of C4 HSL because they are likely to be found in the same environment as C4 HSL.

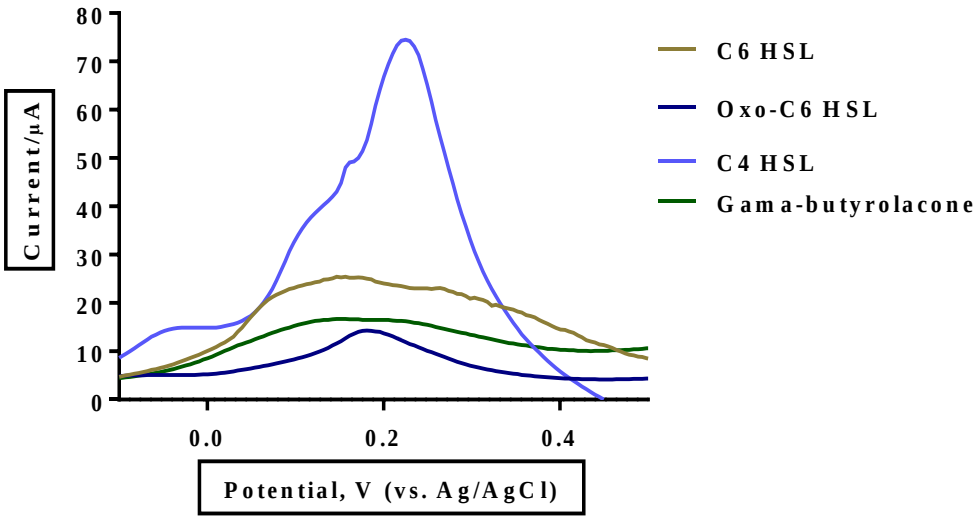

Figure 4.16: Sensor selectivity for C4 HSL and its analogues

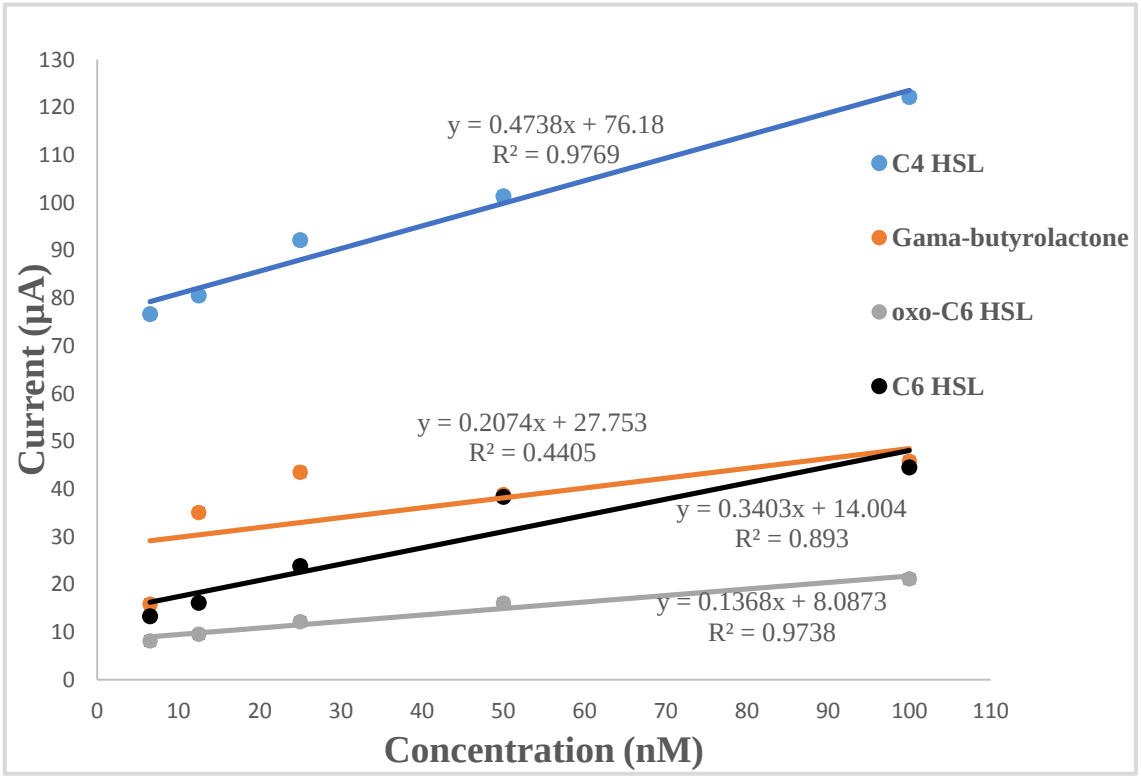

Figure 4.17: Calibration curve for C4 HSL and its analogues

The results of these experiments, as shown in Figure 4.16 and Figure 4.17 confirm that the MIP sensor had three times higher response for the target molecule than analouges with no interfrences effect from the structural analogues, demonstrating that this sensor was specific to HSL structure. The chain length and functionality might be the reason for variations in sensor response to the analogues. In addition, in case of γ-butyrolactone, the curve was non-linear with low value of R^2 (0.440).

As conclusion, a highly sensitive and selective MIP sensor for the detection of C4 HSL was successfully developed by the measurement of the oxidative current of redox mediator (FMAA), an electrochemical probe, located onto MIP surface, after the template molecules were added, and which could represent a useful method for practical analyses.

4.11.6 Detection of Trypsin Using the DPV Sensor

After the characterisation steps, FMAA was used to create electroactive nanoparticles. After the washing, separation and concentration processes, the DPV sensor as based on the EMIP was tested to evaluate the interaction between EMIPs and trypsin. According to the results illustrated in Figure 4.18, the current response for the DPV sensor increased with increasing trypsin concentration. However, optinisation steps are required to overcome the small shift in the oxidation peak.

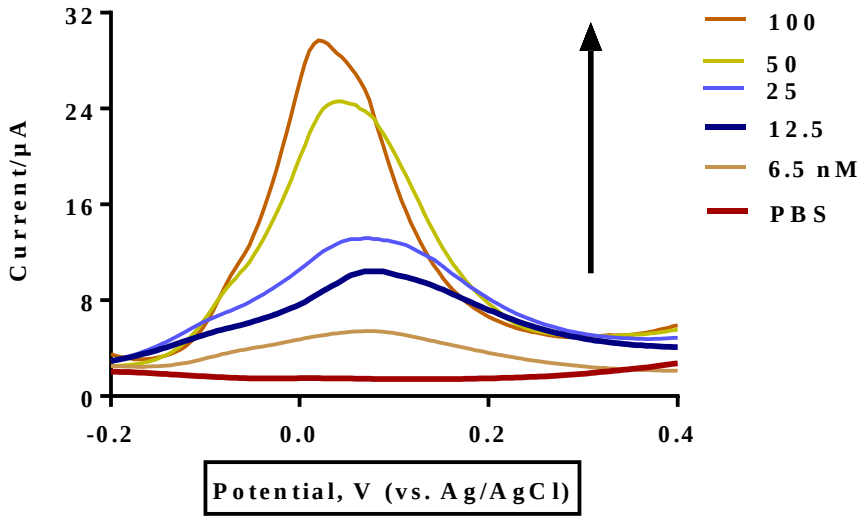

Figure 4.18: DPV voltammogram for trypsin sensor

4.11.7 Selectivity of Trypsin FMAA-MIP Sensor

MIPs with the anchored redox mediator were immobilised by covalent bonding to the functionalised electrode surface. MIPs containing a carboxylic group were activated by EDC to form a reactive O-acylisourea, which reacts with the gold-bound amine to form an amide. Subsequently, the process of electrochemical determination of analytes using MIP nanoparticles in sensors was performed successfully. As shown in Figure 4.19, there is a considerable difference between the current response for trypsin itself and other proteins, whilst at the same time there is no response for bare electrode (without MIP). This can be explained by the fact that the polymer cavities are specific to the imprinted molecule; when the MIP recognises the analyte a conformational change in structure occurs during the binding which increases the number of exposed electroactive moieties that can be detected on the electrode-polymer interface as a result of the particles swelling (Figure 4.3).

To be sure that the prepared EMIP particles have affinity for the target trypsin, the DPV sensor-based EMIP templated for trypsin was tested by studying the influence of other proteins (pepsin and avidin). The analogue was chosen as it had a similar isoelectric point (avidin) and is likely to be found in the same environment and matrix (pepsin). The current response increased propotinally with the increase of the analyteconcentration, while the response of the analogues was considerably lower than that of the target species. Trypsin could therefore be detected in the presence of other molecules.

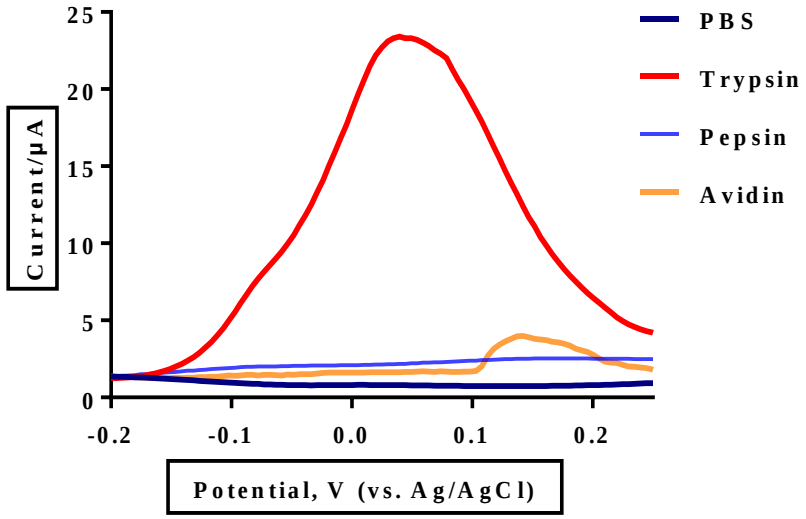

Figure 4.19: Selectivity of the trypsin sensor

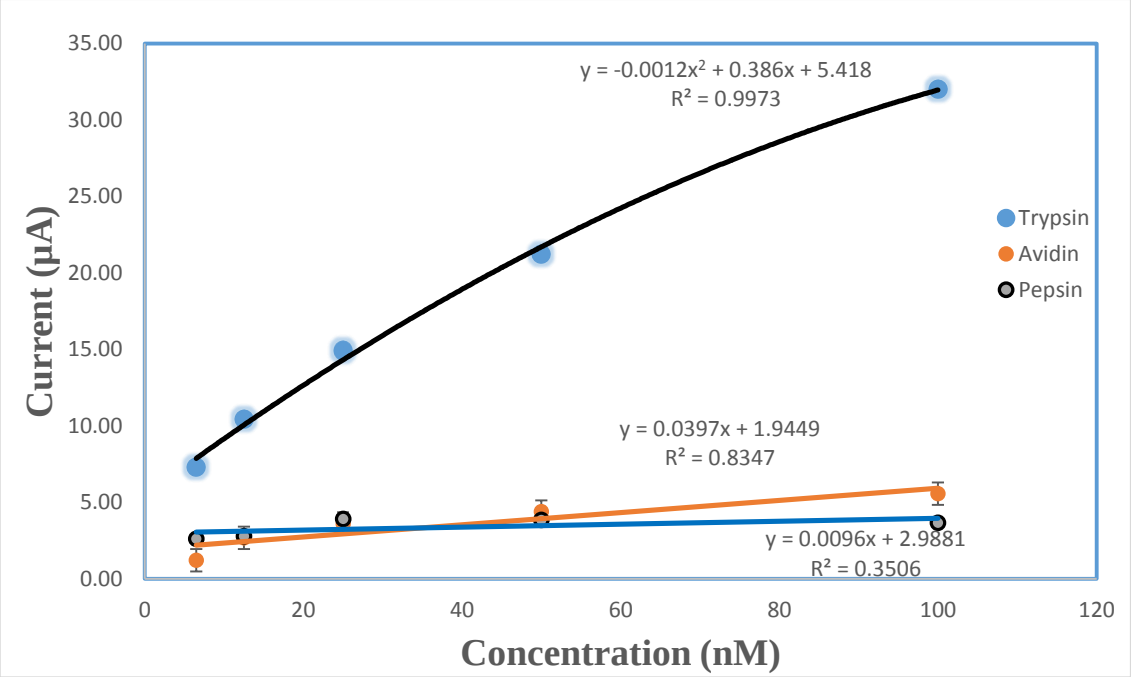

Figure 4.20: Calibration curve for trypsin and its analogues

4.11.7.1 Real Sample Detection of Trypsin

To confirm the possibility of using the DPV sensor for detection of trypsin in a real sample, the proposed DPV sensor based on EMIP NPs as a receptor was used to detect trypsin in human plasma. Human plasma was disssolved in PBS (0.01M) then centrifuged (20 min/4000 rpm) to remove the participated part. A 1.2 µm filter membrane was used to eliminate undissolved material. After that, the supernatant was dissolved in 100 ml of PBS buffer. The detection of trypsin in diluted plasma was conducted voltametrically, accordingly to the protocol described earlier[66]. A serial dilution of trypsin was prepared using diluted plasma. The results indicated that the EMIP NPs-based sensor showed some promise in terms of the accurate and rapid determination of trypsin in complex biological samples and without any interferences. The proposed sensor shows excellent characteristics such as high selectivity and straightforward measurements which would be necessary for routine work. However, there is a small shift in the oxidation peak as a results for the pH.

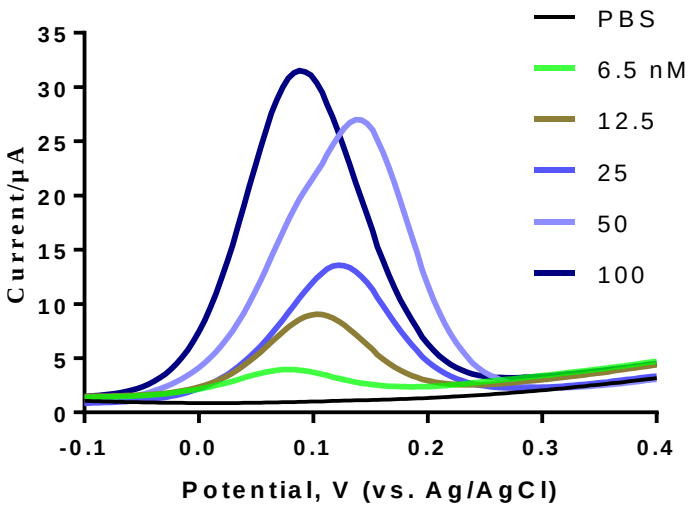

Figure 4.21: Voltammogram for Trypsin sensor in plasma

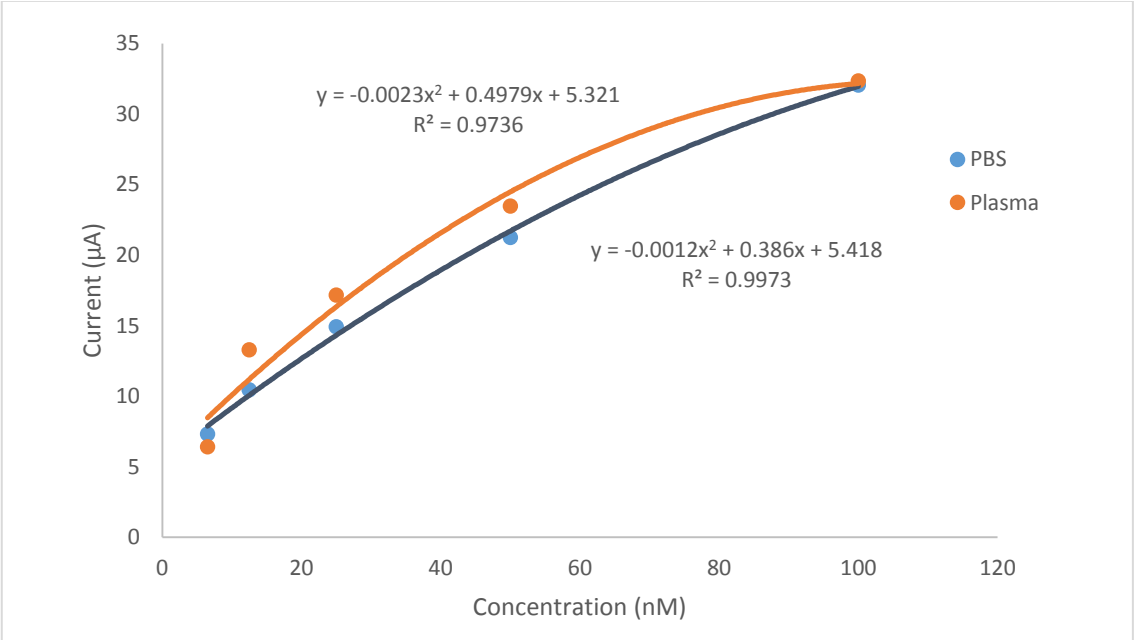

Figure 4.22: Calibration curve for Trypsin in PBS buffer and Plasma

4.11.8 Solution Polymerisation for Glucose

As known, it is difficult to immobilise glucose on a solid phase as solid phase approach requires a functional group for immobilisation. As a result, glucose imprinting was carried out in solution (without glass beads). In solution polymerisation, the monomer, cross-linker, template, initiator and resulting polymer are all soluble in the solvent. This polymerisation can involve a simple process in which a monomer, initiator, catalyst, and solvent are stirred together to form a solution that reacts without the need for heating or indeed any other from of special handling[331]. The capability of molecularly imprinted polymer cavities to bind selectively to the target molecule is derived from the removal of analogues from their corresponding cavities. EMIP formed in solution might include unreacted monomer and small particles which can be reduced or eliminated during the subsequent washing step using a centrifuge cartridge filter (10 K). If the wash step is not successful in removing the template from the MIP, then the recognition site will be not available. As mentioned in the introduction, most glucose sensor based on enzyme activities (glucose oxidase) while labelling the MIP with an electroactive mediator could be used for the direct detection of the template.

4.11.9 Electrochemical Measurements of Glucose

All experiments were carried out using the DPV technique. Experiments were performed under the following experimental conditions: the potential was recorded over the range of -0.4 to +0.8 V whilst the step potential and modulation amplitude were set to 50 mV. The current signal measured the redox potential of the redox marker in EMIPs versus an AgCl reference electrode. The DPV responses of the EMIP-coated electrodes to glucose solutions are illustrated in Figure 4.23 . For the control measurements, a MIP templated for dopamine was used as a control, which showed a negligible response to glucose. Furthermore, the selectivity of the DPV sensor was tested by studying the impact of analogues (maltose, lactose and fructose). The glucose sensor did not show any considerable cross-reactivity for fructose, maltose or lactose (Figure 4.24). The present results are significant in at least two major respects, namely the direct measurement of glucose (non-enzymatic sensor) and the ability to detect glucose in the presence of glucose analogues.

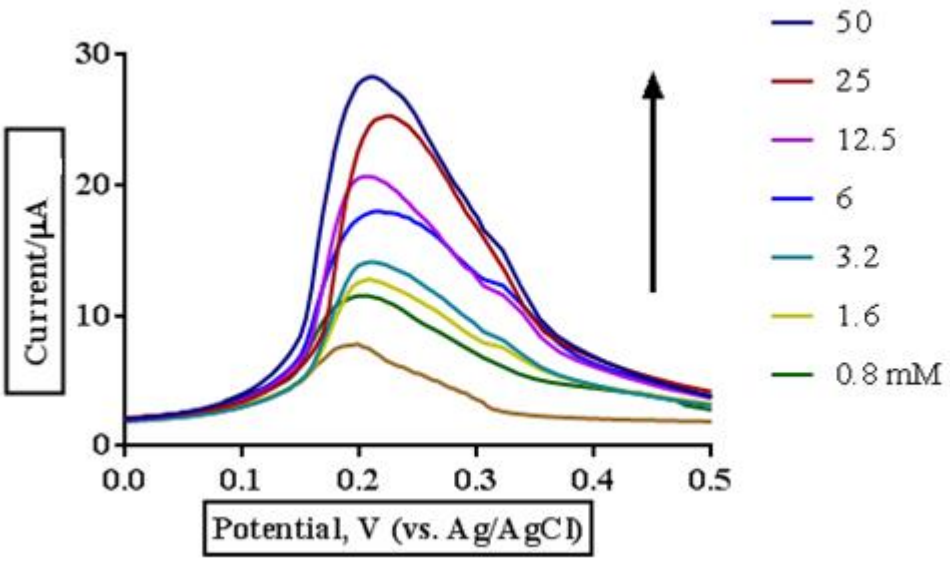

Figure 4.23: DPV voltammogram for the glucose sensor

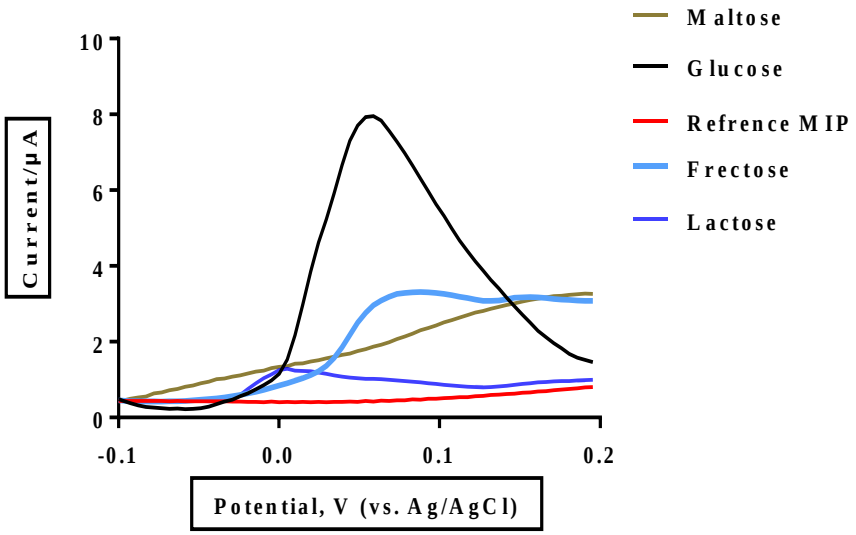

Figure 4.24: DPV voltammogram for glucose and its analogues

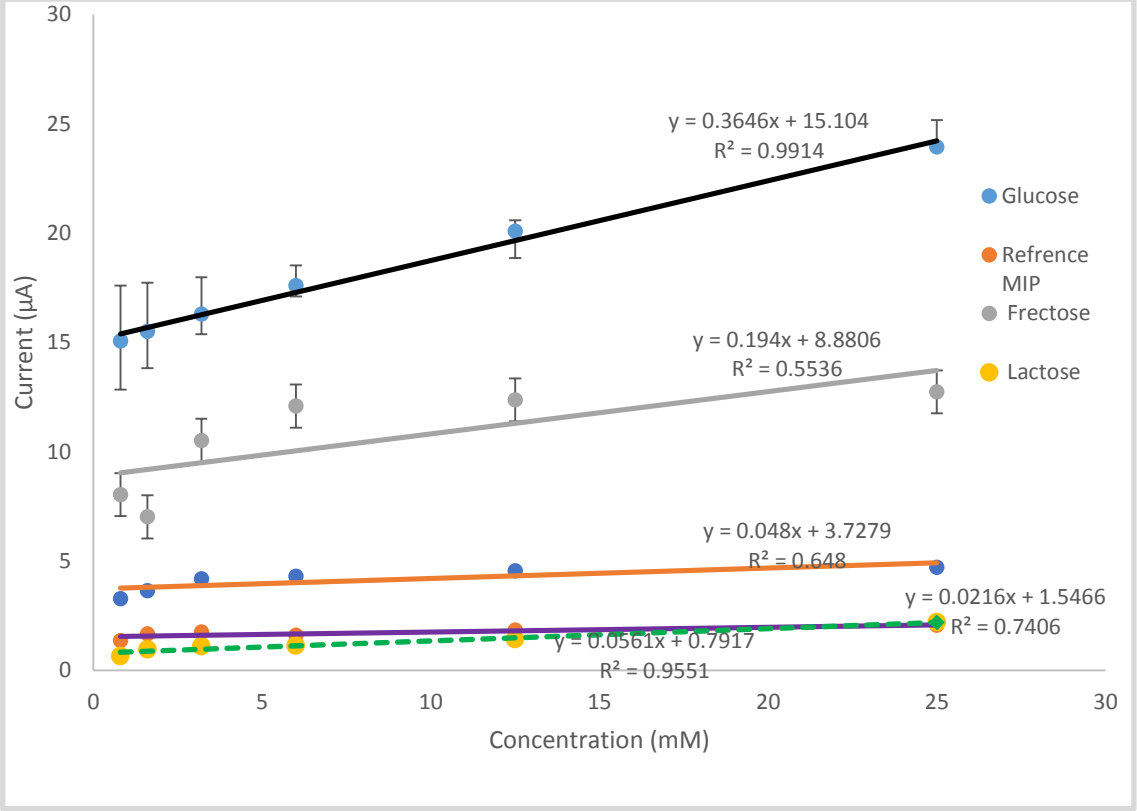

Figure 4.25: Calibration curves for glucose and its analogues

As shown in Figure 4.25 the current response was higher for glucose and there is no interferences effect from glucose analogues in the concertation range (0.8-25 mM). However, in case of fructose, the curve was non-linear with the R^2 value 0.5536.

4.12 Conclusion

It was exciting to confirm that the proposed DPV sensor based on EMIP had a wide detection range for analytes (HSL, trypsin and glucose) sensing. The wide detection range was attributed to the large surface area of the EMIP nanoparticles and the specificity of the cavities therein. The nanosized particles have small dimensions with a high surface-to-volume ratio and thus more homogeneous recognition sites could be accommodated, resulting in a large number of active binding cavities being available in the fabricated EMIP sensor. Additionally, the conformational structure change of the EMIP

nanoparticles was found to enhance and increase the number of exposed electroactive moieties detected on the electrode-polymer interface, again resulting in a larger number of active binding sites being available. Furthermore, the SPE technology is an excellent technique by which to fabricate electrochemical sensors. The sensor was tested using the DPV technique. The detection limits for these assays were 0.3×10^{-9}, 0.22×10^{-9} and 0.13×10^{-6} M for C4 HSL, trypsin and glucose respectively. There was little to no cross-reactivity observed for the template analogues. The EMIP sensor exhibited a higher response than the control MIP. We think this approach can be applied to a wide range of molecules. The EMIP-based electrochemical sensor is a valuable new tool that allows quantitative measurement with particular analyte molecules. It has potential applications in the fields of clinical diagnosis, food analysis and other industrial applications in terms of real-time detection with high specificity.

Chapter Five: General Conclusion and Future Work

5.1 General Conclusion

In this project, MIP NPs were synthesised using a solid phase approach. The MIP NPs have been used for the imprinting of small molecules and big molecules (proteins)[332]. MIPs are rapidly becoming viable alternatives to natural antibodies in sensor technology. Moreover, MIPs offer many benefits regarding shelf-life, stability, robustness, cost and ease of preparation. Particularly exciting are advances with formation of MIP NPs for proteins by solid phase approach[136,323,333].

In the first part of work, a potentiometric sensor based on MIP NPs was developed for the detection of cocaine. As a target analogue, benzoylecgonine was used as a template because cocaine does not have a functional group that can be used to immobilise it onto the glass beads' surface. Different polymerisation techniques were applied in this work (organic and aqueous polymerisation). The composition of polymers with high affinity monomers for cocaine was optimised using molecular modelling. Nanoparticles synthesised using solid phase approach were incorporated within a PVC matrix to create a membrane, which was then used to fabricate an ion-selective electrode. The use of nanoparticles with high affinity and specificity allowed for label-free detection and quantification of cocaine in real samples with short response times. The developed potentiometric sensor exhibited good sensitivity and selectively allowing to quantify cocaine in human serum sample over the range of concentrations from $1x10^{-9}$-$1x10^{-3}$ M.

For non-charged compounds such as HSL, MIP NPs were prepared and immobilised on the surface of a QCR sensor. An acoustic technique used in project was based on Fixed Frequency Drive (FFD) that allowed detection of the HSL sample in 10 min. The FFD technique enabled the sensitive, specific, label-free, rapid and real-time detection of C6-HSL in spiked PBS solution. The novel acoustic sensor can potentially be integrated onto a single silicon chip which favours point of care diagnostics of gram-negative bacterial infections. The FFD technique allowed analytical estimation of the frequency shift of the QCR crystal when the template was bound to HSL MIP NPs. The FFD technique enabled the sensitive, specific, label-free, rapid and real-time detection of C6-HSL in spiked PBS solution with a minimum quantification limit down to 1 µM. The results were better than published previously which C6-HSL was measured using frequency sweep (FS) analysis of QCM[326]. The minimum C6 HSL concentration tried for that work was $1x10^{-3}$ M.

Major success in this work came from integration of MIP NPs with electrochemical transducers capable of detecting non-electroactive molecular targets. A new strategy to detect non-electroactive molecular targets is based on the introduction of a redox probe in the form of a functional monomer into MIP NPs prepared by a solid phase approach. In electroactive MIP NPs (EMIP) the ferrocenylmethyl methacrylate group has acted as the redox probe, sensitive to the change in volume of nanoparticles, triggered by their interaction with the template. DPV was used to assess the selectivity and sensitivity of EMIPs toward templates. The detection limits for these sensors were 0.3×10^{-9}, 0.22×10^{-9}, 0.13×10^{-6} M for HSL, trypsin and glucose respectively with no cross reactivity from the compounds with similar structure. The integration of EMIP with screen printed gold electrodes can be made using well-known and established technology for mass producing electrodes. Comparing our results with these published earlier[334], we can conclude that our sensor design is superior to examples when redox label was used in solution. Our sensors did not depend on the diffusion of soluble mediator, additionally, there is no need for Nafion modified electrode or a requirement for changing the buffer solution. In contrast to previously published examples, our approach is generic, allowing detection of small or large templates, requires minimum handling and compatible with standard techniques used in mass manufacturing of sensor devices.

5.2 Future Work

The natural expansion of my work will be incorporation of the electroactive MIP particles in manufacturing process of screen printed electrodes (SPE). SPE present the advantage over traditional electrodes as being easy to handle and allowing production of cheap sensors devices by well-known and established technology suitable for mass producing. MIPs can be integrated in a gold paint ink for production of functionalised screen printed electrodes. Futhermore, the robustness of the sensor could be evaluated by testing on different pH, temperature, solvent and storage time.

Potential area whether these sensors could include clinical, environmental and food analysis. It would be essential to study performance of MIP sensors in complex matrices and in different environmental conditions. The performance of such sensors will have to be validated against standard analytical techniques such as HPLC and HPLC-MS.

Morever, enhancing the MIP NPs yield by optimising the polymerisation condition or using amino bulk polymer as a solid phase support instead of glass beads.

Yet another area for future research involves integration of developed sensor with mobile phones and commercial sensor platforms. This development however is fundamentally engineering task and beyond the scope of my work.

5.3 List of Publications

1. **New potentiometric sensor based on molecularly imprinted nanoparticles for cocaine detection.** Biosensors and Bioelectronics (2017); 96, 49-54.
2. **Molecularly Imprinted Polymers in electrochemical and optical sensor**. Trends in biotechnology (2019) 37, 3, 294-309.
3. **Label free acoustic detection of gram negative bacterial infection biomarker using a fixed frequency drive (in preparation).**
4. **Process for determination of analytes using conformational changes in redox labelled molecularly imprinted polymer nanoparticles** (submitted patent with application number1809276.7).
5. **Electrochemical sensor based on electroactive molecularly imprinted polymer nanoparticles (EMIP).** In preparation to submit in Nature protocol.

Chapter Six: Bibliography

6.1 References

1. M. Polyakov, *Zhur Fiz Khim*, 1931, **2**, 799-805.
2. M. D. Sousa and C. M. Barbosa, *Quimica Nova*, 2009, **32**, 1609-1619.
3. F. H. Dickey, *Proceedings of the national academy of sciences*, 1949, **35**, 227-229.
4. R. Walsh, Waterford Institute of Technology, 2010.
5. N. Samarth, V. Kamble, P. Mahanwar, A. Rane and V. Abitha, *Chem. Int*, 2015, **1**, 202-210.
6. V. Grassi, Universidade de São Paulo, 2008.
7. T. Takagishi and I. M. Klotz, *Biopolymers*, 1972, **11**, 483-491.
8. G. Wulff, *Angrew. Chem. Internat. Edit.*, 1972, **11**, 341.
9. R. Arshady and K. Mosbach, *Die Makromolekulare Chemie*, 1981, **182**, 687-692.
10. L. Andersson, B. Sellergren and K. Mosbach, *Tetrahedron Lett.*, 1984, **25**, 5211-5214.
11. S. A. Piletsky, N. W. Turner and P. Laitenberger, *Med. Eng. Phys.*, 2006, **28**, 971-977.
12. N. Lavignac, C. J. Allender and K. R. Brain, *Anal. Chim. Acta*, 2004, **510**, 139-145.
13. G. Vlatakis, L. I. Andersson, R. Müller and K. Mosbach, *Nature*, 1993, **361**, 645.
14. P. Zhao and J. Hao, *Food Chem.*, 2013, **139**, 1001-1007.
15. A. Poma, A. Guerreiro, M. J. Whitcombe, E. V. Piletska, A. P. Turner and S. A. Piletsky, *Advanced functional materials*, 2013, **23**, 2821-2827.
16. A. Poma, A. Guerreiro, S. Caygill, E. Moczko and S. Piletsky, *RSC Adv.*, 2014, **4**, 4203-4206.
17. K. Haupt and K. Mosbach, *Chem. Rev.*, 2000, **100**, 2495-2504.
18. K. Haupt, *Journal*, 2003.
19. A. Poma, A. Guerreiro, M. J. Whitcombe, E. V. Piletska, A. P. F. Turner and S. A. Piletsky, *Advanced Functional Materials*, 2013, **23**, 2821-2827.
20. O. Ramström, L. Ye and K. Mosbach, *Chem. Biol.*, 1996, **3**, 471-477.
21. M. J. Whitcombe, C. Alexander and E. N. Vulfson, *Trends in Food Science & Technology*, 1997, **5**, 140-145.
22. L. Longo and G. Vasapollo, *Mini Rev. Org. Chem.*, 2008, **5**, 163-170.
23. A. Bossi, F. Bonini, A. Turner and S. Piletsky, *Biosensors and Bioelectronics*, 2007, **22**, 1131-1137.
24. S. Scorrano, L. Mergola, R. Del Sole and G. Vasapollo, *International journal of molecular sciences*, 2011, **12**, 1735-1743.

25. F. Puoci, G. Cirillo, M. Curcio, F. Iemma, U. Spizzirri and N. Picci, *Anal. Chim. Acta*, 2007, **593**, 164-170.

26. C. Baggiani, L. Anfossi and C. Giovannoli, *Anal. Chim. Acta*, 2007, **591**, 29-39.

27. L. I. Andersson, *Journal of Chromatography B: Biomedical Sciences and Applications*, 2000, **745**, 3-13.

28. V. Pichon and F. Chapuis-Hugon, *Analytica chimica acta*, 2008, **622**, 48-61.

29. Y. Uludağ, S. A. Piletsky, A. P. Turner and M. A. Cooper, *The FEBS journal*, 2007, **274**, 5471-5480.

30. W. Li and S. Li, in *Oligomers-Polymer Composites-Molecular Imprinting*, Springer, 2006, pp. 191-210.

31. F. Puoci, F. Iemma and N. Picci, *Current drug delivery*, 2008, **5**, 85-96.

32. S. Pardeshi, R. Dhodapkar and A. Kumar, *Food Chem.*, 2014, **146**, 385-393.

33. K. J. Shea and E. Thompson, *The Journal of Organic Chemistry*, 1978, **43**, 4253-4255.

34. K. J. Shea, E. A. Thompson, S. D. Pandey and P. S. Beauchamp, *J. Am. Chem. Soc.*, 1980, **102**, 3149-3155.

35. J. Damen and D. Neckers, *J. Am. Chem. Soc.*, 1980, **102**, 3265-3267.

36. E. L. Holthoff and F. V. Bright, *Anal. Chim. Acta*, 2007, **594**, 147-161.

37. B. Sellergren and A. J. Hall, *Molecularly imprinted polymers*, Wiley Online Library, 2012.

38. M. Yan, *Molecularly imprinted materials: science and technology*, CRC press, 2004.

39. G. V. Lisichkin and Y. A. Krutyakov, *Russian chemical reviews*, 2006, **75**, 901-918.

40. M. Kempe, K. Mosbach and L. Fischer, *J. Mol. Recognit.*, 1993, **6**, 25-29.

41. J. Haginaka and H. Sanbe, *Chem. Lett.*, 1999, **28**, 757-758.

42. K. Sreenivasan, *Talanta*, 1997, **6**, 1137-1140.

43. M. J. Whitcombe, M. E. Rodriguez, P. Villar and E. N. Vulfson, *J. Am. Chem. Soc.*, 1995, **117**, 7105-7111.

44. C.-C. Hwang and W.-C. Lee, *J. Chromatogr. A*, 2002, **962**, 69-78.

45. K. Haupt, *The Analyst*, 2001, **126**, 747-756.

46. J. Haginaka, H. Tabo and C. Kagawa, *J. Pharm. Biomed. Anal.*, 2008, **46**, 877-881.

47. J.-f. He, Q.-h. Zhu and Q.-y. Deng, *Spectrochimica Acta Part A: Molecular and Biomolecular Spectroscopy*, 2007, **67**, 1297-1305.

48. L. I. Andersson and K. Mosbach, *J. Chromatogr. A*, 1990, **516**, 313-322.

49. M. T. Koesdjojo, Y. H. Tennico and V. T. Remcho, in *Separation Science and Technology*, Elsevier, 2007, vol. 8, pp. 479-503.

50. S. Al-Kindy, R. Badía, J. L. Suárez-Rodríguez and M. E. Díaz-García, *Critical Reviews in Analytical Chemistry*, 2000, **30**, 291-309.

51. J. Matsui, I. A. Nicholls and T. Takeuchi, *Tetrahedron: Asymmetry*, 1996, **7**, 1357-1361.

52. J. Matsui, I. A. Nicholls and T. Takeuchi, *Anal. Chim. Acta*, 1998, **365**, 89-93.

53. B. R. Hart and K. J. Shea, *J. Am. Chem. Soc.*, 2001, **123**, 2072-2073.

54. J. L. Urraca, A. J. Hall, M. C. Moreno- Bondi and B. Sellergren, *Angewandte Chemie*, 2006, **118**, 5282-5285.

55. K. Karim, T. Cowen, A. Guerreiro, E. Piletska, M. J. Whitcombe and S. A. Piletsky, 2017.

56. K. Muzyka and M. Rozhitskii, *Системи обробки інформації*, 2012, 237-240.

57. X. Fu, Q. Yang, Q. Zhou, Q. Lin and C. Wang, *Open Journal of Organic Polymer Materials*, 2015, **5**, 58.

58. B. Sellergren, *TrAC Trends in Analytical Chemistry*, 1999, **18**, 164-174.

59. C. Yu and K. Mosbach, *The Journal of Organic Chemistry*, 1997, **62**, 4057-4064.

60. M. Avila, M. Zougagh, Á. Ríos and A. Escarpa, *TrAC Trends in Analytical Chemistry*, 2008, **27**, 54-65.

61. T. S. Rebelo, C. Santos, J. Costa-Rodrigues, M. Fernandes, J. P. Noronha and M. G. F. Sales, *Electrochimica Acta*, 2014, **132**, 142-150.

62. P. A. Cormack and A. Z. Elorza, *Journal of Chromatography B*, 2004, **804**, 173-182.

63. E. Yilmaz, K. Mosbach and K. Haupt, *Analytical Communications*, 1999, **36**, 167-170.

64. T. Zhang, F. Liu, W. Chen, J. Wang and K. Li, *Anal. Chim. Acta*, 2001, **450**, 53-61.

65. W. M. Mullett, M. F. Dirie, E. P. Lai, H. Guo and X. He, *Anal. Chim. Acta*, 2000, **414**, 123-131.

66. K. Smolinska-Kempisty, O. S. Ahmad, A. Guerreiro, K. Karim, E. Piletska and S. Piletsky, *Biosensors and Bioelectronics*, 2017, **96**, 49-54.

67. F. Canfarotta, Department of Chemistry, 2016.

68. X. Zhang, F. Shen, Z. Zhang, Y. Xing and X. Ren, *Analytical Methods*, 2014, **6**, 9483-9489.

69. M. Kempe and K. Mosbach, *Tetrahedron Lett.*, 1995, **36**, 3563-3566.

70. F. Canfarotta, A. Poma, A. Guerreiro and S. Piletsky, *Nat. Protoc.*, 2016, **11**, 443-455.

71. K. Yoshimatsu, K. Reimhult, A. Krozer, K. Mosbach, K. Sode and L. Ye, *Anal. Chim. Acta*, 2007, **584**, 112-121.

72. G. Vasapollo, R. D. Sole, L. Mergola, M. R. Lazzoi, A. Scardino, S. Scorrano and G. Mele, *International journal of molecular sciences*, 2011, **12**, 5908-5945.

73. B. Sellergren and K. J. Shea, *J. Chromatogr. A*, 1993, **635**, 31-49.

74. S. Scorrano, L. Longo and G. Vasapollo, *Anal. Chim. Acta*, 2010, **659**, 167-171.

75. K. Yoshizako, K. Hosoya, Y. Iwakoshi, K. Kimata and N. Tanaka, *Anal. Chem.*, 1998, **70**, 386-389.

76. U. Athikomrattanakul, M. Katterle, N. Gajovic-Eichelmann and F. W. Scheller, *Biosensors and Bioelectronics*, 2009, **25**, 82-87.

77. D. Spivak, M. A. Gilmore and K. Shea, *J. Am. Chem. Soc.*, 1997, **119**, 4388-4393.

78. A. R. Kannurpatti, S. Lu, G. M. Bunker and C. N. Bowman, *Macromolecules*, 1996, **29**, 7310-7315.

79. E. V. Piletska, A. R. Guerreiro, M. J. Whitcombe and S. A. Piletsky, *Macromolecules*, 2009, **42**, 4921-4928.

80. B. Sellergren, M. Lepistoe and K. Mosbach, *J. Am. Chem. Soc.*, 1988, **110**, 5853-5860.

81. N. Marchyk, J. Maximilien, S. Beyazit, K. Haupt and B. T. S. Bui, *Nanoscale*, 2014, **6**, 2872-2878.

82. S. A. Piletsky, I. Mijangos, A. Guerreiro, E. V. Piletska, I. Chianella, K. Karim and A. P. Turner, *Macromolecules*, 2005, **38**, 1410-1414.

83. T. Cowen, K. Karim and S. Piletsky, *Anal. Chim. Acta*, 2016, **936**, 62-74.

84. S. A. Piletsky, K. Karim, E. V. Piletska, A. P. F. Turner, C. J. Day, K. W. Freebairn and C. Legge, *The Analyst*, 2001, **126**, 1826-1830.

85. I. Chianella, M. Lotierzo, S. A. Piletsky, I. E. Tothill, B. Chen, K. Karim and A. P. Turner, *Anal. Chem.*, 2002, **74**, 1288-1293.

86. S. Wei, M. Jakusch and B. Mizaikoff, *Anal. Bioanal. Chem.*, 2007, **389**, 423-431.

87. C. F. Silva, K. B. Borges and C. S. do Nascimento, *Analyst*, 2018, **143**, 141-149.

88. K. Puzio, R. Delépée, R. Vidal and L. A. Agrofoglio, *Anal. Chim. Acta*, 2013, **790**, 47-55.

89. F. Bates, M. Busato, E. Piletska, M. J. Whitcombe, K. Karim, A. Guerreiro, M. del Valle, A. Giorgetti and S. Piletsky, *Separation Science and Technology*, 2017, **52**, 1441-1453.

90. K. Farrington, E. Magner and F. Regan, *Anal. Chim. Acta*, 2006, **566**, 60-68.

91. M. Yoshida, Y. Hatate, K. Uezu, M. Goto and S. Furusaki, *Colloids and Surfaces A: Physicochemical and Engineering Aspects*, 2000, **169**, 259-269.

92. K. Farrington and F. Regan, *Biosensors and Bioelectronics*, 2007, **22**, 1138-1146.

93. E. Toorisaka, K. Uezu, M. Goto and S. Furusaki, *Biochemical Engineering Journal*, 2003, **14**, 85-91.

94. T. Takeuchi, A. Dobashi and K. Kimura, *Anal. Chem.*, 2000, **72**, 2418-2422.

95. D. B. Henthorn and N. A. Peppas, *Ind. Eng. Chem. Res.*, 2007, **46**, 6084-6091.

96. I. A. Nicholls, H. S. Andersson, C. Charlton, H. Henschel, B. C. Karlsson, J. G. Karlsson, J. O'Mahony, A. M. Rosengren, K. J. Rosengren and S. Wikman, *Biosensors and Bioelectronics*, 2009, **25**, 543-552.

97. W. Dong, M. Yan, M. Zhang, Z. Liu and Y. Li, *Anal. Chim. Acta*, 2005, **542**, 186-192.

98. T. Ogawa, K. Hoshina, J. Haginaka, C. Honda, T. Tanimoto and T. Uchida, *J. Pharm. Sci.*, 2005, **94**, 353-362.

99. I. A. Nicholls, H. S. Andersson, K. Golker, H. Henschel, B. C. Karlsson, G. D. Olsson, A. M. Rosengren, S. Shoravi, S. Suriyanarayanan and J. G. Wiklander, *Anal. Bioanal. Chem.*, 2011, **400**, 1771.

100. L. Ye, R. Weiss and K. Mosbach, *Macromolecules*, 2000, **33**, 8239-8245.

101. S. Tokonami, H. Shiigi and T. Nagaoka, *Anal. Chim. Acta*, 2009, **641**, 7-13.

102. R. Schirhagl, P. A. Lieberzeit and F. L. Dickert, *Advanced materials*, 2010, **22**, 2078-2081.

103. R. Schirhagl, *Anal. Chem.*, 2013, **86**, 250-261.

104. L. Ye, P. A. Cormack and K. Mosbach, *Analytical Communications*, 1999, **36**, 35-38.

105. S. Slomkowski, J. V. Alemán, R. G. Gilbert, M. Hess, K. Horie, R. G. Jones, P. Kubisa, I. Meisel, W. Mormann and S. Penczek, *Pure Appl. Chem.*, 2011, **83**, 2229-2259.

106. S. Subrahmanyam, A. Guerreiro, A. Poma, E. Moczko, E. Piletska and S. Piletsky, *European Polymer Journal*, 2013, **49**, 100-105.

107. G. Wulff, B. O. Chong and U. Kolb, *Angewandte Chemie International Edition*, 2006, **45**, 2955-2958.

108. J. M. Beierle, K. Yoshimatsu, B. Chou, M. A. Mathews, B. K. Lesel and K. J. Shea, *Angewandte Chemie International Edition*, 2014, **53**, 9275-9279.

109. P. A. Lieberzeit, A. Afzal, G. Glanzing and F. L. Dickert, *Anal. Bioanal. Chem.*, 2007, **389**, 441-446.

110. E. Asadi, S. Azodi-Deilami, M. Abdouss and S. Khaghani, *Appl. Biochem. Biotechnol.*, 2012, **167**, 2076-2087.

111. F. G. Tamayo, M. M. Titirici, A. Martin-Esteban and B. Sellergren, *Anal. Chim. Acta*, 2005, **542**, 38-46.

112. A. Poma, A. P. F. Turner and S. A. Piletsky, *Trends in biotechnology*, 2010, **28**, 629-637.

113. P. A. Lieberzeit, A. Afzal, A. Rehman and F. L. Dickert, *Sensors and Actuators B: Chemical*, 2007, **127**, 132-136.

114. Z. Chen and L. Ye, *J. Mol. Recognit.*, 2012, **25**, 370-376.

115. D. Vaihinger, K. Landfester, I. Kräuter, H. Brunner and G. E. Tovar, *Macromolecular Chemistry and Physics*, 2002, **203**, 1965-1973.

116. M. E. Çorman and S. Akgöl, *Artificial Cells, Blood Substitutes, and Biotechnology*, 2012, **40**, 245-255.

117. G. Congur, H. Senay, C. Turkcan, E. Canavar, A. Erdem and S. Akgol, *Comb. Chem. High Throughput Screen.*, 2013, **16**, 503-510.

118. G. Sener, E. Ozgur, E. Yılmaz, L. Uzun, R. Say and A. Denizli, *Biosensors and Bioelectronics*, 2010, **26**, 815-821.

119. G. Sener, L. Uzun, R. Say and A. Denizli, *Sensors and Actuators B: Chemical*, 2011, **160**, 791-799.

120. A. Martín-Esteban, *TrAC Trends in Analytical Chemistry*, 2013, **45**, 169-181.

121. G. Ceolin, Á. Orbán, V. Kocsis, R. E. Gyurcsányi, I. Kézsmárki and V. Horváth, *Journal of Materials Science*, 2013, **48**, 5209-5218.

122. Y. Li, H.-H. Yang, Q.-H. You, Z.-X. Zhuang and X.-R. Wang, *Anal. Chem.*, 2006, **78**, 317-320.

123. F. Vandevelde, J. Pantigny, I. Pezron, L. Gheber and K. Haupt, *International Journal of Nanotechnology*, 2008, **5**, 757-768.

124. E. Yilmaz, K. Haupt and K. Mosbach, *Angewandte Chemie International Edition*, 2000, **39**, 2115-2118.

125. G. Erturk and B. Mattiasson, *Sensors*, 2017, **17**.

126. E. Pellizzoni, 2016.

127. A. R. Guerreiro, I. Chianella, E. Piletska, M. J. Whitcombe and S. A. Piletsky, *Biosensors and Bioelectronics*, 2009, **24**, 2740-2743.

128. C. Cáceres, F. Canfarotta, I. Chianella, E. Pereira, E. Moczko, C. Esen, A. Guerreiro, E. Piletska, M. J. Whitcombe and S. Piletsky, *Analyst*, 2016, **141**, 1405-1412.

129. J. Xu, K. Haupt and B. Tse Sum Bui, *ACS applied materials & interfaces*, 2017, **9**, 24476-24483.

130. I. Chianella, A. Guerreiro, E. Moczko, J. S. Caygill, E. V. Piletska, I. M. P. De Vargas Sansalvador, M. J. Whitcombe and S. A. Piletsky, *Anal. Chem.*, 2013, **85**, 8462-8468.

131. D. García-Mutio, A. Gómez-Caballero, A. Gotiandia, I. Larrauri, M. A. Goicolea and R. J. Barrio, *Electrochimica Acta*, 2018, **279**, 57-65.

132. G. Mustafa and P. A. Lieberzeit, in *Designing Receptors for the Next Generation of Biosensors*, Springer, 2013, pp. 167-187.

133. S. Ambrosini, S. Beyazit, K. Haupt and B. Tse Sum Bui, *Chemical communications*, 2013, **49**, 6746-6748.

134. Y. Garcia, K. Smolinska-Kempisty, E. Pereira, E. Piletska and S. Piletsky, *Analytical Methods*, 2017, **9**, 4592-4598.

135. S. Korposh, I. Chianella, A. Guerreiro, S. Caygill, S. Piletsky, S. W. James and R. P. Tatam, *Analyst*, 2014, **139**, 2229-2236.

136. A. Guerreiro, A. Poma, K. Karim, E. Moczko, J. Takarada, I. P. de Vargas-Sansalvador, N. Turner, E. Piletska, C. S. de Magalhães and N. Glazova, *Advanced healthcare materials*, 2014, **3**, 1426-1429.

137. I. Basozabal, A. Guerreiro, A. Gomez-Caballero, M. Aranzazu Goicolea and R. J. Barrio, *Biosensors & bioelectronics*, 2014, **58**, 138-144.

138. Y. Hoshino, W. W. Haberaecker III, T. Kodama, Z. Zeng, Y. Okahata and K. J. Shea, *J. Am. Chem. Soc.*, 2010, **132**, 13648-13650.

139. K. Yoshimatsu, B. K. Lesel, Y. Yonamine, J. M. Beierle, Y. Hoshino and K. J. Shea, *Angewandte Chemie International Edition*, 2012, **51**, 2405-2408.

140. D. Garcia-Mutio, A. Gomez-Caballero, A. Guerreiro, S. Piletsky, M. Goicolea and R. Barrio, *Sensors and Actuators B: Chemical*, 2016, **236**, 839-848.

141. M. Abdin, Z. Altintas and I. Tothill, *Biosensors and Bioelectronics*, 2015, **67**, 177-183.

142. F. Canfarotta, J. Czulak, K. Betlem, A. Sachdeva, K. Eersels, B. Van Grinsven, T. Cleij and M. Peeters, *Nanoscale*, 2018.

143. E. Piletska, H. Yawer, F. Canfarotta, E. Moczko, K. Smolinska-Kempisty, S. S. Piletsky, A. Guerreiro, M. J. Whitcombe and S. A. Piletsky, *Sci. Rep.*, 2017, **7**, 11537.

144. S. Piletsky, *Molecular imprinting of polymers*, Crc Press, 2006.

145. S. A. Piletsky, E. V. Piletskaya, T. L. Panasyuk, A. V. El'Skaya, R. Levi, I. Karube and G. Wulff, *Macromolecules*, 1998, **31**, 2137-2140.

146. T. Alizadeh, M. R. Ganjali, M. Zare and P. Norouzi, *Electrochimica Acta*, 2010, **55**, 1568-1574.

147. T. Kamra, *Nano-and Micro-sized Molecularly Imprinted Polymer Particles on Solid Surfaces*, Department of Physics, Lund University, 2015.

148. N. K. Chaki and K. Vijayamohanan, *Biosensors and Bioelectronics*, 2002, **17**, 1-12.

149. T. Kamra, S. Chaudhary, C. Xu, L. Montelius, J. Schnadt and L. Ye, *J. Colloid Interface Sci.*, 2016, **461**, 1-8.

150. A. Poma, A. P. Turner and S. A. Piletsky, *Trends Biotechnol.*, 2010, **28**, 629-637.

151. Y.-F. Chang, W.-H. Wang, Y.-W. Hong, R.-Y. Yuan, K.-H. Chen, Y.-W. Huang, P.-L. Lu, Y.-H. Chen, Y.-M. A. Chen and L.-C. Su, *Anal. Chem.*, 2018, **90**, 1861-1869.

152. ThermoFisher scientific Carbodiimide Crosslinker Chemistry, https://www.thermofisher.com/uk/en/home/life-science/protein-biology/protein-biology-learning-center/protein-biology-resource-library/pierce-protein-methods/carbodiimide-crosslinker-chemistry.html

(accessed viewed in 26 th october 2015, 2015).

153. L. Yuan, L. Jiang, T. Hui, L. Jie, X. Bingbin, Y. Feng and L. Yingchun, *Sensors and Actuators B: Chemical*, 2015, **206**, 647-652.

154. O. S. Ahmad, T. S. Bedwell, C. Esen, A. Garcia-Cruz and S. A. Piletsky, *Trends in biotechnology*, 2019, **37**, 294-309.

155. Y. Yoshimi, Y. Yagisawa, R. Yamaguchi and M. Seki, *Sensors and Actuators B: Chemical*, 2018, **259**, 455-462.

156. M. F. Frasco, L. A. Truta, M. G. F. Sales and F. T. Moreira, *Sensors*, 2017, **17**, 523.

157. P. Qi, J. Wang, X. Wang, Z. Wang, H. Xu, S. Di, Q. Wang and X. Wang, *RSC Advances*, 2018, **8**, 25334-25341.

158. Ş. Sağlam, A. Üzer, E. Erçağ and R. Apak, *Anal. Chem.*, 2018.

159. V. Gupta, H. Karimi-Maleh, S. Agarwal, F. Karimi, M. Bijad, M. Farsi and S.-A. Shahidi, *Sensors*, 2018, **18**, 2817.

160. A. Afzal, A. Mujahid, R. Schirhagl, S. Bajwa, U. Latif and S. Feroz, *Chemosensors*, 2017, **5**, 7.

161. S. Piletsky, I. Butovich and V. Kukhar, *Zh. Anal. Khim*, 1992, **47**, 1681-1684.

162. S. Emir Diltemiz, R. Keçili, A. Ersöz and R. Say, *Sensors*, 2017, **17**, 454.

163. J. J. BelBruno, *Chem. Rev.*, 2018.

164. A. Seifner, P. Lieberzeit, C. Jungbauer and F. L. Dickert, *Anal. Chim. Acta*, 2009, **651**, 215-219.

165. A. G. Ayankojo, J. Reut, R. Boroznjak, A. Öpik and V. Syritski, *Sensors and Actuators B: Chemical*, 2018, **258**, 766-774.

166. N. Maouche, N. Ktari, I. Bakas, N. Fourati, C. Zerrouki, M. Seydou, F. Maurel and M. M. Chehimi, *J. Mol. Recognit.*, 2015, **28**, 667-678.

167. A. G. Ayankojo, A. Tretjakov, J. Reut, R. Boroznjak, A. Öpik, J. r. Rappich, A. Furchner, K. Hinrichs and V. Syritski, *Anal. Chem.*, 2016, **88**, 1476-1484.

168. A. Hulanicki, S. Glab and F. Ingman, *Pure Appl. Chem.*, 1991, **63**, 1247-1250.

169. F. Bates and M. del Valle, *Microchimica Acta*, 2015, **182**, 933-942.

170. B. B. Prasad and R. Singh, *Sensors and Actuators B: Chemical*, 2015, **212**, 155-164.

171. E. Mazzotta, R. Picca, C. Malitesta, S. Piletsky and E. Piletska, *Biosensors and Bioelectronics*, 2008, **23**, 1152-1156.

172. H. Bai, C. Wang, J. Chen, J. Peng and Q. Cao, *Biosensors and Bioelectronics*, 2015, **64**, 352-358.

173. J. Bai, X. Zhang, Y. Peng, X. Hong, Y. Liu, S. Jiang, B. Ning and Z. Gao, *Sensors and Actuators B: Chemical*, 2017, **238**, 420-426.

174. D. Kriz, O. Ramstroem, A. Svensson and K. Mosbach, *Anal. Chem.*, 1995, **67**, 2142-2144.

175. M. Blanco-Lopez, S. Gutierrez-Fernandez, M. Lobo-Castanon, A. Miranda-Ordieres and P. Tunon-Blanco, *Anal. Bioanal. Chem.*, 2004, **378**, 1922-1928.

176. G. Selvolini and G. Marrazza, *Sensors*, 2017, **17**, 718.

177. W. Li, Y. Zheng, T. Zhang, S. Wu, J. Zhang and J. Fang, *Sensors*, 2018, **18**, 828.

178. E. Mazzotta, A. Turco, I. Chianella, A. Guerreiro, S. A. Piletsky and C. Malitesta, *Sensors and Actuators B: Chemical*, 2016, **229**, 174-180.

179. T. Alizadeh, M. Akhoundian and M. R. Ganjali, *New Journal of Chemistry*, 2018, **42**, 4719-4727.

180. A. Turco, S. Corvaglia and E. Mazzotta, *Biosensors & bioelectronics*, 2015, **63**, 240-247.

181. S. Rebocho, C. M. Cordas, R. Viveiros and T. Casimiro, *The Journal of Supercritical Fluids*, 2018.

182. V. M. Ekomo, C. Branger, R. Bikanga, A.-M. Florea, G. Istamboulie, C. Calas-Blanchard, T. Noguer, A. Sarbu and H. Brisset, *Biosensors and Bioelectronics*, 2018, **112**, 156-161.

183. I. Svancara, K. Kalcher, A. Walcarius and K. Vytras, *Electroanalysis with carbon paste electrodes*, Crc Press, 2012.

184. W. D. Report, *World Drug Report* 2017.

185. N. J. Connors and R. S. Hoffman, *J. Pharmacol. Exp. Ther.*, 2013, **347**, 251-257.

186. H. H. Maurer, C. Sauer and D. S. Theobald, *Ther. Drug Monit.*, 2006, **28**, 447-453.

187. R. T. Jones, *NIDA Res. Monogr.*, 1998, **175**, 221-234.

188. M. Barroso, E. Gallardo and J. Queiroz, *Bioanalysis*, 2009, **1**, 977-1000.

189. W. M. Bosker and M. A. Huestis, *Clin. Chem.*, 2009, **55**, 1910-1931.

190. UNODC, 2016.

191. J. Mann, *The Guardian*, 2014, **5**.

192. V. Almeida, R. Cassella and W. Pacheco, *Forensic Sci. Int.*, 2015, **251**, 50-55.

193. A. S. Emrani, N. M. Danesh, M. Ramezani, S. M. Taghdisi and K. Abnous, *Biosensors and Bioelectronics*, 2016, **79**, 288-293.

194. J. Y. Zhang and R. L. Foltz, *J. Anal. Toxicol.*, 1990, **14**, 201-205.

195. M. Janicka, A. Kot-Wasik and J. Namieśnik, *TrAC Trends in Analytical Chemistry*, 2010, **29**, 209-224.

196. L. Asturias-Arribas, M. A. Alonso-Lomillo, O. Domínguez-Renedo and M. J. Arcos-Martínez, *Anal. Chim. Acta*, 2014, **834**, 30-36.

197. V. Spiehler, D. S. Isenschmid, P. Matthews, P. Kemp and T. Kupiec, *J. Anal. Toxicol.*, 2003, **27**, 587-591.

198. J. C. Vidal, J. R. Bertolín, L. Bonel, L. Asturias, M. J. Arcos-Martínez and J. R. Castillo, *J. Pharm. Biomed. Anal.*, 2016, **125**, 54-61.

199. T. H. Nguyen, S. A. Hardwick, T. Sun and K. T. Grattan, *IEEE Sensors Journal*, 2012, **12**, 255-260.

200. C.-y. Zhang and L. W. Johnson, *Anal. Chem.*, 2009, **81**, 3051-3055.

201. Y. Wen, H. Pei, Y. Wan, Y. Su, Q. Huang, S. Song and C. Fan, *Anal. Chem.*, 2011, **83**, 7418-7423.

202. B. R. Srijanto, C. P. Cheney, D. L. Hedden, A. C. Gehl, P. B. Crilly, M. A. Huestis and T. L. Ferrell, *Sensor Letters*, 2012, **10**, 850-855.

203. E. V. Piletska, N. W. Turner, A. P. Turner and S. A. Piletsky, *J. Control. Release*, 2005, **108**, 132-139.

204. F. Breton, R. Rouillon, E. V. Piletska, K. Karim, A. Guerreiro, I. Chianella and S. A. Piletsky, *Biosensors and Bioelectronics*, 2007, **22**, 1948-1954.

205. I. Tsyrulneva, O. Zaporozhets, E. Piletska and S. Piletsky, *Analytical Methods*, 2014, **6**, 3429-3435.

206. S. A. Piletsky, E. V. Piletska, A. Bossi, K. Karim, P. Lowe and A. P. Turner, *Biosensors and Bioelectronics*, 2001, **16**, 701-707.

207. E. V. Piletska, B. H. Abd, A. S. Krakowiak, A. Parmar, D. L. Pink, K. S. Wall, L. Wharton, E. Moczko, M. J. Whitcombe and K. Karim, *Analyst*, 2015, **140**, 3113-3120.

208. S. E. Shim, Y. Shin, J. W. Jun, K. Lee, H. Jung and S. Choe, *Macromolecules*, 2003, **36**, 7994-8000.

209. T. Otsu, *Journal of Polymer Science Part A: Polymer Chemistry*, 2000, **38**, 2121-2136.

210. S. A. Piletsky, E. V. Piletska, K. Karim, K. W. Freebairn, C. H. Legge and A. P. Turner, *Macromolecules*, 2002, **35**, 7499-7504.

211. E. A. El Hadji Mamour Sakho and O. S. Oluwafemi, *Thermal and Rheological Measurement Techniques for Nanomaterials Characterization*, 2017, **3**, 37.

212. E. Botosoa, M. Maillasson, M. Mougin-Degraef, R.-L. Saëc, J.-F. Gestin, Y. Jacques, J. Barbet and A. Faivre-Chauvet, *Journal of drug delivery*, 2011, **2011**.

213. J. F. Biebuyck, J. A. Fleming, R. Byck and P. G. Barash, *Anesthesiology: The Journal of the American Society of Anesthesiologists*, 1990, **73**, 518-531.

214. S. P. Wren, T. H. Nguyen, P. Gascoine, R. Lacey, T. Sun and K. T. Grattan, *Sensors and Actuators B: Chemical*, 2014, **193**, 35-41.

215. R. Gutiérrez-Climente, A. Gómez-Caballero, N. Unceta, M. A. Goicolea and R. J. Barrio, *Electrochimica Acta*, 2016, **196**, 496-504.

216. R. A. Weinstein, R. Gaynes, J. R. Edwards and N. N. I. S. System, *Clin. Infect. Dis.*, 2005, **41**, 848-854.

217. V. Ki and C. Rotstein, *Canadian Journal of Infectious Diseases and Medical Microbiology*, 2008, **19**, 173-184.

218. S. Tokonami and T. Iida, *Anal. Chim. Acta*, 2017, **988**, 1-16.

219. T. Boyles and S. Wasserman, *SAMJ: South African Medical Journal*, 2015, **105**, 419-419.

220. W. C. Fuqua, S. C. Winans and E. P. Greenberg, *J. Bacteriol.*, 1994, **176**, 269.

221. S. Swift, J. P. Throup, P. Williams, G. P. Salmond and G. S. Stewart, *Trends Biochem. Sci.*, 1996, **21**, 214-219.

222. B. L. Bassler, *Curr. Opin. Microbiol.*, 1999, **2**, 582-587.

223. C. Gera and S. Srivastava, *Curr. Sci.*, 2006, **90**, 666-676.

224. C. M. Waters and B. L. Bassler, *Annu. Rev. Cell Dev. Biol.*, 2005, **21**, 319-346.

225. H. Lade, D. Paul and J. H. Kweon, *BioMed research international*, 2014, **2014**.

226. G. Stavroulakis, PhD Thesis PhD Thesis, Cranfield University, 2010.

227. H. Withers, Swift, S. and Williams, P, *Curr. Opin. Microbiol.*, 2001, 186-191.

228. H. Jiang, D. Jiang, J. Shao and X. Sun, *Biosensors & bioelectronics*, 2016, **75**, 411-419.

229. A. Kumari, P. Pasini and S. Daunert, *Anal. Bioanal. Chem.*, 2008, **391**, 1619-1627.

230. K. Lakshmana Gowda, J. John, M. A. Marie, G. Sangeetha and S. R. Bindurani, *APMIS*, 2013, **121**, 886-889.

231. W.-F. Yin, K. Purmal, S. Chin, X.-Y. Chan, C.-L. Koh, C.-K. Sam and K.-G. Chan, *Sensors*, 2012, **12**, 3472-3483.

232. C. Okano, M. Arai, E. Nasuno, K.-i. Iimura, T. Morohoshi, T. Ikeda and N. Kato, *Transactions of the Materials Research Society of Japan*, 2012, **37**, 315-318.

233. A. Annapoorani, A. K. K. A. Jabbar, S. K. S. Musthafa, S. K. Pandian and A. V. Ravi, *Indian J. Microbiol.*, 2012, **52**, 160-166.

234. A. Kumari, P. Pasini, S. K. Deo, D. Flomenhoft, H. Shashidhar and S. Daunert, *Anal. Chem.*, 2006, **78**, 7603-7609.

235. M. Cooley, S. R. Chhabra and P. Williams, *Chem. Biol.*, 2008, **15**, 1141-1147.

236. Q. Yang, Y. Han and X. H. Zhang, *J. Appl. Microbiol.*, 2011, **110**, 1438-1448.

237. L. Ravn, A. B. Christensen, S. Molin, M. Givskov and L. Gram, *J. Microbiol. Methods*, 2001, **44**, 239-251.

238. C. García- Aljaro, G. Vargas- Cespedes and A. Blanch, *J. Appl. Microbiol.*, 2012, **112**, 383-389.

239. Q. Yang, Y. Han, N. T. N. Tinh, N. T. Hien and P. Bossier, *Indian J. Microbiol.*, 2012, **52**, 581-586.

240. K. Tang, Y. Zhang, M. Yu, X. Shi, T. Coenye, P. Bossier and X. Zhang, *Journal*, 2013.

241. E. J. Leaman, B. Q. Geuther and B. Behkam, *ACS synthetic biology*, 2018, **7**, 1030-1042.

242. J. B. Andersen, A. Heydorn, M. Hentzer, L. Eberl, O. Geisenberger, B. B. Christensen and M. Givskov, *Appl. Environ. Microbiol.*, 2001, **67**, 575-585.

243. C. E. Chambers, M. B. Visser, U. Schwab and P. A. Sokol, *FEMS Microbiol. Lett.*, 2005, **244**, 297-304.

244. S. Poonguzhali, M. Madhaiyan and T. Sa, *J. Microbiol. Biotechnol.*, 2007, **17**, 226.

245. B. Middleton, H. C. Rodgers, M. Cámara, A. J. Knox, P. Williams and A. Hardman, *FEMS Microbiol. Lett.*, 2002, **207**, 1-7.

246. J. Liu, K. Fu, Y. Wang, C. Wu, F. Li, L. Shi, Y. Ge and L. Zhou, *Frontiers in microbiology*, 2017, **8**, 1097.

247. H. Sheng, Y. Song, Y. Bian, W. Wu, L. Xiang, G. Liu, X. Jiang and F. Wang, *Analytical Methods*, 2017, **9**, 688-696.

248. J. S. Kumar, S. Umesha, K. S. Prasad and P. Niranjana, *Curr. Microbiol.*, 2016, **72**, 297-305.

249. R. Taghadosi, M. R. Shakibaie and S. Masoumi, *Reports of biochemistry & molecular biology*, 2015, **3**, 56.

250. K. Wöllner, X. Chen, E. Kremmer and P. Krämer, *Anal. Chim. Acta*, 2010, **683**, 113-118.

251. W. R. Galloway, J. T. Hodgkinson, S. D. Bowden, M. Welch and D. R. Spring, *Chem. Rev.*, 2011, **111**, 28-67.

252. S. Susmel and C. Comuzzi, *Chemosensors*, 2017, **5**, 5.

253. S. K. Ghosh, University of Cambridge, 2011.

254. H. Zhang, M. Zhao and Y. Yang, *Biomedical Nanomaterials; Zhao, Y., Shen, Y., Eds*, 2016.

255. M. Allen and D. Tildesley, *Computer simulation of liquids*.

256. E. V. Piletska, G. Stavroulakis, K. Karim, M. J. Whitcombe, I. Chianella, A. Sharma, K. E. Eboigbodin, G. K. Robinson and S. A. Piletsky, *Biomacromolecules*, 2010, **11**, 975-980.

257. E. M. d. S. Cavaleiro, PhD PhD, 2014.

258. E. V. Piletska, G. Stavroulakis, L. D. Larcombe, M. J. Whitcombe, A. Sharma, S. Primrose, G. K. Robinson and S. A. Piletsky, *Biomacromolecules*, 2011, **12**, 1067-1071.

259. R. Weiss, M. Freudenschuss, R. Krska and B. Mizaikoff, *Food Addit. Contam.*, 2003, **20**, 386-395.

260. L. Ye and K. Mosbach, *J. Incl. Phenom. Macrocycl. Chem.*, 2001, **41**, 107-113.

261. R. J. Young and P. A. Lovell, *Introduction to polymers*, CRC press, 2011.

262. M. J. Fischer, in *Surface plasmon resonance*, Springer, 2010, pp. 55-73.

263. J. Lim, S. P. Yeap, H. X. Che and S. C. Low, *Nanoscale research letters*, 2013, **8**, 1-14.

264. Z. Farka, D. Kovář and P. Skládal, *Sensors*, 2014, **15**, 79-92.

265. D. Johannsmann, *The Quartz Crystal Microbalance in Soft Matter Research*, Springer, 2014.

266. C. Solano, M. Echeverz and I. Lasa, *Curr. Opin. Microbiol.*, 2014, **18**, 96-104.

267. D. G. Davies, M. R. Parsek, J. P. Pearson, B. H. Iglewski, J. W. Costerton and E. P. Greenberg, *Science*, 1998, **280**, 295-298.

268. L. Hall-Stoodley, J. W. Costerton and P. Stoodley, *Nature reviews microbiology*, 2004, **2**, 95.

269. N.Muthukumar, *Indian Jornal of Experimental Biology*, 2003, **14**, 1012-1022.

270. C. Fuqua and E. P. Greenberg, *Nature reviews. Molecular cell biology*, 2002, **3**, 685.

271. J. M. Henke and B. L. Bassler, *Trends Cell Biol.*, 2004, **14**, 648-656.

272. P. Williams, K. Winzer, W. C. Chan and M. Camara, *Philosophical Transactions of the Royal Society of London B: Biological Sciences*, 2007, **362**, 1119-1134.

273. Y. Y. Lau, J. Sulaiman, J. W. Chen, W.-F. Yin and K.-G. Chan, *Sensors*, 2013, **13**, 14189-14199.

274. C. Fuqua, M. R. Parsek and E. P. Greenberg, *Annu. Rev. Genet.*, 2001, **35**, 439-468.

275. C. N. Berger, S. V. Sodha, R. K. Shaw, P. M. Griffin, D. Pink, P. Hand and G. Frankel, *Environ. Microbiol.*, 2010, **12**, 2385-2397.

276. J. C. Heaton and K. Jones, *J. Appl. Microbiol.*, 2008, **104**, 613-626.

277. P. Skandamis and G.-J. E. Nychas, *Appl. Environ. Microbiol.*, 2012, AEM. 00468-00412.

278. M. B. Miller and B. L. Bassler, *Annual Reviews in Microbiology*, 2001, **55**, 165-199.

279. E. Vandermarliere, M. Mueller and L. Martens, *Mass Spectrom. Rev.*, 2013, **32**, 453-465.

280. M. Kondo, T. Fukao, S. Shinoda, N. Kawamoto, H. Kaneko, Z. Kato, E. Matsui, T. Teramoto, T. Nakano and N. Kondo, *Allergy, Asthma & Clinical Immunology*, 2007, **3**, 1.

281. M. Hirota, M. Ohmuraya and H. Baba, *J. Gastroenterol.*, 2006, **41**, 832-836.

282. W. A. See and J. L. Smith, *Transplantation*, 1991, **52**, 630-633.

283. L. Hu, S. Han, S. Parveen, Y. Yuan, L. Zhang and G. Xu, *Biosensors and Bioelectronics*, 2012, **32**, 297-299.

284. J. Artigas, M. E. Garcia, M. Faure and A. Gimeno, *Postgrad. Med. J.*, 1981, **57**, 219-222.

285. L. Chen, X. Fu and J. Li, *Nanoscale*, 2013, **5**, 5905-5911.

286. C. Mizon, M. Balduyck, D. Albani, C. Michalski, T. Burnouf and J. Mizon, *J. Immunol. Methods*, 1996, **190**, 61-70.

287. J. Carrere, R. Grataroli, J. Marfin, B. Ferrua, J. Thouvenot and C. Figarella, *J. Immunol. Methods*, 1983, **60**, 235-242.

288. G. M. Homer, B. J. Katchman and R. E. Zipf, *Clin. Chem.*, 1963, **9**, 428-437.

289. G. Jang, S. Seo and T. S. Lee, *Sensors and Actuators B: Chemical*, 2015, **221**, 1229-1235.

290. X. A. Ton, B. Tse Sum Bui, M. Resmini, P. Bonomi, I. Dika, O. Soppera and K. Haupt, *Angewandte Chemie*, 2013, **125**, 8475-8479.

291. R. E. Ionescu, S. Cosnier and R. S. Marks, *Anal. Chem.*, 2006, **78**, 6327-6331.

292. X. Li, S. Zhu, B. Xu, K. Ma, J. Zhang, B. Yang and W. Tian, *Nanoscale*, 2013, **5**, 7776-7779.

293. W. Xue, G. Zhang, D. Zhang and D. Zhu, *Organic letters*, 2010, **12**, 2274-2277.

294. J. Wackerlig and R. Schirhagl, *Anal. Chem.*, 2015, **88**, 250-261.

295. S. M. Reddy, Q. T. Phan, H. El-Sharif, L. Govada, D. Stevenson and N. E. Chayen, *Biomacromolecules*, 2012, **13**, 3959-3965.

296. O. Hayden, C. Haderspöck, S. Krassnig, X. Chen and F. L. Dickert, *Analyst*, 2006, **131**, 1044-1050.

297. G. Ertürk, M. Hedström and B. Mattiasson, *Biosensors and Bioelectronics*, 2016, **86**, 557-565.

298. *Diabetes Care*, 2014, **37**, S81-S90.

299. Y. Cui, L. Zhang, M. Zhang, X. Yang, L. Zhang, J. Kuang, G. Zhang, Q. Liu, H. Guo and Q. Meng, *Sci. Rep.*, 2017, **7**, 11195.

300. C. Wanner, S. E. Inzucchi, J. M. Lachin, D. Fitchett, M. von Eynatten, M. Mattheus, O. E. Johansen, H. J. Woerle, U. C. Broedl and B. Zinman, *N. Engl. J. Med.*, 2016, **375**, 323-334.

301. C. S. Fox, S. H. Golden, C. Anderson, G. A. Bray, L. E. Burke, I. H. De Boer, P. Deedwania, R. H. Eckel, A. G. Ershow and J. Fradkin, *Circulation*, 2015, CIR. 230.

302. K. Aung, C. Lorenzo, M. A. Hinojosa and S. M. Haffner, *The Journal of Clinical Endocrinology & Metabolism*, 2014, **99**, 462-468.

303. A. Heller and B. Feldman, *Chem. Rev.*, 2008, **108**, 2482-2505.

304. J. Wang, *Chem. Rev.*, 2008, **108**, 814-825.

305. P. D'Orazio, *Clin. Chim. Acta*, 2003, **334**, 41-69.

306. A. Harper and M. R. Anderson, *Sensors*, 2010, **10**, 8248-8274.

307. N. Gupta, Glucose sensor, https://www.slideshare.net/nikita_liferocks/glucose-sensor-48338483, 2018).

308. J. S. Skyler, *Diabetes Technol. Ther.*, 2009, **11**, S-5-S-10.

309. T.-W. Tsai, G. Heckert, L. s. F. Neves, Y. Tan, D.-Y. Kao, R. G. Harrison, D. E. Resasco and D. W. Schmidtke, *Anal. Chem.*, 2009, **81**, 7917-7925.

310. T. Wungu and S. Marsha, 2017.

311. T. D. K. Wungu, *Procedia engineering*, 2017, **170**, 84-87.

312. M. M. Farid, L. Goudini, F. Piri, A. Zamani and F. Saadati, *Food Chem.*, 2016, **194**, 61-67.

313. B.-C. Iacob, E. Bodoki, C. Farcau, L. Barbu-Tudoran and R. Oprean, *Electrochimica Acta*, 2016, **217**, 195-202.

314. D. Dechtrirat, B. Sookcharoenpinyo, P. Prajongtat, C. Sriprachuabwong, A. Sanguankiat, A. Tuantranont and S. Hannongbua, *RSC Advances*, 2018, **8**, 206-212.

315. S. Rahmadhani, H. Setiyanto and M. A. Zulfikar, 2017.

316. S. M. Khor, G. Liu, C. Fairman, S. G. Iyengar and J. J. Gooding, *Biosensors and Bioelectronics*, 2011, **26**, 2038-2044.

317. H. H. Girault, *Analytical and physical electrochemistry*, EPFL press, 2004.

318. J. Wang, *Analytical electrochemistry*, John Wiley & Sons, 2006.

319. I. Basozabal, A. Guerreiro, A. Gomez-Caballero, M. A. Goicolea and R. J. Barrio, *Biosensors and Bioelectronics*, 2014, **58**, 138-144.

320. W. Luo, L. Zhu, C. Yu, H. Tang, H. Yu, X. Li and X. Zhang, *Anal. Chim. Acta*, 2008, **618**, 147-156.

321. J. M. Walker, in *Basic Protein and Peptide Protocols*, Springer, 1994, pp. 321-328.

322. E. Poli, V. Chaleix, C. Damia, Z. Hjezi, E. Champion and V. Sol, *Analytical Methods*, 2014, **6**, 9622-9627.

323. J. Xu, P. X. Medina-Rangel, K. Haupt and B. T. S. Bui, in *Methods Enzymol.*, Elsevier, 2017, vol. 590, pp. 115-141.

324. T. Kondo, H. Hoshi, K. Honda, Y. Einaga, A. Fujishima and T. Kawai, *The Journal of Physical Chemistry C*, 2008, **112**, 11887-11892.

325. G. Inzelt and L. Szabo, *Electrochimica Acta*, 1986, **31**, 1381-1387.

326. E. A. Mun, C. Hannell, S. E. Rogers, P. Hole, A. C. Williams and V. V. Khutoryanskiy, *Langmuir*, 2013, **30**, 308-317.

327. V. Filipe, A. Hawe and W. Jiskoot, *Pharm. Res.*, 2010, **27**, 796-810.

328. A. Ulman, *Chem. Rev.*, 1996, **96**, 1533-1554.

329. J. C. Love, L. A. Estroff, J. K. Kriebel, R. G. Nuzzo and G. M. Whitesides, *Chem. Rev.*, 2005, **105**, 1103-1170.

330. W. C. Mak, R. Georgieva, R. Renneberg and H. Bäumler, *Advanced Functional Materials*, 2010, **20**, 4139-4144.

331. R. O. Ebewele, *Polymer science and technology*, CRC press, 2000.

332. H. El-Sharif, D. Stevenson and S. Reddy, *Sensors and Actuators B: Chemical*, 2017, **241**, 33-39.

333. S. Ambrosini, S. Beyazit, K. Haupt and B. T. S. Bui, *Chemical communications*, 2013, **49**, 6746-6748.

334. M. Arredondo, M. Stoytcheva, R. Zlatev and S. Cosnier, *ECS Electrochemistry Letters*, 2012, **1**, B1-B3.